Synthesis and characterization of photoactivatable NADPH mimics

Clément Polese

université PARIS-SACLAY

Synthesis and characterization of photoactivatable NADPH mimics

Synthèse et caractérisation d'analogues photoactivables de NADPH

Thèse de doctorat de l'université Paris-Saclay

École doctorale n° 571, Sciences chimiques: molécules, matériaux, instrumentation et biosystèmes (2MIB)
Spécialité de doctorat: Chimie
Graduate School : Chimie, Référent : ENS Paris-Saclay

Thèse préparée dans l'unité de recherche PPSM (Université Paris-Saclay, ENS Paris-Saclay, CNRS), sous la direction de Joanne XIE, Professeure, le co-encadrement de Eric DEPREZ, Directeur de recherche, et de Nicolas BOGLIOTTI, Maître de conférences

Thèse soutenue à Paris-Saclay, le 07 janvier 2022, par

Clément POLESE

Composition du jury

Hamid Dhimane Professeur, Université de Paris	Rapporteur & Examinateur
Gilles Lemercier Professeur, Université de Reims Champagne-Ardenne	Rapporteur & Examinateur
Patricia Busca Maîtresse de conférences, Université de Paris	Examinatrice
Isabelle Leray Directrice de recherche, CNRS	Examinatrice & Présidente du jury
Joanne Xie Professeure, ENS Paris-Saclay	Directrice de thèse

THESE DE DOCTORAT

NNT : 2022UPASF001

Contents

List of Acronyms

AC adenylate cyclase
ACh acetylcholine
AcOEt ethyl acetate
ADMA asymmetric L-dimethylarginine
ALDH2 mitochondrial aldehyde dehydrogenase or aldehyde dehydrogenase-2
AMP adenosine 5'-monophosphate

BH_4 tetrahydrobiopterin

CaM calcium-modulated protein or calmodulin
CARS coherent anti-Stokes Raman scattering
C-geNOp cyan genetically encoded NO probe
cAMP cyclic adenosine 3',5'-monophosphate
cGMP cyclic guanosine 3',5'-monophosphate
cNOS constitutive NOS
cyt P450 cytochrome P450
cyt c ox cytochrome c oxidase

DCM dichloromethane
DEA/NO diethylamine NONOate
DEPT distortionless enhancement by polarization transfer
DHFR dihydrofolate reductase
DHP 3,4-dihydro-*2H*-pyrane
DIAD diisopropylazodicarboxylate
DMAP 4-dimethylaminopyridine
DMF *N*,*N*-dimethylformamide
DMSO dimethylsulphoxide
DNA deoxyribonucleic acid
DPI diphenylene iodonium
DPPA diphenylphosphoryl azide

EDC·HCl 1-ethyl-3-(3-dimethylaminopropyl)carbodiimide hydrochloride
EDRF endothelium-derived relaxing factor
eNOS endothelial Nitric Oxide Synthase
EPR electron paramagnetic resonance spectroscopy
EtOH ethanol

FAD flavin adenine dinucleotide
FMN flavin mononucleotide
Foxo forkhead box O
FTIR Fourier-transform infrared spectroscopy

GC guanylate cyclase
GDN 1,2-glyceryl dinitrate
GLPC gas-liquid partition chromatography

GMN glyceryl mononitrate
GMP guanosine 5'-monophosphate
GTN glyceryl trinitrate
GTP guanosine triphosphate
GUI graphical user interface

HOBt hydroxybenzotriazole
HPLC high pressure liquid chromatography
hr hour
HRMS high-resolution mass spectroscopy
hsp90 heat shock protein 90
HUVECs human umbilical vein endothelial cells
HWE Horner-Wadsworth-Emmons

IC_{50} half maximal inhibitory concentration
ICT intramolecular charge transfer
IET interdomain electron transfer
iNOS inducible Nitric Oxide Synthase
iPrOH isopropanol
ISDN isosorbide dinitrate
ISMN isosorbide mononitrate

LE locally excited
L-SMTC *S*-methyl-L-thiocitrulline
L-TC L-thiocitrulline
L-NMMA N^{ω}-monomethyl-L-arginine
LC light chain
LPS lipopolysaccharide
LTP long term potentiation

mCPBA *meta*-chloroperoxybenzoic acid
MeCN acetonitrile
MeOH methanol
min minute
MLC myosin light chain
mRNA messenger RNA

NADPH reduced form of nicotinamide adenine dinucleotide phosphate
NBF nitro-benzofurazan
NCS *N*-chlorosuccinimide
NF-κB nuclear factor κB
NMO *N*-methylmorpholine *N*-oxide
NMR nuclear magnetic resonance
nNOS neuronal Nitric Oxide Synthase
NO nitric oxide
NOS Nitric Oxide Synthase
NOSIP NOS interacting protein
NT nanotrigger

PAPA/NO propylamine propylamine NONOate
PDE phosphodiesterase
PE petroleum ether
PEDN pentaerythritol dinitrate
PEMN pentaerythritol mononitrate

PET polyethylene terephtalate
PETN pentaerythritol tetranitrate
PETriN pentaerythritol trinitrate
PG prostaglandin
pGC particulate guanylate cyclase
PGI$_2$ prostaglandin I$_2$
PIC pre-initiation complex
PKG GMPc-dependent protein kinase
PKG Iα GMPc-dependent protein kinase type Iα
PPM part per million
PPTS pyridinium *para*-toluenesulfonate
PROLI/NO proline NONOate
PTFE polytetrafluoroethylene
PTSA *para*-toluenesulfonic acid

R$_f$ retention factor
RNA ribonucleic acid
ROS reactive oxygen species
RPM rotation per minute

S$_N$2 second order nucleophilic substitution
sGC soluble guanylate cyclase
SI International System of Units
SNP sodium nitroprusside
SOD superoxide dismutase

TAF TBP associated factor
TBP TATA binding protein
TFA trifluoroacetic acid
THF tetrahydrofuran
THP 2-tetrahydropyranyl
TICT twisted intramolecular charge transfer
TLC thin layer chromatography
TMS tetramethylsilane
TPIF two-photon-induced fluorescence
TPPO triphenylphosphine oxide
tRNA transfer RNA
TS transition state

UDEFT uniform driven equilibrium Fourier transform
UV ultraviolet light

VBA Visual Basic for Applications
VEGF vascular endothelial growth factor
VNTR variable number of tandem repeats

XO xanthine oxidase

Background introduction

Nitric oxide (NO) was found fairly recently to be a major signalling molecule in various biological processes. It is involved in the relaxation induced by nitrovasodilators, some of which clinically used for more than 150 years in the treatment of cardiac pathologies, and in a much more complex signal transduction pathway discovered in the late 1980s. Numerous physiopathologies were correlated with endogenous or exogenous NO, such as cardiovascular diseases, renal dysfunction, obesity, erectile dysfunction or cancer, in addition to an important role in apoptosis by upregulation of *p53*. In order to elucidate further the bioprocesses regulated by NO and their underlying mechanism, a highly resolved release both in space and time would be of the greatest interest. To that extent, light-triggered phenomena would be the most promising candidates, achieving among the most precise space-time control available if using a modern light source. Several strategies towards NO release were developped but one of particular interest relies on photoactivatable mimics of NADPH, called nanotriggers, that are able to competitively bind the NO-producing enzyme and trigger its catalytic transformation upon photo-induced electron transfer under irradiation. The main objective of this work is to synthesize and characterize new NADPH analogs targeted at the Nitric Oxide Synthases, designed with insights from molecular modelling.

The first chapter contextualizes the topic of this research, summarizing briefly the discovery of the biological relevance of NO and the main bioprocesses it is involved in, from its biosynthesis to its effects.

The second chapter describes the synthesis of a new generation of nanotriggers by convergent synthesis of a photoactivatable moiety linked to functionalized adenosines. The linkages aimed at would be either an amide or thiourea functional group.

The third chapter summarizes the spectroscopic characterizations carried out on the synthesized compounds.

Various additional figures and discussions can be found in the *appendixes*, when referenced.

Chapter 1

Physiology of Nitric Oxide and its modulation

Contents

1.1 Discovery of the physiological relevance of Nitric Oxide in biological processes

1.1.1 Nitrovasodilators

Nitrovasodilators are among the very first molecules obtained by chemical synthesis that would be used to therapeutical ends. Their effects on living organisms were so particular and intense that they were mostly discovered trying to list their chemical properties, simply by handling them.

Balard first synthesized amyl nitrite[1] in 1844, and Guthrie studied the properties of this newly available compounds and its derivatives. One of its most important finding was the effects produced by inhaling its vapors, which doubled the heart rate, flushed the face of the subject and provoked throbbing of the carotid artery for a short period of time[2]. Later on, Brunton would later show the potency of nitrite of amyl in treating angina pectoris[3], a pathology mainly caused by insufficient oxygenation of the heart muscle.

Shortly after Balard's synthesis, Sobrero described the synthesis of a dense slightly yellow oily liquid from glycerin, much better known today as nitroglycerin[4] or glyceryl trinitrate (GTN). He already described at the time its migraine inducing potency experienced by himself and his coworkers by tasting it, as it was a quite common analytical technique at the time. It was described to be of great therapeutic use by Murell a few decades later[5], as a powerful treatment for angina pectoris. Patients were relieved of much of their pain and the occasional downside was a short migraine. A growing interest would arise as GTN was shown to be potent in various heart pathologies and is still widely used to this day[6], alongside more recent organic nitrates[7]. The chemical structures of several nitrovasodilators are presented on **Scheme** 1.1, such as pentaerythritol tetranitrate (PETN), isosorbide mononitrate (ISMN) and sodium nitroprusside (SNP).

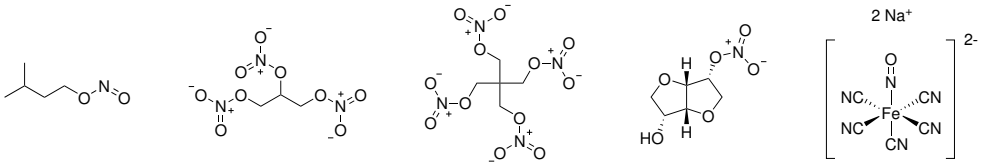

Scheme 1.1: Chemical structures of some nitrovasodilators.

Despite being clinically used, the biochemical processes involved in vasodilation mediated by nitrovasodilators remained unknown for a very long time. Organic nitrates were thought to be transformed into nitrites, as it was shown that nitroglycerin would turn blue an iodine and starch solution after alkali degradation[8]. Furthermore, nitrites were known to have similar physiological effect but with a notable difference in intensity. Nonetheless, no nitrites could be detected in the blood of dogs who received either an injection of organic nitrate or their hydrolysate in alkaline conditions[9,10]. Interestingly, an unexpected result of these experiments was that no decrease of

[1] Balard, A.-J. *Ann. Chim. Phys.* **1844**, *12*, 294–330.
[2] Guthrie, F. *Q. J. Chem. Soc.* **1859**, *11*, 245–252.
[3] Brunton, T. L. *Lancet* **1867**, *90*, 97–98.
[4] Sobrero, A. *C. r. hebd. séances Acad. sci.* **1847**, 247–248.
[5] Murrell, W. *Lancet* **1879**, *113*, 80–81.
[6] Hill, N. S. et al. *CHEST* **1981**, *79*, 69–76.
[7] Miller, M. R.; Megson, I. L. *Br. J. Pharmac.* **2007**, *151*, 305–321.
[8] Hay, M. *Earth Environ. Sci. Trans. R. Soc. Edinb.* **1883**, *32*, 67–86.
[9] Krantz, J. C. et al. *J. Pharmacol. Exp. Ther.* **1940**, *70*, 323–327.
[10] Rath, M. M.; Krantz, J. C. *J. Pharmacol. Exp. Ther.* **1942**, *76*, 33–38.

blood pressure would be observed with the hydrolysates, meaning the organic nitrates needed to be injected pure to be effective.

SNP was found to increase cellular cyclic guanosine 3',5'-monophosphate (cGMP)[11], and some other nitrogen-bearing compounds would demonstrate a similar behavior but in a tissue-dependent fashion, such as sodium azide, GTN or hydroxylamine[12]. Additionally, cGMP formation was inhibited by the presence of either hemoglobin or myoglobin[13], preventing activation of the guanylate cyclase (GC), a family of enzyme synthesizing cGMP from guanosine triphosphate (GTP). The mechanical effect of vasodilation was then shown to be posterior to that increase in cGMP levels[14]. The cause underlying the formation of cGMP was still assumed to come from nitrite release[15], despite a staggering 1000 fold difference in potency in favor of GTN *versus* sodium nitrite, which was thought to be explained by a poor membrane permeability to nitrites. That hypothesis lost credibility when Parks showed the same year that nitrite was almost evenly distributed amongst the tissues in rabbits and mice very shortly after injection[16]. From this observation arose an intriguing question, as formulated by Bennett in 1984[17], regarding the mechanism by which nanomolar levels of GTN could produce micromolar levels of nitrites, as it would be required to obtain the same physiological effect. This last interrogation was solved a few years afterwards by Romanin[18], demonstrating that at an equipotent concentration of GTN and sodium nitrite towards 95% activation of GC, a 1000 fold difference in nitrite concentration subsisted, strongly indicating that its activation is not mediated by nitrites. In the meantime, L-arginine was proven to activate GC in an indirect fashion[19], in a similar way to the one induced by nitroso compounds. That feat could not be easily explained, and there would not be any breakthrough on that matter until a parallel investigation progressed and helped uncover the mechanism of nitrovasodilator-mediated vasodilation.

1.1.2 Endothelium-Derived Relaxing Factor

The vascular tone was known to be regulated by numerous vasoactive agents acting on the vessel wall either *via* the bloodstream, like epinephrine, or by release on site by the terminal end of a adrenergic or cholinergic nervous fiber. The possibility that these vasoactive substances could be synthesized and released by the constitutive cells of the vessel walls would not be suspected until the discovery of a new prostaglandin (PG) by Moncada[20]. The latter, called prostacyclin or prostaglandin I_2 (PGI_2), was shown to be a vasodilator produced by the vascular endothelium, and sparked the research for new endogenous vasodilators synthesized within the vascular system. A detailed scheme of vascular vessels is presented in **Appendix A.1**.

At the time, acetylcholine (ACh), a powerful hypotensive agent would occasionally show a different behavior *in-vitro*, having either no effect or even contracting smooth muscle. Furchgott demonstrated that ACh needed the presence of the endothelium in order to provoke the relaxation of arterial smooth muscle[21], and that its alternative behavior was due to the unintentional removal of endothelial cells in samples. Furthermore, indomethacin, inhibiting the synthesis of PGs thus preventing PGI_2 release by the endothelium[22], did not suppress the relaxation induced

[11] Schultz, K.-D. et al. *Nature* **1977**, *265*, 750–751.
[12] Katsuki, S. et al. *J. Cyclic Nucleotide Res.* **1977**, *3*, 23–35.
[13] Murad, F. et al. *Adv. Cyclic Nucleotide Res.* **1978**, *9*, 145–158.
[14] Kukovetz, W. R. et al. *Naunyn-Schmiedeberg's Arch. Pharmacol.* **1979**, *310*, 129–138.
[15] Ignarro, L. J. et al. *J. Pharmacol. Exp. Ther.* **1981**, *218*, 739–749.
[16] Parks, N. J. et al. *Science* **1981**, *212*, 58–60.
[17] Bennett, B. M.; Marks, G. S. *Trends Pharmacol. Sci.* **1984**, *5*, 329–332.
[18] Romanin, C.; Kukovetz, W. R. *J. Mol. Cell. Cardiol.* **1988**, *20*, 389–396.
[19] Deguchi, T.; Yoshioka, M. *J. Biol. Chem.* **1982**, *257*, 10147–10151.
[20] Moncada, S. et al. *Nature* **1976**, *263*, 663–665.
[21] Furchgott, R. F.; Zawadzki, J. V. *Nature* **1980**, *288*, 373–376.
[22] Ferreira, S. H. et al. *Nat. New Biol.* **1971**, *231*, 237–239.

by ACh. The latter would be suspected to be caused by a another humoral substance released by the endothelium which would be called endothelium-derived relaxing factor (EDRF).

Endothelium-dependent relaxation of arteries could be triggered by various types of stimuli[23,24], such as injection of bradykinin or vasopressin, hypoxia or increase in blood flow. In order to unify the studies about this kind of relaxation of the smooth muscle, a superfusion technique using a modified syringe with the barrel covered in endothelial cells was developped[25], as shown on **Figure** 1.2. An improvement of that method[26], based on Vane's cascade superfusion bioassay[27], involved covering spherical beads with endothelial cells and packing them in an appropriate heated chromatographic column, allowing the effluent to incubate a cascade of chosen arterial strips in a very short timespan, enabling a more rigorous and precise study of the endothelium-dependent relaxation phenomena and EDRF.

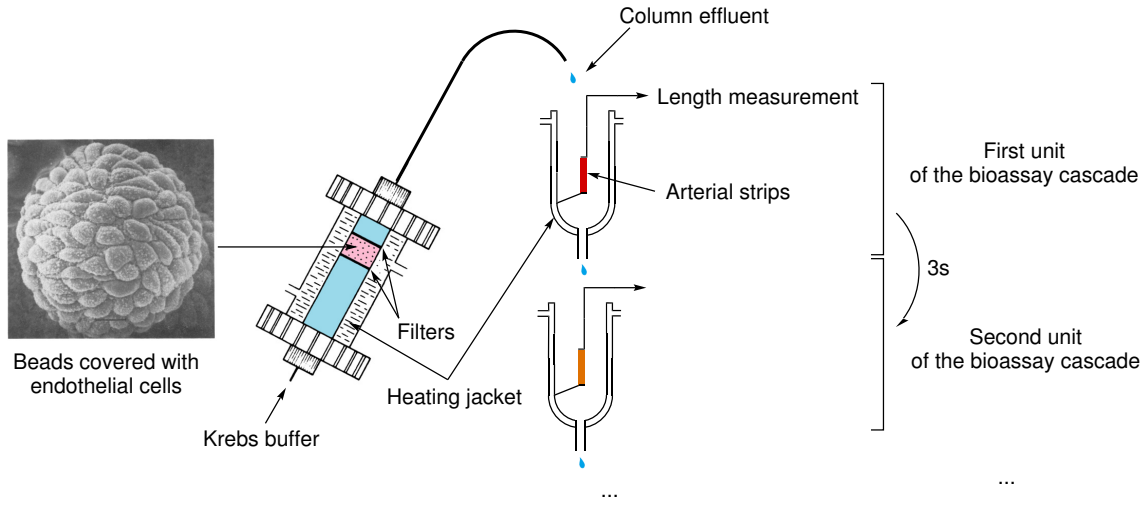

Figure 1.2: Schematic of the superfusion cascade bioassay technique, adapted from Gryglewski[26].

Using this useful methodology, properties and caracteristics of EDRF would start to add up very quickly. EDRF was shown to inhibit natural[28] or induced[29] platelet aggregation and their adhesion to endothelial cells[30]. Furthermore, inhibitors of cGMP diesterases increased EDRF relaxing potency, by preventing the enzymatic cleavage of cGMP[31]. This observation supported previous observations that methylene blue, a GC inhibitor, prevented the action of EDRF[32]. Thus, cGMP increase was within the signaling pathway towards vascular relaxation and stemmed from EDRF production, similarly to nitrovasodilators as discussed previously.

Additionally, superoxide dismutase (SOD) was shown to increase the lifetime of EDRF, implying that superoxide anions were involved in its instability[33,34]. This hypothesis was further supported

[23] Moncada, S. et al. In *Biology and Pathology of Platelet-Vessel Wall Interactions*, Academic Press, London; Orlando, 1986, pp 289–304.
[24] Busse, R. et al. *Basic Res. Cardiol.* **1985**, *80*, 475–490.
[25] Cocks, T. M. et al. *J. Cell. Physiol.* **1985**, *123*, 310–320.
[26] Gryglewski, R. J. et al. *Br. J. Pharmac.* **1986**, *87*, 685–694.
[27] Vane, J. R. *Br. J. Pharmacol. Chemother.* **1964**, *23*, 360–373.
[28] Azuma, H. et al. *Br. J. Pharmac.* **1986**, *88*, 411–415.
[29] Radomski, M. W. et al. *Br. J. Pharmacol.* **1987**, *92*, 181–187.
[30] Radomski, M. W. et al. *Lancet* **1987**, *330*, 1057–1058.
[31] Radomski, M. W. et al. *Biochem. Biophys. Res. Commun.* **1987**, *148*, 1482–1489.
[32] Gruetter, C. A. et al. *J. Pharmacol. Exp. Ther.* **1981**, *219*, 181–186.
[33] Gryglewski, R. J. et al. *Nature* **1986**, *320*, 454–456.
[34] Rubanyi, G. M.; Vanhoutte, P. M. *Am. J. Physiol. Heart Circ.* **1986**, *250*, H822–H827.

by the reversal of EDRF inhibition in presence of SOD[35]. If SOD was added, degrading superoxide anions, several substances that were inhibitory of the action of EDRF would lose this property.

1.1.3 Nitric oxide as an endogenous humoral relaxing factor

1.1.3.1 Link between EDRF and NO

Going slightly back in time, a small gaseous molecule bearing a radical was added to the list of compounds able to activate the GC, NO[36]. Shortly after, the importance of the nitrosyl-heme complex towards the activation of GC was described[37]. The purification of the enzyme decreased its activity, but the addition of a solution of 10µM of NO-hemoglobin could restore it more than 20-folds. Moreover, free NO would not show any activation in presence of hemoglobin, and oxygenating the solution of NO-hemoglobin decreased GC activation as well because of the competitive binding of NO and oxygen to hemoglobin. Thus, the NO-hemoglobin complex could improve the GC activation, possibly because of the heme presence. The ferrous heme of GC could then be studied as a receptor for NO, EDRF and endogenous stimulants of GC. Following these insights, the interaction of hemoglobin with azide or GTN was probed, as an inhibitor of their effects, but none was found[38]. The latter could be explained by the binding of an active metabolic intermediate by hemoglobin.

By combination of available data, Ignarro[39] and Furchgott[40] formulated independantly in 1986 the hypothesis that EDRF was, in fact, NO.

Aiming at proving EDRF is NO, Ignarro[41] based most of his reasoning on knowledge previously discussed, adding a particularly speaking experiment. The absorption spectra in the lower wavelength of the visible region of deoxyhemoglobin would be compared after incubation in several conditions, and no distinction could be made between an incubation with NO or endothelial cells. Furthermore, using calcium ionophore as an EDRF inhibitor and adding deoxyhemoglobin to endothelial cells would result in the same absorbance profile as deoxyhemoglobin alone. Previously, EDRF was chemically and pharmacologically identified as NO in perfusates recovered after stimulation of endothelial cells, both substances induce indistinguishable actions, are antagonized by the same inhibitors, are inactivated by superoxide anions but stabilized by SOD. The authors conclude that all converging evidences are consistent with the criteria introduced by Dale[42] to recognize a chemical substance as a biological mediator, thus identifying EDRF as nitric oxide.

The discovery of NO as the endogenous vasodilator formerly known as EDRF was recognized almost immediately, as it was already widely known that both substances behaved very similarly. Moncada summarized available properties for EDRF and NO in a simple way, as shown in **Table** 1.1[43,44].

[35] Moncada, S. et al. *Proc. Natl. Acad. Sci. U. S. A.* **1986**, *83*, 9164–9168.
[36] Arnold, W. P. et al. *Proc. Natl. Acad. Sci. U. S. A.* **1977**, *74*, 3203–3207.
[37] Craven, P. A.; DeRubertis, F. R. *J. Biol. Chem.* **1978**, *253*, 8433–8443.
[38] Martin, W. et al. *Br. J. Pharmac.* **1986**, *89*, 563–571.
[39] Ignarro, L. J. et al. In *Vasodilation: Vascular Smooth Muscle Peptides, Autonomic Nerves and Endothelium*, Vanhoutte, P. M., Ed.; Raven Press, pp 401–414.
[40] Furchgott, R. F. In *Vasodilation: Vascular Smooth Muscle Peptides, Autonomic Nerves and Endothelium*, Vanhoutte, P. M., Ed.; Raven Press, pp 401–414.
[41] Ignarro, L. J. et al. *Proc. Natl. Acad. Sci. U. S. A.* **1987**, *84*, 9265–9269.
[42] Dale, H. H. *Bull. Johns Hopkins Hosp.* **1933**, *53*, 297–347.
[43] Moncada, S. et al. *Biochem. Pharmacol.* **1988**, *37*, 2495–2501.
[44] Moncada, S. et al. *Hypertension* **1988**, *12*, 365–372.

Property	EDRF	NO
Released by endothelial cells	+	+
Relaxes vascular smooth muscle	+	+
Inhibits platelet aggregation	+	+
Induces platelet disaggregation	+	+
Inhibits platelet adhesion	+	+
$t_{\frac{1}{2}}$ (s) - Down cascade	3.6 ± 0.1	4.1 ± 0.2
$t_{\frac{1}{2}}$ (s) - Through polypropylene tubes	30.9 ± 1.9	30.4 ± 2.2
Receptor	soluble GC	soluble GC
2^{nd} messenger	cGMP	cGMP
Inhibited directly by hemoglobin	+	+
Inhibited indirectly by redox compounds	+	+
Potentiated by SOD, cytochrome c	+	+
Potentiated by M&B22948[†], MY 5445[†]	+	+
Not affected by methemoglobin, HL 725[‡]	+	+
Reacts with superoxide anions	+	+
Reacts with O_2	+	+
Binds to ion exchange columns	±	±

Table 1.1: Summary of the comparison experiments trying to differenciate EDRF from nitric oxide, reproduced from Moncada[44].

[†] Both are specific cGMP phosphodiesterases inhibitors.

[‡] A specific cyclic adenosine 3',5'-monophosphate (cAMP) phosphodiesterase inhibitor.

A decade later, Furchgott, Ignarro and Murad received the Nobel Prize in Physiology or Medicine 1998[45] "for their discoveries concerning nitric oxide as a signalling molecule in the cardiovascular system".

1.1.3.2 Nitrovasodilators metabolization into NO

Numerous interrogations were still unanswered. Firstly, the pathway by which nitrovasodilators are converted into NO towards smooth muscle relaxation was yet to be found, and secondly the mechanism behind the endogenous synthesis of NO was even more obscure.

The first clue about the metabolic pathway of nitrovasodilators towards NO would come from an enzyme expressed in mitochondria called mitochondrial aldehyde dehydrogenase or aldehyde dehydrogenase-2 (ALDH2), which was found to transform GTN into 1,2-glyceryl dinitrate (GDN), consuming a reducing thiol cofactor and releasing one equivalent of nitrite[46], as shown on **Figure** 1.3. This process of GTN transformation would still happen at therapeutical concentrations, in the nanomolar range[47]. Nonetheless, no evidence of its conversion into NO was found. Much later, an endogenous fluorescent proteic NO sensor, the cyan genetically encoded NO probe (C-geNOp), was expressed in vascular smooth muscle cells and enabled the detection of NO production by ALDH2[48]. GTN-mediated NO production was continous if enough reductant was available in the cytosol. The enzyme was also able to produce relevant short bursts of NO from GTN by stoechiometric reaction of the enzyme, without the third step reduction of the disulfide bond shown on **Figure** 1.3[49].

[45] The Nobel Prize in Physiology or Medicine 1998, https://www.nobelprize.org/prizes/med icine/1998/summary/.

[46] Chen, Z. et al. *Proc. Natl. Acad. Sci. U. S. A.* **2002**, *99*, 8306–8311.

[47] Kleschyov, A. L. et al. *Circ. Res.* **2003**, *93*, e104–e112.

[48] Opelt, M. et al. *J. Biol. Chem.* **2016**, *291*, 24076–24084.

[49] Opelt, M. et al. *Mol. Pharmacol.* **2018**, *93*, 335–343.

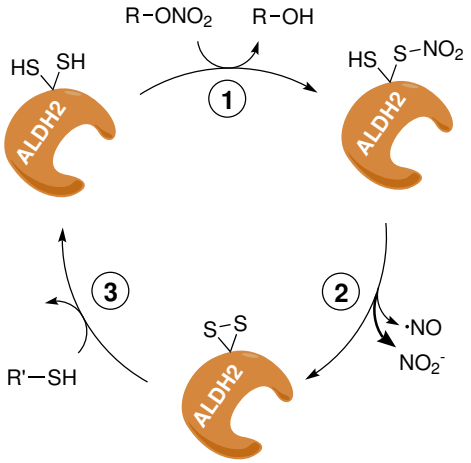

Figure 1.3: Catalytic formation of nitric oxide and nitrite from an organic nitrate by ALDH2 involving a reducing thiol[46,48].

Regarding the mechanism of endogenous synthesis of NO that will be discussed thoroughsly later, the reader only needs to know it is performed by enzymes called Nitric Oxide Synthases (NOSs) for the moment.

Nitric oxide is the active substance responsible for vasodilation, among many other effects, produced either endogenously by NOSs or exogenously by nitrovasodilators. It could behave as an hormone-like signaling molecule spreading *via* the circulatory system, thanks to being a pretty unreactive radical with a decent half-life ranging from a few seconds to a few minutes in physiological conditions, having a very high diffusion rate because of its small size and an elimination pathway that does not involve any external action. Unfortunately, NO is so reactive towards oxyhemoglobin in red blood cells that its half-life is decreased in the bloodstream to around 2 ms as its free form[50], enough for a cell-to-cell diffusion but not enough at an entire mammal scale. Nitric oxide is most likely part of a much more complex signal transduction system.

1.1.3.3 The NO-cGMP signal transduction pathway

Several isoforms of GC were described quite early[51], and their presence in soluble and particulate fractions of homogenates from mammalian tissues would give them their names[52]. Activity ratio between particulate guanylate cyclase (pGC) and soluble guanylate cyclase (sGC) are tissue-dependant. Additionally, NO-induced increase in GC activity was described quite early to be more important on sGC[36]. Two decades later, the quaternary structures of the nucleotides cyclases would finally be elucidated, and shown a strong conservation of the cyclase domains, as pictured by the yellow regions in **Figure** 1.4[53]. Adenylate cyclase (AC) and pGC are regulated enzymes and their cofactors are not of a great interest towards understanding the relaxing effect caused by NO. On the other hand, sGC only has one regulatory site, its iron heme, where nitric oxide can form a nitrosyl-iron complex[54]. Furthermore, very recent results showed the allosteric activation described in **Figure** 1.4 to be slightly more complex despite being a reasonable approximation. The enzyme only becomes fully active when the cytosolic concentration of NO is sufficient. Beforehand, when the enzyme binds the first NO molecule at the heme site, it reaches an intermediate equilibrium state between an inactive and an active form in a roughly 3 to 1 ratio[55].

[50] Liu, X. et al. *J. Biol. Chem.* **1998**, *273*, 18709–18713.
[51] Goridis, C.; Morgan, I. *FEBS Lett.* **1973**, *34*, 71–73.
[52] Kimura, H.; Murad, F. *Life Sci.* **1975**, *17*, 837–843.
[53] Denninger, J. W.; Marletta, M. A. *Biochim. Biophys. Acta - Bioenerg.* **1999**, *1411*, 334–350.
[54] Bellamy, T. C. et al. *Proc. Natl. Acad. Sci. U. S. A.* **2002**, *99*, 507–510.
[55] Horst, B. G. et al. *eLife* **2019**, *8*, ed. by van der Donk, W. A. et al., e50634.

More precisely, the previous statements only concerns an already existing enzyme, and another level of regulation of sGC activity exists with the modulation of the expression of the associated gene. Regulatory sequences in deoxyribonucleic acid (DNA) associated with proteic transcription factors can influence the cytosolic concentration of an enzyme, thus its apparent activity, but the latter will not be discussed further. For a structural reminder of eukaryotic cells see **Appendix A.2** and for further details on the possible regulations of genetic expression see **Appendix A.3**.

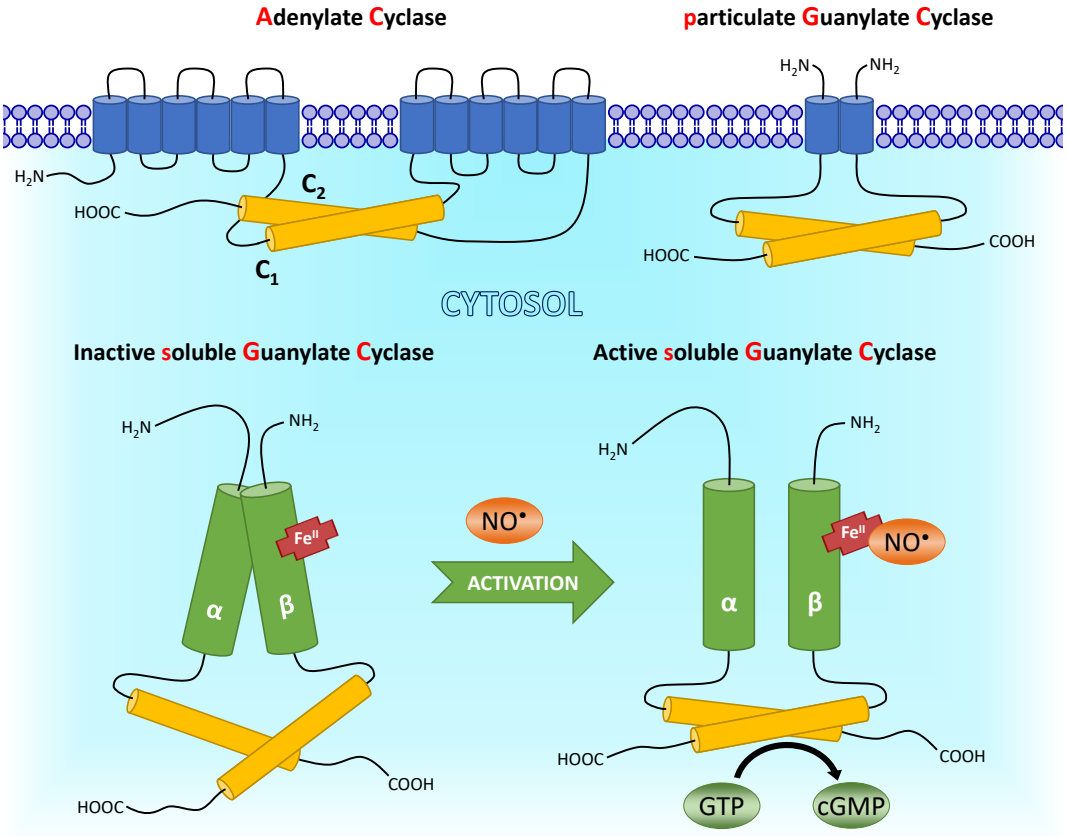

Figure 1.4: Quaternary structures of adenylate cyclase, particulate guanylate cyclase and soluble guanylate cyclase, with a simplified representation of the allosteric activation of sGC by NO binding to the prosthetic iron heme towards cGMP synthesis from GTP[53,54,55]. Transmembranar α-helixes in blue; conserved catalytic regions in yellow; simplified α and β subunits in green; iron heme in red.

Once the sGC is activated, cellular levels of cGMP will increase and have many consequences, which can be divided among three main categories[56]. The cGMP can diffuse out of some cells or interact with gated ion channels, opening sodium and potassium specific ones, influencing calcium concentration as well[57]. It can also activate phosphodiesterases (PDEs) specific of cAMP and cGMP, enabling their elimination respectively towards adenosine 5'-monophosphate (AMP) and guanosine 5'-monophosphate (GMP)[58,59]. The latter acts as a self regulation of cGMP and cross-talk with the signal transduction pathway of cAMP. The most interesting consequence towards vascular relaxation is the activation of GMPc-dependent protein kinases (PKGs), and particularly of GMPc-dependent protein kinase type Iα (PKG Iα). This kinase is able to activate the myosin light chain phosphatase, enabling dephosphorylation of myosin light chain (MLC) and muscle relaxation[60]. A summary of the NO-mediated activation of sGC by endogenous NO or nitrovasodi-

[56] Kots, A. Y. et al. In *cGMP: Generators, Effectors and Therapeutic Implications*, Schmidt, H. H. H. W. et al., Eds.; Handbook of Experimental Pharmacology; Springer: Berlin, Heidelberg, 2009, pp 1–14.
[57] Stryer, L. *Annu. Rev. Neurosci.* **1986**, *9*, 87–119.
[58] Francis, S. H.; Corbin, J. D. *Urol. Clin. North Am.* **2005**, *32*, 419–429.
[59] Francis, S. H. et al. *Pharmacol. Rev.* **2010**, *62*, 525–563.
[60] Surks, H. K. et al. *Science* **1999**, *286*, 1583–1587.

lators[61] towards dephosphorylation of MLC and smooth muscle relaxation is presented in **Figure** 1.5.

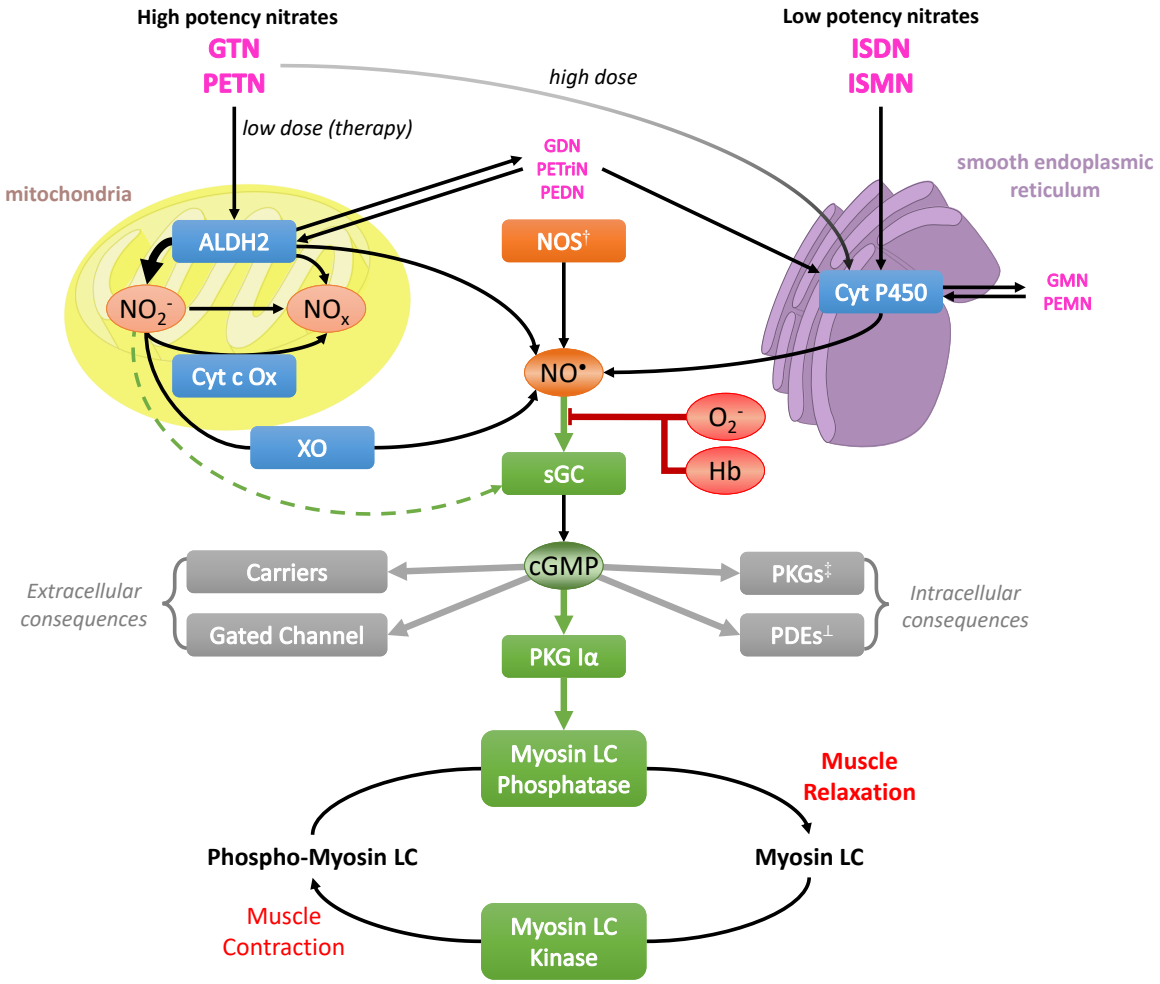

Figure 1.5: Mechanisms involved in the relaxation of smooth muscle induced by nitrovasodilators or endogenous NO, through activation of the guanylate cyclase transduction pathway until dephosphorylation of MLC[61,58,59]. Enzymes are represented as rectangles, blue for non-specific and orange for specific NO production, green for the NO-cGMP transduction pathway towards muscle relaxation, grey towards other consequences; Substances involved in the signaling cascade are depicted in ovals. Black arrows represent substance production proportional to their width, green arrows activation of enzymes, red flat-headed arrows inhibition, grey arrows modulation of activity (activation or inhibition). Abbreviations: isosorbide dinitrate (ISDN); pentaerythritol trinitrate (PETriN); pentaerythritol dinitrate (PEDN); pentaerythritol mononitrate (PEMN); glyceryl mononitrate (GMN); cytochrome c oxidase (cyt c ox); cytochrome P450 (cyt P450); xanthine oxidase (XO); light chain (LC).

† NOSs localization and activity will be discussed later.
‡ PKG Iα is a PKG but separated on the scheme for convenience.
⊥ The cross communication between the signal transduction pathways of cAMP and cGMP induced by the not complete selectivity of PDEs will not be discussed.

1.1.4 Ubiquitous role of Nitric Oxide

The main focus of the previous discussion was on the vasodilation properties of NO, because it was the feature that lead Ignarro, Murad and Furchgott to the discovery of its importance in the cardiovascular system, rewarded by a *Nobel prize*. Nonetheless, many other biological functionalities are tied to NO and will be superficially described hereafter.

[61] Münzel, T. et al. *Circulation* **2011**, *123*, 2132–2144.

NO is also an important inflammatory mediator, as pro-inflammatory cytokines induce its production in cells from the immune system such as macrophages by a factor able to reach 1000-fold of the physiological levels[62]. At this concentration, NO can have two very distinct effects. First a pro-inflammatory action, attracting other immune cells by chemotaxis towards the source of inflammation such as microbes and eliminate it. The second effect encountered at higher concentrations of NO is the destruction of tissues[63].

The latter is caused by another feature of NO, able to promote or prevent apoptosis based on the concentration and the cellular type considered[64]. Interestingly, when exposed to low doses of NO the apoptosis of B lymphocytes is inhibited, whereas higher concentration induced apoptosis in macrophages, neurons and a other cell types. Macrophages are still more resistant to NO-mediated apoptosis[65], increasing their survival in inflammatory environments.

NO is an important neurotransmitter, found in both retrograde and anterograde neurotransmission[66]. Its production at postsynaptic junctions is able to trigger retrograde processes such as spine growth. Its fairly unique ability to diffuse out towards the presynaptic neuron enables a loop formation called long term potentiation (LTP) involved in memory and learning.

NO is also involved in the regulation of oxidative stress, for example by reaction with reactive oxygen species (ROS).

The role and biological functions of NO are a constantly expanding field of research, and the former descriptions are merely a glimpse over decades of work. Nonetheless, these overviews should be helpful setting a wider context towards upcoming discussions.

[62] Sharma, J. N. et al. *Inflammopharmacology* **2007**, *15*, 252–259.
[63] Pfeilschifter, J. et al. *Cell Biol. Int.* **1996**, *20*, 51–58.
[64] Kim, Y.-M. et al. *Circ. Res.* **1999**, *84*, 253–256.
[65] Brüne, B. et al. *J. Biol. Chem.* **1997**, *272*, 7253–7258.
[66] Picón-Pagès, P. et al. *Biochim. Biophys. Acta Mol. Basis Dis.* **2019**, *1865*, 1949–1967.

1.2 Biosynthesis of Nitric Oxide

1.2.1 Nitric Oxide Synthases

1.2.1.1 Isoforms

As previously introduced, NO is endogenously synthesized by three isoforms of NOS[67]. An additional prefix letter is added for each form, as a remnant of a property or the origin tissue, and are still widely used. Despite being proven to be not completely accurate and sometimes misleading, these names will still be used as commonly accepted. The neuronal Nitric Oxide Synthase (nNOS), also known as NOS1, was first purified from neuronal tissue. The inducible Nitric Oxide Synthase (iNOS), also known as NOS2, was first isolated from macrophages but only after immunoactivation induced by inflammatory stimuli. The endothelial Nitric Oxide Synthase (eNOS), also known as NOS3, was first extracted from vascular endothelium[68]. Sometimes nNOS and eNOS are grouped under the name of constitutive NOS (cNOS), as opposed to iNOS.

Nonetheless, nNOS was shown to be expressed in other tissues such as skeletal muscle[69] and its expression can be induced by nerve injury[70], iNOS was found to be expressed constitutively in human airway epithelium[71] and eNOS was observed in other cells type such as cardiomyocytes where its transcription is modulated[72].

1.2.1.2 Structure

The sequences of all three isoforms are relatively similar, as shown on **Figure** 1.6, sharing binding sites for an iron heme, tetrahydrobiopterin (BH_4), calcium-modulated protein or calmodulin (CaM), flavin mononucleotide (FMN), flavin adenine dinucleotide (FAD) and reduced form of nicotinamide adenine dinucleotide phosphate (NADPH), but several important differences shall be noted[73].

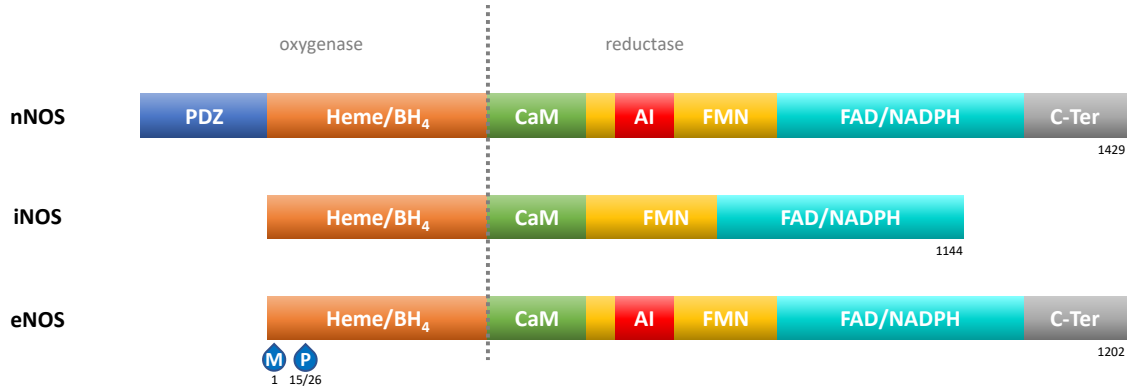

Figure 1.6: Sequence alignment of the conserved domains of the three isoforms of NOS[73].

A PDZ domain is found only in nNOS at its N-terminus, enabling its localization at synaptic junctions in neurons[74]. Post-translational modifications of eNOS, such as N-myristoylation, al-

[67] Knowles, R. G.; Moncada, S. *Biochem. J.* **1994**, *298*, 249–258.
[68] Michel, T.; Feron, O. *J. Clin. Invest.* **1997**, *100*, 2146–2152.
[69] Kobzik, L. et al. *Nature* **1994**, *372*, 546–548.
[70] Vizzard, M. A. et al. *J. Neurosci.* **1995**, *15*, 4033–4045.
[71] Guo, F. H. et al. *Proc. Natl. Acad. Sci. U. S. A.* **1995**, *92*, 7809–7813.
[72] Belhassen, L. et al. *J. Clin. Invest.* **1996**, *97*, 1908–1915.
[73] Daff, S. *Nitric Oxide* **2010**, *23*, 1–11.
[74] Brenman, J. E. et al. *Cell* **1996**, *84*, 757–767.

lows for membrane association and Golgi apparatus addressing[75], and palmitoylation at Cys16 and/or Cys26 is required for a maximum NO release[76]. An insertion of about 45 amino acids in the sequence of nNOS and eNOS was shown to be a key difference between iNOS and cNOSs, as it enables regulation of the enzymes activity by CaM interaction, thus refered as an autoinhibitory domain[77].

The active forms of the enzymes are homodimers, as shown on **Figure** 1.7, and the main interaction between the two units was shown to come from the oxygenases subunits[78]. Additionally, the electron transfer from the reductase domain of the first unit proceeds towards the oxygenase domain of a second unit through a mobile FMN shuttle, explaining the homodimer requirement for an active enzyme. The dimer formation process and regulation depends on the isoform and will not be further detailed.

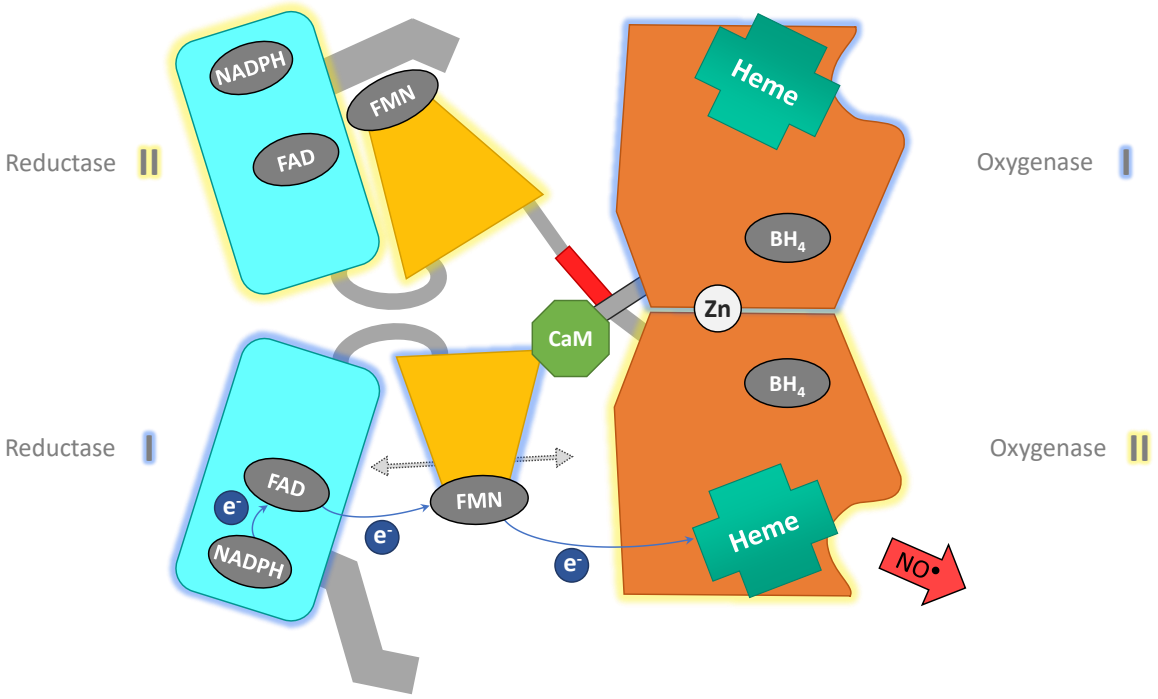

Figure 1.7: Quaternary structure of cNOSs and electron transfer chain towards NO biosynthesis, modified from Daff[73].

1.2.1.3 Electron transfer chain

The autoinhibitory sequence was found to be in close interaction with the FMN subdomain of eNOS and influence CaM binding as well as the electron transfer in the reductase subunit[79]. The C-terminal domain of cNOSs are also part of the enzyme regulation by CaM, as shown by a mutant enzyme without that sequence losing its ability to be CaM-activated[80]. Furthermore, CaM binding and phosphorylation of a serine at position 1412 was found to unlock the FMN shuttle in cNOSs by displacing the C-terminal peptide[81]. The latter is depicted on the **Figure** 1.7 with the yellow glowing unit having its FMN binding domain locked, while the other subunit is able to transfer electrons if CaM is bound.

[75] Sessa, W. C. et al. *J. Biol. Chem.* **1995**, *270*, 17641–17644.
[76] Liu, J. et al. *Biochemistry* **1996**, *35*, 13277–13281.
[77] Roman, L. J. et al. *Chem. Rev.* **2002**, *102*, 1179–1190.
[78] Stuehr, D. J. *Biochim. Biophys. Acta - Bioenerg.* **1999**, *1411*, 217–230.
[79] Chen, P.-F.; Wu, K. K. *J. Biol. Chem.* **2000**, *275*, 13155–13163.
[80] Roman, L. J. et al. *J. Biol. Chem.* **2000**, *275*, 29225–29232.

The FMN is able to transfer electrons from the reductase domain towards the oxygenase domain through a tethered shuttle mechanism, as shown on **Figure** 1.7. The FMN binding domain was observed to lock the FMN around 5 Å of the FAD in an electron-accepting position[81], very similarly to the stuctural arrangement found in cyt P450 reductase[82] associated with a fast electron transfer. Thus the limiting step would be its movement towards the heme in order to deliver harvested electrons and enable the catalytic formation of NO[83]. The importance of the interaction between the FAD and FMN was further investigated *via* mutation R1229E in the reductase region, replacing a positively charged arginine by a negatively charged glutamate within the FMN-binding domain. A new repulsive interaction with Glu762, Glu816 and Glu819 took place, replacing the former stabilizing one and preventing the formation of the locked state that allowed the interdomain electron transfer (IET) from the FAD to the FMN. In the mutant, the IET was highly impacted and showed that the FMN shuttle was a key step in the electron transfer chain of NOSs and an important feature of the relationship between the structure and activity of these enzymes[84].

The role of CaM was also shown to be of great interest while studying the IET from the FMN to the heme. A truncated nNOS only composed of the FMN binding domain and the oxygenase region would show a 10-fold increase in activity in presence of CaM[83]. Additionally, an FMN-heme IET in nNOS holoenzyme could not be observed in absence of CaM[85].

1.2.1.4 Catalytic cycle

The catalytic transformation performed by NOSs to produce NO was discovered way before the enzymes. Using ^{15}N radiomarkers, NO was found to be formed by conversion of L-arginine into L-citrulline[86]. This process is now well documented and known to consume one and a half equivalent of NADPH alongside two equivalents of dioxygen in order to fully oxidize L-arg with NO release[73], as shown on **Figure** 1.8.

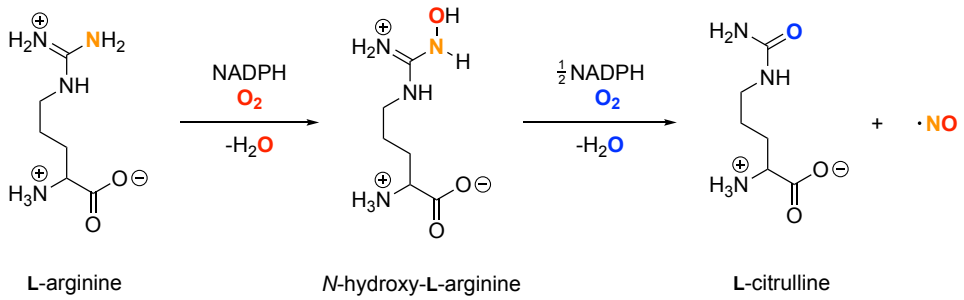

Scheme 1.8: Catalytic transformation of L-arginine into L-citrulline with NO release.

The catalytic cycle including the multiple necessary cofactors is shown on **Scheme** 1.9, summarizing the electron transfer chain discussed previously. A detailed scheme of the catalytic transformations occuring at the heme are detailed in **Appendix A.4**.

The many intermediate cofactors involved in the latter increase the complexity of its mechanism, requiring two IETs per electron transfered to the heme. These elements combined highlight the key importance of the electron transport in NOSs and the complexity of its regulation[87]. Fur-

[81] Garcin, E. D. et al. *J. Biol. Chem.* **2004**, *279*, 37918–37927.
[82] Bredt, D. S.; Snyder, S. H. *Proc. Natl. Acad. Sci. U. S. A.* **1990**, *87*, 682–685.
[83] Feng, C. et al. *Biochemistry* **2006**, *45*, 6354–6362.
[84] Welland, A. et al. *Biochemistry* **2008**, *47*, 9771–9780.
[85] Feng, C. et al. *J. Am. Chem. Soc.* **2007**, *129*, 5621–5629.
[86] Palmer, R. M. J. et al. *Nature* **1988**, *333*, 664–666.
[87] Feng, C. *Coord. Chem. Rev.* **2012**, *256*, 393–411.

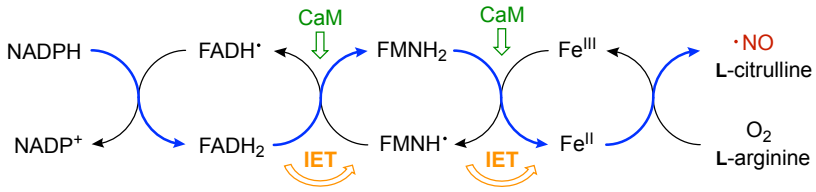

Figure 1.9: Catalytic cycle in NOSs forming NO from L-arginine. Electron transfer represented by blue arrows; CaM activation in cNOSs by green hollow arrows; Interdomain electron transfert by orange hollow arrows.

thermore, ubiquitous NO production among most living organisms is another clue of its physiological relevance, as it was observed in mammals but also in fishes, birds, invertebrates, plants and bacteria[88]. Thus, the pathologies associated with NO or NOSs are quite numerous and an expanding field of clinical research.

1.3 NO-Associated physiopathologies

The relationship between several pathologies and NO were intensively investigated in the last decades, following the discovery of NO as an endogenous vasodilator and its biosynthesis by NOSs.

Nitrovasodilators, now also known as exogenous NO donors, are to this day commonly clinically used for cardiac diseases such as angina pectoris or hypertension[89]. They also inhibit platelet function and adhesion as well as show antithrombotic and anti-inflammatory properties. The latter mainly derives from NO production following their uptake. After its discovery as the endogenous nitrovasodilator, NO was rapidly associated with various physiological phenomena, such as renal activity[90], apoptosis[65], tumoral angiogenesis[91] in addition to the previously discussed vascular tone and platelet adhesion[31,30] and function[92]. From these observations was deduced that endogenous NO was most likely involved in much more physiopathological disorders[93].

Congenital heart disease is a structural defect of the heart and vessel found in 1 to 2% of newborns, and is a major cause of child mortality. The endothelial isoform of NOS was shown to be a key factor in embryonic development of the heart[94]. Heart muscle proliferation, development of the vascular system (coronary artery, myocardial capillaries) as well as the modeling of the aortic valve all stem from the crucial role of eNOS in the formation of the embryonic and postnatal heart development. Thus eNOS could be a therapeutic target of choice towards prevention of congenital heart diseases.

NO is also promising towards improving the viability of vascular grafts[95]. For patients requiring a coronary bypass graft, the best option would be to use a piece of another artery but they often are diseased as well. In those scenarios, the only other available option is to graft a polytetrafluoroethylene (PTFE) or polyethylene terephtalate (PET) tubing, but the success rate is interesting only for the bigger arteries. For smaller vascular vessels, the grafts failure rate increase sharply mainly because thrombotic complications that cannot be fully adressed by antiplatelet therapy. A strategy

[88] Liu, Q.; Gross, S. S. In *Methods in Enzymology*; Nitric Oxide Part A: Sources and Detection of NO; NO Synthase, Vol. 268; Academic Press: 1996, pp 311–324.
[89] Divakaran, S.; Loscalzo, J. *J. Am. Coll. Cardiol.* **2017**, *70*, 2393–2410.
[90] Vidal, M. J. et al. *Eur. J. Pharmacol.* **1988**, *149*, 401–402.
[91] Cooke, J. P.; Losordo, D. W. *Circulation* **2002**, *105*, 2133–2135.
[92] Sinzinger, H. et al. *Lancet* **1990**, *335*, 627–628.
[93] Pacher, P. et al. *Physiol. Rev.* **2007**, *87*, 315–424.
[94] Liu, Y.; Feng, Q. *Differentiation* **2012**, *84*, 54–61.
[95] de Mel, A. et al. *Chem. Rev.* **2011**, *111*, 5742–5767.

that could improve the viability of this surgery could be the use of an NO releasing polymeric graft preventing platelet adhesion and formation of blood clots. Nonetheless, the NO donating polymer could not release it continuously as it would contain only a fixed amount of precursor.

An other effect of NO, further away from health and diseases, was found in its pro-apoptotic properties[96]. NO promotes p53, a key cellular transcription factor involved in the regulation of cellular cycle and apoptosis voted *molecule of the year* by the magazine *Science* in 1993[97]. Caspases are a family of cysteine proteases cleaving peptidic sequences after an aspartic acid known to be involved in the apoptotic process. Endogenous or exogenous NO activates their activity after p53 accumulation, triggering a controlled cellular death. Nonetheless, NO is also involved in cellular protection by prevention of oxidative stress by reaction with superoxides anions or other mechanisms, such as modification of thiols inhibiting the caspases activity. Thus, NO has a dual effect on apoptosis regulation, tightly related to its concentration.

The involvement of NO in apoptosis and angiogenesis makes it a target of choice for cancer study and therapy[98]. Tumoral cells were shown to induce neoangiogenesis, stimulating growth by vascularization[99], a phenomenon that could be induced by NO. Using the radiosensitizing effects of NO, delivery platforms were developped with photo-induced or stimuli-induced release with an improved efficiency compared to free NO donors. The increased vascularization around tumors added to the vasodilation properties of NO also helps concentrating the active drugs at the delivery site.

A correlation between several physiopathologies and some of the most studied eNOS polymorphisms is presented in **Table** 1.2[100].

polymorphism / associated disease	g.-786T→C[†]	4b/4a VNTR[‡]	E298D[§]
Hypertension	(+)	(+)	(+)
Preeclampsia	(+)	(+)	(+)
Obesity (children)	+	+	+
Diabetes	(+)	(+)	+
Migraine	(+)	∅	(+)
Erectile dysfunction	+	+	+

Table 1.2: Diseases associated with various polymorphisms of eNOS gene, adapted from Oliveira-Paula[100]. +: Established; (+): Described in specific populations.

[†] (rs2070744) g.-786T→C mutation in the promoter sequence of eNOS.
[‡] 4 (4b) or 5 (4a) copies of a 27bp sequence within intron 4 of eNOS gene.
[§] (rs1799983) g.-894G→T mutation in exon 7 leading to Glu298Asp mutated protein.

The three presented polymorphs all bear a genome difference expressed at a different level of the enzyme biosynthesis but correlated with various humans physiopathologies. The genomic mutaion g.-786T→C in the promoter sequence of eNOS, modifies its transcription but not the peptidic sequence. The 4b/4a polymorph has an intron variable number of tandem repeats (VNTR) respectively modified from 4 to 5 copies, which influences the maturation process of a specific kind

[96] Brüne, B. et al. *Eur. J. Pharmacol.* **1998**, *351*, 261–272.
[97] Koshland, D. E. *Science* **1993**, *262*, 1953–1953.
[98] Park, D. et al. In *Therapeutic Application of Nitric Oxide in Cancer and Inflammatory Disorders*, Morbidelli, L., Bonavida, B., Eds.; Academic Press: 2019, pp 191–218.
[99] Andrade, S. P. et al. *Br. J. Cancer* **1992**, *66*, 821–826.
[100] Oliveira-Paula, G. H. et al. *Gene* **2016**, *575*, 584–599.

of ribonucleic acid (RNA), messenger RNA (mRNA), but still does not interfere with the amino acid sequence of the protein. The g.-894G→T mutation in an exon of the enzyme leads to a Glu298Asp mutated protein, changing the peptidic sequence. Further details about the transcription and translation processes can be found in **Appendix A.3**.

Consequently, NO regulation is an important factor in various diseases and is a thriving therapeutic target.

1.4 Nitric Oxide regulation

1.4.1 Endogenous regulation

1.4.1.1 Expression

nNOS An antisense mRNA was shown to be coexpressed in snails neurons, leading to a stable RNA-RNA adduct that prevented nNOS translation[101].

iNOS Murine iNOS gene has two upstream activating regions inducing cooperatively hundreds of fold increase in proteic expression, by binding pro-inflammatory cytokines and lipopolysaccharide (LPS)[102].

eNOS In addition to an increase of expression under shear stress conditions, transciption of eNOS is regulated by various transcriptional factors such as nuclear factor κB (NF-κB) or forkhead box O (Foxo)[103].

1.4.1.2 post-translational regulation

nNOS The nNOS regulated by Ca^{2+} and CaM, as well as interaction of its PDZ domain with other proteins which can change its subcellular localization[104]. Phosphorylation of Ser847 in nNOS by a CaM-dependant proteine kinase was shown to modulate its activity[104]. NO has a negative feedback regulatory effect on the enzyme, as shown by the linearized formation of L-citrulline by addition of an NO scavenger[105].

iNOS CaM and Ca^{2+} do not regulate iNOS activity. NO also has a negative feedback regulatory effect on this enzyme[106].

eNOS The endothelial isoform is regulated by CaM and Ca^{2+}, similarly to nNOS, but also by various proteins and many post-translational modifications. A chaperone protein, heat shock protein 90 (hsp90), can serve as an allosteric activator of eNOS and promote the active dimer formation[104]. Caveolae are small inward invaginations of the cellular plasma membrane, mainly involved in endocytosis. Caveolins are proteins recruited at caveolae as a mechanical support, and caveolin-1 inhibits eNOS activity. A joint action of CaM and hsp90 can restore the enzyme activity by displacing the peptidic inhibitor. A peptide, named NOS interacting protein (NOSIP), was found to modulate eNOS activity by enabling delocalization of the enzyme to intracellular compartments, inhibiting NO synthesis[107]. Phosphorylation of several key residues of eNOS are also involved in

[101] Korneev, S. A. et al. *J. Neurosci.* **1999**, *19*, 7711–7720.
[102] Lowenstein, C. J. et al. *Proc. Natl. Acad. Sci. U. S. A.* **1993**, *90*, 9730–9734.
[103] Balligand, J.-L. et al. *Physiol. Rev.* **2009**, *89*, 481–534.
[104] Nakane, M. et al. *Biochem. Biophys. Res. Commun.* **1991**, *180*, 1396–1402.
[105] Bernátová, I. *Interdiscip. Toxicol.* **2011**, *4*, 63–68.
[106] Bernátová, I. *Interdiscip. Toxicol.* **2011**, *4*, 63–68.
[107] Dedio, J. et al. *FASEB J.* **2001**, *15*, 79–89.

the regulation of protein-protein interactions[108]. Additionally, phosphorylation of Ser1177[109] and Ser1179[110] by a kinase bears a crucial regulatory role in eNOS, as well as Thr497 which decreases the binding ability of CaM when phosphorylated, thus its activity[111]. A negative regulatory feedback also exists in eNOS by NO itself. Increasing levels of intracellular NO leads to S-nitrosylation of the enzyme, decreasing eNOS activity by monomerization, as cysteins play an important role in maintaining the dimeric active form[112].

As previously stated, CaM plays a key role in the electron transfer chain, thus in the catalytic activity cNOSs[87]. CaM binding is regulated by intracellular Ca^{2+} concentration, which can itself be modulated by opening and closing of gated channels in response to chemical stimuli, as shown in **Figure** 1.10. ACh released by cholinergic neurons in the tunica externa trigger the opening of calcium channels in endothelial cells, promoting eNOS activity. Similarly, glutamate enable increase of intracellular Ca^{2+} in neurons, increasing nNOS activity.

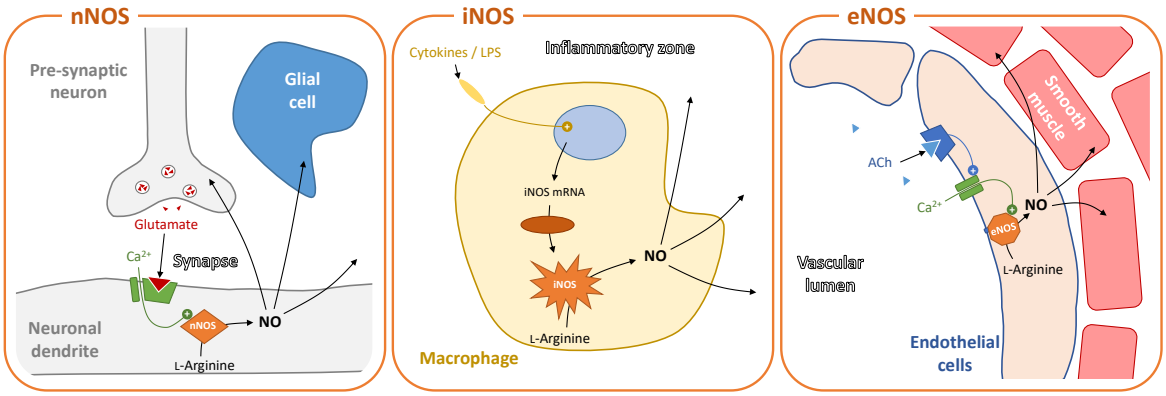

Figure 1.10: Mechanism of NO production from cNOSs activation by Ca^{2+} intracellular increase and iNOS induced expression by cytokines and LPS[67].

1.4.2 Exogenous control

1.4.2.1 Inhibition of NOS activity

Inhibition of NOSs activity can be divided in three main categories: Inhibition of the reductase activity, prevention of the electronic transfer between the two domains or inhibition of the oxygenase activity.

Reductase inhibition

Flavins: A flavoprotein inhibitor, diphenylene iodonium (DPI) and some of its analogs were tested in mouse macrophages and porcine endothelial cells, resulting in a high irreversible inhibition of NOS activity[113]. Nonetheless, as flavins are also the cofactors of numerous other enzymes that inhibition is not NOS-specific.

NADPH: A more recent approach involves the use of NADPH analogs, as shown on **Scheme** 1.11, bearing the same recognition moiety represented as the green adenosine. Unlike the natural cofactor, the conjugated moiety of the molecule, designed towards π-interactions with the FAD in

[108] Bauer, P. M. et al. *J. Biol. Chem.* **2003**, *278*, 14841–14849.
[109] Dimmeler, S. et al. *Nature* **1999**, *399*, 601–605.
[110] Fulton, D. et al. *Nature* **1999**, *400*, 792–792.
[111] Matsubara, M. et al. *J. Biochem* **2003**, *133*, 773–781.
[112] Ravi, K. et al. *Proc. Natl. Acad. Sci. U. S. A.* **2004**, *101*, 2619–2624.
[113] Stuehr, D. J. et al. *FASEB J.* **1991**, *5*, 98–103.

cNOSs, is functionalized with an electron withdrawing group, preventing an electron transfer but enabling imaging. They were designed as fluorescent two-photon cNOSs imaging probes[114], but also demonstrated potent inhibition of angiogenesis in vascular endothelial growth factor (VEGF)-stimulated matrigel-grown human umbilical vein endothelial cells (HUVECs) and interruption of the cellular cycle in metastatic melanoma[115].

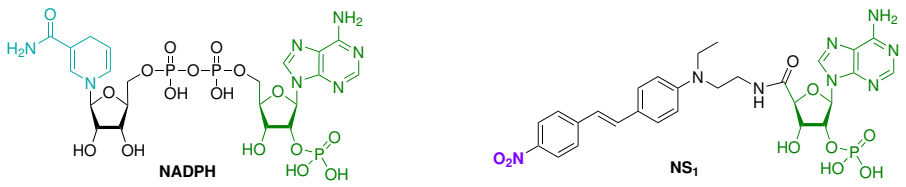

Scheme 1.11: Structure of the natural NADPH and a fluorescent analog NS1 (electron donating group in dark cyan; electron withdrawing group in deep purple; docking moiety in green).

Prevention of the electronic transfer from reductase to oxygenase

As previously discussed, CaM is a necessary cofactor towards cNOSs activity. As such, a specific CaM inhibitor, calmidazolium, is able to inhibit the activity of nNOS and eNOS but not in the CaM-independant iNOS[116]. Similarly to the flavins, CaM being involved in various other cellular processes, its inhibition is not NOS-specific.

Oxygenase inhibition

BH_4: Analogs of BH_4 with similar association constant showed potency in competitive inhibition of nNOS[117]. Nonetheless, the basal NOS activity without BH_4 would be preserved. A major issue using these inhibitors comes from the great variety of enzymes using BH_4 as a cofactor, making them non-specific of NOS and mostly not suitable for NOSs study.

L-Arginine: Several analogs of L-arginine and L-citrulline are good competitive inhibitors of NOSs, as shown in **Scheme** 1.12[118]. Asymmetric L-dimethylarginine (ADMA) and N^{ω}-monomethyl-L-arginine (L-NMMA) were among the first discovered inhibitors of NO signalling pathway[119] and ADMA biological accumulation related to chronic renal failure[120]. Citrulline derivatives such as L-thiocitrulline (L-TC) are also able to show inhibitory activity by binding the oxygenase domain of NOSs, further increased by alkylation of the thiol like in *S*-methyl-L-thiocitrulline (L-SMTC). An interesting challenge in that matter is the selective inhibition of one or several isoform of NOS, enabling *in-vivo* studies. Indeed, using a non-selective inhibitor to study iNOS would result in various undesired side effects in the cardiovascular system of the living organism studied because of unwanted eNOS inhibition. GW274150 is an inhibitor found by more recent biochemical screening, and shows great potency towards a selective iNOS inhibition, with an half maximal inhibitory concentration (IC_{50}) over 300 fold higher for eNOS and 100 fold higher for nNOS *versus* iNOS[121].

[114] Li, Y. et al. *Proc. Natl. Acad. Sci. U. S. A.* **2012**, *109*, 12526–12531.
[115] Rouaud, F. et al. *Oncotarget* **2014**, *5*, 10650–10664.
[116] Schini, V. B.; Vanhoutte, P. M. *J. Pharmacol. Exp. Ther.* **1992**, *261*, 553–559.
[117] Werner, E. R. et al. *Biochem. J.* **1996**, *320*, 193–196.
[118] Víteček, J. et al. *Mediators Inflamm.* **2012**, *2012*, e318087.
[119] Macallister, R. et al. *Kidney Int.* **1994**, *45*, 737–742.
[120] Vallance, P. et al. *Lancet* **1992**, *339*, 572–575.
[121] Young, R. J. et al. *Bioorganic Med. Chem. Lett.* **2000**, *10*, 597–600.

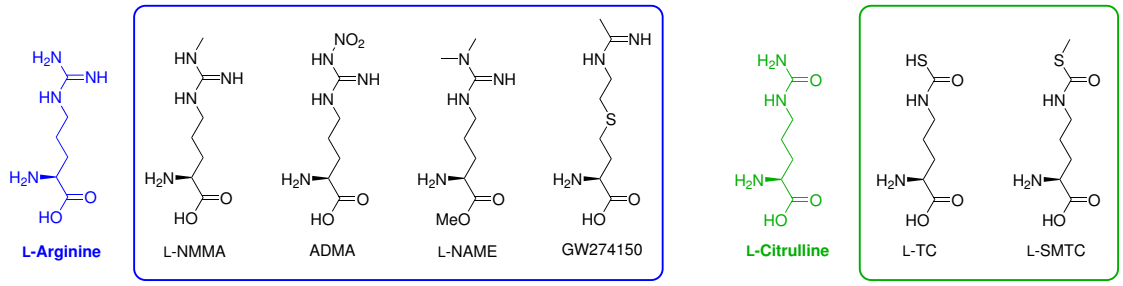

Scheme 1.12: Example of some NOSs inhibitors with structures similar to L-arginine and L-citrulline.

Heme: Imidazole and some of its phenylic derivatives are NOSs inhibitors by acting as an iron ligand at the heme site, competing with oxygen binding, thus considerably slowing down the oxidation of L-arginine and production of L-citrulline, most likely correlated with a drop in NOS-dependent NO production[122]. Once more, iron heme are quite common making this family of inhibitors not NOS-specific.

1.4.2.2 Exogenous modulation of NO release

Kinetic release

NONOates are a family of compounds discovered in the 60s[123], able to kinetically release two molar equivalents of NO at physiological pH. The half-life of these compounds can be very different with respect to their structure, as shown in **Scheme** 1.13. Historically, diethylamine NONOate (DEA/NO) was the first synthesized with an half-life of a couple of minutes, but many more compounds are available today, with longer lifespans such as propylamine propylamine NONOate (PAPA/NO) or much shorter with the example of proline NONOate (PROLI/NO). A major inconvenient of these NO donors comes from their first order kinetics, related to a poor spatial resolution of the released dose.

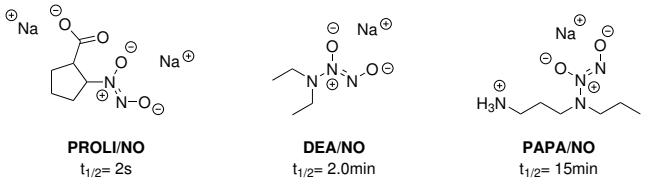

Scheme 1.13: Structure of several NONOates with various half-lives[98].

A more spatially acurate NO dose was demonstrated with a particular compound, **RRx-001**, shown on **Scheme** 1.14. The latter is currently under clinical testing towards cancer therapy, related to its interesting pharmacokinetics[124,125]. After injection, this compound binds hemoglobin and remains in the bloodstream for the entire lifetime of the bound red blood cell. Upon encounter of an hypoxic tissue, as found in tumors, production of NO is promoted and used as a radiosensitizer for radiotherapy, additionally producing on-site ROS. However, the resulting high levels of NO can have systemic effects such as hypotension. Nonetheless, that treatment can resensitize tumors that were unresponsive to conventional substances.

[122] Wolff, D. J. et al. *J. Biol. Chem.* **1993**, *268*, 9425–9429.
[123] Drago, R. S.; Paulik, F. E. *J. Am. Chem. Soc.* **1960**, *82*, 96–98.
[124] Scicinski, J. et al. *Redox Biol.* **2015**, *6*, 1–8.
[125] Scicinski, J. et al. *Drug Metab. Dispos.* **2012**, *40*, 1810–1816.

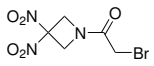

RRx-001

Scheme 1.14: Structure of RRx-001[125].

The kinetic NO donors have their respective usefulness, but a way of delivering NO with a fully controlled spatiotemporal delivery would be of great interest. First enabling a better understanding of its associated signalling pathway, and allowing more precise therapeutical approaches. Towards that sharp spatiotemporal control, light-induced release seem like a promising candidate.

Photoinduced release

Spatial and time resolution achieved by modern light sources can be quite astonishing. As such, molecules able to be activated by light are the most promising candidates towards the most precise release of drugs, such as NO. To that end, several strategies were developped to enable drug photorelease, as presented in the upcoming discussion. Caged molecules are functionalized with a photolabile group able to be cleaved under irradiation, releasing a precursor of an enzymatic transformation such as NADPH[126], with two-photon variants also available[127]. Alternatively, other structures were described to enable NO release directly upon irradiation[128]. The first method would use the endogenous enzymatic pathway whereas the second strategy produces NO independantly from NOSs.

Photoactivatable molecules have already been used to study enzymes, such as the caged compounds shown on **Scheme** 1.15[129]. The use of such compounds enabled the study of an enzyme/-substrate complex with a lifetime in the tens of milliseconds. The temporal resolution is limited by the diffusion rate of the photoreleased substance, preventing the study of high turnover enzymes. Cryophotolysis would enable the trapping of intermediates at low temperature (100K - 150K) in order to reduce their apparent turnover, enabling the crystallographic studies of the enzyme/substrate intermediates[130]. Intermediates of GTPase were also studied following the photorelease of caged GTP by time-resolved Fourier-transform infrared spectroscopy (FTIR)[131].

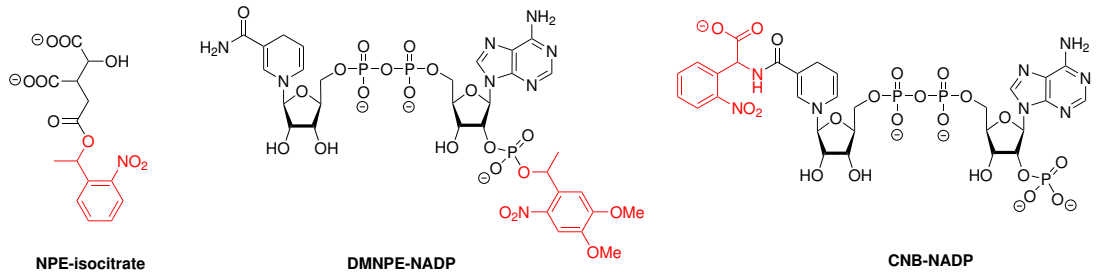

NPE-isocitrate DMNPE-NADP CNB-NADP

Scheme 1.15: Structure of caged compounds able to photorelease an active species by light-induced cleavage of the red moieties[129].

Modified Ruthenium bipyridine complexes were designed towards binding a cyt P450 substrate site. Under light irradiation, these compounds showed the ability to potently reduce the heme

[126] Ellis-Davies, G. C. R. *Nat. Methods* **2007**, *4*, 619–628.
[127] Vuilleumier, J. et al. *ACS Appl. Mater. Interfaces* **2019**, *11*, 27443–27452.
[128] Fraix, A. et al. *Chem. Eur. J.* **2021**, *27*, 12714–12725.
[129] Stoddard, B. L. et al. *Nat. Struct. Biol.* **1998**, *5*, 891–897.
[130] Ursby, T. et al. *Acta Crystallogr. D. Biol. Crystallogr.* **2002**, *58*, 607–614.
[131] Allin, C. et al. *Proc. Natl. Acad. Sci. U. S. A.* **2001**, *98*, 7754–7759.

Fe^{3+} at the tens of nanoseconds timescale[132]. The same research group next aimed at the iNOS in a similar fashion, with Rhenium complexes, breaching the sub-nanosecond timescale[133]. These techniques do not enable catalytic activity.

A fluoroxan derivative was described to photorelease NO upon irradiation in the low-wavelength visible region but with a very low release efficiency, requiring hours of irradiation towards full conversion[134]. Despite showing interesting spatial resolution, the photorelease low kinetics does not allow experiments at low timescale. Even more recent investigations showed the potency of photorelease of NO by derivatives of nitro-benzofurazan (NBF) under blue-light irradiation, as presented in **Scheme** 1.16[135]. Nonetheless, this compound seem to have a quite low solubility in aqueous medium, requiring the use of mycelles which remarkably also improve its NO-release efficiency. Interestingly the fluorescent product formed can be used as a probe towards determining the amount of NO photoreleased.

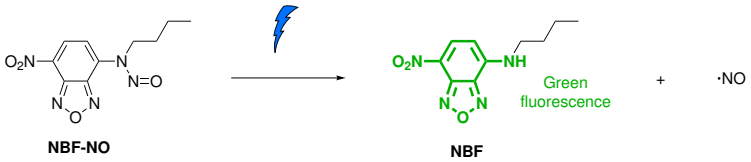

Scheme 1.16: Structure of **NBF-NO**, a blue-light photoactivatable NO prodrug[135].

A photactivatable compound shown on **Scheme** 1.17 based on a different structure was shown to be able to modulate NO concentration in a biological buffer, under red-light irradiation. Furthermore, it enabled a photocontrolled increase of intracavernous pressure *versus* the mean arterial pressure in rats. The latter was further evidenced to originate from NO by spin trapping[136].

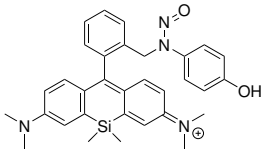

Scheme 1.17: Structure of **NORD-1**, a near-infrared photoactivatable NO prodrug[136].

Another promising approach was to use multiphoton processes to promote a substance activity. To that extent, a construct made of an inhibitor and a cage was synthesized. The latter was demonstrated to efficiently inhibit iNOS activity upon multiphoton photolysis[137]. Multiphoton processes are particularly interesting towards *in-vivo* experiments for several reasons. First and foremost, the ability to use at least two photons to enter a molecular excited state enable the use of an excitation wavelength two fold higher, because of the relationship $E = h\nu = hc/\lambda$. The latter is particularly interesting in biological experiments, as ultraviolet light (UV) excitation can cause DNA damages, either triggering genome reparation processes that may interfere with the desired experiment, or induced toxicity might simply lead to cellular death. Enabling excitation with deep red or infrared light requires powerful laser sources which are more and more accessible. Another benefit of multiphoton processes at a full body scale is the penetration potency of red light through

[132] Dunn, A. R. et al. *J. Am. Chem. Soc.* **2003**, *125*, 12450–12456.
[133] Belliston-Bittner, W. et al. *J. Am. Chem. Soc.* **2005**, *127*, 15907–15915.
[134] Seymour, C. P. et al. *J. Org. Chem.* **2017**, *82*, 9647–9654.
[135] Parisi, C. et al. *ChemPhotoChem* **2020**, *4*, 742–748.
[136] Ieda, N. et al. *ACS Chem. Biol.* **2020**, *15*, 2958–2965.
[137] Perdicakis, B. et al. *Bioorg. Med. Chem.* **2005**, *13*, 47–57.

tissues, with respect to blue or UV light. Furthermore, multiphoton processes are non-linear, making focalization of a laser beam a very efficient way of exciting molecules in a very restrained volume (a cube with micrometric sides) while keeping a very high time resolution. Unfortunately, this spatial resolution is also the limitation of the technique. As a high photon flux is necessary to enable multiphoton processes, sustaining such a flux in a larger volume would require monstruous laser sources. Nonetheless, this strategy enables experiments with a very high spatial resolution as well as a very high time resolution.

A combination of these strategies took the shape of the first photoactivatable nanotrigger (NT), **NT1**[138,139]. As presented in **Scheme** 1.18, its structure is also very similar to NADPH, displaying the same binding site as the natural molecule.

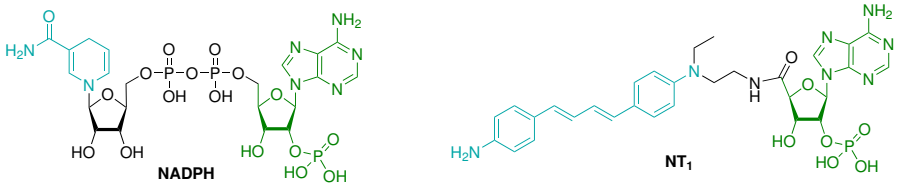

Scheme 1.18: Structure of the natural NADPH and NT_1 (electron donating group in dark cyan; docking moiety in green).

The electron transfer from **NT1** towards the FAD of a truncated eNOS reductase domain was shown to be successfully photoinitiated. The NT was also demonstrated to be an effective competitor of NADPH at the reductase binding site of eNOS, with a binding constant of around 7µM[140]. Additionally, irradiation of **NT1** in a solution of nNOS showed partial nitrosylation of the iron heme, involving a photinduced electron transfer from **NT1** at the reductase binding site. This NT was also capable of promoting the electron transfer to the FAD cofactor under two-photon illumination, pushing further the possibilities of photoinitiation of NADPH-driven enzymatic activities[141]. Nitric oxide photoproduction from the nanotrigger was then observed by cryotrapping the ferrous nitrosyl at 77K and performing an electron paramagnetic resonance spectroscopy (EPR) analysis[142]. As previously discussed, reductase domains with NADPH binding sites are commonly found in numerous enzymes. Despite displaying the same activity, different reductase sites can be slightly different in structure. Thus, **NT1** ability to photoinduce a catalytic activity in another reductase binding site was probed, the latter incarnated by dihydrofolate reductase (DHFR). Unlike eNOS, **NT1** was not able to photoinitate the DHFR catalysis, discriminating between the reductase binding sites of the two enzymes[143]. These results were supported by modeling experiments, which indicated that a precise positioning of the NT against the electron accepting moiety was necessary for an efficient electron transfer.

From these observations would stem the synthesis of a new generation of mimics, $\mathbf{NT}_{2-x}$,probing several synthetic modifications towards a better electron transfer of a more selective binding[144,145]. Interestingly, a good bioisostere for the phosphate moiety in 2' position found in NADPH and **NT1** was found, a more readily available carboxymethyl functionalization at position 3'[146]. The lat-

[138]Beaumont, E. et al. *Nitric Oxide* **2006**, *14*, 14–15.
[139]Robin, A.-C. et al. *Chem. Commun.* **2007**, 1334–1336.
[140]Beaumont, E. et al. *J. Am. Chem. Soc.* **2007**, *129*, 2178–2186.
[141]Beaumont, E. et al. *ChemPhysChem* **2008**, *9*, 2325–2331.
[142]Beaumont, E. et al. *ChemBioChem* **2009**, *10*, 690–701.
[143]Lambry, J.-C. et al. *J. Mol. Recognit.* **2010**, *23*, 379–388.
[144]Nguyen, N.-H. Synthèse de Nano-Déclencheurs Photo-Activables Pour Le Contrôle Spatio-Temporel de La Formation de NO, These de Doctorat, Ecole normale supérieure de Cachan, 2015.
[145]Nguyen, N.-H. et al. *Org. Biomol. Chem.* **2016**, *14*, 9519–9532.
[146]Chennoufi, R. et al. *Biochim. Biophys. Acta Gen. Subj.* **2019**, *1863*, 1127–1137.

ter was shown multiphotonic illumination of HUVECss incubated with several NTs, as shown on **Scheme** 1.19, displaying a clear pro-apoptotic effect exclusively for compounds functionalized in 3' position. In order to increase the selectivity towards NOSs, the methyl group could be replaced by an *anchor*, a structure exploiting the known structure of their reductase domain comparatively to other enzymes.

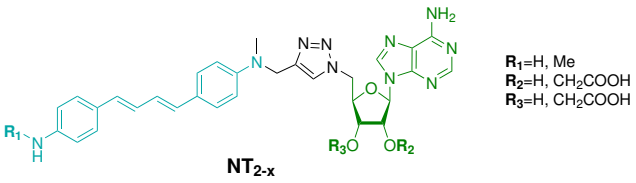

Scheme 1.19: Structure of the second generation of nanotriggers NT_{2-x}, designed towards photoactivation of NOS (electron-donating group in dark cyan; docking moiety in green).

The aim of the work presented hereafter constitutes a continuation of the search for more efficient and more selective mimics towards a better understanding of NOSs catalytic process. To that end, the targets presented in **Scheme** 1.20 bearing either an amide or thiourea linkage should enable an improved electron transfer efficiency towards the enzyme, as supported by modelisation, with respect to the previous nanotriggers linked by a triazole $\mathbf{NT}_{2-x}$.

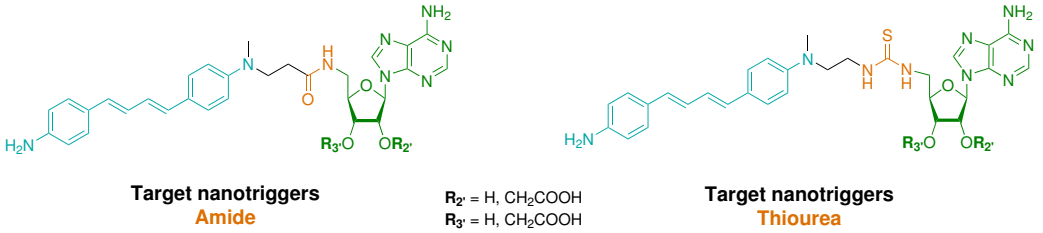

Scheme 1.20: Structure of the targets of this work, bearing an amide or thiourea linkage, designed towards photoactivation of NOS (electron-donating group in dark cyan; docking moiety in green; linkage in orange).

Chapter 2

Synthesis of photoactivatable NADPH mimics

Contents

2.1 Introduction

In addition to previous work[144], molecular dynamic modelisation results suggested that a triazole linkage was too rigid to allow the electron-donating moiety to properly face the FAD. Thus, the electron transfer from the nanotrigger towards the FAD could be improved *via* a more flexible linker, enabling a better overlap of the conjugated systems of the electron-donating diaryldiene and the FAD. Alongside this lead, a carboxymethyl functionalization in 3' position of the adenosine seemed to be a good bioisostere for the usual 2'-phosphate found in the natural NADPH[145,146]. Thus, targets described in **Scheme** 2.1 should be more efficient than the previous nanotriggers $\mathbf{NT}_{2-x}$, with an improved flexibility of the linker and a removed source of instability. The synthetic strategy towards the novel nanotriggers would be a convergent synthesis of the two distincts parts of the targets, the docking and the photoactivatable moieties, before a coupling step forming the desired linker.

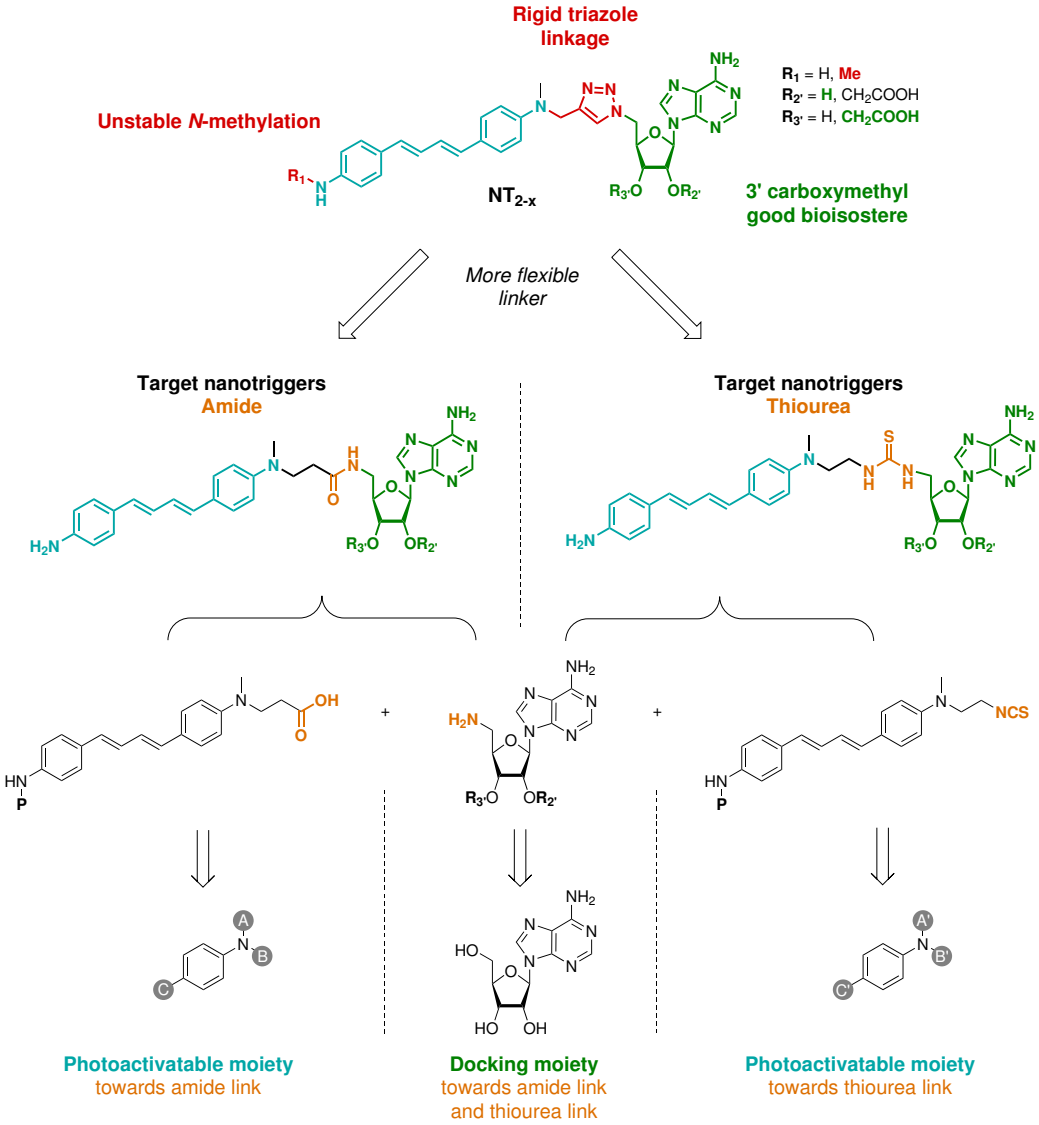

Scheme 2.1: General strategy towards the obtention of the desired target nanotriggers following insights from $\mathbf{NT}_{2-x}$.

The intermediates might need appropriate protecting groups in order to progress as planned along the synthetic pathway. The docking moiety should bear an amine at the 5' position of the adenosine towards the formation of the amide or the thiourea linker. The photoactivatable moiety

would be functionalized either with a carboxylic acid or an isothiocyanate respectively towards the formation of the amide bond or the thiourea linkage. Obtaining both functionalizations from a common intermediate would be interesting but the synthetic schemes would not be designed to that end, as it can be difficult to foresee the reactions outcome before performing them. The starting material for the docking part would be the commercially available adenosine and for the photoactivatable moiety it would be an arylamine derivative.

2.2 Synthesis of the docking moiety

2.2.1 Retrosynthesis

As stated previously, the most appealing structures for the docking moiety would be either a 2'-phosphate or a carboxymethyl functionalization at the 3' position, as well as a free amine at the 5' position. Carboxymethyl functionalization at the 2' or 2' and 3' positions would still be very valuable targets as well, as they would be used as controls in biological experiments.

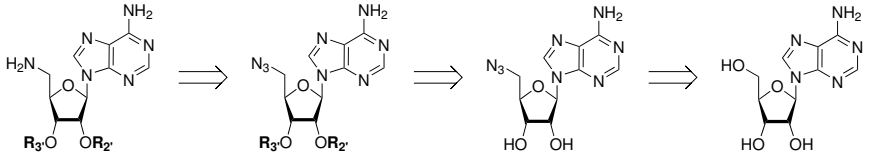

Scheme 2.2: Retrosynthetic scheme of the docking moieties starting from adenosine.

In order to obtain these adenosine derivatives, several important milestones appeared. The first one being the synthesis of the 5'-azido-5'-deoxyadenosine, before the regioselective functionalization of the 2' and 3' positions of the latter derivative or their separation, and finally introducing the 5'-amino functionality which could be readily used towards a coupling reaction with the photoactivatable moiety bearing an adequate functional group.

2.2.2 Synthesis of 5'-azido-5'-deoxyadenosine

First, positions 2' and 3' of the adenosine were protected by introducing a bridging isopropylidene, as shown in **Scheme** 2.3. Treating adenosine with an excess of triethyl orthoformate and *para*-toluenesulfonic acid (PTSA) in acetone would give compound **A-1** isolated in 87% yield. Following this protection, the remaining free hydroxy in 5' position was substituted with an azido group *via* a modified[147,148] Mitsunobu[149,150,151] reaction, using diphenylphosphoryl azide (DPPA) alongside triphenylphosphine and diisopropylazodicarboxylate (DIAD) in tetrahydrofuran (THF), with all respective ratios being one to one[152]. The desired compound was obtained with a decent 65% yield, but required tedious consecutives column chromatography over silica gel to get rid of the triphenylphosphine oxide (TPPO). The deprotection of the isopropylidene moiety was achieved in a mixture of water and trifluoroacetic acid (TFA) with a quantitative yield if the mixture was carefully evaporated at a temperature never rising above 20°C. A few more degrees and the yield would drop drastically, at around 50% for a temperature of 27°C. An explanation comes from the loss of the adenyl moiety in very acidic conditions but can be quite easily avoided. This procedure gave the desired 5'-azido-5'-deoxyadenosine with a yield of 60% over 3 steps.

[147] Overman, L. E.; Paone, D. V. *J. Am. Chem. Soc.* **2001**, *123*, 9465–9467.
[148] Lal, B. et al. *Tetrahedron Lett.* **1977**, *18*, 1977–1980.
[149] Mitsunobu, O. et al. *J. Org. Chem.* **1965**, *30*, 1071–1073.
[150] Mitsunobu, O.; Yamada, M. *BCSJ* **1967**, *40*, 2380–2382.
[151] Mitsunobu, O. et al. *BCSJ* **1967**, *40*, 935–939.
[152] Comstock, L. R.; Rajski, S. R. *Tetrahedron* **2002**, *58*, 6019–6026.

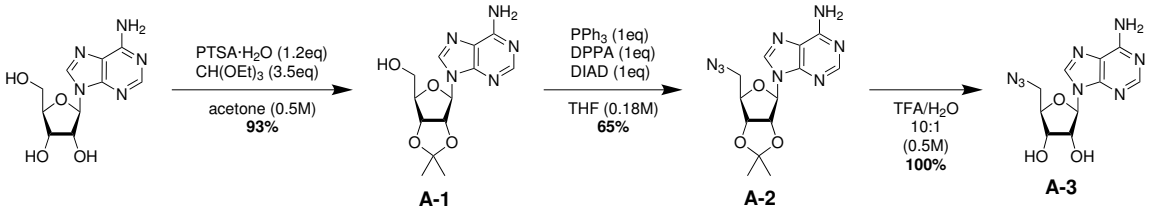

Scheme 2.3: Synthetic pathway towards 5'-azido-5'-deoxyadenosine *via* a modified Mitsunobu reaction[152].

According to a recent review[153], despite being one of the broadest and most useful tool an organic chemist can use, especially near the end of a synthesis, the Mitsunobu reaction suffers from non-negligible drawbacks. The stoechiometric amount of triphenylphosphine and azodicarboxylate is costly, and additionnally the final separation of the triphenylphosphosphine oxide from the desired product can be quite challenging.

In order to prevent the solvent and silica waste due to the several consecutive purifications needed to remove the TPPO, a selective precipitation of the latter by complexation with $ZnCl_2$ solubilized in warm ethanol[154] was tested out. Unfortunately, the desired compound **A-2** showed to have a similar affinity towards Zn^{2+} ions, according to the ^{1}H NMR spectra of the filtrate and precipitate which were both roughly the same mixture of adenosine derivative and TPPO. However that outcome was to be expected, as stated in the reference, because of the aromatic amine in the adenyl moiety. Another subtle approach was given a try, using a postulated difference of solubility of TPPO[155] and the desired adenosine derivative **A-2**. The crude residue of the Mitsunobu reaction was dissolved in ethyl acetate (AcOEt) then petroleum ether (PE) was added, and the proportion of the two compounds in solution was followed by thin layer chromatography (TLC) for AcOEt/PE ratios from 1:1 to 1:50. Once more, the relative proportion of both molecules did not sensibly change, thus was not useful towards improving the later purification over silica gel of the crude mixture.

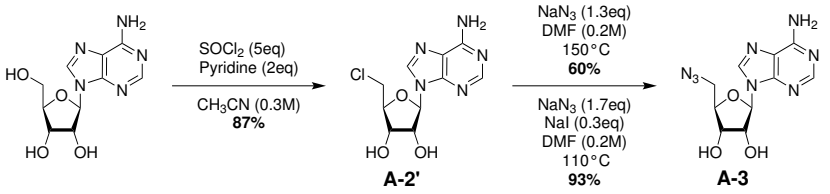

Scheme 2.4: Synthetic pathway towards 5'-azido-5'-deoxyadenosine *via* a Darzens halogenation followed by a second order nucleophilic substitution (S_N2) using an azide anion.

Another synthetic route was preferred, as shown on **Scheme** 2.4, involving a more recent procedure[156] of a Darzens' halogenation[157]. By using an excess of thionyl chloride and pyridine in acetonitrile (MeCN), adenosine was converted to 5'-chloro-5'-deoxyadenosine with 82% yield. The latter halogenated compound could undergo a S_N2 with an azide anion[158], giving the desired 5'-azido-5'-deoxyadenosine in 60% yield at a temperature of 150°C, or 93% yield at 110°C using 30mol% of sodium iodide. This 2 steps procedure gave the desired 5'-azido-5'-deoxyadenosine with an overall 81% yield. In addition to improving the yield, the purification of the final compound was much easier, leading to quite a lot of time saved over the course of several syntheses.

[153]Beddoe, R. H. et al. *Org. Biomol. Chem.* **2018**, *16*, 7774–7781.
[154]Batesky, D. C. et al. *J. Org. Chem.* **2017**, *82*, 9931–9936.
[155]Hu, F.-H. et al. *J. Chem. Eng. Data* **2009**, *54*, 1382–1384.
[156]Sun, H. et al. *Angew. Chem. Int. Ed.* **2016**, *55*, 14277–14280.
[157]Darzens, A. G. *C. r. hebd. séances Acad. sci.* **1911**, *152*, 1601–1603.
[158]Peterson, M. A. et al. *Bioorganic Med. Chem. Lett.* **2009**, *19*, 6775–6779.

Surprisingly, the addition of sodium iodide while keeping the temperature at 150°C would lead to a decrease in yield. A temperature decrease towards 110°C was necessary to see a substantial increase in yield. These observations could indicate a side reaction involving the secondary alcohols.

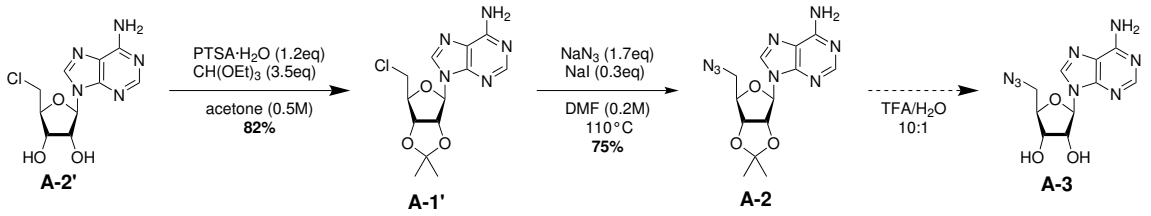

Scheme 2.5: Alternative pathway towards 5'-azido-5'-deoxyadenosine *via* Darzens halogenation followed by S_N2 with an intermediate isopropylidene protection.

Another pathway was investigated before the previous optimised S_N2 conditions were found. In order to prevent degradation, an intermediate isopropylidene protection was inserted in the pathway, alongside the according deprotection as a last step, as shown in **Scheme** 2.5. The protection of the chlorinated compound gave **A-1'** with a slightly decreased yield compared to the previous synthesis of **A-1**. The increased solubility of the chlorinated compound in AcOEt during the washing step could explain a decreased recovery of **A-1'** *versus* **A-1**. This pathway was not interesting anymore when even the optimised S_N2 conditions gave lower yield on **A-1'** than on the unprotected derivative **A-2'**. The additional steps and lower yields were of no use in this synthesis.

2.2.3 Synthesis of functionalized 5'-amino-5'-deoxyadenosines

2.2.3.1 *O*-alkylation

After the introduction of the azide on the 5' position, the remaining nucleophilic groups in **A-3** were the hydroxyl groups at positions 2' and 3' and the lesser nucleophilic amine within the adenine moiety due to its lone pair delocalization. This intermediate should be easily *O*-alkylated at these positions without making the *N*-alkylation an issue[145].

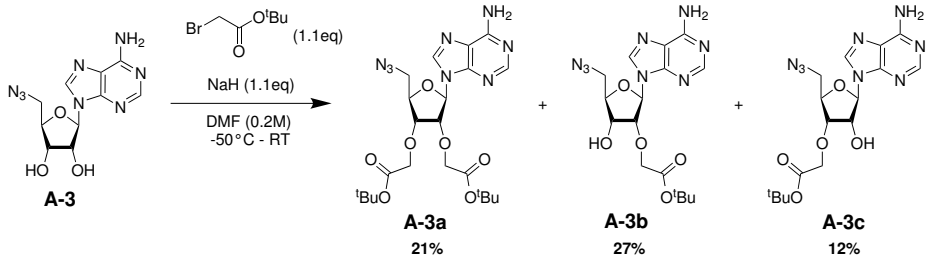

Scheme 2.6: Reaction conditions for the formation of 2' and/or 3' carboxymethyl *tert*-butyl ester *O*-alkylated 5'-azido-5'-deoxyadenosine.

The *O*-alkylation of the latter hydroxyl groups, as shown on **Scheme** 2.6, using sodium hydride and *tert*-butyl bromoacetate in *N,N*-dimethylformamide (DMF) at very low temperature would convert 60% of the starting adenosine towards the 3 possible *O*-alkylated products, and only traces of the *N*-alkylated ones which were not isolated. Despite the three compounds having very close retention factors, they could be purified without many troubles over silica gel using a very slow slope of gradient elution. The resulting mixture composition would depend on the scale of the reaction, and the highest conversion would be observed for an input of around 1g of **A-3**.

Appropriately, towards the desired amide or thiourea linkages in the final nanotriggers, an amine group at the 5' position of the adenosine moiety would allow its use towards both linkers and could be readily available through a single additional reduction step.

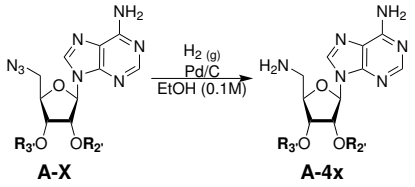

Scheme 2.7: Reaction conditions for the reduction of azide into amine using palladium on carbon and dihydrogen.

Azide	$R_{2'}$	$R_{3'}$	Amine A-4x	Yield
A-3	-H	-H	**A-4**	90%
A-3a	$-CH_2COO^tBu$	$-CH_2COO^tBu$	**A-4a**	90%
A-3b	$-CH_2COO^tBu$	-H	**A-4b**	82%
A-3c	-H	$-CH_2COO^tBu$	**A-4c**	31%
A-2	$-C(CH_3)_2-$		**A-4i**	99%

Table 2.1: Summary of the Pd/C reductions under H_2 atmosphere on the previously isolated *O*-alkylated 5'-azido-5'-deoxyadenosines.

The azide reduction using palladium on carbon under a dihydrogen atmosphere[159,160,161] in ethanol (EtOH) shown on **Scheme** 2.7 would give decent yields on all *O*-alkylated 5'-azido-5'-deoxyazidoadenosines except **A-3c**, see the yields summarized in **Table** 2.1. These compounds were quite surprisingly difficult to recover after filtration of the Pd/C on silica or Celite®, most likely because of the high polarity of the compounds. Methanol (MeOH) would solubilize silica and was therefore avoided.

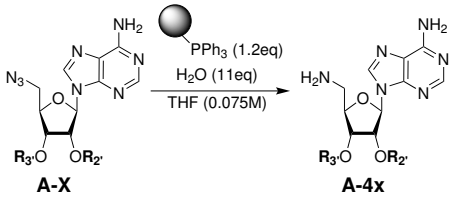

Scheme 2.8: Reaction conditions for the Staudinger reduction of the azide into amine.

Azide	$R_{2'}$	$R_{3'}$	Amine A-4x	Yield
A-3	-H	-H	**A-4**	19%
A-3a	$-CH_2COO^tBu$	$-CH_2COO^tBu$	**A-4a**	100%
A-3b	$-CH_2COO^tBu$	-H	**A-4b**	100%
A-3c	-H	$-CH_2COO^tBu$	**A-4c**	85%

Table 2.2: Summary of the azides reduction *via* a Staudinger reaction on the previously isolated *O*-alkylated 5'-azido-5'-deoxyadenosines.

[159] Bertho, A.; Maier, J. *Liebigs Ann.* **1932**, *498*, 50–61.
[160] Wang, T. et al. *Bioorganic Med. Chem. Lett.* **2007**, *17*, 4456–4459.
[161] Zhang, G. et al. *Org. Biomol. Chem.* **2015**, *13*, 4149–4154.

Another strategy was carried out, as shown on **Scheme** 2.8, performing a Staudinger reaction[162] with supported triphenylphoshine[163] in presence of water in THF. These conditions allowed a very simple recovery of the amine by filtration over filter paper. The yields obtained for all the *O*-alkylated compounds would substantially increase, as shown in **Table** 2.2. Oddly, the non-substituted compound **A-3** could not be efficiently reduced in these conditions. Moreover, as this method would require more time because of the heterogenous phosphine, the reduction of **A-3c** would start to show some degradation hints on TLC after a few days, possibly because of an intramolecular side reaction forming the ε-lactame, hypothesis that was left unverified. Thus, this reduction was stopped slightly before completion as seen on TLC, eventhough nuclear magnetic resonance (NMR) experiments would not show traces of the starting azide (meaning less than 5% in amount of substance).

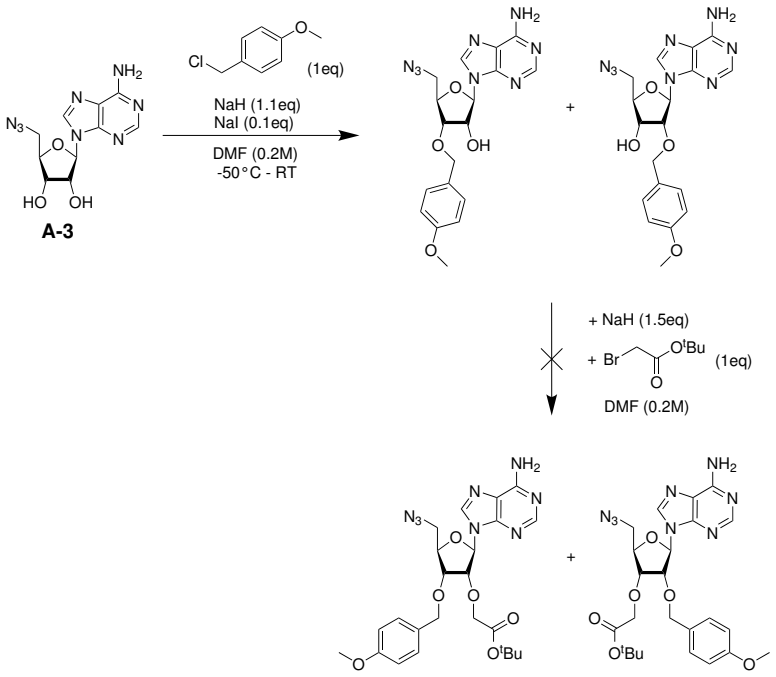

Scheme 2.9: Alternative pathway involving a *para*-methoxybenzene protection on the free hydroxy groups.

The free hydroxyl groups on the mono *O*-alkylated adenosines **A-3b** and **A-3c** might lead to side reactions at later stages of the synthesis. A strategic protection in the same step as the *O*-alkylations was tested out with *para*-methoxybenzene chloride, which was expected to be quite similar in reactivity with respect to *tert*-butylbromoacetate. Unfortunately, as shown on **Scheme** 2.9, the carboxymethyl *tert*-butyl ester could not be introduced afterwards, most likely because of an increased steric hindrance.

2.2.3.2 Phosphorylation tryouts

In spite of the carboxymethyl functionalization at the 3' position being a good bioisostere of the 2' phosphate as previously stated and described[145,146], those were empirical results and not easily understandable. Thus, being able to obtain and compare the nanotriggers bearing either a phosphate or a carboxymethyl group on their docking moieties would be of great interest. The 2' and 3' phosphorylated adenosines were previously[144] obtained through formation of the cyclic phosphate bridging the two positions, before enzymatic opening of the phosphodiester. Opening

[162] Staudinger, H.; Meyer, J. *Helv. Chim. Acta* **1919**, *2*, 635–646.
[163] Xie, J. *Eur. J. Org. Chem.* **2002**, *2002*, 3411–3418.

with ribonuclease T2[164] would give the 3' phosphate and snake venom phosphodiesterase[165,166] the 2' phosphate. Hereafter the aim was to get access to these phosphorylated compounds *via* a more classical chemical pathway.

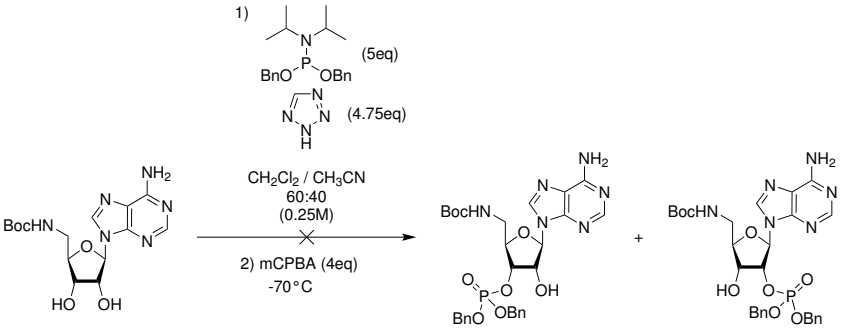

Scheme 2.10: Phosphorylation tryout using diisopropyldibenzylphosphoramidite, 1*H*-tetrazole before a low temperature oxidation with *meta*-chloroperbenzoic acid.

A phosphorylation tryout[167] was carried out on an available Boc protected 5'-amino-5'-deoxy-adenosine using 1*H*-tetrazole and dibenzyloxy diisopropylaminophosphine in a mixture of dichloromethane (DCM) and MeCN before a low temperature oxidation with *meta*-chloroperoxybenzoic acid (mCPBA), as shown on **Scheme** 2.10, but none of the regioisomer could be observed by TLC nor isolated.

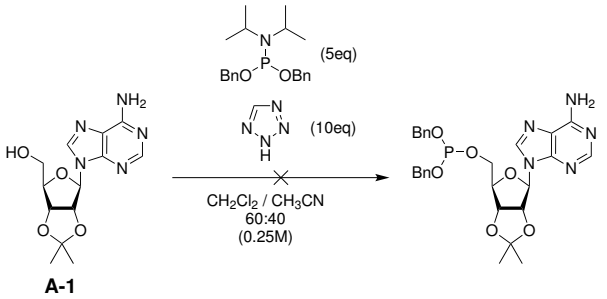

Scheme 2.11: Phosphorylation tryout on a described reaction to check the 1*H*-tetrazole solution.

In order to verify that the previous phosphorylation failure was not because of a degraded reagent, a described[167] phosphorylation of the primary alcohol at the 5' position of **A-1** was performed, as shown on **Scheme** 2.11. Yet again, the reaction did not show formation of a new product, implying that at least one of the reagent was degraded. Some ^{1}H and ^{31}P NMR spectra cleared the phosphoramidite, leaving the sensitive 1*H*-tetrazole solution as the most likely degraded reagent.

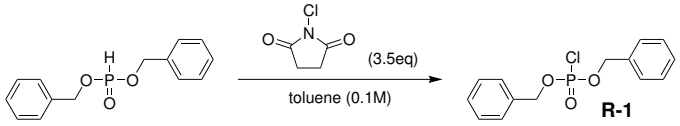

Scheme 2.12: Synthesis of dibenzyl chlorophosphonate, a reactive phosphorylating agent.

[164] Uchida, T.; Egami, F. *J. Biochem* **1967**, *61*, 44–53.
[165] Uzawa, S. *J. Biochem* **1932**, *15*, 1–10.
[166] Fox, J. W. *Toxicon* **2013**, *62*, 75–82.
[167] Borio, A. et al. *Tetrahedron Lett.* **2017**, *58*, 2826–2829.

Some other promising procedures required a sensitive phosphorylating reagent that could be readily synthesized from available chemicals[168], as shown on **Scheme** 2.12. The desired dibenzyl chlorophosphonate **R-1** was successfully obtained after stirring dibenzyl phosphite with an excess of *N*-chlorosuccinimide (NCS) overnight under an inert atmosphere. The conversion was controlled by ^{31}P NMR as detailed in **Appendix B.1**. The transformation lead to a clean compound but the latter would be degraded overnight even if carefully placed in a fridge and under inert atmosphere.

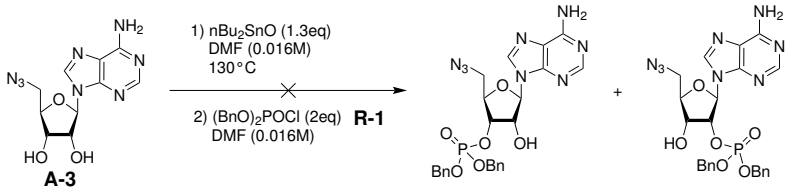

Scheme 2.13: Phosphorylation tryout *via* an organotin.

A well known phosphorylation reaction on nucleosides[169,114] was carried out, as shown on **Scheme** 2.13. This transformation was tried on **A-3** but could not give access to the desired phosphorylated compounds. The formation in the first step of the cyclic organotin intermediate bridging the 2' and 3' positions could not be observed by TLC, which was expected because of its degradation over silica. The second step was nevertheless carried out, but no change would be observed by TLC and NMR experiments confirmed the only presence of the starting material after the work-up of the crude. This would not be troublesome, because introducing a step involving an organotin in the convergent synthesis of a bioactive molecule was not very attractive, as tin is quite difficult to get rid of. It could still have been useful to have a reference towards phosphorylation tryouts, for TLC and NMR references.

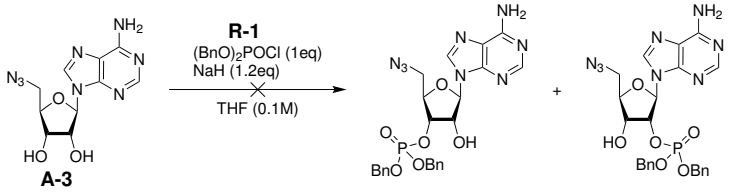

Scheme 2.14: Phosphorylation tryout involving dibenzylphoryl chloride and sodium hydride.

A last procedure[170] was performed, as shown on **Scheme** 2.14, involving a straightforward phosphorylation with sodium hydride and the previously obtained dibenzyl chlorophosphonate. The reaction should give acceptable yields on primary alcohols but did not show any progress by TLC on our 2' and 3' secondary alcohols.

The desired docking moieties of the nanotriggers bearing a carboxymethyl bioisostere were successfully obtained, but their phosphate counterparts could not be synthesized. Molecular dynamics experiments[171] confirmed at that moment that the analogs bearing a carboxymethyl group at position 3' would interact in a very similar fashion with the reductase binding domain of eNOS with respect to the natural phosphate group at position 2'. This hypothesis was already observed[146] but could not yet find a thorough explanation. In fact, the flexible $-CH_2-$ would enable the 3' negatively charged carboxylate at a physiological pH to interact with the positively

[168] Lehar, S. M. et al. *Nature* **2015**, *527*, 323–328.
[169] Wagner, D. et al. *J. Org. Chem.* **1974**, *39*, 24–30.
[170] Wei, W.-C.; Chang, C.-C. *Eur. J. Org. Chem.* **2017**, *2017*, 3033–3040.
[171] Dilly, S. et al. *Antioxidants* **2020**, *9*, 89.

charged arginines R1165 and R1049 as presented in **Figure** 2.15, with electrostatic stabilization energies in the same range as a 2' phosphate group has. The photoactivatable moiety would also be more planar and correctly facing the FAD, easing the primary electron transfer by π-stacking. The easier synthetic route added to the molecular modeling results would make the carboxymethyl functionalized nanotriggers the primary targets of this work.

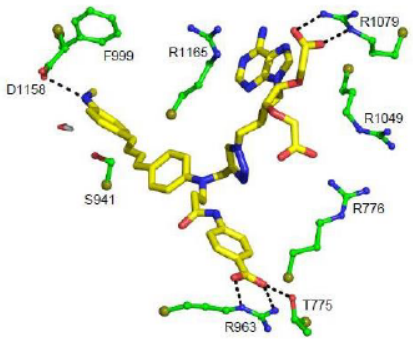

Scheme 2.15: Interaction of residues within the reductase domain of eNOS with a previous nanotrigger *O*-alkylated at positions 2' and 3' bearing an *anchor*[171].

2.3 Synthesis of the photoactivatable moiety towards an amide linker

2.3.1 Three carbons amide linkage

2.3.1.1 Retrosynthesis

As stated previously, the strategy to get the nanotriggers would be to proceed to a mild and simple coupling reaction between the different moieties prepared accordingly. In order to obtain an amide linker, the most straightforward retrosynthetic pathway would be the simple peptidic coupling between an amine at the 5' position of a functionalized adenosine and the photoactivatable moiety bearing a carboxylic acid at the end of its three carbons linker, as shown on **Scheme** 2.16.

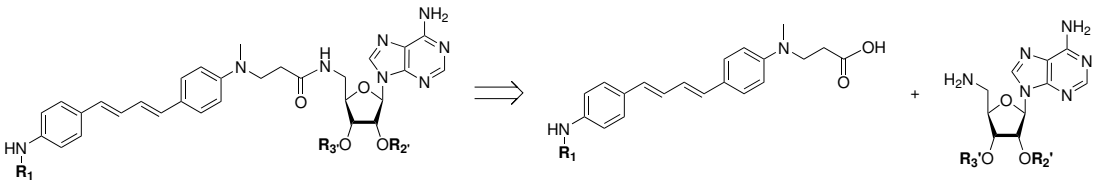

Scheme 2.16: Easiest retrosynthetic pathway towards the nanotriggers bearing an amide linker.

One of the major challenges arising through this pathway would be the formation of the diaryldiene moiety by a Horner-Wadsworth-Emmons olefination. As shown by previous work[144], the reaction between a protected diethyl-4-aminobenzylphosphonate and an α,β-insaturated aldehyde bearing an ethyl ester in presence of sodium hydride would lead only to a degradation of the starting material, as shown in **Scheme** 2.17. The ester functional group seemed to be responsible, as the reaction would proceed as intended if the latter was replaced with a methyl group.

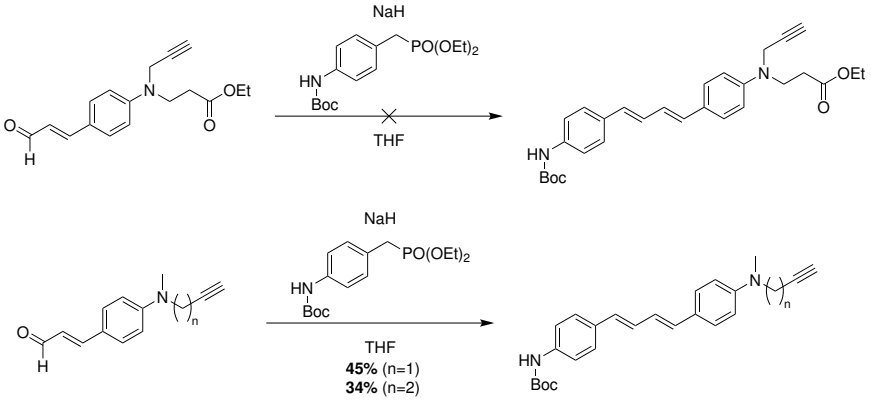

Scheme 2.17: Horner-Wadsworth-Emmons olefination on different substrates in previous work.

A way around the issue could be to form the amide linkage between the adenosine moiety and the α,β-insaturated aldehyde first, followed by the Horner-Wadsworth-Emmons coupling, as presented in **Scheme** 2.18. An advantage of this pathway would be the versatility of the functionalization of the adenosine: At every step the functional groups $\mathbf{R}_{2'}$ and $\mathbf{R}_{3'}$ could represent either a protective bridging isopropylidene (*via* **A-4i**) or the desired functionality (*via* **A-4**, **A-4a**, **A-4b** or **A-4c**). On the one hand, functionalization before the coupling would be the most efficient, to prevent additionnal steps on highly transformed, thus precious compounds. On the other hand, the presence of free hydroxyl groups (in **A-4**, **A-4b** and **A-4c**) was expected to rise side reactions issues, and a later functionalization would bypass this problem.

The cinnamaldehyde would be synthesized as described in **Scheme** 2.19 starting from *N*-methylaniline. The latter would undergo a Michael's addition with ethyl acrylate, before proceeding to

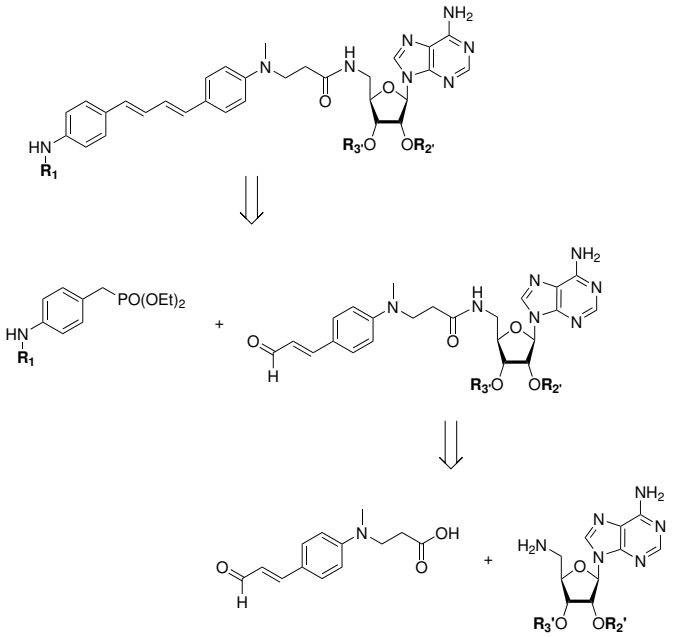

Scheme 2.18: Retrosynthetic scheme of the three carbons amide linkage nanotriggers.

a Vilsmeier's formylation and extending the conjugated system with a Wittig reaction. Lastly, the ethyl ester would be deprotected in a saponification reaction to give the desired α,β-insaturated aldehyde ready for peptidic coupling.

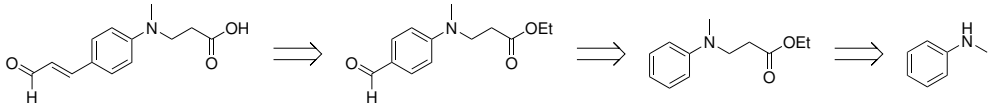

Scheme 2.19: Retrosynthetic scheme of the photoactivatable moiety towards three carbons amide linkage starting from commercially available *N*-methyl anilline.

2.3.1.2 Michael's addition

The first step towards the synthesis of the cinnamaldehyde was a solvent free Michael's addition[172,173,174], as shown in **Scheme** 2.20.

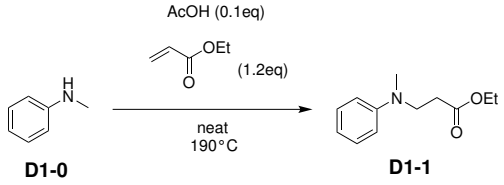

Scheme 2.20: Reaction conditions of the Michael's addition of ethyl acrylate on *N*-methyl anilline.

A slight excess of ethyl acrylate was added to *N*-methylaniline in presence of a catalytic amount of acetic acid, and upon heating to 190°C overnight the mixture would be worked up. The crude residue was a mixture of the desired compound **D1-1** and *N*-methylaniline in a 6 to 1 ratio, as well as a small remainder of ethyl acrylate. The mixture would be used without further purification in the next step.

[172]Komnenos, T. *Liebigs Ann.* **1883**, *218*, 145–167.
[173]Michael, A. *J. prakt. Chem.* **1887**, *35*, 349–356.
[174]Tokoroyama, T. *Eur. J. Org. Chem.* **2010**, *2010*, 2009–2016.

2.3.1.3 Vilsmeier's formylation

The next step would be the Vilsmeier's formylation[175,176] of the previously obtained Michael adduct, as shown in **Scheme** 2.21.

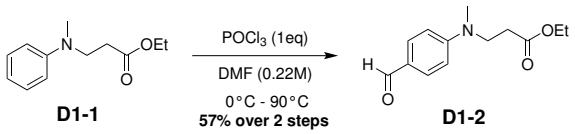

Scheme 2.21: Reaction conditions of the Vilsmeier's formylation.

Vilsmeier's reagent was carefully formed by dropwise addition of phosphoryl chloride to ice-cold DMF, before addition of **D1-1** at room temperature and heating at 90°C overnight. After neutralization and extraction, the crude residue was purified over silica gel to afford **D1-2** with a decent yield of 57% over two steps.

2.3.1.4 Extension of the conjugated system by Wittig's olefination

The cinnamaldehyde **D1-3** would be obtained through a two-step procedure, as shown in **Scheme** 2.22. A Wittig's reaction[177,178] would give the desired compound as its protected acetal[179], before the latter was cleaved in acidic conditions to recover the desired α,β-insaturated aldehyde **D1-3**.

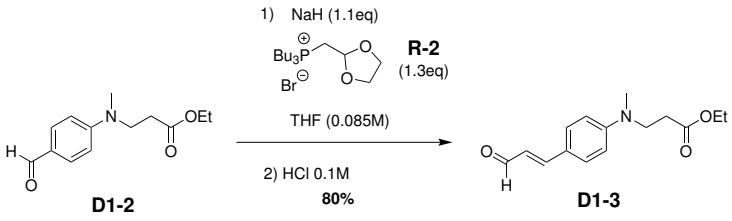

Scheme 2.22: Reaction conditions of the Wittig's transformation and acidic hydrolysis of the acetal.

A complete *trans* stereoselective olefination would be of great interest in order to maximize the yield towards the desired *E* olefin and avoid a potentially difficult purification. Various stereoselective Wittig's transformations were developped[180], and such a variant by Tamura[181,182] using tributylphosphorus ylides could achieve such an excess of *E* isomer (> 95%) that the *Z* olefin was not quantifyable by ^{1}H NMR or gas-liquid partition chromatography (GLPC). The straightforward solventless synthesis of the phosphonium bromide **R-2** (see Experimental Section) enabled the Wittig's olefination with the previously obtained benzaldehyde **D1-2** to give the desired *E* olefin **D1-3** in 80% yield over two steps. The reaction gave a non-isolated intermediate acetal before acidic cleavage with hydrochloric acid and exclusive recovery of the *trans* α,β-insaturated aldehyde. As expected, no traces of the *Z* isomer were detected by ^{1}H NMR experiments. More details are discussed in **Appendix B.2**.

[175] Fischer, O. et al. *J. prakt. Chem.* **1925**, *109*, 69–87.
[176] Vilsmeier, A.; Haack, A. *Ber. Dtsch. Chem. Ges.* **1927**, *60*, 119–122.
[177] Wittig, G.; Geissler, G. *Liebigs Ann.* **1953**, *580*, 44–57.
[178] Wittig, G.; Schöllkopf, U. *Chem. Ber.* **1954**, *87*, 1318–1330.
[179] Spangler, C. W.; McCoy, R. K. *Synth. Commun.* **1988**, *18*, 51–59.
[180] Gu, Y.; Tian, S.-K. In *Stereoselective Alkene Synthesis*, Wang, J., Ed.; Topics in Current Chemistry; Springer: Berlin, Heidelberg, 2012, pp 197–238.
[181] Tamura, R. et al. *J. Org. Chem.* **1987**, *52*, 4121–4124.
[182] Tamura, R. et al. *J. Org. Chem.* **1988**, *53*, 2723–2728.

2.3.1.5 Amide bond formation

A cleavage of the ethyl ester would be needed in order perform the coupling with an amine.

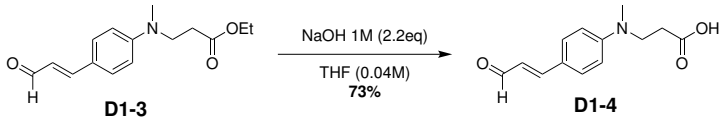

Scheme 2.23: Deprotection of the ethyl ester towards a carboxylic acid

The ester linkage was hydrolysed in basic conditions using aqueous sodium hydroxide in THF. Upon acidification at a pH of 2, an extraction gave the desired carboxylic acid **D1-4** with a yield of 73%.

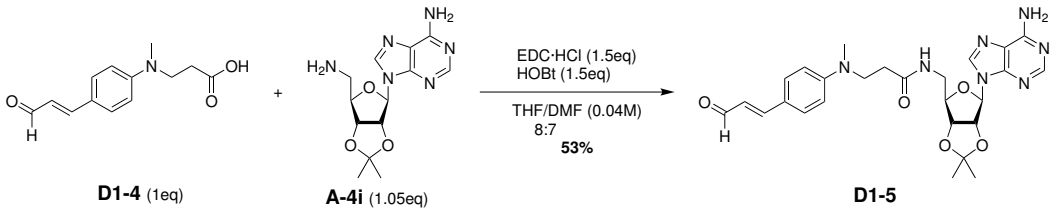

Scheme 2.24: Synthesis of the α,β-insaturated aldehyde linked *via* an amide bond to the protected docking moiety.

The formation of the three carbons amide linkage between the α,β-insaturated aldehyde **D1-4** and the isopropylidene-protected adenosine moiety **A-4i** was achieved with a 53% yield in presence of 1-ethyl-3-(3-dimethylaminopropyl)carbodiimide hydrochloride (EDC·HCl) and hydroxybenzotriazole (HOBt). The latter compound could now be tested in a Horner-Wadsworth-Emmons (HWE) olefination.

2.3.1.6 Horner-Wadsworth-Emmons olefination

The reaction known as the Horner-Wadsworth-Emmons olefination stems from modifications of the Wittig reaction. Horner used diphenylphosphine oxides to obtain olefins from aldehydes or ketones[183,184] and a few years later Wadsworth and Emmons showed that replacing the phenyl groups by *O*-alkyl groups could improve many aspects of the olefination[185,186], mainly the reactivity, stereoselectivity and purification. Additional details are presented in **Appendix B.3**.

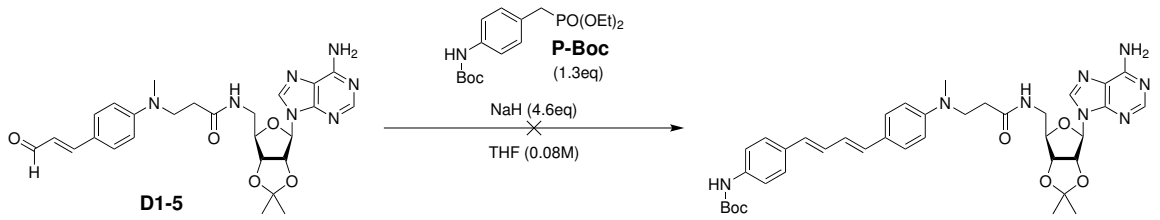

Scheme 2.25: Horner-Wadsworth-Emmons olefination tryouts with diethyl 4-benzoylamino-benzylphosphonate and sodium hydride.

[183] Horner, L. et al. *Chem. Ber.* **1958**, *91*, 61–63.
[184] Horner, L. et al. *Chem. Ber.* **1959**, *92*, 2499–2505.
[185] Wadsworth, W. S.; Emmons, W. D. *J. Am. Chem. Soc.* **1961**, *83*, 1733–1738.
[186] Wadsworth, D. H. et al. *J. Org. Chem.* **1965**, *30*, 680–685.

The tryouts of HWE olefination on **D1-5** would not give a more favorable outcome than the one discussed earlier, as shown in **Scheme** 2.25. The starting **D1-5** would disappear from the mixture as followed by TLC and seemed to undergo degradation, possibly because of retro-Michael's reaction. To avoid the latter side reaction, a new linker bearing two carbons would be targeted towards the synthesis of the nanotriggers, as it should not undergo this kind of degradation.

2.3.2 Two carbons amide linkage

2.3.2.1 Retrosynthesis

Following the previous insights on the synthesis of three carbons amide linkage nanotriggers, the next targets would be bearing a two carbons linkage in order to avoid the postulated retro-Michael's reaction. As already described[144,171], some further functionalization $\mathbf{R}_4$ on the nitrogen, named *hook* or *anchor*, can improve the selectivity towards binding the reductase domain of eNOS compared to iNOS or nNOS. The synthetic pathway was changed accordingly in order to enable a more versatile synthesis of the methyl or hook bearing nanotriggers, as shown on **Scheme** 2.26, depending on the step the $\mathbf{R}_4$ functionality could be introduced. The final reaction would still be an amide bond formation by peptidic coupling before deprotection.

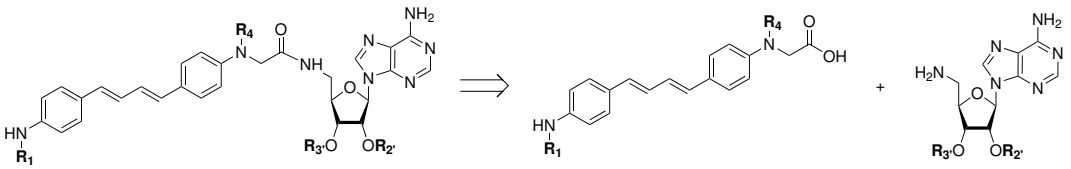

Scheme 2.26: Retrosynthetic scheme of the two carbons amide linked nanotriggers.

The photoactivatable moiety would be synthesized starting from the commercially available 4-vinylaniline, as shown in **Scheme** 2.27. The latter would be *N*-alkylated and its amine protected, before formation of the complete diaryldiene moiety by successive Wittig and HWE olefinations after alkene cleavage. The ethyl ester would then be cleaved in order to react it with the desired functionalized 5'-aminoadenosines.

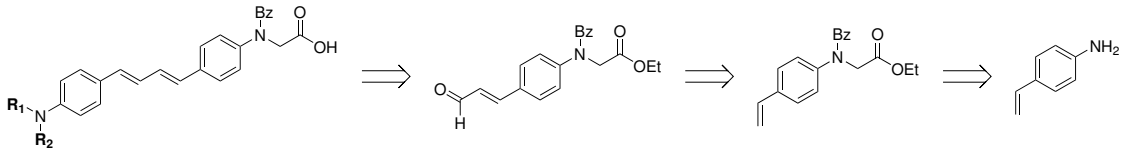

Scheme 2.27: Retrosynthetic scheme of the photoactivatable moiety towards two carbons amide linkage starting from 4-vinylanilline.

2.3.2.2 *N*-alkylation

In the first steps, the aim would be to introduce a functional group bearing the ethyl ester that will be used to form the amide linkage and at the same time introduce a protection on the last position of the arylamine. The absence of any acidic protons on the amine could prove helpful towards the later HWE olefination which requires a strong base such as NaH. In these conditions the increased nucleophilicity of the deprotonated amine could lead to side reactions on the aldehyde or the ester and must be avoided.

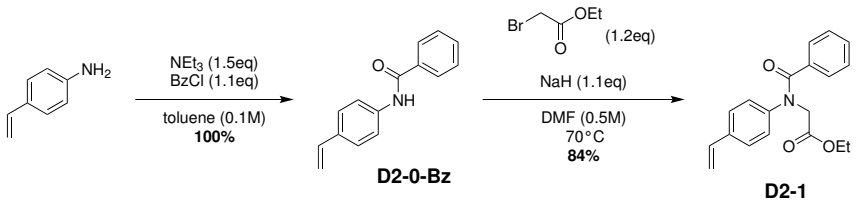

Scheme 2.28: Reaction conditions for the preparation of ethyl *N*-benzoyl-*N*-(4-vinylphenyl)-2-aminoethanoate.

A benzoyl protecting group was introduced quantitatively *via* a Schotten-Baumann[187,188] reaction in toluene, using a slight excess of benzoyl chloride in presence of triethylamine, as shown on **Scheme** 2.28. The obtained compound would undergo *N*-alkylation with a small excess of sodium hydride and ethyl bromoacetate in DMF while heated at 70°C. The desired compound fully substituted on the nitrogen **D2-1** was obtained with a 84% yield after purification by column chromatography.

2.3.2.3 Upjohn dihydroxylation and Lemieux-Johnson oxidation

A preparation step towards the extension of the conjugated system was a two step oxidative cleavage of the alkene group. Osmium-mediated hydroxylations are known for decades to be efficient[189] and many very useful developments towards racemic[190] or asymmetric[191,192] synthesis were developped. In our case, a simple Upjohn dihydroxylation[193] would give a vicinal diol, which could be cleaved by a Lemieux-Johnson oxidation[194] to give the desired aldehyde **D2-2**, as shown on **Scheme** 2.29.

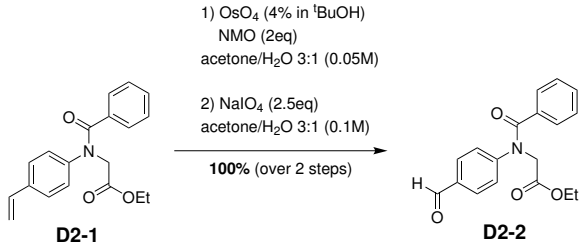

Scheme 2.29: Upjohn dihydroxylation followed by a Lemieux-Johnson oxidation on the *N*-benzoyl-*N*-alkyl-4-vinylanilline.

After addition of a few drops of osmium tetroxide in *tert*-butanol and two equivalents of *N*-methylmorpholine *N*-oxide (NMO) in a water/acetone solution of compound **D2-1**, it would be quantitatively dihydroxylated as monitored by TLC. Then acetone was removed under reduced pressure and a saturated sodium thiosulfate solution was added in order to neutralize OsO_4 before extracting the solution. The crude residue would be dissolved again in a water/acetone mixture before addition of an excess of sodium periodate and converted to the desired benzaldehyde **D2-2** with a quantitative yield.

[187] Schotten, C. *Ber. Dtsch. Chem. Ges.* **1884**, *17*, 2544–2547.
[188] Baumann, E. *Ber. Dtsch. Chem. Ges.* **1886**, *19*, 3218–3222.
[189] Milas, N. A.; Sussman, S. *J. Am. Chem. Soc.* **1936**, *58*, 1302–1304.
[190] Eames, J. et al. *J. Chem. Soc., Perkin trans. 1* **1999**, 1095–1104.
[191] Jacobsen, E. N. et al. *J. Am. Chem. Soc.* **1988**, *110*, 1968–1970.
[192] Sharpless, K. B. et al. *J. Org. Chem.* **1992**, *57*, 2768–2771.
[193] VanRheenen, V. et al. *Tetrahedron Lett.* **1976**, *17*, 1973–1976.
[194] Pappo, R. et al. *J. Org. Chem.* **1956**, *21*, 478–479.

2.3.2.4 Extension of the conjugated system by Wittig's olefination

A Wittig reaction was carried out in the same conditions as previously described[179], as shown on **Scheme** 2.30.

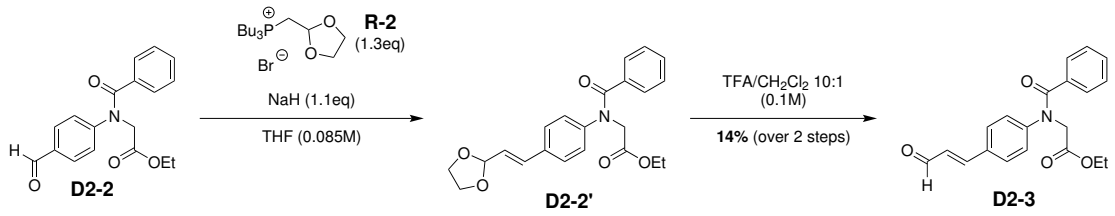

Scheme 2.30: Formation of the α,β insaturated aldehyde *via* a Wittig's reaction and acetal deprotection using TFA.

The acetal formed was removed before the column chromatography in order to increase the polarity difference between the stoechiometric phosphine oxide produced in the Wittig step and the desired α,β-insaturated aldehyde **D2-3**, improving the separation efficiency. The cleavage of the acetal moiety using TFA was very fast but too acidic to be able to proceed without cleaving the ethyl ester as well, leading to a very low yield of 14%. The amount of **D2-3** recovered would still be enough to test the feasibility of the next HWE olefination step.

2.3.2.5 Horner-Wadsworth-Emmons olefination

The HWE olefination step was the limiting step towards the obtention of the nanotriggers, and as such several more phosphonates were synthesized, as shown on **Scheme** 2.31 (see Eperimental Section for the procedures).

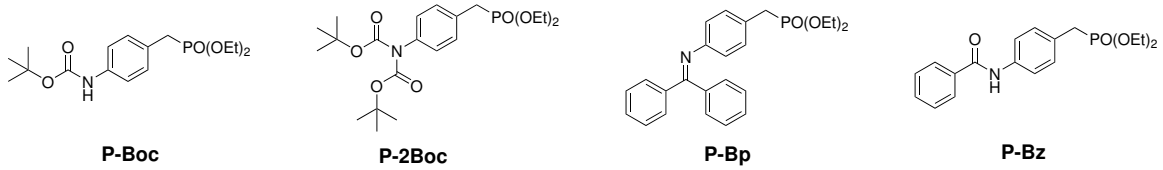

Scheme 2.31: Diethyl 4-aminobenzylphosphonates synthesized towards the HWE olefination.

Alongside **P-Boc** and **P-Bz**[195] displaying an acidic proton on the nitrogen, two more phosphonates with a tertiarized amine either by two Boc groups such as **P-2Boc** or condensation of benzophenone with **P-Bp** were synthesized. The amine deprotonation on the phosphonate moiety could give side reactions preventing the proper olefination, for the same reasons discussed before on the synthesis of **D2-1** in **Scheme** 2.28.

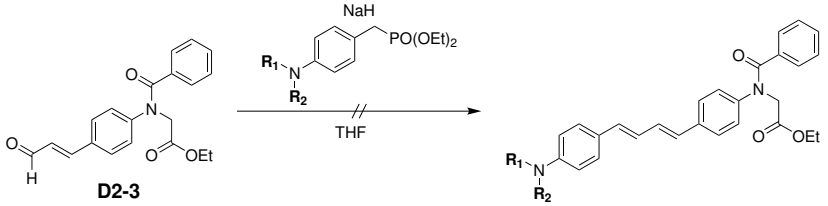

Scheme 2.32: HWE tryouts on the α,β insaturated aldehyde using several phosphonates.

[195] Bellucci, C. et al. *Eur. J. Med. Chem.* **1987**, *22*, 473–477.

Phosphonate	equivalents	Base	equivalents	Yield
P-Boc	1eq.	NaH	6+4eq.	∅
P-Boc	1eq.	NaH	10eq.	∅
P-Boc	1.1eq.	NaH	6eq.	∅
P-2Boc	1eq.	NaH	1.3eq.	∅
P-Bp	1.1eq.	NaH	1.3eq.	∅
P-Bp	1.1eq.	NaH	1.66eq.	∅
P-Bp	1.1eq.	NaH	6eq.	∅

Table 2.3: Summary of the different conditions tested towards the HWE olefination on **D2-3**.

As summarized in **Table** 2.3, the desired diaryldiene moiety could not be obtained. The presence of a stoechiometric amount or an excess of sodium hydride with respect to the phosphonate did not change the outcome. The most coherent hypothesis would be that the ester functionality itself is preventing the reaction. The absence of an acidic proton on the amine of the phosphonates did not improve the outcome either, and its presence did not prevent the reaction from proceeding as stated on **Scheme** 2.17. Thus, a slightly different synthetic scheme was designed.

2.3.2.6 Alternative pathway on *N*-benzoyl vinylanilline

Possibly, the HWE olefination might as well proceed with an acidic proton on the amine of the cinnamaldehyde moiety, as shown on **Scheme** 2.33. As the ethyl ester was the common group in all failed attemps at this olefination, trying the HWE olefination before introducing the ester by *N*-alkylation might proceed better and even a low yield would be an improvement.

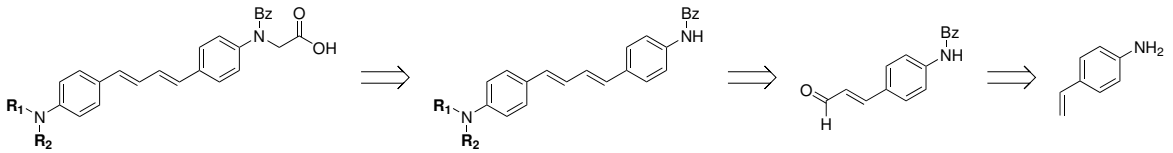

Scheme 2.33: Alternative retrosynthetic scheme of the photoactivatable moiety towards a two carbons amide linkage with *N*-alkylation after the HWE olefination step.

The synthesis of the α,β-insaturated aldehyde would proceed in the same conditions as already described[179], as shown on **Scheme** 2.34.

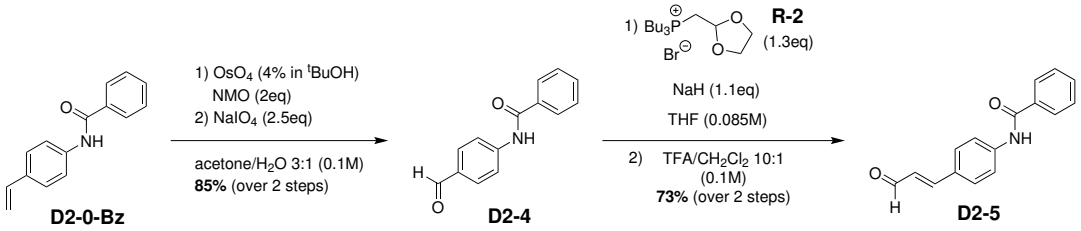

Scheme 2.34: Reaction conditions towards the (*E*) *N*-*para*-(3-oxoprop-1-en-yl)phenyl benzamide.

Starting from the *N*-benzoyl protected 4-vinylanilline **D2-0-Bz**, an Upjohn dihydroxylation followed by a Lemieux-Johnson oxidation was carried out, giving the corresponding aldehyde **D2-4** with 85% yield. The Wittig's reaction and acetal acidic deprotection towards the α,β-insaturated aldehyde yielded 73% of the desired compound **D2-5**, with an overall 62% yield for this five-steps procedure, including the prior benzoyl protection.

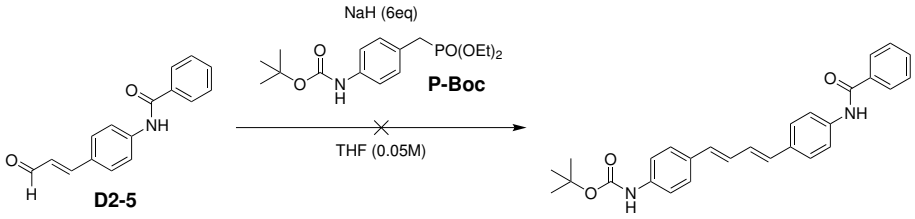

Scheme 2.35: HWE tryouts on the α,β-insaturated aldehyde.

Phosphonate	equivalents	Base	equivalents	Yield
P-Boc	1.1eq.	NaH	6eq.	∅
P-Boc	1.3eq.	NaH	6eq.	∅
P-Boc	2eq.	NaH	6eq.	∅

Table 2.4: Summary of the several conditions tried out towards the HWE olefination on aldehyde **D2-5**.

The HWE olefination tryouts on compound **D2-5** would not lead to the desired compound, as shown on **Scheme** 2.35, with tested conditions summarized in **Table** 2.4. These results would call in for a new synthetic strategy in order to obtain the desired nanotriggers.

2.4 Synthesis of the photoactivatable moiety towards a thiourea linker

2.4.1 Retrosynthesis

A new approach was to put aside the amide linkage and focus on the similarly flexible thiourea linkage. It could provide more hydrogen bondings in the reductase domain of the enzyme with an acceptor sulfur atom and two donors nitrogens. Additionally, the thiourea targets could be obtained from the same 5'-amino-5'-deoxyadenosine derivatives already prepared, by coupling with a photoactivatable moiety bearing an isothiocyanate, as shown in **Scheme** 2.36. Furthermore, on the new synthetic route towards these targets a common intermediate could be found, enabling a divergent synthesis.

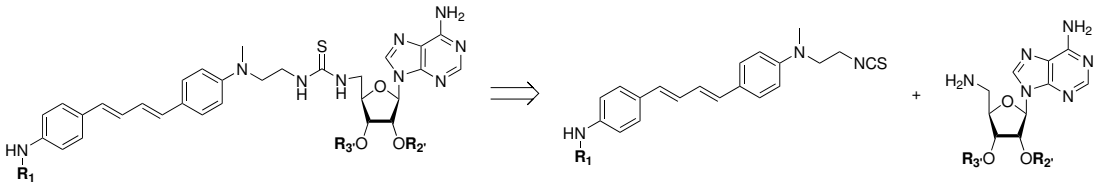

Scheme 2.36: Retrosynthetic scheme towards the thiourea linkage targets.

The retrosynthetic pathway towards the photoactivatable moiety, as shown on **Scheme** 2.37, was inspired by the synthetic scheme of the first described nanotrigger[139].

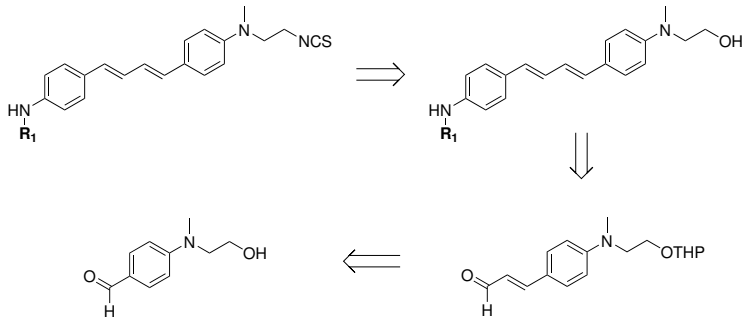

Scheme 2.37: Retrosynthetic scheme of the photoactivatable towards an isothiocyanate bearing (*E,E*) *p,p*-butadien-diyl-dianiline.

The commercially available *N*-methyl-*N*-hydroxyethyl-4-aminobenzaldehyde would be protected on the alcohol before a Wittig and a HWE olefinations. The primary alcohol would then be deprotected and changed to an isothiocyanate in several steps.

2.4.2 Synthesis

2.4.2.1 Extension of the conjugated system by Wittig's olefination

First, the alcohol was protected with a 2-tetrahydropyranyl (THP) group[196]. To a solution of *N*-methyl-*N*-hydroxyethyl-4-aminobenzaldehyde in DCM was added an excess of 3,4-dihydro-*2H*-pyrane (DHP) with a catalytic amount of pyridinium *para*-toluenesulfonate (PPTS) to obtain the desired compound in near quantitative 96% yield.

Compound **D3-1** could then undergo a Wittig's olefination in the same conditions as previously described[179], as shown on **Scheme** 2.39.

[196] Mladenova, M. et al. *Tetrahedron Lett.* **1999**, *40*, 6923–6926.

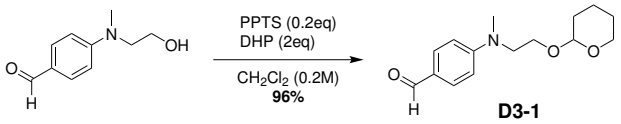

Scheme 2.38: Reaction conditions for the hydroxyl protection using a THP protection.

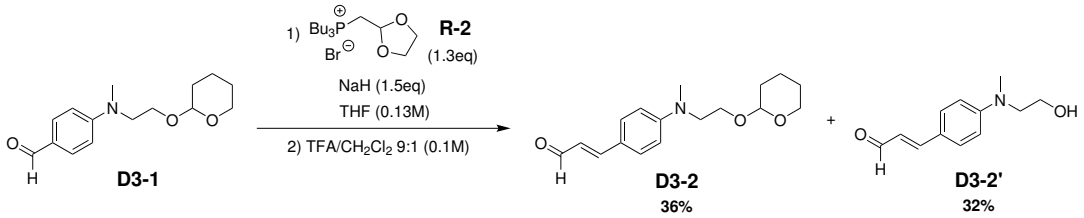

Scheme 2.39: Formation of the cinnamaldehyde moiety by Wittig's reaction and acetal deprotection.

The Wittig's olefination would transform a decent 68% of the aldehyde **D3-1**, but the TFA deprotection of the acetal was also so strong it would proceed in less than an hour but also remove the THP protection from almost half of the desired compound. Even if the **D3-2'** could be protected again, some milder conditions could be interesting. The challenge rises from a selective deprotection towards the newly formed 1,3-dioxolan acetal while not reacting with the THP acetal protection.

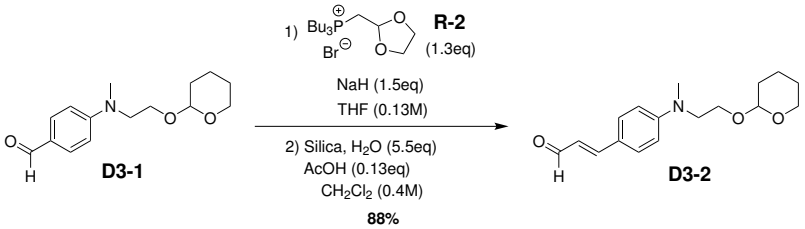

Scheme 2.40: Formation of the cinnamaldehyde moiety using milder deprotection conditions.

A good balance between reactivity and mildness was found with the conditions described in **Scheme** 2.40. As previously shown, it is possible to discriminate between two acetals using the acidity of silica[197]. Towards the formation of the desired cinnamaldehyde **D3-2**, an addition of a catalytic amount of acetic acid was still necessary to push forward the reaction, yielding 88% over 10 days and leaving the protecting THP untouched.

2.4.2.2 Formation of the photoactivatable moiety by HWE

The determining HWE step could then be carried out on the previously obtained cinnamaldehyde **D3-2**. The chosen phosphonate was protected by a benzoyl group, which is insensitive towards acidic conditions that will be needed for the deprotection of the THP group.

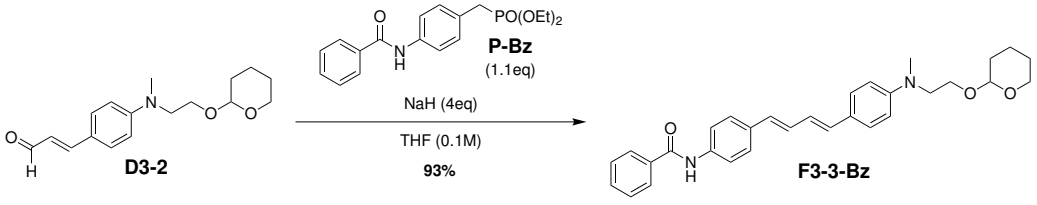

Scheme 2.41: Formation of the photoactivatable moiety *via* HWE.

[197] Leonelli, F. et al. *Eur. J. Org. Chem.* **2019**, *2019*, 1594–1599.

The HWE olefination between **D3-2** and a slight excess of diethyl 4-aminobenzylphosphonate **P-Bz** would proceed smoothly in THF, after portionwise addition of sodium hydride. The reaction would not progress anymore after 4 days, yielding 93% of the desired compound **F3-3-Bz** after a clean purificationless work-up as HWE reactions are known for. From this step, the diaryldiene moiety would always show an intense turquoise fluorescence when irradiated at 365nm, which will be discussed thoroughsly in the third chapter and explains the **F** denomination.

2.4.2.3 Introduction of the isothiocyanate

Next, the aim would be to replace the protecting THP with the desired isothiocyanate functionality. To that end, the alcohol protection would be cleaved in acidic conditions[139], as shown in **Scheme** 2.42.

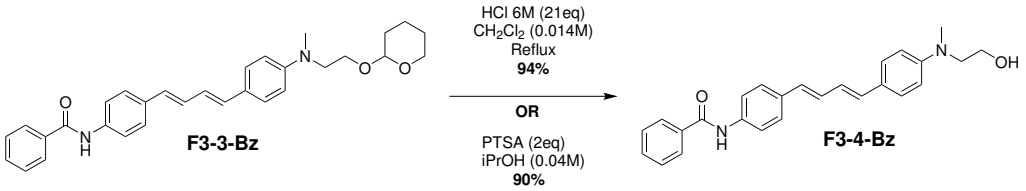

Scheme 2.42: Reaction conditions used for the tetrahydropyran acidic cleavage.

Heating a solution of **F3-3-Bz** in DCM at 55°C after adding an excess of an aqueous solution of hydrochloric acid for an hour and a half would almost completely remove the THP group. The reaction progress could conveniently be monitored by the color of the organic phase, as the deprotected compound would precipitate as an ammonium salt, slowly clearing up the solution. Despite the great efficiency of this reaction, judging by the high yield of 94%, the work up was very tedious. The crude ammonium salt was neutralized with aqueous sodium hydroxide and an extraction was performed by adding a large amount of DCM to solubilize the desired compound, around 1L per gram. In order to save solvent and maybe save some time, some other reaction conditions were carried out. **F3-3-Bz** was mixed with two equivalents of PTSA in isopropanol (iPrOH) at 55°C. The reaction needed to be monitored by TLC this time, and reached completion overnight. Upon removal under *vacuum* of the solvents, a saturated solution of sodium hydrogenocarbonate would be poured on the crude residue. The solution would produce carbon dioxide bubbles as it was neutralizing the acid and solubilizing the sulfonate, thus leaving only the desired compound as an insoluble. Upon thorough mixing and sonication, the mixture was filtered over a sintered glass funnel and the solid was washed with distilled water several times, to give the desired compound **F3-4-Bz** with a yield of 90%.

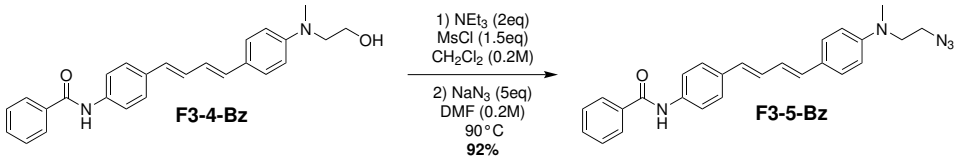

Scheme 2.43: Azide introduction *via* an intermediate mesylation of the free hydroxy followed by an SN_2.

The primary alcohol was then converted to an azide using a well known two-steps procedure[163]. In a first step, the hydroxyl group was mesylated using an excess of mesyl chloride in DCM and a further excess of triethylamine acting as an hydrogen chloride scavenger. After quenching of the leftover mesylating agent with methanol, the crude mixture was thoroughlsy evaporated then dried under reduced pressure to prevent any danger in the next step. The latter residue was dissolved in DMF and heated to 90°C after addition of a five fold excess of sodium azide, leading to a S_N2 of the mesylate group by an azide with 92% yield over two-steps.

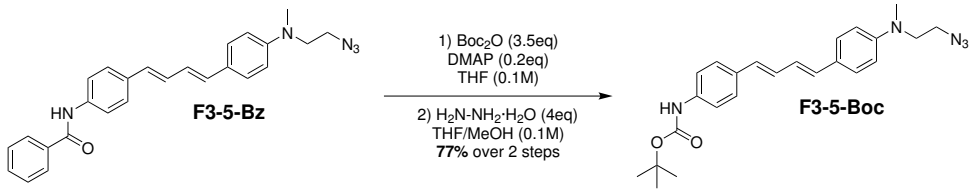

Scheme 2.44: Reaction conditions for the aromatic amine protecting group switch from -Bz to -Boc.

A little adjustment was then required on the arylamine, in order to have at that position another protecting group that could be cleaved in the same conditions as the *tert*-butyl esters and isopropylidene group on the docking moiety. Such an amine protecting group could be impersonated by the *tert*-butyloxycarbonyl group. That would induce the possibility of a one-pot cleavage of all the protecting groups in acidic conditions in a last step towards the nanotriggers. A way of switching these two protecting groups on an amine was previously published in a two-steps procedure[198], as shown on **Scheme** 2.44. Firstly a Boc protecting group was forced onto the benzoylated amine using an excess of di-*tert*-butyl dicarbonate in THF using a catalytic amount of 4-dimethylaminopyridine (DMAP). Upon completion, methanol was added to destroy the leftover Boc anhydride, then a four fold excess of hydrazine hydrate was carefully added to the reaction mixture and removed the benzoyl moiety, giving the desired compound **F3-5-Boc** with a 77% yield over two steps.

Several ways of introducing the isothiocyanate from an amine were found, adding a simple azide reduction step. An issue with these procedures would be the need for purification due to an incomplete conversion[199,200] risking the isothiocyanate degradation over silica, and the toxicity of some reagents used like thiophosgene[201]. Another strategy would be to reduce *in situ* the azide by forming an iminophosphorane *via* a Staudinger's reduction[162] before converting it to an isothiocyanate with carbon disulfide, either sequentially[202] or in one-pot[203]. An interesting balance between all these procedures would be found by the use of supported triphenylphosphine[204], as shown on **Scheme** 2.45, which would enable removal of the reagents by filtration and drying under reduced pressure.

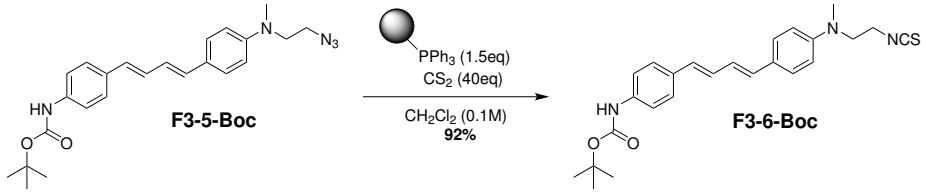

Scheme 2.45: Formation of the isothiocyanate *via* an iminophosphorane.

Compound **F3-5-Boc** was dissolved in dry DCM before addition of an excess of supported triphenylphosphine and carbon disulfide under an argon atmosphere. Upon completion as followed by TLC, the heterogenous mixture was carefully filtered over a paper filter and the filtrate was dried under reduced pressure. Purification over silica gel would be risky with respect to the isothiocyanate electrophilicity, so the quality of the crude was verified by ^{1}H NMR. As shown on **Figure** 2.46, the spectra for the starting and desired compound were very similar, except for the two

[198] Burk, M. J.; Allen, J. G. *J. Org. Chem.* **1997**, *62*, 7054–7057.
[199] Janczewski, Ł. et al. *Eur. J. Org. Chem.* **2019**, *2019*, 2528–2532.
[200] Li, H. et al. *Adv. Synth. Catal.* **2012**, *354*, 2264–2274.
[201] Rodríguez-Lucena, D. et al. *J. Org. Chem.* **2008**, *73*, 2967–2979.
[202] Xiong, J. et al. *Synlett* **2017**, *28*, 1075–1078.
[203] Despras, G. et al. *Chem. Eur. J.* **2017**, *23*, 10838–10847.
[204] García-Moreno, M. I. et al. *Carbohydr. Res.* **2002**, *337*, 2329–2334.

$-CH_2-$ highlighted in red. The isothiocyanate moiety symmetrized the chemical environment of these four protons, leading to them appearing as a 4H singlet, whereas the azide lead to a distinction between the two groups of two protons. Considering the crude of the transformation did not show any traces of the two caracteristic 2H triplets of **F3-5-Boc**, no further purification was needed yielding 92% of the desired compound **F3-6-Boc**. An explanation for the loss of a fraction of the starting material could be that the intermediate iminophosphoranes are bound to the support of the triphenylphosphine, thus they were removed in the filtration step. As no starting material was found in the product, the Staudinger's reaction was complete and the slightly reduced yield comes from a kinetic or thermodynamic factor. Thus, this transformation did not proceed through the transient phosphazide mechanistic pathway[204].

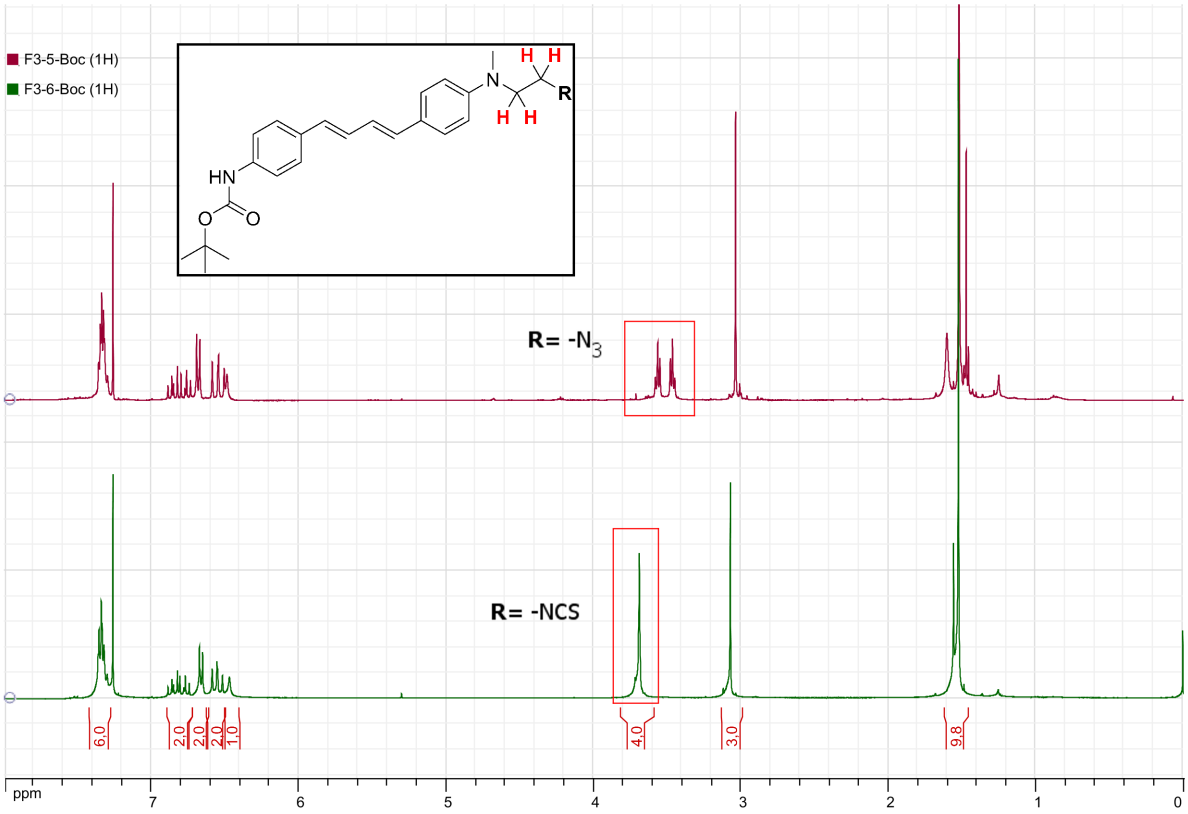

Figure 2.46: Superimposed ^{1}H NMR spectra of **F3-5-Boc** (red) and **F3-6-Boc** (green).

The coupling between the adenosines derivatives and the photoactivatable moiety could now be tested out, in order to obtain the corresponding thioureas linkage protected nanotriggers.

2.5 Coupling of the docking and photoactivatable moieties

The coupling of amines with isothiocyanates is straightforward and the products contain exactly the same starting atoms, meaning an atom economy of 100%. Eventhough some procedures may use an additional base such as pyridine[203,201], its absence does not change drastically the output yield[202,200]. Furthermore, the presence of pyridine might harden the purification process, as no acidic washing would be advisable with the two protecting groups that could be destroyed in these conditions. For these reasons, the simple coupling in THF with no additive was chosen, as shown on **Scheme** 2.47.

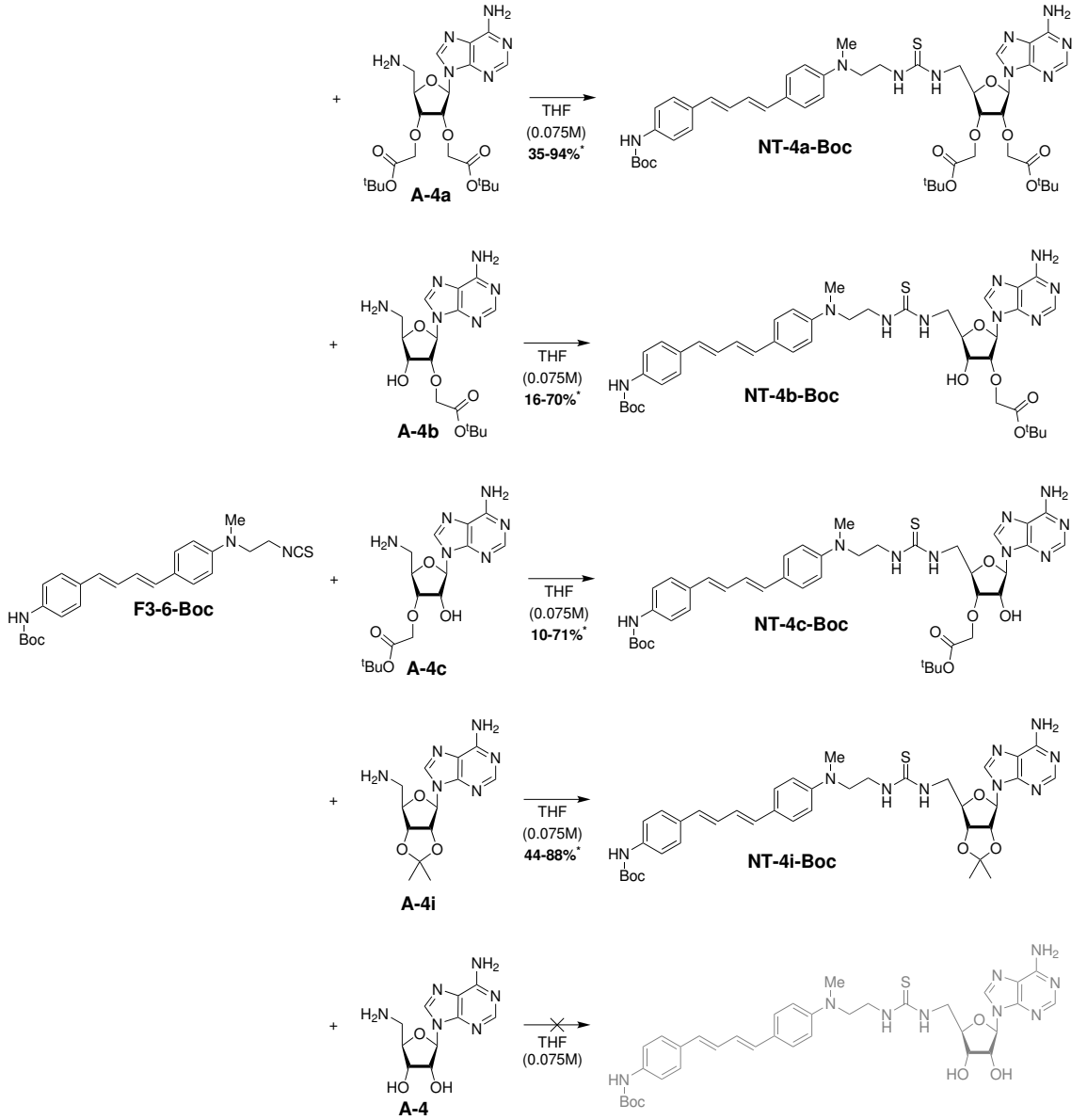

Scheme 2.47: Coupling of the docking moiety and the -Boc protected photoactivatable moiety *via* formation of the thiourea bond.

* Indicative yields given based on recovered unpure compounds after inefficient purification over silica gel (DCM/EtOH from 100:0 to 90:10) over respectively 3, 4, 7 and 4 batches for **NT-4a-Boc**, **NT-4b-Boc**, **NT-4c-Boc** and **NT-4i-Boc**.

The reaction progressed over several days, and after removal of the solvent, none of the desired compounds could be readily purified over silica gel. The reactions outcome showed issues of re-

peatability, with no clear explanation. The crude residues were analized by high pressure liquid chromatography (HPLC) to determine their respective purity. Unsurprisingly, the 5'-amino-5'-deoxyadenosine **A-4** would not form a major compound when reacting with the isothiocyanate, as monitored by TLC, most likely because of side reactions involving the hydroxyl groups.

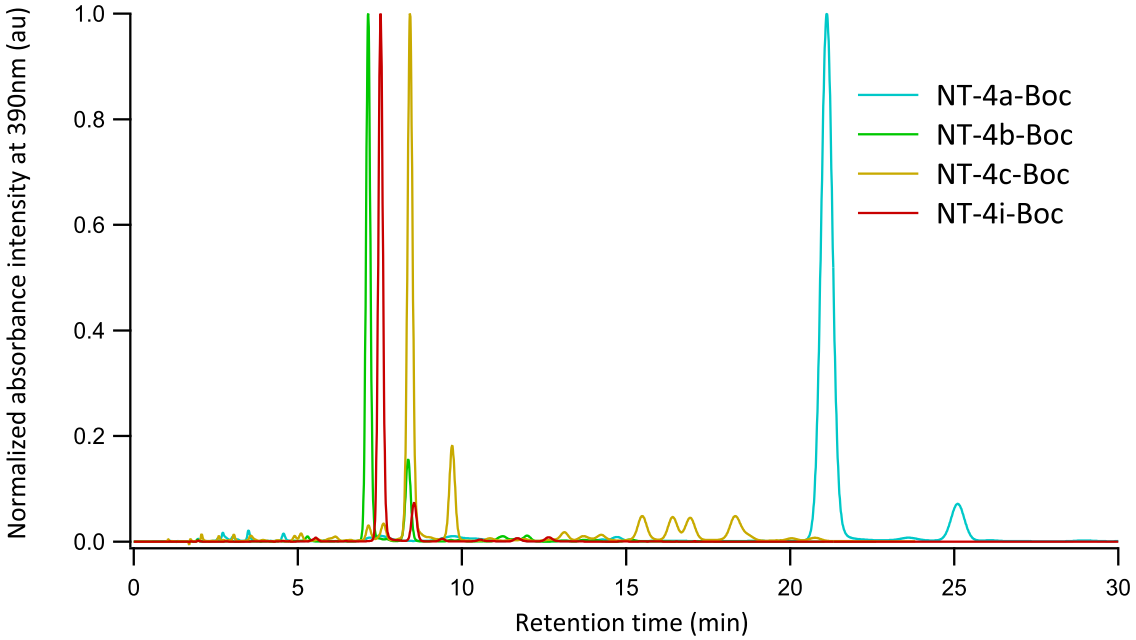

Figure 2.48: HPLC chromatograms[§] of the crude protected nanotriggers in optimized elution conditions[♮].

[§] Chromatograms were truncated after 30mins for the sake of clarity, as no peak was observed afterwards for any of the compounds.

[♮] Analytical C18 column 5µ 250×4.6mm eluted with MeCN/H_2O 65:35 at a flowrate of 1.75mL/min under a pressure of 97bar.

After optimizing the elution conditions, the chromatograms showed the presence of a major compound and one or several minor impurities as represented on **Figure** 2.48. As water and acetonitrile absorb slightly at 190nm and 254nm, quantifying the composition by integration could not be practical at such wavelengths. The diaryldiene moiety have its absorption maximum around 390nm, depending on the solvent, where the eluant is fully transparent. Thus, this wavelength was used towards quantification to help assessing the compounds purity. Available batches were reunited for each compound and their optical purity was determined by this method, as summarized in **Table** 2.5.

Entry	RT (min)[†]	Optical Purity at 390nm[‡]
NT-4a-Boc	20.74	79.7%
NT-4b-Boc	7.05	77.4%
NT-4c-Boc	8.32	52.4%
NT-4i-Boc	7.43	88.2%

Table 2.5: Optical purity and retention time measured by HPLC of the crude protected nanotriggers.

[†] In optimized elution conditions on a C18 analytical column.

[‡] Represents the integral of the absorption intensity at 390nm for the peak at that retention time divided by the sum of the integrals of the absorption intensity at 390nm for all the detected peaks over 60min, more details in **Appendix D.1**.

After purification over C18 silica with a gradient elution MeCN/H_2O 50:50 → 90:10, the compounds would show a purity above 90%, as shown in **Table** 2.6. Even if better would be advised for spectroscopic measurements, it was deemed decent enough to carry on the deprotection tryout.

Entry	RT (min)[†]	Optical Purity at 390nm
NT-4a-Boc	21.12	95.5%
NT-4b-Boc	7.15	94.1%
NT-4c-Boc	8.42	90.6%
NT-4i-Boc	7.52	96.2%

Table 2.6: Optical purity and retention time measured by HPLC of the protected nanotriggers purified over C18 silica.

[†] In optimized elution conditions on a C18 analytical column.

Later would be found by high-resolution mass spectroscopy (HRMS) that the major peaks corresponded to the fractions of desired compounds. More informations about HPLC methodology are detailed in **Appendix B.4** and **Appendix D.1**.

2.6 Cleavage of the protecting groups

The deprotection of the various protective moieties in the four previous molecules was tested on less valuables compounds in model reactions, shown in **Scheme** 2.49. In order to avoid any risk of degrading the higher value compounds, increasingly acidic conditions were tested out on three model compounds, as shown in **Table** 2.7. The main goal was to have the three protecting groups able to be cleaved over the same duration to avoid degradation in such acidic media.

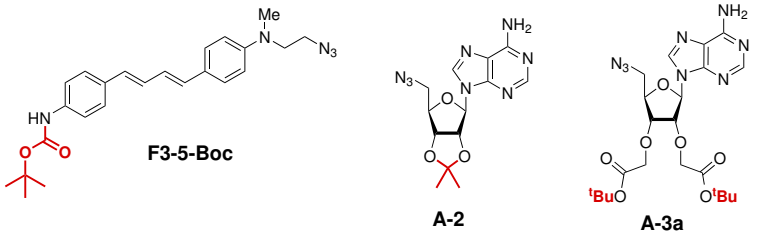

Scheme 2.49: Model compounds chosen to test acidic deprotection conditions.

On the one side, the *tert*-butyloxycarbamate **F3-5-Boc** was easily cleaved with 10%v/v TFA in DCM in 2 hours[205], just as the di-*tert*-butyl ester **A-3a**[206]. The reaction was quantitative and clean, as supported by ^{1}H NMR experiments that only showed the desired deprotected compounds, without any traces of starting material or other degradation products. It was assumed that if these conditions could cleave the two esters in **A-3a**, it would cleave one in the same way in **A-3b** and **A-3c**.

Entry	Protecting group	Conditions	Time to completion
F3-5-Boc	Boc	CH_2Cl_2/TFA (9:1)	2hrs
A-2	Isopropylidene	CH_2Cl_2/TFA/H_2O (9:1:0.5)	$\gg$2hrs
A-2	Isopropylidene	CH_2Cl_2/TFA/EtOH (8:1:1)	>2hrs
A-2	Isopropylidene	TFA/EtOH (1:1)	>2hrs
A-2	Isopropylidene	TFA/EtOH (9:1)	2hrs
A-3a	*tert*-butyl ester	CH_2Cl_2/TFA (9:1)	2hrs

Table 2.7: Reaction conditions for the acidic cleavage of the protecting groups.

The isopropylidene, on the other side, was expected to be quite harder to cleave. Its deprotection would require very concentrated TFA with water, as previously discussed in subsection **2.2.2**, or methanol[207] to make the reaction possible at room temperature. A mixture of ethanol/TFA/water (110:16:10) was described to need thorough heating for hours barely reaching 50% yield[208]. Nonetheless ethanol was tried out first to increase the much needed solubility of the protected compounds, and with TFA/EtOH 9:1 the reaction would be completed in around 2 hours at room temperature. It was assumed that these conditions would deprotect the Boc as cleanly as previously. Furthermore, as discussed in section **2.2.2**, the TFA needed to be carefully removed under reduced pressure at a temperature not rising over 20°C in order to avoid the degradation of the compounds *via* an acidic desadenylation.

The protective moieties could be quantitatively cleaved from the protected compounds in the optimized conditions determined on the model compounds, as shown on **Scheme** 2.50. Thus the

[205] Li, R. et al. *J. Med. Chem.* **2012**, *55*, 2474–2478.
[206] Doknic, D. et al. *Eur. J. Org. Chem.* **2013**, *2013*, 5303–5314.
[207] Banik, B. K. et al. *J. Org. Chem.* **1993**, *58*, 307–309.
[208] Ramage, R. et al. *Tetrahedron* **1991**, *47*, 5625–5636.

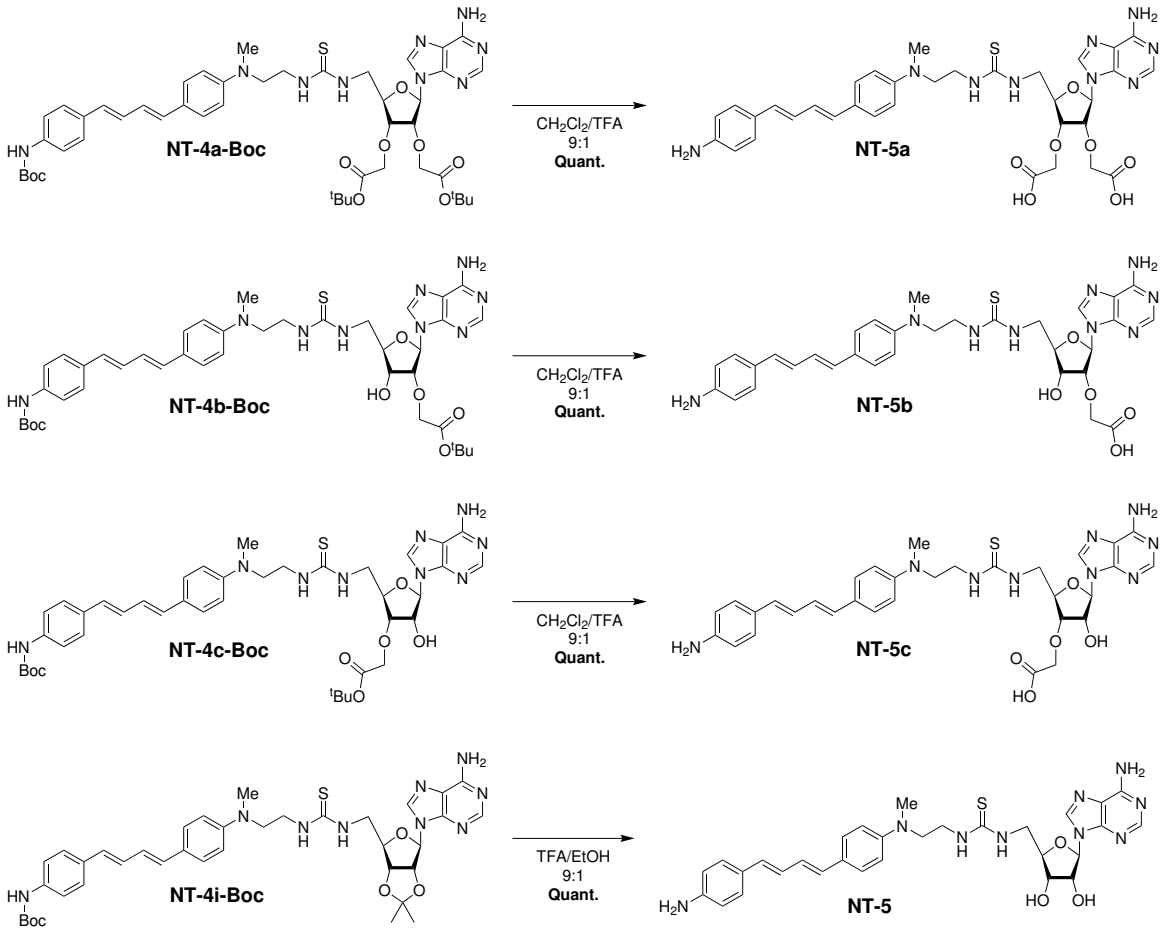

Scheme 2.50: Deprotection conditions carried out to obtain the desired non-, mono-2', mono-3' or di-substituted nanotriggers.

desired nanotriggers **NT-5a**, **NT-5b**, **NT-5c** and **NT-5** were isolated at the tens of milligrams scale after careful removal of the solvents under reduced pressure. NMR experiments neither showed traces of the usually very high peaks corresponding to the 9H *tert*-butyl group or the two 3H peaks of the isopropylidene, nor of the starting materials.

2.7 Conclusion

Four new photoactivatable NADPH analogues were synthesized, bearing a carboxymethyl functionalization at positions 2', 3', both or none as a bioisostere for the natural 2'-phosphate. These mimics have the photoactivatable diaryldiene moiety linked to the docking moiety by a flexible thiourea linkage that should improve the electron transfer to the FAD in eNOS. These nanotriggers need to be tested in eNOS studies, in order to probe their relative potency compared to the previous ones and hopefully enable the NO-mediated angiogenesis.

These nanotriggers were obtained at the tens of milligrams scale, which should be enough to carry spectroscopic caracterization and biological experiments.

Chapter 3

Absorption and emission properties of the nanotriggers

Contents

3.1 Properties of the synthesized nanotriggers

3.1.1 Preliminary remarks

In order to proceed to biological experiments *in-cellulo*, it is of great use to have some basic knowledge on the spectroscopic behaviors of the synthesized nanotriggers. For that matter, the compounds were characterized in two solvents with characteristics similar to the environment of NOS-bound or free nanotriggers. The first one being dimethylsulphoxide (DMSO) which mimics the polarity of the NADPH-binding pocket of eNOS, and the second one a Tris buffer pH7.4 which can be considered closer to the cytosolic medium.

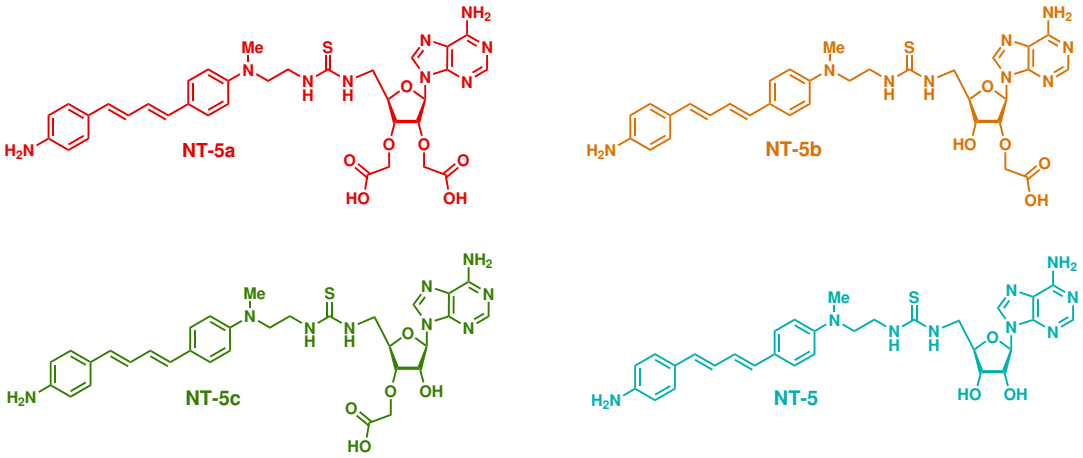

Scheme 3.1: Structure of the compounds characterized with matching colors in upcoming graphs.

For the sake of clarity, the colors representing the various compounds in **Scheme** 3.1 will be matched with the graphs presented in the upcoming discussion, unless explicitely stated otherwise.

3.1.2 Characterization in a model apolar environment: DMSO

3.1.2.1 Absorption properties

The molar absorption coefficient ε of the 4 nanotriggers were measured in a conventional fashion, using the Beer-Lambert law. The absorbance was divided by the concentration of the solution and the length of the quartz cuvette used, yielding ε as a function of the wavelength, as plotted for all the compounds in **Figure** 3.2.

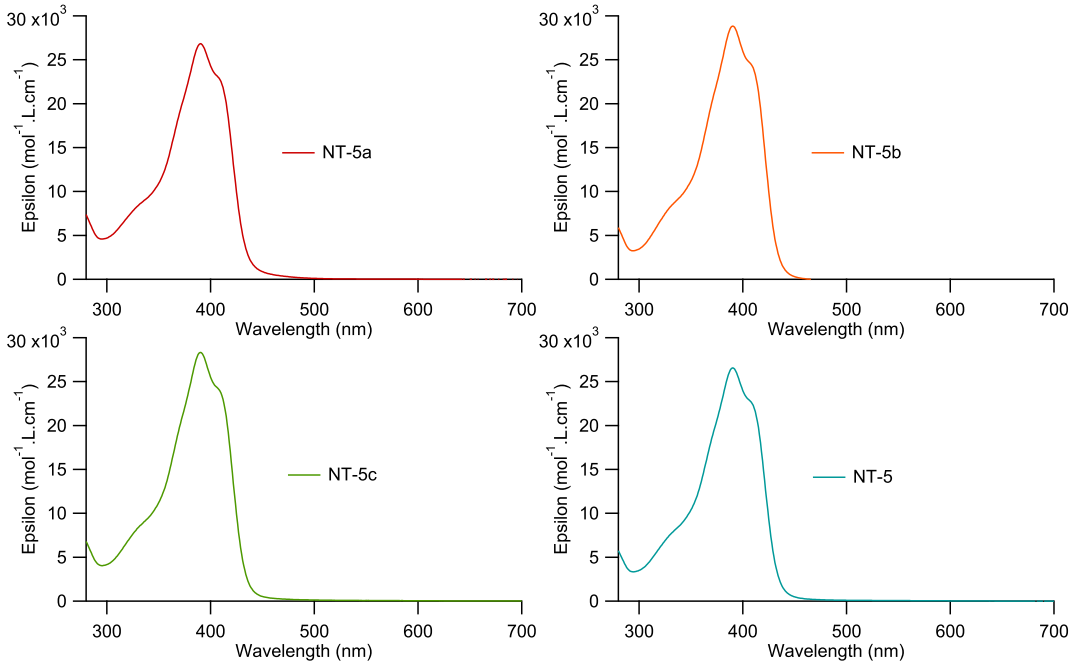

Figure 3.2: Absorption coefficient in DMSO of the synthesized compounds.

Increasing the number of measurements enabled the use of a statistical approach in order to increase the reliability of the results, as presented in **Table** 3.1.

Compound	**Solvent**	$\lambda_{max,abs}$ (nm)	$\varepsilon^{\dagger}$(L.mol^{-1}.cm^{-1})	$\sigma^{\dagger}$(L.mol^{-1}.cm^{-1})
NT-5a	DMSO	390	26 800	± 800
NT-5b	DMSO	390	28 700	± 500
NT-5c	DMSO	390	28 000	± 1000
NT-5	DMSO	390	26 200	± 500

Table 3.1: Summary of the absorption coefficient in DMSO at $\lambda_{max,abs}$ of the synthesized compounds.

† Determined by statistical analysis over 4 independant experiments. Standard deviation $\sigma < 5\%$.

3.1.2.2 Fluorescence

The absorption spectra of the nanotriggers are very similar and have their maxima at 390nm in DMSO. Thus in order to study the fluorescence emission of these molecules, the easiest and most consistent procedure would be to excite at this wavelength and record the light emitted perpendicularly, as shown on **Figure** 3.3. The nanotriggers emission spectra are quite similar showing two overlapped bands and have their maxima at 462−463nm.

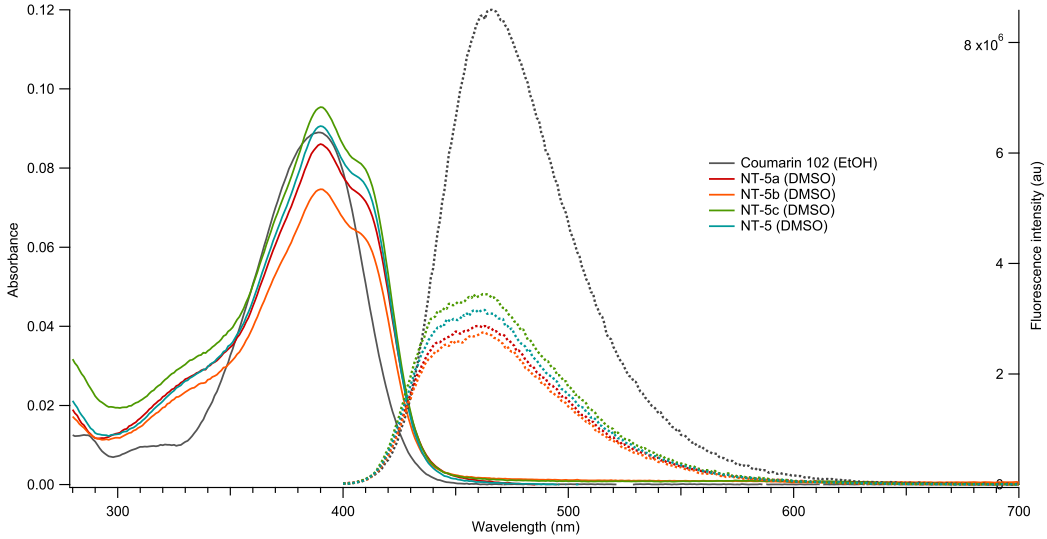

Figure 3.3: Absorbance (plain) and fluorescence (dotted lines) with excitation at 390nm of the nanotriggers and coumarin 102. Spectra are not normalized for an easier reading.

Excitation spectra

The emission and absorption spectra presented earlier display overlapped bands, and this can be caused by several phenomena. First, the emitting state can differ from the absorbing state. Second, if the both emitting and absorbing states are the same, the vibrational resolution observed in the emission and absorption spectra should be the same. The bands should then be separated by the same energy, meaning a slightly larger difference in emission when converted into wavelength. This observation could as well come from the presence of two fluorescent emitters in the prepared solutions. If the first hypothesis does not rise any concern, the second one should be eliminated before investigating further into the fluorescence properties of the nanotriggers. To that extent, excitation spectra were carried out on the compounds, as shown on **Figure** 3.4, for one wavelength in each plausible emission band, respectively 430nm and 500nm.

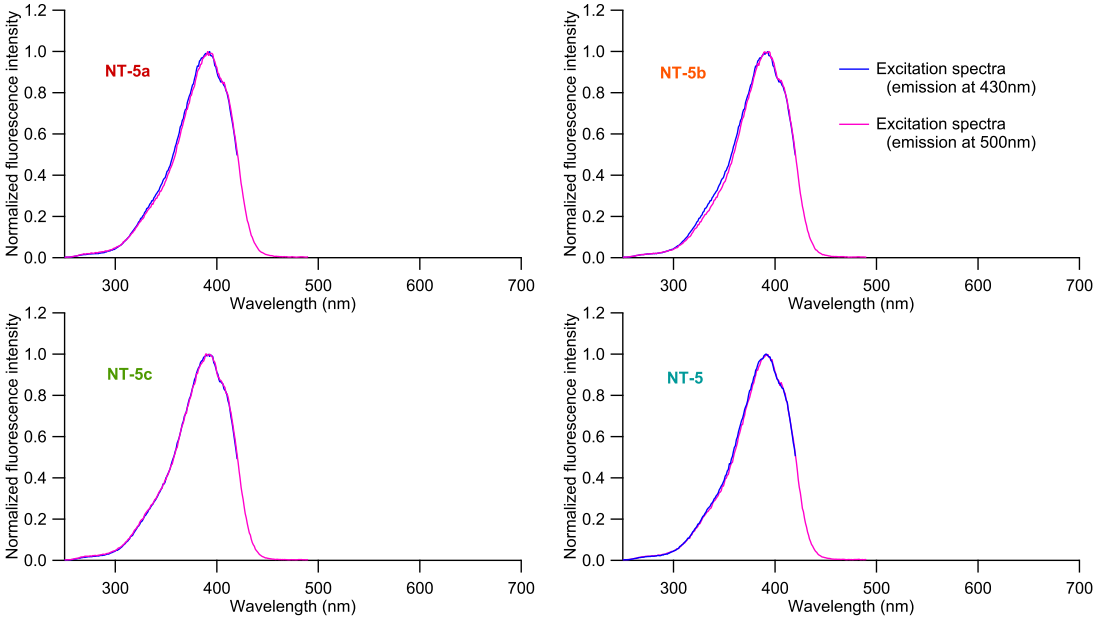

Figure 3.4: Normalized excitation spectra of the synthesized nanotriggers for an emission at 430nm or 500nm, respectively in blue and magenta.

The two spectra overlap decently for all the compounds, and fit the look of the absorption band in that region. Based on these measurements, the probability of the emission shape coming from a second emitter seems pretty low, thus enabling the quantum yields characterization. Additionally, the solvatochromic properties of the compounds were studied, as shown in **Appendix C**, in order to probe for the existence of a twisted intramolecular charge transfer (TICT) excited state[209].

Fluorescence quantum yield

Quantum yields ϕ are characteristics of the processes by which molecules can be excited and deactivated. The fluorescence quantum yield ϕ_F is the ratio of excited molecules that emits a fluorescence photon to come back to the ground state over the total amount of absorbed photons, thus it is comprised between 0 and 1 and very often expressed as a percentage.

Several procedures enable the measurements of fluorescence quantum yields. One of the most precise involves the use of an integration sphere, allowing to precisely measure the quantum yield as the ratio of output over the input photons. A much simpler approach exists but requires a known molecular reference with similar absorption and emission properties in order to avoid corrections due to the detection system[209]. The absorption and emission spectra of the coumarin 102, as displayed on **Figure** 3.3, are very similar to the nanotriggers and its quantum yield of fluorescence is known[210]. Using the following equation, one can deduce the fluorescence quantum yield of an unknown compound by measuring the integration of the fluorescence intensities F^x of the compounds, adding a correction on the absorbance and refractive index if different[211]. The dependency of the quantum yield ϕ^F with the wavelength within an absorption band will not be investigated.

$$\phi_F^i = \frac{F^i \cdot n_i^2}{F^r \cdot n_r^2} \times \frac{1-10^{-A_r}}{1-10^{-A_i}} \times \phi_F^r$$

Using this method, the fluorescence quantum yields of the nanotriggers were measured and are summarized in **Table** 3.2.

Compound	**Solvent**	$\lambda_{max,em}$ (nm)	$\phi_F{}^\dagger$	$\sigma^\dagger$
NT-5a	DMSO	463	0.36	± 0.005
NT-5b	DMSO	463	0.36	± 0.04
NT-5c	DMSO	462	0.36	± 0.03
NT-5	DMSO	462	0.35	± 0.03
Coumarin 102[210]	EtOH	466	0.766	± 0.041

Table 3.2: Determined quantum yields of the synthesized nanotriggers in DMSO. Measured with λ_{exc} =390nm.

† Determined by statistical analysis over 2 independant experiments. $\sigma < 10\%$, as accepted for fluorescence quantum yields.

[209] Valeur, B. In *Molecular Fluorescence*; John Wiley & Sons, Ltd: 2001; Chapter 3, pp 34–71.
[210] Rurack, K.; Spieles, M. *Anal. Chem.* **2011**, *83*, 1232–1242.
[211] Brouwer, A. M. *Pure Appl. Chem.* **2011**, *83*, 2213–2228.

3.1.3 Characterization in a model polar environment: Tris buffer

As previously stated, the nanotriggers were also characterized in a Tris buffer pH7.4 20mM, containing 1% of DMSO to help in the preparation of samples and is commonly accepted in biological experiments.

3.1.3.1 Absorption properties

The measurements carried out previously were repeated on solutions of nanotriggers in Tris buffer pH7.4 20mM (1% DMSO) for various concentrations, as presented in **Figure** 3.5.

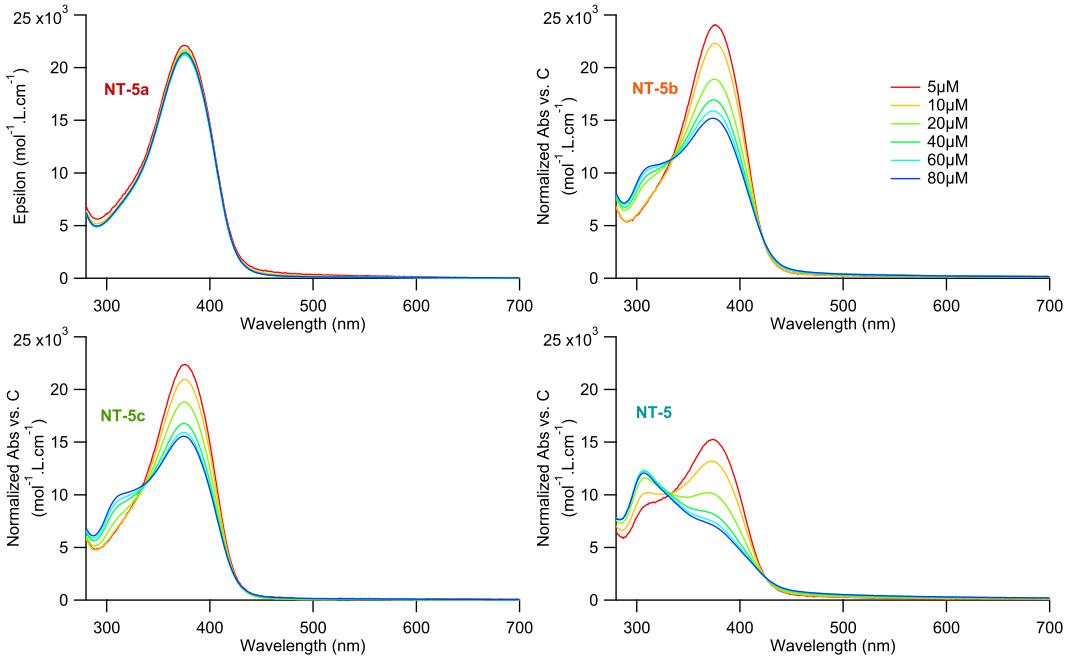

Figure 3.5: Absorption spectra of the synthesized compounds in Tris buffer pH7.4 20mM (1% DMSO) normalized with respect to the concentration and cuvette length, for concentration ranging from 5µM (red) to 80µM (blue).

As expected, the shape of the absorbance of **NT-5a** does not depend on the concentration. Surprisingly, the three other compounds do not behave similarly. The superimposition of spectra shows an isobestic point near 335nm for these nanotriggers, suggesting an equilibrium between two species. An aggregation of the molecules caused by a lower solubility could explain this observation, as the two carboxylic acids in **NT-5a** are deprotonated at physiological pH, increasing the solubility compared to **NT-5b** and **NT-5c** bearing only one carboxylate and even more with respect to **NT-5**. The spectra evolution is very similar for the two monoacids, and the change is even larger in **NT-5**.

An aggregation equilibrium does not rise issues towards biological experiments, as consumption of the free nanotriggers will displace the equilibrium towards their release from aggregates. This can be seen in the spectra previously described, as the lowest concentrations in red seem to tend towards the behavior observed for **NT-5a**, and increasing the concentration also increases the spectra discrepancy. Nonetheless, no absorption coefficient nor fluorescence quantum yields can be measured for these three compounds in this solvent. The results obtained are given in **Table** 3.3.

Compound	Solvent	$\lambda_{max,abs}$ (nm)	$\varepsilon^{\dagger}$(L.mol^{-1}.cm^{-1})	$\sigma^{\dagger}$(L.mol^{-1}.cm^{-1})
NT-5a	Tris buffer	376	20 600	± 100
NT-5b	Tris buffer	376	∅	∅
NT-5c	Tris buffer	376	∅	∅
NT-5	Tris buffer	374‡	∅	∅

Table 3.3: Summary of the molar attenuation coefficient of the synthesized compounds in Tris pH7.4 20mM (1% DMSO).

† Determined by statistical analysis over 2 independant experiments. σ < 5%.
‡ For concentrations below 10µM, above $\lambda_{max,abs}$ = 307nm.

Additionnally, the negative solvatochromic nature of the nanotriggers can be seen by a 25nm hypsochromic shift of the maxima of absorbance.

3.1.3.2 Fluorescence

The emission upon excitation at 375nm was recorded and is presented in **Figure** 3.6.

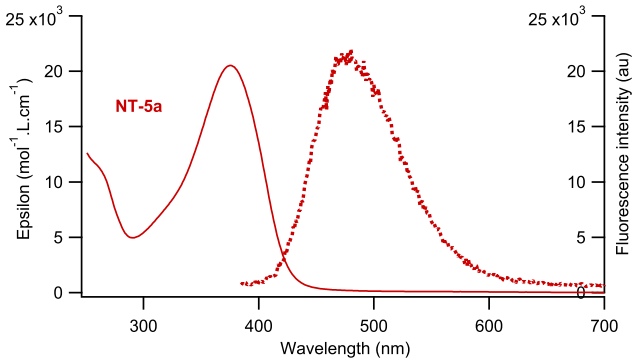

Figure 3.6: Absorbance and fluorescence emission with excitation at 375nm of **NT-5a**. Absorbance shown as continuous curves and fluorescence emission as dashed curves.

The emission spectrum of **NT-5a** shows a bathochromic shift of 20nm in Tris buffer with respect to DMSO, showing its maximum at 480nm. The absorption and emission spectra do not show any vibrational structure. The fluorescence quantum yield was measured and the results are summarized in **Table** 3.4.

Compound	Solvent	$\lambda_{max,em}$ (nm)	$\phi_F{}^{\dagger}$	$\sigma^{\dagger}$
NT-5a	Tris buffer	480	0.035	± 0.001
NT-5b	Tris buffer	474	∅	∅
NT-5c	Tris buffer	475	∅	∅
NT-5	Tris buffer	481	∅	∅

Table 3.4: Measured quantum yields of the nanotriggers in Tris buffer pH7.4 20mM (1% DMSO). Measured with λ_{exc} =375nm.

† Determined by statistical analysis over 2 independant experiments. σ < 10%, as accepted for fluorescence quantum yields.

3.2 Properties of the previous generation of nanotriggers

3.2.1 Preliminary remarks

The same properties were determined on nanotriggers synthesized by a previous PhD student[144] bearing a triazole linkage, as shown on **Figure** 3.7. These compounds also display an additional structure, named *anchor*, designed to increase the specificity towards the reductase domain of NOSs compared to other enzymes[171].

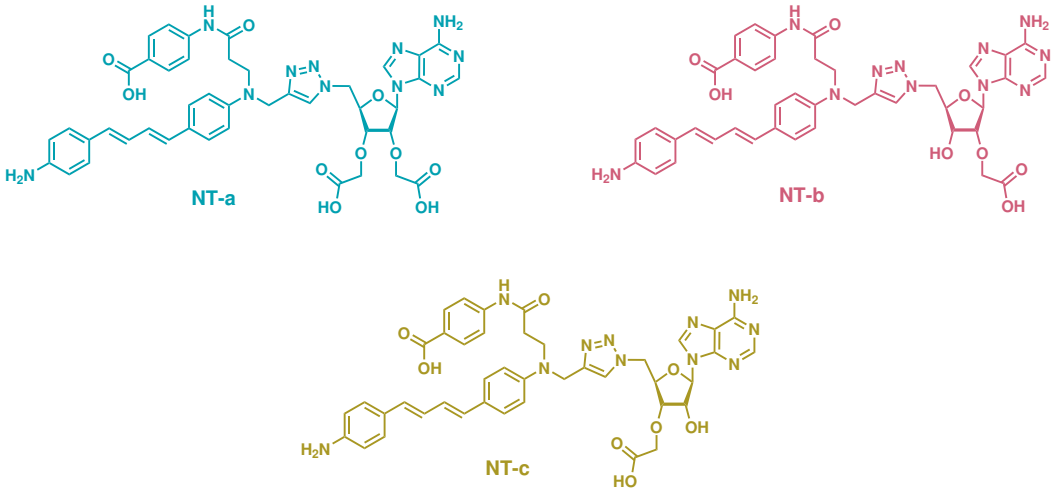

Scheme 3.7: Structure of the previous generation of nanotriggers characterized with matching colors in upcoming graphs.

For the sake of clarity, the colors representing the various compounds in **Scheme** 3.7 will be matched with the graphs presented in the upcoming discussion.

3.2.2 One-photon characterization

The absorption coefficient and emission properties of the previous generation of nanotriggers were determined in DMSO and Tris buffer, as shown on **Figure** 3.8.

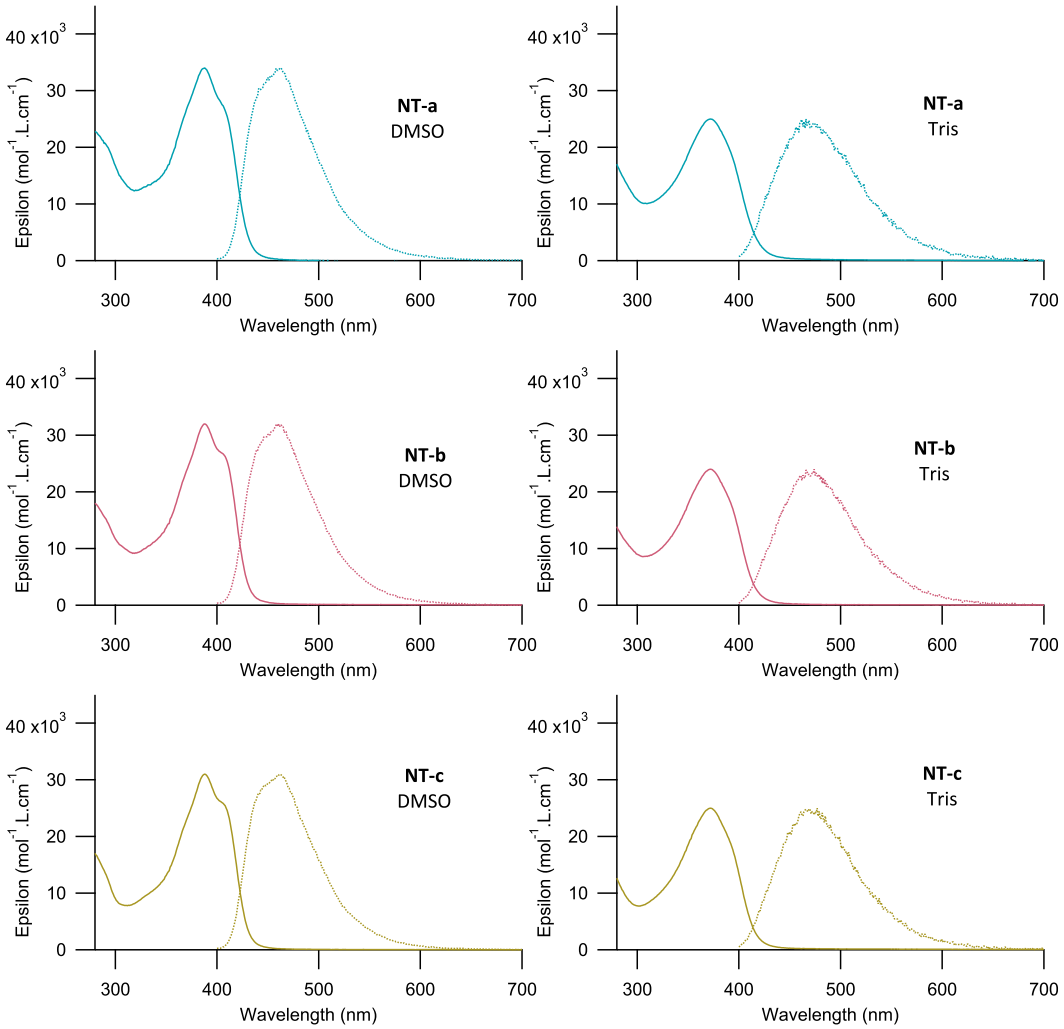

Figure 3.8: Molar absorption coefficient (plain lines) in DMSO (left panel) and Tris buffer pH7.4 20mM (1% DMSO) (right panel) of the previous generation of nanotriggers, alongside their normalized emission spectra (dotted lines).

Compound	Solvent	$\lambda_{max,abs}$ (nm)	ε (L.mol^{-1}.cm^{-1})	σ (L.mol^{-1}.cm^{-1})
NT-a†	DMSO	388	34 000	± 6000
NT-b‡	DMSO	388	32 000	± 5000
NT-c‡	DMSO	388	31 000	± 5000
NT-a*	Tris buffer	372	25 000	± 4000
NT-b*	Tris buffer	372	24 000	± 4000
NT-c*	Tris buffer	372	25 000	± 4000

Table 3.5: Summary of the absorption coefficient at $\lambda_{max,abs}$ in DMSO and Tris buffer pH7.4 20mM (1% DMSO) of the previous generation of nanotriggers.

† Determined by statistical analysis over 7 independant experiments.
‡ Determined by statistical analysis over 5 independant experiments.
* Determined by statistical analysis over 4 independant experiments.

Independant measurements were carried out in order to gain statistical precisions over the results. However, as shown in **Table** 3.5, the observed standard deviation is quite high compared to the previously presented results. This discrepancy can be explained by the use of an older scale, before a much more precise one was purchased. The precision on the weights used in these measurements was two orders of magnitude lower with respect to the ones used in **3.1**, as they were carried out earlier chronologically.

The absorption coefficients measured for compounds **NT-a**, **NT-b** and **NT-c** in DMSO show a maximum at 388nm, very similar to the one observed for **NT-5a**, **NT-5b**, **NT-5c** and **NT-5**. The values obtained are also slightly higher, which can be explained by the addition of the aromatic *anchor* absorbing in that range of wavelength. Interestingly, the absorption spectra of these nanotriggers did not show differences after normalization *versus* the concentration in Tris buffer, as observed previously in **3.1.3.1**. Considering these compounds are functionalized with 2 to 3 carboxylates at pH7.4 because of an additional one on the *anchor* moiety, if the presence of charges is hypothesized as the major factor towards solubility, they should all be at least as soluble as **NT-5a**. This observation is not contradictory of the previously formulated hypothesis on the low solubility of **NT-5b**, **NT-5c** and **NT-5** in Tris buffer.

Compound	Solvent	$\lambda_{max,em}$ (nm)	$\phi_F{}^{\dagger}$	$\sigma^{\dagger}$
NT-a	DMSO	462	0.179	± 0.004
NT-b	DMSO	459	0.218	± 0.003
NT-c	DMSO	462	0.24	± 0.01
NT-a	Tris buffer	466	0.032	± 0.004
NT-b	Tris buffer	474	0.03	± 0.01
NT-c	Tris buffer	477	0.36	± 0.03

Table 3.6: Measured quantum yields of the previous generation of nanotriggers in DMSO and Tris buffer pH7.4 20mM (1% DMSO). Measured with λ_{exc} =390nm in DMSO, λ_{exc} =370nm in Tris buffer.

† Determined by statistical analysis over 2 independant experiments.

The fluorescence quantum yields measured for this series of nanotriggers are slightly lower compared to the newly synthesized ones, as shown in **Table** 3.6. Once more, this fact is consistent with the presence of the *anchor* moiety, bearing an aromatic structure that can absorb light in the range of the excitation wavelength before a non-radiative deactivation. Similarly, this moiety could also absorb the emission of the diarylbutadiene. These remarks are consistent with the lower quantum yield observed, as a lower ratio of photons are absorbed by the diarylbutadiene fluorescent moiety, and some of its fluorescence emission can be re-absorbed by the *anchor*.

Nonetheless, the absorption and emission properties of the previous generation of nanotriggers are quite similar to the those obtained for the new compounds, and the variation can be explained by their structural difference.

3.2.3 Two-photon characterization

The two-photon absorption properties of compounds **NT-a**, **NT-b** and **NT-c** were also investigated. The two-photon equivalent of the molar absorption coefficient ε is called the two-photon absorption cross-section σ_{TPA}, expressed in Goeppert-Mayer (GM) referencing the theorizer of this phenomenon[212]. These measurements require a more sophisticated setup with respect to the one-photon and rely on more complex mathematics[213,214], as slightly discussed in **Appendix C.2**.

[212] Göppert-Mayer, M. *Ann. Phys.* **1931**, *401*, 273–294.
[213] Rumi, M.; Perry, J. W. *Adv. Opt. Photon.* **2010**, *2*, 451–518.
[214] Friedrich, D. M. *J. Chem. Educ.* **1982**, *59*, 472.

The method used in order to determine σ_{TPA} of these nanotriggers involved their two-photon-induced fluorescence (TPIF). In a simple manner, it is very similar to the method used previously to determine the fluorescence quantum yields by comparison with a known reference. The TPIF intensity I_{TPIF} is proportional the two-photon fluorescence quantum yield $\phi_{F,2P}$ and σ_{TPA}:

$$I_{TPIF} \propto \phi_{F,TP} \times \sigma_{TPA}$$

A very commonly used approximation is $\phi_{F,TP} \approx \phi_F$, enabling the calculation of σ_{TPA} for **NT-a**, **NT-b** and **NT-c** knowing their fluorescence quantum yield, by comparison with Coumarin 102 which is a described two-photon reference[215], and fixing every other parameters of the setup, including the laser power. Reasoning on the energy levels of the ground state and emitting excited state, the deactivation pathways of the latter leading to fluorescence and vibrational relaxation should not be so different upon one or two-photon excitation, thus the respective quantum yields should not be far apart. The spectra of two-photon absorption cross-section of **NT-a**, **NT-b** and **NT-c** in DMSO obtained by this method are displayed on **Figure** 3.9.

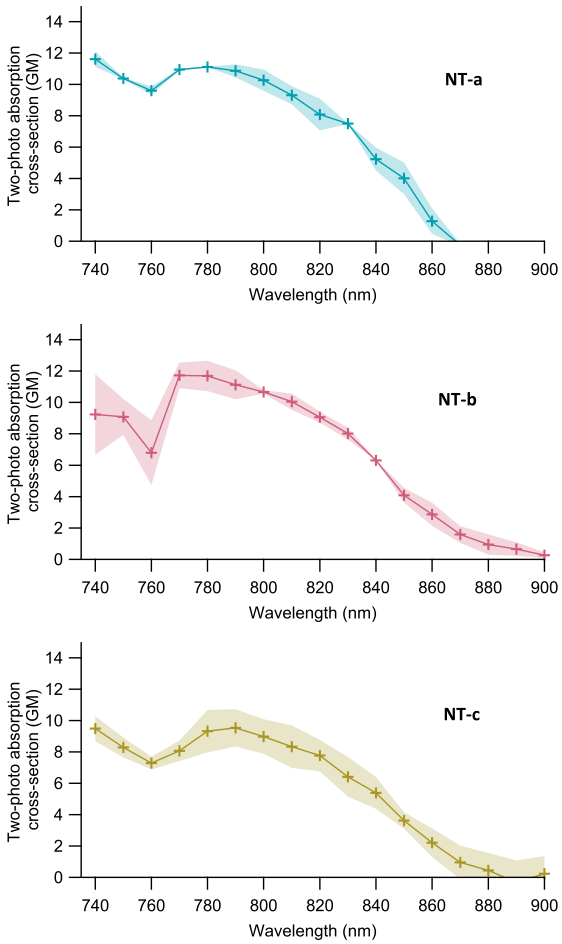

Figure 3.9: Two-photon absorption cross-section (σ_{TPA}) for the previous generation of nanotriggers, expressed in Goeppert-Mayer (GM). Measurements using Coumarin 102 in MeOH as reference: ϕ_F=0.88, $\sigma_{TPA,780nm}$=26 ± 7GM. Mean of two sets of experiments displayed with the standard deviation represented as shaded area. 1GM = 10^{-50}cm^4·s·photon^{-1}.

The $\sigma_{TPA}(\lambda)$ obtained are quite similar, which was expected from the relatively small structural differences between the compounds. Their respective maxima are within the 770−790nm range,

[215] Melnikov, A. S. et al. *J. Phys.: Conf. Ser.* **2017**, *917*, 062029.

consistent with the doubling of the wavelength observed for the one-photon maxima at 390nm. The values described for nanotriggers without an *anchor* (replaced by a methyl group) are about twice higher, around 25GM at 770nm[145]. For the same reasons described earlier, the *anchor* could absorb the fluorescence of the diarylbutadiene moiety, leading to a decrease of σ_{TPA}.

A two-photon excitation of these nanotriggers leading to the same excited state as one-photon is of the highest interest, especially in the context of our studies. Most tissues are much more transparent to red-shifted light enabling an efficient penetration of an excitation beam. Additionally, the usual energetic UV excitation can lead to DNA degradation, possibly interfering with the biological process studied in cellular experiments. The excited state would still be able to induce the electron transfer to the reductase domain, as previously demonstrated[141].

3.3 Conclusion

The synthesized nanotriggers **NT-5a**, **NT-5b**, **NT-5c** and **NT-5** have been characterized in DMSO, with the determination of their molar absorption coefficient ε and fluorescence quantum yields. Excitation spectra were carried out in order to verify the presence of only one emitting entity. Compound **NT-5a** was characterized in a similar fashion in a Tris buffer containing 1% of DMSO. On the other hand, **NT-5b**, **NT-5c** and **NT-5** could not be characterized in this solvent, most likely because of an aggregation process. These properties will be of great use in future cellular experiments.

Another series of nanotriggers, **NT-a**, **NT-b** and **NT-c** bearing an *anchor* have been characterized, with the measurement of their molar absorption coefficient ε and fluorescence quantum yield ϕ_F in DMSO and Tris buffer. The two-photon absorption cross-section σ_{TPA} of these compounds in DMSO was also determined. These spectroscopic properties will be useful in future cellular experiments.

Concluding remarks & prospects

The main matter of this work is based on the synthesis of novel nanotriggers and the spectroscopic studies of their properties.

The first chapter emphasized the context of this research, encompassing therapeutical avenues and new biological studies that could be enabled by light-triggered NO-producing NOS activity because of the high resolutions achievable both in space and time.

The second chapter described the strategies used towards the synthesis of several nanotriggers bearing different linkages. The 5'-amino-5'-deoxyadenosine derivatives serving as recognition moieties could be *O*-alkylated in several steps from adenosine. The photoactivatable moieties were more troublesome to form due to degradation in the HWE olefination step. The desired diarylbutadiene towards amide linkages could not be obtained, but the structure bearing an isothiocyanate towards the formation of a thiourea linkage was synthesized. The latter was successfully coupled with the former adenosines to get the protected thiourea-linked nanotriggers. The protecting groups could be efficiently and cleanly cleaved in a single step, leading to 4 new NADPH mimics.

The third chapter summarized the spectroscopic properties of the 4 new nanotriggers synthesized, displaying similar molar absorption coefficients and fluorescence quantum yields in DMSO with respect to previous results. The compounds could not be all studied in Tris buffer, most likely because of an aggregative behaviour. A previous generation of nanotriggers was studied and successfully characterized in DMSO and Tris buffer with respect to their molar absorption coefficients and fluorescence quantum yields, as well as their two-photon absorption cross-section in DMSO.

The synthesized nanotriggers have yet to be characterized with respect to their two-photon absorption cross-section.

The obtained and characterized nanotriggers should be tested out in cellular experiments in HUVECs, in order to probe their respective activity and compare it to the other generations of nanotriggers already described. Their cytotoxicity, Golgi localization after incubation and photoinduced apoptosis should be investigated and compared with previous work. Their selectivity towards NOSs NADPH binding site should be evaluated *versus* other reductase domains such as DHFR, and if positive, a difference in affinity between the NOSs isoforms should be probed.

Finally, if the previous cellular experiments display an improvement with respect to the previous generations of nanotriggers as modelling experiments suggested, these new nanotriggers might be used to study the angiogenic effect induced by NO, *via* a highly resolved photoreleased dose.

Experimental Section

Contents

1 Materials and methods

Solvents and reagents

Commercial solvents and reagents were used without purification. Reactions conducted under anhydrous conditions were carried out under an argon or dinitrogen atmosphere with glassware dried in a 110°C oven or with a heatgun. Anhydrous solvents were obtained *via* a purification system mBraun MB-SPS-800, giving access to anhydrous DCM, DMF, MeCN, THF and toluene. The solvents water content was checked weekly and compared with reference values obtained by sodium/benzophenone distillation for THF and toluene, or calcium hydride for DCM. Water was purified by a Milli-Q®apparatus by Merck.

Chromatography

TLC analysis were conducted on SDS silica or C18 silica coated aluminium plates with a fluorescent indicator absorbing at 254nm. Revelation was performed either by irradiation with an UV lamp at 254nm or 365nm, or dipping in solutions of sulfuric acid, ninhydrin, vanillin or potassium permanganate, alongside the use of a heatgun to fully reveal the plates. The retention factor (R_f) were measured as a ratio of the length between the highest intensity within a TLC spot over the total distance of eluant migration. The purifications by column chromatography were carried out on SDS silica gel 40-63µm, or on a CombiFlash R_f apparatus from Serlabo with its respective pre-packed silica columns. Precolumns were packed with 63-200µm SDS silica.

HPLC

The HPLCs were carried out on either an apparatus from Shimadzu. Chromatograms were analyzed from a separation with an analytical column made by Phenomenex, a Luna C18 with 5µ particle size, 250mm×4.6mm or a semi-preparative column also made by Phenomenex, a Luna C18 with 5µ particle size, 250mm×10mm. Details about the software processing are presented in **Appendix D.1**.

NMR spectroscopy

NMR spectra were recorded on a JEOL ECS400 spectrometer (400 MHz for ^{1}H, 101 MHz for ^{13}C and 162 MHz for ^{31}P). The chemical shifts δ are expressed in part per million (PPM) using tetramethylsilane (TMS) as a reference if available or the deuterated solvent residual peak[216]. Deuterated solvents were obtained from Eurisotop. The signal multiplicity is described as a combination of the following shapes: singlet (s), doublet (d), triplet (t), quadruplet (q), unresolved multiplet (m) and broad singlet (bs). In order to attribute the ^{13}C signals, distortionless enhancement by polarization transfer (DEPT) experiments[217] enabled to determine the nature of signals obtained by classical ^{13}C or a more recent uniform driven equilibrium Fourier transform (UDEFT) sequence[218]. The carbons signal is attributed as follows: quaternary carbons (C_q), aromatic or vinylic carbons (C_{Ar}). The conversion of NMR spectra into the presented condensed form was performed as presented in **Appendix D.2**. The usual atom numbering of adenosine was used towards the interpretation of NMR spectra for adenosine derivatives, as displayed in **Appendix E**.

Mass spectroscopy

The HRMS analysis were carried out externally at the HRMS platform of the *Institut de Chimie Organique et Analytique* (ICOA) in Orléans (FR 2708 CBM-ICOA).

[216] Gottlieb, H. E. et al. *J. Org. Chem.* **1997**, *62*, 7512–7515.
[217] Doddrell, D. M. et al. *J. Magn. Reson.* **1982**, *48*, 323–327.
[218] Piotto, M. et al. *Magn. Reson. Chem.* **2006**, *44*, 943–947.

UV-Vis absorption spectroscopy

The absorbance spectra were recorded on a Cary-100, Cary-4000 or Cary-5000 made by Agilent. The solvents used were spectroscopic grade. The mass were measured with a microbalance MYA 4Y.P Plus made by Radwag. Some details about the data processing is presented in **Appendix D.3**.

Fluorescence spectroscopy

The fluorescence emission and excitation spectra were recorded on a Fluoromax-3, Fluoromax-4 or Fluorolog-3 from Jobin-Yvon. The solvents used were spectroscopic grade. The mass were measured with a microbalance MYA 4Y.P Plus from Radwag.

Two-photon absorption cross-section

The two-photon absorption cross-section were measured with an available homemade setup[114]. A 80 MHz mode-locked Mai-Tai®Ti:Sapphire tunable laser (690nm−1040nm, 100 fs laser pulse) from Spectra Physics was focused inside of a quartz cuvette. The TPIF was collected at 90°from the excitation beam through an optical fiber towards a QE65000 spectrometer from Ocean Optics. Raw data analysis was carried out as described in **Appendix C.2.3**.

Fusion temperature

Fusion temperature was measured with a Wagner & Munz Köfler WME system, calibrated with Reichert test substances. Fusion temperature are given when a clear solid/liquid interface was observed. Substances bearing the *decomposition* tag would show a clear color change, an ambiguous softening or both around the given temperature.

FTIR

FTIR spectra were recorded on a ThermoFisher FTIR Nexus 670 spectrometer equipped with an ATR module. The absorption bands were interpreted using published references[219]. The vibration modes are described as stretching (*str*) or deformation (*def*), with a symmetric (*sym*) or asymmetric (*asym*) character if three or more atoms are involved.

[219] Socrates, G., *Infrared and Raman Characteristic Group Frequencies: Tables and Charts*, 3rd ed; Wiley: Chichester ; New York, 2001.

2 Synthesis

2.1 General procedures

Azide reduction with palladium and dihydrogen[159]

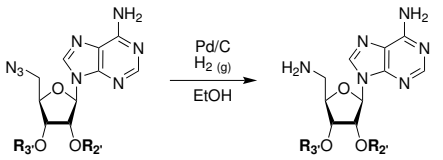

Procedure A: To a solution of functionalized 5'-azido-5'-deoxyadenosine moiety (1 eq.) in EtOH (0.1M) was added 10% palladium on carbon (30wt%). Dihydrogen was introduced in the flask using 3 cycles of vacuum/dihydrogen, and the reaction mixture was stirred at least overnight. The reaction progress was monitored by TLC (DCM/EtOH 95:5) and upon completion the reaction mixture was filtered and solvents were removed under reduced pressure to obtain the desired compound, used without further purification.

Staudinger reduction with supported triphenylphosphine[163]

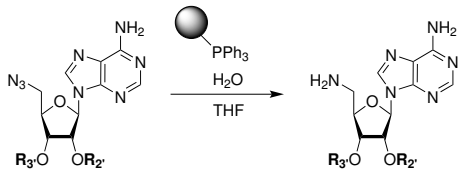

Procedure B: Functionalized 5'-azido-5'-deoxyadenosine (1 eq.), supported triphenylphosphine (1.2 eq.) and distilled water (11 eq.) were stirred in THF (0.075 M) under an argon atmosphere for 4 days. The reaction progress was monitored by TLC (DCM/EtOH 95:5) and upon completion the reaction mixture was filtered over filter paper and solvents were removed under reduced pressure to obtain the desired compound, used without further purification.

Isothiocyanate formation[204]

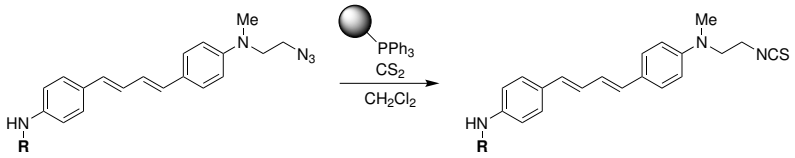

Procedure C: To the azide moiety (1 eq.) was added supported triphenylphosphine (1.5 eq.), carbon disulfide (40 eq.) and anhydrous DCM (0.1 M) before flushing with argon. The mixture was then stirred for 4 days, and was monitored by TLC (DCM/EtOH 95:5 or PE/AcOEt 70:30). Upon completion, the reaction mixture was filtered on a paper filter and solvents were removed under reduced pressure to obtain the desired compound, used without any further purification due to isothiocyanate's poor stability.

Formation of the thiourea linkage[202]

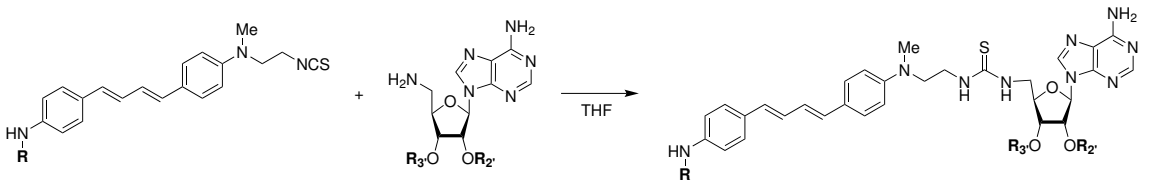

Procedure D: The isothiocyanate moiety (1 eq.) and the functionalized adenosines **A-4x** (1 eq.) were dissolved in THF (0.075 M) and the mixture was stirred under an argon atmosphere for 3 days. The reaction progress was monitored by TLC (DCM/EtOH 95:5) and upon completion solvents were removed under reduced pressure. The crude residue was purified over silica gel (DCM/EtOH from 100:0 to 90:10) or C18 silica ($MeCN/H_2O$ 50:50 to 90:10) to give the desired compound.

2.2 Synthesis of adenosine derivatives

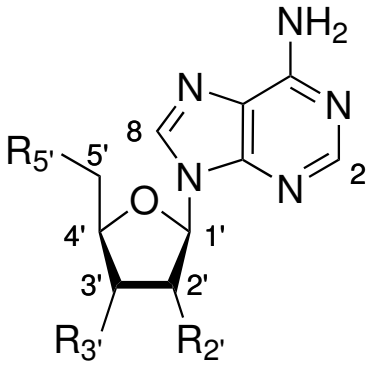

Figure 3.10: Atom numbering used towards NMR attributions based on the commonly accepted nomenclature for adenosine

2',3'-isopropylideneadenosine (A-1)[144,220]

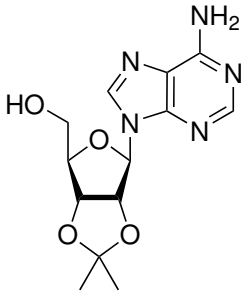

Chemical formula: $C_{13}H_{17}N_5O_4$

Molecular weight: 307.31 g.mol^{-1}

To adenosine (10.0g, 37.4mmol) and PTSA monohydrate (8.54g, 44.9mmol) under an argon atmosphere was added acetone (70mL) and the mixture was stirred until the solids were solubilized. Triethyl orthoformate (22.0mL, 135mmol) was then added, and the reaction medium was stirred for 3 days. The reaction progress was monitored by TLC (AcOEt/EtOH 80:20). Upon completion aqueous ammonia (5mL, 26%wt) and distilled water (100mL) were added, and the mixture was stirred another 10 minute (min) before removing solvents under reduced pressure. Distilled water (50mL) was then added to the dry residue, and the mixture was filtered on a sintered glass funnel, and the solid was further rinsed with distilled water (50mL). The glassware was washed with AcOEt in the filtrate, and the latter was extracted 3 times with AcOEt, organic phases were combined, dried over magnesium sulfate, filtered on cotton and poured over the previously recovered solid in a flask, and dried under reduced pressure to yield 10.71g (93%) of the desired compound as a white solid.

R$_f$: 0.50 (AcOEt/EtOH 80:20)

T$_f$: 216°C

FTIR (cm^{-1}): 3270 (O−H *str*), 3109 (N−H *str*), 2986 (CH_3 *asym str*), 2939 (CH_2 *asym str*), 1684 (C−N= *str*), 1605 (N−H primary aromatic amine *def*), 1571, 1475, 1418, 1375, 1339, 1300, 1240, 1208, 1176, 1157, 1116, 1085, 1036, 1009, 947, 919, 867, 844, 795, 712.

^{1}H NMR (CD_3OD, 400 MHz): δ 8.33 (s, 1H, H_2), 8.20 (s, 1H, H_8), 6.16 (d, 1H, J = 3.6 Hz, H_1'), 5.28 (dd, 1H, J = 6.1, 3.6 Hz, H_2'), 5.04 (dd, 1H, J = 6.1, 2.3 Hz, H_3'), 4.38 (ddd, 1H, J = 3.9, 3.2, 2.3 Hz, H_4'), 3.79 (dd, 1H, J = 12.1, 3.2 Hz, H_{5a}'), 3.71 (dd, 1H, J = 12.1, 3.9 Hz, H_{5b}'), 1.62 (s, 3H, CH_3), 1.38 (s, 3H, CH_3).

^{13}C NMR (CD_3OD, 101 MHz): δ 153.93 (CH_{Ar}), 150.17 (C_q), 141.90 (CH_{Ar}), 115.41 (C_q), 93.00 (CH), 88.24 (CH), 85.45 (CH), 83.13 (CH), 63.72 (CH_2), 27.75 (CH_3), 25.67 (CH_3).

[220] Devkota, K. et al. *ACS Med. Chem. Lett.* **2014**, *5*, 293–297.

5'-azido-5'-deoxy-2',3'-isopropylideneadenosine (A-2)[144,148,221]

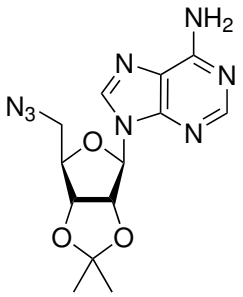

Chemical formula: $C_{13}H_{16}N_8O_3$

Molecular weight: 332.32 g.mol^{-1}

Procedure 1: To a triphenylphosphine (8.14g, 31.0mmol) solution in anhydrous THF (175mL, 0.18M) was added diisopropyl azodicarboxylate (6.1mL, 31mmol) at 0°C, under an argon atmosphere. After stirring for 5min at room temperature, diphenylphosphoryl azide (6.7mL, 31mmol) was added dropwise. Then **A-1** (9.53g, 31.0mmol) was added in two portions and the reaction mixture was stirred in the dark for 4 days. The reaction progress was monitored by TLC (AcOEt/DCM/MeOH 30:10:1). When the reaction did not show further progress, solvents were removed under reduced pressure and the crude residue was purified over silica gel twice (DCM/AcOEt/MeOH from 100:0:0 to 25:72.6:2.4, then DCM/iPrOH from 100:0 to 90:10) to give 6.70g (65%) of the desired compound as a white solid.

Procedure 2: Compound **A-2'** (2.00g, 6.14mmol), sodium azide (676mg, 10.4mmol) and sodium iodide (276mg, 1.84mmol) were dissolved in anhydrous DMF (30mL, 0.2M). The reaction mixture was then stirred and heated at 110°C for 4 days. Solvents were removed under reduced pressure and the crude residue was purified over silica gel (DCM with 1% triethylamine/EtOH from 100:0 to 90:10) to give 1.53g (76%) of the desired compound as a white solid.

R_f: 0.25 (DCM/iPrOH 98:2); 0.49 (AcOEt/DCM/MeOH 30:20:1)

T_f: 140°C

IR (cm^{-1}): 3134 (N−H *str*), 2987 (CH_3 *asym str*), 2102 (N_3 *asym str*), 1687 (C−N= *str*), 1608 (N−H primary aromatic amine *def*), 1576, 1483, 1422, 1376, 1331, 1298, 1259, 1210, 1177, 1155, 1110, 1083, 1042, 1024, 1005, 916, 891, 855, 831, 797, 787, 773, 761, 750, 742, 723, 694, 683.

^{1}H NMR ($CDCl_3$, 400 MHz): δ 8.35 (s, 1H, H_2), 7.95 (s, 1H, H_8), 6.10 (d, 1H, J = 2.3 Hz, H_1'), 6.02 (bs, 2H, NH_2), 5.40 (dd, 1H, J = 6.4, 2.3 Hz, H_2'), 5.03 (dd, 1H, J = 6.4, 3.5 Hz, H_3'), 4.38 (td, 1H, J = 5.5, 3.5 Hz, H_4'), 3.58 (d, 2H, J = 5.5 Hz, H_{5a}',H_{5b}'), 1.60 (s, 3H, CH_3), 1.38 (s, 3H, CH_3).

[221] Swarbrick, J. M. et al. *Chem. Commun.* **2014**, *50*, 2458–2461.

^{13}C NMR (CD_3OD, 101 MHz): δ 157.57 (C_q), 154.19 (CH), 150.41 (C_q), 141.93 (CH), 120.70 (C_q), 115.82 (C_q), 91.72 (CH), 87.05 (CH), 85.29 (CH), 83.44 (CH), 53.47 (CH_2), 27.56 (CH_3), 25.63 (CH_3).

5'-chloro-5'-deoxy-2',3'-isopropylideneadenosine (A-1')[222]

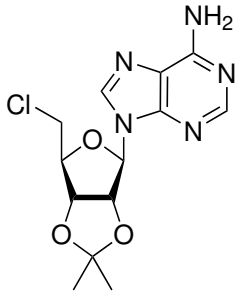

Chemical formula: $C_{13}H_{16}N_5O_3Cl$

Molecular weight: 325.75 g.mol^{-1}

To a solution of **A-2'** (2.92g, 10.2mmol) in acetone (20mL) was added PTSA (2.34g, 12.3mmol), triethyl orthoformate (6.0mL, 36mmol) and the solution was stirred overnight. The progress was monitored by TLC (DCM/EtOH 80:20) and upon completion aqueous ammonia (2.5mL, 26%wt) was added. The reaction mixture was stirred another 10min before removing solvents under reduced pressure. The crude residue was purified over silica gel (DCM/EtOH from 100:0 to 80:20) to give 2.71g (82%) of the desired compound as a white solid.

R$_f$: 0.24 (DCM/EtOH 95:5)

^{1}H NMR (CD$_3$OD, 400 MHz): δ 8.27 (s, 1H, H_2), 8.23 (s, 1H, H_8), 6.23 (d, 1H, J = 2.5 Hz, $H_{1'}$), 5.50 (dd, 1H, J = 6.2, 2.5 Hz, $H_{2'}$), 5.14 (dd, 1H, J = 6.2, 2.9 Hz, $H_{3'}$), 4.47-4.39 (m, 1H, $H_{4'}$), 3.81 (dd, 1H, J = 11.4, 7.0 Hz, $H_{5'a}$), 3.68 (dd, 1H, J = 11.4, 5.6 Hz, $H_{5'b}$), 1.60 (s, 3H, CH_3), 1.39 (s, 3H, CH_3).

^{13}C NMR (DMSO-*d6*, 101 MHz): δ 154.20 (CH_{Ar}), 141.94 (CH_{Ar}), 115.73 (C_q), 92.11 (CH), 88.09 (CH), 85.46 (CH), 84.25 (CH), 44.87 (CH_2), 27.50 (CH_3), 25.58 (CH_3).

[222] Tang, K.-C. et al. *J. Med. Chem.* **1981**, *24*, 1277–1284.

5'-chloro-5'-deoxyadenosine (A-2')[223,156]

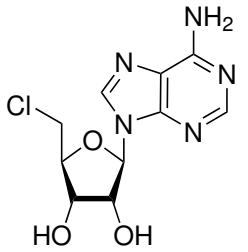

Chemical formula: $C_{10}H_{12}N_5O_3Cl$

Molecular weight: 285.69 g.mol^{-1}

To a stirred solution of adenosine (11.55g, 43.22mmol) in anhydrous MeCN (145mL) was added pyridine (7.0mL, 86mmol), then the reaction mixture was placed in an ice bath. Thionyl chloride (15.7mL, 216mmol) was added slowly to the reaction medium, before flushing with dinitrogen, removing the ice bath and stirring overnight. The next day a precipitate had formed. The flask was placed on an ice bath, then the mixture was filtered on sintered glass. The residue was dissolved in a mixture of MeOH and distilled water (240mL, 5:1) before adding aqueous ammonia (20mL, 26%wt), stirring for 10 min and removing solvents under reduced pressure. The crude residue was purified by recristallisation in water to give 10.68g (87%) of the desired compound as a white solid.

R_f: 0.52 (AcOEt/EtOH 80:20)

$T_{decomposition}$: 96°C

IR (cm^{-1}): 3324 (N−H *str*), 3169 (N−H *str*), 2990 (CH_3 *asym str*), 1646 (C−N= *str*), 1599 (N−H primary aromatic amine *def*), 1476, 1425, 1375, 1330, 1298, 1210, 1156, 1078, 1010, 909, 871, 799, 782, 769, 751, 724, 684.

^{1}H NMR (DMSO-*d6*, 400 MHz): δ 8.35 (s, 1H, H_2), 8.16 (s, 1H, H_8), 7.33 (bs, 2H, NH_2), 5.93 (d, 1H, J = 5.6 Hz, H_1'), 5.62 (d, 1H, J = 6.0 Hz, $O_{2'}H$), 5.48 (d, 1H, J = 5.2 Hz, $O_{3'}H$), 4.75 (ddd, 1H, J = 6.0, 5.6, 5.0 Hz, H_2'), 4.22 (ddd, 1H, J = 5.2, 5.0, 3.7 Hz, H_3'), 4.09 (ddd, 1H, J = 6.3, 5.1, 3.7 Hz, H_4'), 3.94 (dd, 1H, J = 11.5, 5.1 Hz, H_{5a}'), 3.84 (dd, 1H, J = 11.5, 6.3 Hz, H_{5b}').

^{13}C NMR (DMSO-*d6*, 101 MHz): δ 156.13 (C_q), 152.76 (C_2), 149.47 (C_q), 139.78 (C_8), 119.14 (C_q), 87.41 (CH), 83.69 (CH), 72.64 (CH), 71.28 (CH), 44.84 (CH_2).

[223] Anglin, J. L. et al. *J. Med. Chem.* **2012**, *55*, 8066–8074.

5'-azido-5'-deoxyadenosine (A-3)[144,152]

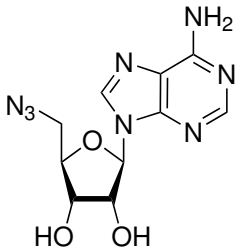

Chemical formula: $C_{10}H_{12}N_8O_3$

Molecular weight: 292.26 g.mol^{-1}

Procedure 1: **A-2** (1.02g, 3.05mmol) was added to a 0°C mixture of TFA (5.75mL) and distilled water (0.60mL) under dinitrogen atmosphere, and upon dissolution of the solid after 35 min, the reaction mixture was allowed to warm up to room temperature and stirred for another 1.25 hour (hr). The reaction mixture was then evaporated under reduced pressure with a temperature not rising above 20°C. The crude residue was then purified over silica gel (AcOEt/EtOH from 100:0 to 60:40) to give 787mg (88%) of the desired compound as a white foam.

Procedure 2: To **A-2'** (2.02g, 7.07mmol), sodium azide (781mg, 12.0mmol) and sodium iodide (321mg, 2.14mmol) was added anhydrous DMF (40mL, 0.18M), before stirring the mixture at 110°C overnight. The reaction progress was monitored by ^{1}H NMR, and upon completion solvents were removed under reduced pressure. The crude residue was purified over silica gel (DCM/MeOH from 100:0 to 80:20) to give 1.92g (93%) of the desired compound as a white foam.

R_f: 0.39 (AcOEt/EtOH 80:20)

T_f: 116°C

IR (cm^{-1}): 3320 (O−H *str* & N−H *str*), 3141 (N−H *str*), 2107 (N_3 *asym str*), 1677, 1648 (C−N= *str*), 1610 (N−H primary aromatic amine *def*), 1575, 1480, 1425, 1339, 1291, 1250, 1215, 1126, 1075, 1062, 1043, 1007, 924, 906, 841, 795, 767, 758, 749, 742, 725, 706, 695, 681.

^{1}H NMR (DMSO-*d6*, 400 MHz): δ 8.36 (s, 1H, H_2), 8.16 (s, 1H, H_8), 7.32 (bs, 2H, NH_2), 5.92 (d, 1H, *J* = 5.5 Hz, H_1'), 5.58 (d, 1H, *J* = 5.9 Hz, $O_{2'}H$), 5.39 (d, 1H, *J* = 5.2 Hz, $O_{3'}H$), 4.75 (ddd, 1H, *J* = 5.9, 5.5, 4.9 Hz, H_2'), 4.19 (ddd, 1H, *J* = 5.2, 4.9, 3.8 Hz, H_3'), 4.04 (ddd, 1H, *J* = 7.1, 3.8, 3.7 Hz, H_4'), 3.69 (dd, 1H, *J* = 13.1, 7.1 Hz, H_{5a}'), 3.54 (dd, 1H, *J* = 13.1, 3.7 Hz, H_{5b}').

^{13}C NMR (DMSO-*d6*, 101 MHz): δ 155.60 (C_q), 152.04 (C_2), 149.31 (C_q), 140.16 (C_8), 119.16 (C_q), 87.73 (CH), 83.00 (CH), 72.74 (CH), 70.91 (CH), 51.69 (CH_2).

_O_-alkylation of A-3

Sodium hydride (60w% dispersed in mineral oil, 150mg, 3.75mmol) was added to anhydrous DMF (17mL) under dinitrogen atmosphere, and the suspension was cooled down to 0°C. 5'-Azido-adenosine (1.00g, 3.42mmol) was then added in 3 portions, with dihydrogen release. A low temperature bath was prepared using acetone and liquid dinitrogen, with a target temperature range between -40°C and -45°C. The reaction mixture was placed in the cold bath which was kept within the same temperature range during the addition of *tert*-butylbromoacetate (550µL, 3.73mmol) at a slow rate of around 1 drop every 2s. After the addition was completed, liquid dinitrogen was not added anymore to the cold bath to allow the reaction mixture to slowly warm up. Upon reaching a bath temperature of -25°C, it was removed and the reaction medium was stirred at room temperature overnight. The reaction progress was monitored by TLC (DCM/EtOH 95:5), and a saturated solution of ammonium chloride (15mL) was added when the latter showed no more evolution. The mixture was stirred for 10mins before removing solvents under reduced pressure. The crude residue was purified over silica gel (DCM/EtOH from 100:0 to 90:10 over 90 min) to give 377mg (21%) of **A-3a**, 371mg (27%) of **A-3b** and 169mg (12%) of **A-3c** as white foams.

5'-azido-5'-deoxy-2',3'-di(methyl *tert*-butoxycarbonyl)adenosine (A-3a)[145]

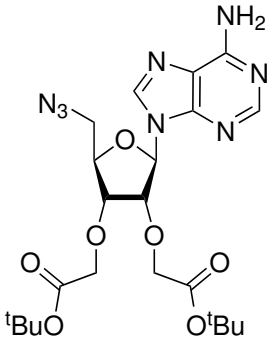

Chemical formula: $C_{22}H_{32}N_8O_7$

Molecular weight: 520.55 g.mol^{-1}

R$_f$: 0.35 (DCM/EtOH 95:5)

T$_f$: 58°C

IR (cm^{-1}): 3335 (N−H *str*), 3184 (N−H *str*), 2979 (CH_3 *asym str*), 2932 (CH_2 *asym str*), 2104 (N_3 *asym str*), 1741 (C=O ester *str*), 1641 (C−N= *str*), 1597 (N−H primary aromatic amine *def*), 1475, 1424, 1394, 1368, 1330, 1296, 1237, 1145, 1091, 920, 846, 823, 799, 779, 740, 725, 692, 683.

^{1}H NMR (CD_3OD, 400 MHz): δ 8.31 (s, 1H, H_2), 8.20 (s, 1H, H_8), 6.19 (d, 1H, J = 4.6 Hz, H_1'), 4.97 (dd, 1H, J = 5.2, 4.6 Hz, H_2'), 4.47 (t, 1H, J = 5.2 Hz, H_3'), 4.36-4.31 (m, 1H, H_4'), 4.30-4.25 (m, 2H, CH_2), 4.23 (s, 2H, CH_2), 3.77-3.65 (m, 2H, H_{5a}',H_{5b}'), 1.51 (s, 9H, ^{t}Bu), 1.39 (s, 9H, ^{t}Bu).

^{13}C NMR (CD_3OD, 101 MHz): δ 171.53 (C_q), 171.18 (C_q), 157.48 (C_q), 154.04 (CH), 150.74 (C_q), 141.90 (CH), 120.86 (C_q), 89.14 (CH), 83.18 ($2C_q$), 83.07 (CH), 81.64 (CH), 79.44 (CH), 69.24 ($2CH_2$), 53.01 (CH_2), 28.52 ($3CH_3$ (^{t}Bu)), 28.40 ($3CH_3$ (^{t}Bu)).

5'-azido-5'-deoxy-2'-(methyl *tert*-butoxycarbonyl)adenosine (A-3b)[145]

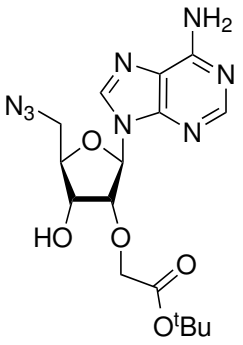

Chemical formula: $C_{16}H_{22}N_8O_5$

Molecular weight: 406.40 g.mol^{-1}

R_f: 0.23 (DCM/EtOH 95:5)

T_f: 130°C

IR (cm^{-1}): 3336 (O−H *str* & N−H *str*), 3179 (N−H *str*), 2983 (CH_3 *asym str*), 2929 (CH_2 *asym str*), 2105 (N_3 *asym str*), 1746 (C=O ester *str*), 1724, 1654 (C−N= *str*), 1597 (N−H primary aromatic amine *def*), 1577, 1483, 1443, 1425, 1414, 1394, 1367, 1353, 1331, 1295, 1252, 1242, 1161, 1145, 1133, 1123, 1088, 1049, 1008, 987, 935, 890, 852, 830, 799, 767, 741, 731, 687.

^{1}H NMR (CD_3OD, 400 MHz): δ 8.31 (s, 1H, H_2), 8.21 (s, 1H, H_8), 6.18 (d, 1H, J = 4.7 Hz, H_1'), 4.81 (dd, 1H, J = 5.2, 4.7 Hz, H_2'), 4.50 (dd, 1H, J = 5.2, 4.9 Hz, H_3'), 4.21 (s, 2H, CH_2), 4.20-4.15 (m, 1H, H_4'), 3.71-3.57 (m, 2H, H_{5a}', H_{5b}'), 1.39 (s, 9H, ^{t}Bu).

^{13}C NMR (DMSO-*d6*, 101 MHz): δ 171.82 (C_q), 157.48 (C_q), 154.07 (CH), 150.78 (C_q), 141.87 (CH), 120.80 (C_q), 88.93 (CH), 84.69 (CH), 83.48 (C_q), 83.41 (CH), 71.73 (CH), 69.76 (CH_2), 53.07 (CH_2), 28.34 ($3CH_3$ (^{t}Bu)).

5'-azido-5'-deoxy-3'-(methyl *tert*-butoxycarbonyl)adenosine (A-3c)[145]

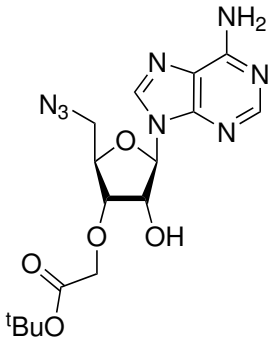

Chemical formula: $C_{16}H_{22}N_8O_5$

Molecular weight: 406.40 g.mol^{-1}

R$_f$: 0.17 (DCM/EtOH 95:5)

T$_f$: 84°C

IR (cm^{-1}): 3324 (O−H *str* & N−H *str*), 3175 (N−H *str*), 2980 (CH_3 *asym str*), 2931 (CH_2 *asym str*), 2105 (N_3 *asym str*), 1739 (C=O ester *str*), 1644 (C−N= *str*), 1601 (N−H primary aromatic amine *def*), 1578, 1477, 1426, 1394, 1370, 1331, 1296, 1249, 1141, 1084, 911, 848, 834, 809, 797, 780, 770, 760, 750, 736, 724, 702, 690, 680.

^{1}H NMR (CD_3OD, 400 MHz): δ 8.30 (s, 1H, H_2), 8.21 (s, 1H, H_8), 6.03 (d, 1H, J = 4.7 Hz, H_1'), 4.94-4.90 (m, 1H, H_2'), 4.37-4.32 (m, 1H, H_3'), 4.32-4.28 (m, 1H, H_4'), 4.28-4.19 (m, 2H, CH_2), 3.72-3.64 (m, 2H, H_{5a}', H_{5b}'), 1.50 (s, 9H, ^{t}Bu).

^{13}C NMR (CD_3OD, 101 MHz): δ 172.08 (C_q), 157.51 (C_q), 154.11 (CH), 150.82 (C_q), 141.53 (CH), 120.68 (C_q), 90.31 (CH), 83.47 (C_q), 83.11 (CH), 81.14 (CH), 74.34 (CH), 69.61 (CH_2), 53.14 (CH_2), 28.45 ($3CH_3$).

5'-amino-5'-deoxyadenosine (A-4)[160]

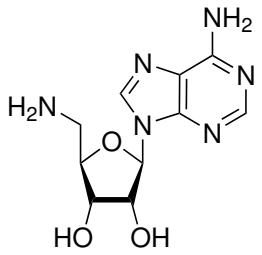

Chemical formula: $C_{10}H_{14}N_6O_3$

Molecular weight: 266.26 g.mol^{-1}

Compound obtained using procedure A and B on **A-3**, yielding respectively 126mg (90%) and 52mg (19%) of the desired compound as a white solid.

R_f: 0.05 (DCM/EtOH 80:20)

$T_{decomposition}$: 143°C

IR (cm^{-1}): 3296 (O−H *str* & N−H *str*), 3142 (N−H *str*), 2932 (CH_2 *asym str*), 1683, 1651 (C−N= *str*), 1607 (N−H primary aromatic amine *def*), 1578, 1477, 1421, 1373, 1332, 1295, 1250, 1202, 1131, 1074, 1052, 1013, 967, 902, 835, 828, 818, 797, 770, 751, 722, 709, 702.

^{1}H NMR (CD_3OD, 400 MHz): δ 8.26 (s, 1H, H_2), 8.20 (s, 1H, H_8), 5.96 (d, 1H, J = 5.6 Hz, H_1'), 4.81 (t, 1H, J = 5.6 Hz, H_2'), 4.30 (dd, 1H, J = 5.6, 3.8 Hz, H_3'), 4.16-4.08 (m, 1H, H_4'), 3.10-3.01 (m, 2H, H_{5a}', H_{5b}').

^{13}C NMR (DMSO-*d6*, 101 MHz): δ 156.12 (C_q), 152.58 (CH), 149.41 (C_q), 140.16 (CH), 119.31 (C_q), 87.50 (CH), 85.39 (CH), 72.90 (CH), 70.87 (CH), 43.43 (CH_2).

HRMS: m/z calculated for $C_{10}H_{15}N_6O_3$ $[M+H]^+$ 267.1200, found: 267.1201;
calculated for $C_{10}H_{16}N_6O_3$ $[M+2H]^{2+}$ 134.0636, found 134.0640;
calculated for $C_{10}H_{14}N_6NaO_3$ $[M+Na]^+$ 289.1020, found 289.1022.

5'-amino-5'-deoxy-2',3'-isopropylideneadenosine (A-4i)

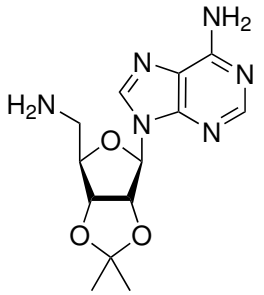

Chemical formula: $C_{13}H_{18}N_6O_3$

Molecular weight: 306.33 g.mol^{-1}

Compound obtained using procedure B on **A-2**, yielding 395mg (99%) of the desired compound as a white solid.

R$_f$: 0.11 (AcOEt/EtOH 70:30)

T$_{decomposition}$: 160°C

IR (cm^{-1}): 3299 (N−H *str*), 3148 (N−H *str*), 2989 (CH_3 *asym str*), 2936 (CH_2 *asym str*), 1678, 1646 (C−N= *str*), 1603 (N−H primary aromatic amine *def*), 1572, 1508, 1475, 1421, 1374, 1332, 1303, 1242, 1210, 1155, 1083, 1009, 969, 908, 872, 798, 757, 745, 707, 692, 680.

^{1}H NMR (CD_3OD, 400 MHz): δ 8.28 (s, 1H, H_2), 8.21 (s, 1H, H_8), 6.19-6.06 (m, 1H, $H_{1'}$), 5.45-5.40 (m, 1H, $H_{2'}$), 5.07-4.92 (m, 1H, $H_{3'}$'), 4.24-4.08 (m, 1H, H4'), 2.81-2.67 (m, 2H, $H_{5'a}$, $H_{5'b}$), 1.60 (s, 3H, CH_3), 1.38 (s, 3H, CH_3).

^{13}C NMR (DMSO-*d6*, 101 MHz): δ 156.15 (C_q), 152.73 (CH), 148.96 (C_q), 139.99 (CH), 119.17 (C_q), 113.17 (C_q), 89.12 (CH), 86.68 (CH), 82.71 (CH), 81.60 (CH), 43.50 (CH_2), 27.06 (CH_3), 25.24 (CH_3).

HRMS: m/z calculated for $C_{13}H_{19}N_6O_3$ $[M+H]^+$ 307.1513, found 307.1514;
calculated for $C_{13}H_{20}N_6O_3$ $[M+2H]^{2+}$ 154.0793, found 154.0798.

5'-amino-5'-deoxy-2',3'-di(methyl *tert*-butoxycarbonyl)adenosine (A-4a)

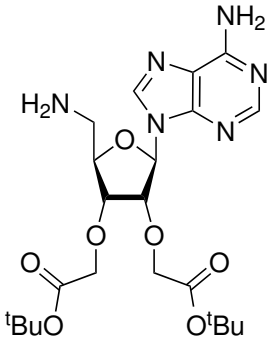

Chemical formula: $C_{22}H_{34}N_6O_7$

Molecular weight: 494.55 g.mol^{-1}

Compound obtained using procedure A and B on **A-3a**, yielding respectively 127mg (90%) and 363mg (quantitative) of the desired compound as a white solid.

R_f: 0.09 (DCM/EtOH 95:5); 0.32 (DCM/EtOH 80:20)

$T_{decomposition}$: 65°C

IR (cm^{-1}): 3330 (N−H *str*), 3183 (N−H *str*), 2976 (CH_3 *asym str*), 2936 (CH_2 *asym str*), 1742 (C=O ester *str*), 1644 (C−N= *str*), 1598 (N−H primary aromatic amine *def*), 1577, 1475, 1424, 1393, 1368, 1329, 1298, 1235, 1145, 1122, 1090, 1039, 943, 919, 848, 823, 799, 776, 764, 748, 742, 726, 710, 693, 685.

^{1}H NMR (CD_3OD, 400 MHz): δ 8.47 (s, 1H, H_2), 8.13 (s, 1H, H_8), 7.32 (bs, 4H, 2xNH_2), 6.08 (d, J = 5.7 Hz, 1H, $H_{1'}$), 4.87 (dd, J = 5.7, 4.5 Hz, 1H, $H_{2'}$), 4.36-4.27 (m, 2H, $H_{3'}$,$H_{4'}$), 4.25-4.21 (m, 2H, CH_2), 4.21-4.17 (m, 2H, CH_2), 3.49-3.42 (m, 2H, $H_{5'a}$,$H_{5'b}$), 1.43 (s, 9H, ^{t}Bu), 1.33 (s, 9H, ^{t}Bu).

^{13}C NMR (DMSO-*d6*, 101 MHz): δ 169.26 (C_q), 168.80 (C_q), 156.20 (C_q), 152.60 (CH), 149.07 (C_q), 140.11 (CH), 119.46 (C_q), 86.20 (2CH), 80.94 (2C_q), 79.01 (CH), 77.71 (CH), 67.10 (CH_2), 60.73 (CH_2), 60.30 (CH_2), 27.77 (CH_3 (^{t}Bu)), 27.58 (CH_3 (^{t}Bu)).

HRMS: m/z calculated for $C_{22}H_{35}N_6O_7$ $[M+H]^+$ 495.2562, found 495.2564;
calculated for $C_{22}H_{34}N_6NaO_7$ $[M+Na]^+$ 517.2381, found 517.2380.

5'-amino-5'-deoxy-2'-(methyl *tert*-butoxycarbonyl)adenosine (A-4b)

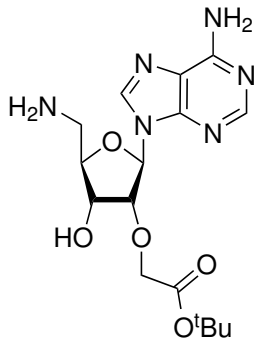

Chemical formula: $C_{16}H_{24}N_6O_5$

Molecular weight: 380.41 g.mol^{-1}

Compound obtained using procedure A and B on **A-3b**, yielding respectively 120mg (82%) and 196mg (54%) of the desired compound as a white solid.

R_f: 0.06 (DCM/EtOH 95:5); 0.16 (DCM/EtOH 80:20)

$T_{decomposition}$: 89°C

IR (cm^{-1}): 3332 (O−H *str* & N−H *str*), 3181 (N−H *str*), 2976 (CH_3 *asym str*), 2932 (CH_2 *asym str*), 1740 (C=O ester *str*), 1646 (C−N= *str*), 1600 (N−H primary aromatic amine *def*), 1576, 1476, 1423, 1369, 1330, 1300, 1246, 1141, 1077, 1001, 909, 842, 825, 799, 749, 728, 694, 679.

^{1}H NMR (DMSO-*d6*, 400 MHz): δ 8.45 (s, 1H, H_2), 8.13 (s, 1H, H_8), 7.30 (bs, 4H, 2xNH_2), 6.10-6.04 (m, 1H, $H_{1'}$), 5.34-5.28 (m, 1H, $H_{2'}$), 4.74-4.64 (m, 1H, $H_{3'}$), 4.39-4.29 (m, 1H, $H_{4'}$), 4.18-4.08 (m, 3H, CH_2; OH), 3.52-3.41 (m, 2H, $H_{5'a}$,$H_{5'b}$), 1.31 (s, 9H, ^{t}Bu).

^{13}C NMR (CD_3OD, 101 MHz): δ 171.89 (C_q), 157.55 (C_q), 153.94 (CH), 150.77 (C_q), 142.55 (CH), 121.12 (C_q), 89.23 (CH), 86.79 (CH), 83.42 (C_q), 83.41 (CH), 71.90 (CH), 69.68 (CH_2), 44.56 (CH_2), 28.31 ($3CH_3$ (^{t}Bu)).

HRMS: m/z calculated for $C_{16}H_{25}N_6O_5$ $[M+H]^+$ 381.1881, found 381.1885;
calculated for $C_{16}H_{24}N_6NaO_5$ $[M+Na]^+$ 403.1700, found 403.1707.

5'-amino-5'-deoxy-3'-(methyl *tert*-butoxycarbonyl)adenosine (A-4c)

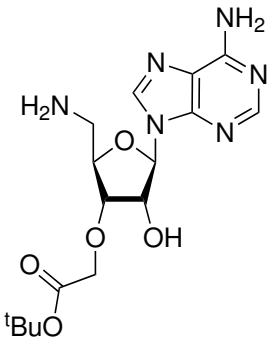

Chemical formula: $C_{16}H_{24}N_6O_5$

Molecular weight: 380.41 g.mol^{-1}

Compound obtained using procedure A and B on **A-3c**, yielding respectively 45mg (31%) and 71mg (35%) of the desired compound as a white solid.

R_f: 0.05 (DCM/EtOH 95:5); 0.11 (DCM/EtOH 80:20)

^{1}H NMR (CD_3OD, 400 MHz): δ 8.27 (s, 1H, H_2), 8.17 (s, 1H, H_8), 5.95 (d, J = 5.5 Hz, 1H, $H_{1'}$), 4.88-4.84 (m, 1H, $H_{2'}$), 4.30-4.18 (m, 4H, CH_2,$H_{3'}$,$H_{4'}$), 3.04-2.97 (m, 2H, $H_{5'a}$,$H_{5'b}$), 1.51 (s, 9H, ^{t}Bu).

^{13}C NMR (DMSO-*d6*, 101 MHz): δ 169.64 (C_q), 156.11 (C_q), 152.56 (CH), 149.44 (C_q), 140.09 (CH), 119.30 (C_q), 87.28 (CH), 84.08 (CH), 80.90 (C_q), 79.22 (CH), 72.37 (CH), 67.70 (CH_2), 43.61 (CH_2), 27.79 ($3CH_3$ (^{t}Bu)).

2.3 Synthesis of the photoactivatable moieties towards an amide linkage

ethyl 3-(methyl(phenyl)amino)propanoate (D1-1)

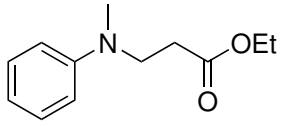

Chemical formula: $C_{12}H_{17}NO_2$

Molecular weight: 207.27 g.mol^{-1}

Ethyl acrylate (6.0mL, 55mmol) and *N*-methyl anilline (5.0mL, 46mmol) were mixed under an argon atmosphere, before dropwise addition of acetic acid (0.31mL, 4.6mmol) and heating at 190°C for 3hrs. The reaction progress was monitored by TLC (PE/AcOEt 10:1) and when no further advance was observed, heating was stopped and when the mixture cooled down, an aqueous saturated solution of sodium hydrogenocarbonate was added. The mixture was then extracted 3 times with DCM, organic phases were combined, dried over magnesium sulfate, filtered over cotton and solvents were removed under reduced pressure. The crude obtained, while still containing a small amount of ethyl acrylate (8.0mol%) and *N*-methylaniline (13.1mol%) as determined by ^{1}H NMR, was used in the next step without further purification.

R$_f$: 0.53 (PE/AcOEt 10:1)

^{1}H NMR (CDCl$_3$, 400 MHz): δ 7.27-7.22 (m, 2H, 2H$_{Ar}$), 6.75-6.69 (m, 3H, 3H$_{Ar}$), 4.10 (q, 2H, *J* = 7.2 Hz, O-CH$_2$), 3.65 (t, 2H, *J* = 7.2 Hz, CH$_2$), 2.92 (s, 3H, N-CH$_3$), 2.55 (t, 2H, *J* = 7.2 Hz, CH$_2$), 1.22 (t, 3H, *J* = 7.2 Hz, CH$_3$).

ethyl 3-((4-formylphenyl)(methyl)amino)propanoate (D1-2)

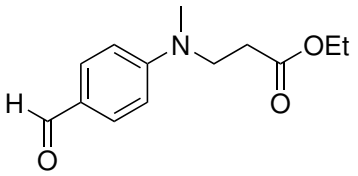

Chemical formula: $C_{13}H_{17}NO_3$

Molecular weight: 235.28 g.mol^{-1}

Phosphoryl chloride (4.34mL, 46.4mmol) was added dropwise to anhydrous DMF (130mL) at 0°C and stirred for 10mins. Then a solution of **D1-1** (9.61g, 46.4mmol) in anhydrous DMF (80mL) was added slowly at 0°C. After stirring 45mins at room temperature, the reaction mixture was heated at 90°C overnight. The reaction progress was monitored by TLC (PE/AcOEt 80:20) and upon maximum progress, an aqueous saturated solution of sodium hydrogenocarbonate was added until the formation of carbon dioxide bubbles stopped. The mixture was then extracted 3 times with ethyl acetate, after addition of an aqueous saturated solution of ammonium chloride and water. Organic phases were combined, dried over magnesium sulfate, filtered over cotton and solvents were removed under reduced pressure. The crude residue was purified over silica gel (PE/AcOEt from 90:10 to 70:30) to give 6.12g (57% over 2 steps) as an orange oil.

R_f: 0.21 (PE/AcOEt 80:20)

IR (cm^{-1}): 1729 (C=O ester *str*), 1680 (C=O aryl aldehyde *str*), 1594, 1557, 1526, 1374, 1314, 1241, 1166, 1112, 1045, 817.

^{1}H NMR ($CDCl_3$, 400 MHz): δ 9.76 (s, 1H, CHO), 7.75 (d, 2H, J = 8.6 Hz, 2H$_{Ar}$), 6.75 (d, 2H, J = 8.6 Hz, 2H$_{Ar}$), 4.14 (q, 2H, J = 7.2 Hz, O-CH_2), 3.78 (t, 2H, J = 7.2 Hz, CH_2), 3.08 (s, 3H, N-CH_3), 2.62 (t, 2H, J = 7.2 Hz, CH_2), 1.25 (t, 3H, J = 7.2 Hz, CH_3).

^{13}C NMR ($CDCl_3$, 101 MHz): δ 190.47 (CHO), 171.82 (C_q), 153.09 (C_q), 132.29 (2CH), 125.72 (C_q), 111.27 (2CH), 61.03 (CH_2), 48.24 (CH_2), 38.72 (CH_2), 32.17 (CH_3), 14.32 (CH_3).

HRMS: m/z calculated for $C_{13}H_{18}NO_3$ $[M+H]^+$ 236.1281, found 236.1286;
calculated for $C_{13}H_{17}NNaO_3$ $[M+Na]^+$ 258.1101, found 258.1106.

ethyl (*E*)-3-(methyl(4-(3-oxoprop-1-en-1-yl)phenyl)amino)propanoate (D1-3)

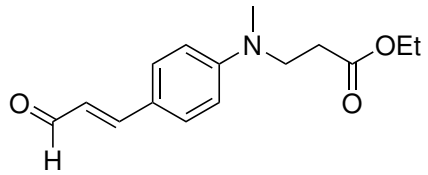

Chemical formula: $C_{15}H_{19}NO_3$

Molecular weight: 261.32 g.mol^{-1}

To a stirred sodium hydride (60w% dispersed in mineral oil, 93.7mg, 2.34mmol) suspension in anhydrous THF (10mL) at 0°C under an argon atmosphere was added dropwise a solution of **R-2** (1.03g, 2.76mmol) in anhydrous THF (5mL). The mixture was stirred 20mins at room temperature before the addition of a solution of **D1-2** (504mg, 2.13mmol) in anhydrous THF (10mL). The reaction was then stirred overnight at room temperature. The reaction progress was monitored by TLC (PE/AcOEt 80:20) and upon completion the mixture was cooled down to 0°C before addition of an aqueous solution of hydrochloric acid (25mL, 0.1M), then solvents were removed under reduced pressure. The residue was extracted 3 times with DCM after addition of distilled water. Organic phases were combined, dried over magnesium sulfate, filtered over cotton and solvents were removed under reduced pressure. The crude was purified over silica gel (PE/AcOEt from 100:0 to 70:30) to give 447mg (80%) of the desired compound as a dark red oil.

R_f: 0.16 (PE/AcOEt 80:20)

IR (cm^{-1}): 1728 (C=O ester *str*), 1663 (C=O α,β insaturated aldehyde *str*), 1592, 1523, 1374, 1329, 1262, 1215, 1185, 1135, 1116, 1045, 967, 809.

^{1}H NMR ($CDCl_3$, 400 MHz): δ 9.32 (d, 1H, *J* = 7.8 Hz, CHO), 7.31 (d, 2H, *J* = 9.0 Hz, 2H$_{Ar}$), 7.26 (d, 1H, *J* = 15.6 Hz, CH=C$_q$), 6.56 (d, 2H, *J* = 9.0 Hz, 2H$_{Ar}$), 6.27 (dd, 1H, *J* = 15.6, 7.8 Hz, CH=C), 3.83 (q, 2H, *J* = 7.1 Hz, CH_2), 3.52 (t, 2H, *J* = 7.1 Hz, CH_2), 2.80 (s, 3H, N-CH_3), 2.36 (t, 2H, *J* = 7.1 Hz, CH_2), 0.94 (t, 3H, *J* = 7.1 Hz, CH_3).

^{1}H NMR (DMSO-*d6*, 400 MHz): δ 10.03 (d, 1H, *J* = 7.8 Hz, CHO), 8.02 (d, 2H, *J* = 9.0 Hz, 2H$_{Ar}$), 7.97 (d, 1H, *J* = 15.6 Hz, CH=C$_{Ar}$), 7.26 (d, 2H, *J* = 9.0 Hz, 2H$_{Ar}$), 6.98 (dd, 1H, *J* = 15.6, 7.8 Hz, CH=C), 4.53 (q, 2H, *J* = 7.1 Hz, CH_2), 4.23 (t, 2H, *J* = 7.1 Hz, CH_2), 3.51 (s, 3H, N-CH_3), 3.07 (t, 2H, *J* = 7.1 Hz, CH_2), 1.65 (t, 3H, *J* = 7.1 Hz, CH_3).

^{13}C NMR ($CDCl_3$, 101 MHz): δ 194.01 (CHO), 172.00 (C$_q$), 153.92 (=CH), 151.00 (C$_q$), 130.84 (2CH$_{Ar}$), 124.29 (=CH), 122.38 (C$_q$), 112.04 (2CH$_{Ar}$), 61.02 (CH_2), 48.31 (CH_2), 38.61 (CH_2), 32.18 (CH_3), 14.37 (CH_3).

HRMS: *m*/*z* calculated for $C_{15}H_{19}NO_3$ $[M+H]^+$ 262.1438, found 262.1437;
calculated for $C_{15}H_{19}NNaO_3$ $[M+Na]^+$ 284.1257, found 284.1254.

(*E*)-3-(methyl(4-(3-oxoprop-1-en-1-yl)phenyl)amino)propanoic acid (D1-4)

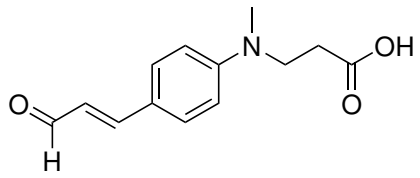

Chemical formula: $C_{13}H_{15}NO_3$

Molecular weight: 233.27 g.mol^{-1}

To a solution of **D1-3** (200mg, 0.77mmol) in anhydrous THF (20mL) was added an aqueous solution of sodium hydroxide (1.20mL, 1M) before stirring overnight at room temperature. The reaction progress was monitored by TLC (DCM/EtOH 95:5) and upon completion the reaction mixture was acidified until *p*H = 2 with an aqueous solution of hydrochloric acid (1M). The solution was then extracted 3 times with DCM, organic phases were combined, dried over magnesium sulfate, filtered over cotton and solvents removed under reduced pressure to give 170mg (73%) of the desired compound as a dark red solid.

R$_f$: 0.37 (DCM/EtOH 95:5)

T$_f$: 130°C

IR (cm^{-1}): 2917 (CH_2 *asym str*), 1730 (C=O carboxylic acid *str*), 1641 (C=O α,β insaturated aldehyde *str*), 1580, 1521, 1461, 1438, 1382, 1351, 1325, 1299, 1274, 1219, 1179, 1149, 1124, 1038, 1012, 1003, 968, 916, 855, 817, 798, 718, 678.

^{1}H NMR ($CDCl_3$, 400 MHz): δ 9.60 (d, 1H, *J* = 7.9 Hz, CHO), 7.47 (d, 2H, *J* = 8.9 Hz, 2H$_{Ar}$), 7.39 (d, 1H, *J* = 15.8 Hz, CH=C$_{Ar}$), 6.73 (d, 2H, *J* = 8.9 Hz, 2H$_{Ar}$), 6.56 (dd, 1H, *J* = 15.8, 7.9 Hz, CH=C), 3.77 (t, 2H, *J* = 7.2 Hz, CH_2), 3.05 (s, 3H, N-CH_3), 2.68 (t, 2H, *J* = 7.2 Hz, CH_2).

^{13}C NMR (DMSO-*d6*, 101 MHz): δ 193.59 (CHO), 173.11 (C$_q$), 154.22 (=CH), 150.87 (C$_q$), 130.82 (2CH$_{Ar}$), 123.40 (=CH), 121.50 (C$_q$), 111.76 (2CH$_{Ar}$), 47.54 (CH_2), 37.94 (CH_2), 31.41 (CH_3).

HRMS: *m*/*z* calculated for $C_{13}H_{16}NO_3$ $[M+H]^+$ 234.1125, found 234.1126;
calculated for $C_{13}H_{15}NNaO_3$ $[M+Na]^+$ 256.0944, found 256.0941.

_N_-5'-2',3'-isopropylidene-5'-deoxyadenosinyl-(_E_)-3-(methyl(4-(3-oxoprop-1-en-1-yl)phenyl)amino)propanamide (D1-5)

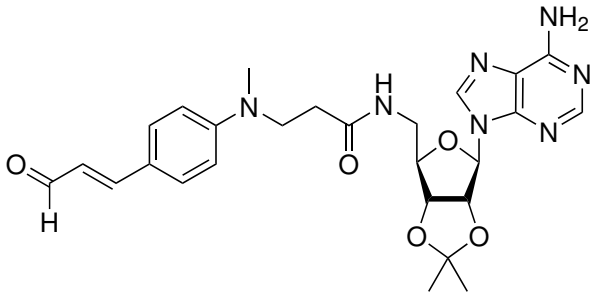

Chemical formula: $C_{26}H_{31}N_7O_5$

Molecular weight: 521.58 g.mol^{-1}

To a solution of **D1-4** (68mg, 0.29mmol) in anhydrous THF (2mL) cooled down to 0°C under an argon atmosphere were added 1-ethyl-3-(3-dimethylaminopropyl)carbodiimide hydrochloride (84mg, 0.44mmol) and hydroxybenzotriazole (60mg, 0.44mmol). After stirring 15mins at room temperature, a solution of **A-4i** (81mg, 0.30mmol) in a mixture of anhydrous THF (2mL) and anhydrous DMF (3.5mL) was added and the mixture was stirred for 3 days. The reaction progress was monitored by TLC (AcOEt/EtOH 70:30) and upon completion, solvents were removed under reduced pressure with the help of 3 co-evaporation with toluene. The crude residue was purified over silica gel (AcOEt/EtOH from 100:0 to 70:30) to give 75mg (53%) of the desired compound as a dark red solid.

R_f: 0.25 (AcOEt/EtOH 85:15)

$T_{decomposition}$: 126°C

IR (cm^{-1}): 3324, 2935 (CH_2 *asym str*), 1648 (C=O secondary amide *str*), 1592, 1524, 1479, 1427, 1382, 1330, 1213, 1187, 1140, 1119, 1097, 969, 855, 811, 798, 748, 726, 696.

^{1}H NMR (DMSO-*d6*, 400 MHz): δ 9.52 (d, 1H, *J* = 8.0 Hz, CHO), 8.32 (s, 1H, H_2), 8.22 (t, 1H, *J* = 6.1 Hz, NH), 8.16 (s, 1H, H_8), 7.60-7.50 (m, 3H, $2H_{Ar}$, CH=C), 7.37 (bs, 2H, NH_2), 6.73 (d, 2H, *J* = 8.7 Hz, $2H_{Ar}$), 6.57 (dd, 1H, *J* = 15.8, 8.0 Hz, CH=C_q), 6.11 (d, 1H, *J* = 2.7 Hz, H_1'), 5.39 (dd, 1H, *J* = 6.3, 2.7 Hz, H_2'), 4.88 (dd, 1H, *J* = 6.3, 3.3 Hz, H_3'), 4.13 (td, 1H, *J* = 6.2, 3.3 Hz, H_4'), 3.63 (dd, 2H, *J* = 6.2, 6.1 Hz, $2H_5$'), 3.33 (s, 3H, N-CH_3), 2.42-2.30 (m, 4H, $2CH_2$), 1.52 (s, 3H, CH_3), 1.29 (s, 3H, CH_3).

^{13}C NMR (DMSO-d6, 101 MHz): δ 156.17 (C_q), 154.18 (CH), 152.71 (CH), 140.03 (CH), 130.69 (CH), 123.25 (CH), 121.34 (CH), 119.26 (C_q), 113.48 (C_q), 111.69 (CH), 88.92 (CH), 84.01 (CH), 82.86 (CH), 81.69 (CH), 48.17 (CH_2), 32.90 (CH_2), 27.03 (CH_3), 25.24 (CH_3).

HRMS: m/z calculated for $C_{26}H_{32}N_7O_5$ $[M+H]^+$: 522.2459, found 522.2452;
calculated for $C_{26}H_{33}N_7O_5$ $[M+2H]^{2+}$ 261.6266, found 261.6266;
calculated for $C_{26}H_{31}N_7NaO_5$ $[M+Na]^+$ 544.2279, found 544.2279.

***N*-(4-vinylphenyl)benzamide[224] (D2-0-Bz)**

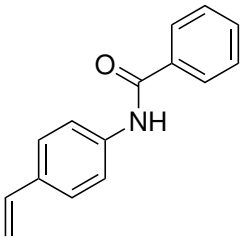

Chemical formula: $C_{15}H_{13}NO$

Molecular weight: 223.28 g.mol^{-1}

To a solution of 4-vinylanilline (1.0mL, 8.5mmol) in toluene (85mL, 0.1M) was added triethylamine (1.73mL, 12.8mmol) then benzoyl chloride (1.09mL, 9.38mmol), dropwise. The reaction progress was monitored by TLC (PE/AcOEt 85:15) and upon completion distilled water (75mL) was added, then the mixture was extracted 3 times with DCM, organic phases were combined, dried over magnesium sulfate, filtered over cotton and solvents were removed under reduced pressure. The crude residue was purified over silica gel (PE/AcOEt from 100:0 to 60:40) to give 2.04g (quant.) of the desired compound as a white solid.

R$_f$: 0.29 (PE/AcOEt 85:15)

T$_f$: 168°C

IR (cm^{-1}): 3336, 1651 (C=O secondary amide *str*), 1626, 1602, 1590, 1515, 1489, 1448, 1424, 1403, 1323, 1260, 1182, 1158, 1120, 1074, 1028, 1016, 987, 928, 899, 837, 794, 741, 716, 690.

^{1}H NMR (CDCl$_3$, 400 MHz): δ 7.86 (bs, 1H, NH), 7.85 (d, 2H, *J* = 7.6 Hz, 2H$_{Ar}$), 7.60 (d, 2H, *J* = 8.4 Hz, 2H$_{Ar}$), 7.53 (t, 1H, *J* = 7.6 Hz, H$_{Ar}$), 7.47 (d, 1H, *J* = 7.6 Hz, H$_{Ar}$), 7.45 (d, 1H, *J* = 7.6 Hz, H$_{Ar}$), 7.40 (d, 2H, *J* = 8.4 Hz, 2H$_{Ar}$), 6.68 (dd, 1H, *J* = 17.6, 10.9 Hz, CH-C$_q$), 5.69 (d, 1H, *J* = 17.6 Hz, CH$_{Trans}$=C), 5.20 (d, 1H, *J* = 10.9 Hz, CH$_{Cis}$=C).

^{13}C NMR (CDCl$_3$, 101 MHz): δ 165.81 (C$_q$), 137.68 (C$_q$), 136.31 (CH), 135.13 (C$_q$), 134.20 (C$_q$), 132.14 (CH), 129.06 (2CH), 127.20 (2CH), 127.17 (2CH), 120.27 (2CH), 113.42 (=CH$_2$).

HRMS: *m*/*z* calculated for $C_{15}H_{14}NO$ $[M+H]^+$ 224.1070, found 224.1072;
calculated for $C_{15}H_{13}NNaO$ $[M+Na]^+$ 246.0889, found 246.0891.

[224] Shah, P. N. et al. *Macromolecules* **2011**, *44*, 7917–7925.

ethyl *N*-benzoyl-*N*-(4-vinylphenyl)ethanoate (D2-1)

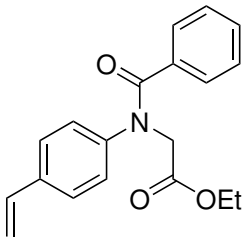

Chemical formula: $C_{19}H_{19}NO_3$

Molecular weight: 309.37 g.mol^{-1}

To a solution of **D2-0-Bz** (998mg, 4.48mmol) in anhydrous DMF (9mL, 0.5M) under an argon atmosphere was added sodium hydride (60w% dispersed in mineral oil, 205mg, 5.13mmol), before heating to 70°C. Then ethyl bromoacetate (0.64mL, 5.38mmol) was added dropwise and the mixture was stirred for 4 days. The reaction progress was monitored by TLC (PE/AcOEt 80:20) and upon completion the heating was stopped and when the flask cooled down an aqueous saturated solution of ammonium chloride (5mL) was added and the mixture was stirred for 10mins. The mixture was extracted 3 times with DCM, organic phases were combined, dried over magnesium sulfate, filtered over cotton and solvents were removed under reduced pressure. The crude residue was purified over silica gel (PE/AcOEt from 100:0 to 20:80) to give 1.16g (84%) of the desired compound as a white solid.

R_f: 0.21 (PE/AcOEt 85:15)

^{1}H NMR ($CDCl_3$, 400 MHz): δ 7.36 (d, 2H, *J* = 7.4 Hz, $2H_{Ar}$), 7.26 (t, 1H, *J* = 7.4 Hz, H_{Ar}), 7.25 (d, 2H, *J* = 8.1 Hz, $2H_{Ar}$), 7.19 (d, 1H, *J* = 7.4 Hz, H_{Ar}), 7.17 (d, 1H, *J* = 7.4 Hz, H_{Ar}), 7.08 (d, 2H, *J* = 8.1 Hz, $2H_{Ar}$), 6.61 (dd, 1H, *J* = 17.6, 10.9 Hz, CH-C_q), 5.67 (d, 1H, *J* = 17.6 Hz, CH_{Trans}=C), 5.23 (d, 1H, *J* = 10.9 Hz, CH_{Cis}=C), 4.59 (s, 2H, CH_2), 4.23 (q, 2H, *J* = 7.1 Hz, CH_2), 1.29 (t, 3H, *J* = 7.2 Hz, CH_3).

^{13}C NMR ($CDCl_3$, 101 MHz): δ 170.82 (C_q), 169.23 (C_q), 143.37 (C_q), 136.24 (C_q), 135.86 (CH_{Ar}), 135.18 (C_q), 130.19 (CH_{Ar}), 129.04 ($2CH_{Ar}$), 127.99 ($2CH_{Ar}$), 127.58 ($2CH_{Ar}$), 127.07 ($2CH_{Ar}$), 114.80 (=CH_2), 61.55 (CH_2), 52.43 (CH_2), 14.34 (CH_3).

ethyl *N*-benzoyl-*N*-(4-formylphenyl)ethanoate (D2-2)

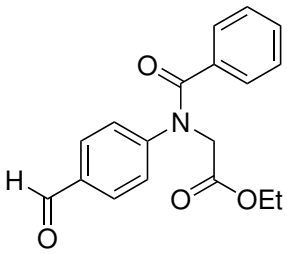

Chemical formula: $C_{18}H_{17}NO_4$

Molecular weight: 311.34 g.mol^{-1}

To a stirred solution of ethyl **D2-1** (433mg, 1.40mmol) in a mixture of acetone and water (3:1, 75mL) were added *N*-methylmorpholine *N*-oxide (345mg, 2.94mmol) and osmium tetraoxide (4% by weight in *tert*-butanol, tip of a pasteur pipette filled by capillarity), and the reaction mixture was stirred overnight. The reaction progress was monitored by TLC (PE/AcOEt 80:20), and upon completion sodium periodate (755mg, 3.53mmol) was added to the mixture. The reaction progress was monitored by TLC (PE/AcOEt 80:20), and upon completion an aqueous saturated solution of sodium thiosulfate (2mL) was added before stirring for 10mins. Acetone was removed under reduced pressure and the resulting mixture was extracted 3 times with DCM, organic phases were combined, dried over magnesium sulfate, filtered over cotton and solvents were removed under reduced pressure. The crude residue was purified over silica gel (PE/AcOEt from 100:0 to 60:40) to give 408mg (85%) of the desired compound as a white solid.

R_f: 0.19 (PE/AcOEt 80:20)

T_f: 99°C

IR (cm^{-1}): 1752 (C=O ester *str*), 1686 (C=O aryl aldehyde *str*), 1645 (C=O secondary amide *str*), 1601, 1579, 1508, 1446, 1423, 1362, 1330, 1293, 1235, 1196, 1164, 1096, 1055, 1024, 1002, 836, 825, 797, 726, 706.

^{1}H NMR ($CDCl_3$, 400 MHz): δ 9.92 (s, 1H, CHO), 7.74 (d, 2H, J = 8.1 Hz, 2H$_{Ar}$), 7.36 (d, 2H, J = 7.5 Hz, 2H$_{Ar}$), 7.31 (t, 1H, J = 7.5 Hz, H$_{Ar}$), 7.25-7.19 (m, 4H, 4H$_{Ar}$), 4.65 (s, 2H, N-CH2), 4.25 (q, 2H, J = 7.2 Hz, CH_2), 1.30 (t, 3H, J = 7.2 Hz, CH_3).

^{13}C NMR ($CDCl_3$, 101 MHz): δ 166.19 (C_q), 158.05 (C_q), 142.64 (C_q), 140.37 (C_q), 130.18 (CH), 127.48 (CH), 126.48 (CH), 124.12 (C_q), 120.91 (CH), 120.73 (CH), 110.06 (CH).

HRMS: m/z calculated for $C_{18}H_{18}NO_4$ $[M+H]^+$ 312.1230, found 312.1233;
calculated for $C_{18}H_{17}NNaO_4$ $[M+Na]^+$ 334.1050, found 334.1054.

ethyl (*E*)-*N*-(4-(2-(1,3-dioxolan-2-yl)vinyl)phenyl)-*N*-benzoylethanoate (D2-2')

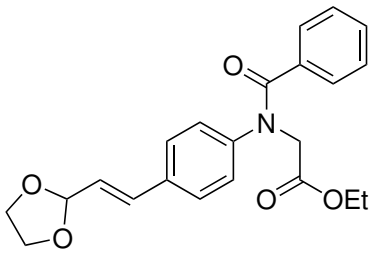

Chemical formula: $C_{22}H_{23}NO_5$

Molecular weight: 381.43 g.mol^{-1}

To a solution of **R-2** (660mg, 1.79mmol) in anhydrous THF (3mL) was added sodium hydride (60w% dispersed in mineral oil, 61mg, 1.53mmol), and after 20mins of stirring a solution of **D2-2** (408mg, 1.31mmol) in anhydrous THF (7mL) was added. The reaction progress was monitored by TLC (PE/AcOEt 70:30) and upon completion, an aqueous saturated solution of ammonium chloride (5mL) was added and the mixture was stirred for another 10mins. The latter was then extracted 3 times with ethyl acetate, organic phases were combined, dried over magnesium sulfate, filtered over cotton and solvents were removed under reduced pressure. The desired compound was obtained mixed with the related phosphine oxide derivative, and was used in the next step without further purification.

R_f: 0.22 (PE/AcOEt 70:30 + NEt_3)

^{1}H NMR ($CDCl_3$, 400 MHz): δ 7.34 (d, 2H, *J* = 8.1 Hz, 2H$_{Ar}$), 7.27-7.22 (m, 3H, 3H$_{Ar}$), 7.18 (d, 1H, *J* = 7.4 Hz, H$_{Ar}$), 7.16 (d, 1H, *J* = 7.4 Hz, H$_{Ar}$), 7.07 (d, 2H, *J* = 8.1 Hz, 2H$_{Ar}$), 6.67 (d, 1H, *J* = 16.0 Hz, CH-C$_q$), 6.09 (dd, 1H, *J* = 16.0, 6.1 Hz, CH=C), 5.38 (d, 1H, *J* = 6.1 Hz, O-CH-O), 4.59 (s, 2H, CO-CH$_2$), 4.09-4.00 (m, 2H, CH$_2$-O), 3.99-3.90 (m, 2H, CH$_2$-O), 3.72 (q, 2H, *J* = 6.9 Hz, CH$_2$), 1.24 (t, 3H, *J* = 6.9 Hz, CH$_3$).

^{13}C NMR ($CDCl_3$, 101 MHz): δ 169.24 (C$_q$), 143.89 (C$_q$), 134.56 (C$_q$), 133.77 (CH), 130.27 (CH), 129.05 (CH), 128.04 (CH), 127.82 (CH), 127.65 (CH), 126.14 (CH), 65.32 (CH$_2$), 61.61 (CH$_2$), 52.38 (CH$_2$), 14.36 (CH$_3$).

ethyl (*E*)-*N*-benzoyl-*N*-(4-(3-oxoprop-1-en-1-yl)phenyl)ethanoate (D2-3)

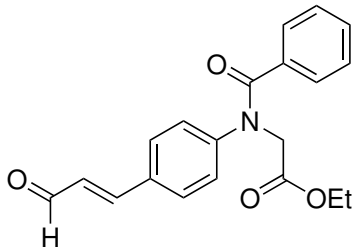

Chemical formula: $C_{20}H_{19}NO_4$

Molecular weight: 337.38 g.mol^{-1}

To a solution of crude ethyl **D2-2'** in anhydrous DCM (10mL) under a dinitrogen atmosphere was added TFA (1mL). The reaction progress was monitored by TLC (PE/AcOEt 70:30 with a drop of triethylamine) and showed completion after 50mins. An aqueous saturated solution of sodium hydrogenocarbonate (5mL) was then added while stirring until no more carbon dioxide bubbles formed. The mixture was then extracted 3 times with DCM, organic phases were combined, dried over magnesium sulfate, filtered over cotton and solvents were removed under reduced pressure. The crude residue was purified over silica gel (PE/AcOEt from 100:0 to 60:40) to give 44mg (14% over two steps) of the desired compound as a deep red oil.

R$_f$: 0.24 (PE/AcOEt 70:30)

^{1}H NMR (CDCl$_3$, 400 MHz): δ 9.67 (d, 1H, *J* = 7.7 Hz, CHO), 7.43 (d, 2H, *J* = 8.1 Hz, 2H$_{Ar}$), 7.40-7.33 (m, 3H, 3H$_{Ar}$), 7.30 (t, 1H, *J* = 7.5 Hz, H$_{Ar}$), 7.24-7.14 (m, 4H, 3H$_{Ar}$,CH=C$_q$), 6.63 (dd, 1H, *J* = 16.0, 7.7 Hz, CH=C), 4.62 (s, 2H, O-CH$_2$), 4.25 (q, 2H, *J* = 7.2 Hz, CH$_2$), 1.30 (t, 3H, *J* = 7.2 Hz, CH$_3$).

***N*-(4-formylphenyl)benzamide (D2-4)**

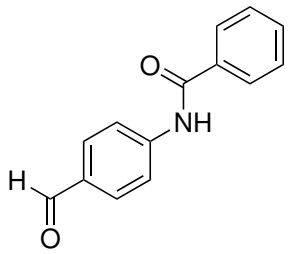

Chemical formula: $C_{14}H_{11}NO_2$

Molecular weight: 225.25 g.mol^{-1}

To a solution of **D2-0-Bz** (2.27g, 10.2mmol) in a mixture of acetone and distilled water (3:1, 120mL) were added *N*-methylmorpholine *N*-oxide (1.81g, 15.4mmol)) and osmium tetraoxide (4w% in *tert*-butanol, tip of a pasteur pipette filled by capillarity). The first step progress was monitored by TLC (PE/AcOEt 70:30) and upon completion, sodium periodate (3.91g, 18.3mmol) was added. The second step was monitored by TLC with the same elution, and upon completion an aqueous saturated solution of sodium thiosulfate (10mL) was added to the mixture, before another 10mins of stirring. The mixture was filtered over cotton to remove sodium periodate, before removing acetone under reduced pressure. The crude mixture was then extracted 3 times with DCM, organic phases were combined, dried over magnesium sulfate, filtered over cotton and solvents were removed under reduced pressure. The crude residue was purified over silica gel (PE/AcOEt from 100:0 to 60:40) to give 1.94g (85%) of the desired compound as a white solid.

R_f: 0.43 (PE/AcOEt 70:30)

T_f: 150°C

IR (cm^{-1}): 3337, 1693 (C=O aryl aldehyde *str*), 1656 (C=O secondary amide *str*), 1590, 1520, 1488, 1414, 1393, 1374, 1317, 1254, 1212, 1166, 1116, 1031, 1001, 901, 826, 803, 791, 718, 689, 676.

^{1}H NMR ($CDCl_3$, 400 MHz): δ 9.96 (s, 1H, CHO), 8.16 (bs, 1H, NH), 7.96-7.84 (m, 6H, $6H_{Ar}$), 7.62-7.56 (m, 1H, H_{Ar}), 7.56-7.49 (m, 2H, $2H_{Ar}$).

^{13}C NMR ($CDCl_3$, 101 MHz): δ 191.22 (CHO), 166.08 (C=O), 143.72 (C_q), 134.55 (C_q), 132.70 (CH,C_q), 131.43 (2CH), 129.17 (2CH), 127.33 (2CH), 119.85 (2CH).

HRMS: m/z calculated for $C_{14}H_{12}NO_2$ $[M+H]^+$: 226.0863, found 226.0864;
calculated for $C_{14}H_{11}NNaO_2$ $[M+Na]^+$ 248.0682, found 248.0682.

(*E*)-*N*-(4-(3-oxoprop-1-en-1-yl)phenyl)benzamide (D2-5)

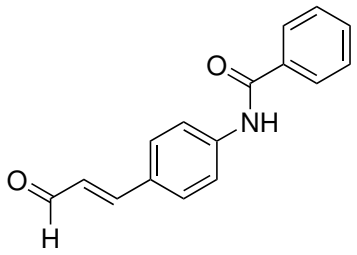

Chemical formula: $C_{16}H_{13}NO_2$

Molecular weight: 251.29 g.mol^{-1}

To a solution of **R-2** (223mg, 0.60mmol) in anhydrous THF (2.5mL) was added sodium hydride (60w% dispersed in mineral oil, 44.3mg, 1.11mmol), and after 20mins of stirring a solution of **D2-4** (100mg, 0.444mmol) in anhydrous THF (2mL) was added. The reaction progress was monitored by TLC (PE/AcOEt 70:30) and upon completion, an aqueous saturated solution of ammonium chloride (10mL) was added and the mixture was stirred for another 10mins before removing THF under reduced pressure. The resulting mixture was then extracted 3 times with DCM, organic phases were combined, dried over magnesium sulfate, filtered over cotton and solvents were removed under reduced pressure. The crude residue was dissolved in a mixture of DCM and TFA (10:1, 11mL) under vigorous stirring for 45mins. Afterwards, an aqueous saturated solution of sodium carbonate (30mL) was added and when carbon dioxide bubbles stopped forming, the mixture was extracted 3 times with DCM, organic phases were combined, dried over magnesium sulfate, filtered over cotton and solvents were removed under reduced pressure. The crude residue was purified over silica gel (PE/AcOEt from 100:0 to 60:40) to give 82mg (73%) of the desired compound as a dark red oil.

R_f: 0.33 (PE/AcOEt 70:30 + NEt_3)

T_f: 178°C

IR (cm^{-1}): 3330, 1668 (C=O α,β insaturated aldehyde *str*), 1652 (C=O secondary amide *str*), 1620, 1600, 1587, 1515, 1493, 1449, 1414, 1322, 1301, 1263, 1208, 1181, 1123, 1078, 1029, 1002, 968, 943, 898, 858, 814, 799, 707, 687, 680.

^{1}H NMR ($CDCl_3$, 400 MHz): δ 9.70 (d, 1H, *J* = 7.7 Hz, CHO), 7.99 (bs, 1H, NH), 7.89 (d, 2H, *J* = 7.6 Hz, $2H_{Ar}$), 7.76 (d, 2H, *J* = 8.4 Hz, $2H_{Ar}$), 7.65-7.55 (m, 3H, $3H_{Ar}$), 7.55-7.49 (m, 2H, $2H_{Ar}$), 7.46 (d, 1H, *J* = 15.9 Hz, CH-C_q), 6.69 (dd, 1H, *J* = 15.9, 7.7 Hz, CH=C).

^{13}C NMR ($CDCl_3$, 101 MHz): δ 193.91 (CHO), 165.94 (C_q), 152.29 (CH), 140.91 (C_q), 134.70 (C_q), 132.49 (CH), 130.26 (C_q), 129.90 (CH), 129.16 (2CH), 127.90 (2CH), 127.27 (2CH), 120.30 (2CH).

HRMS: m/z calculated for $C_{16}H_{14}NO_2$ $[M+H]^+$ 252.1019, found 252.1022;
calculated for $C_{16}H_{13}NNaO_2$ $[M+Na]^+$ 274.0838, found 274.0839.

2.4 Synthesis of the photoactivatable moieties towards a thiourea linkage

4-(methyl(2-((tetrahydro-*2H*-pyran-2-yl)oxy)ethyl)amino)benzaldehyde[225] (D3-1)

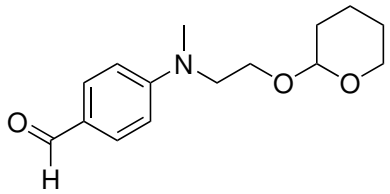

Chemical formula: $C_{15}H_{21}NO_3$

Molecular weight: 263.34 g.mol^{-1}

PPTS (545mg, 2.17mmol) and DHP (2.0mL, 22mmol) were added to a stirred solution of 4-(methyl(2-hydroxyethyl)amino)benzaldehyde (2.02g, 11.2mmol) in anhydrous DCM (50mL) under dinitrogen atmosphere. The reaction progress was monitored by TLC (PE/AcOEt 70:30) and showed completion after 72hrs. Distilled water (60mL) was added to the reaction mixture and phases were separated. The aqueous phase was further extracted 3 times with DCM, then organic layers were combined, dried over magnesium sulfate, filtered on coton and evaporated under reduced pressure. The crude was purified over silica gel (PE/AcOEt from 100:0 to 60:40), yielding 2.82g (96%) of desired compound as a yellow oil.

R_f: 0.36 (PE/AcOEt 70:30)

IR (cm^{-1}): 2941 (CH_2 *asym str*), 1679 (C=O aryl aldehyde *str*), 1594, 1557, 1527, 1438, 1384, 1314, 1241, 1201, 1168, 1121, 1072, 1034, 979, 905, 870, 815, 719.

^{1}H NMR ($CDCl_3$, 400 MHz): δ 9.74 (s, 1H, CHO), 7.73 (d, 2H, J = 8.9 Hz, 2H$_{Ar}$), 6.77 (d, 2H, J = 8.9 Hz, 2H$_{Ar}$), 4.62-4.55 (m, 1H, O-CH (THP)), 3.98-3.89 (m, 1H, N-CH_2-CH_2-O), 3.80-3.73 (m, 1H, N-CH_2-CH_2-O), 3.70-3.58 (m, 3H, N-CH_2-CH_2-O, O-CH2 (THP)), 3.51-3.43 (m, 1H, N-CH_2-CH_2-O), 3.12 (s, 3H, N-CH_3), 1.80-1.63 (m, 2H, CH_2 (THP)), 1.58-1.42 (m, 4H, 2CH_2 (THP)).

^{13}C NMR ($CDCl_3$, 101 MHz): δ 190.43 (CHO), 153.78 (C$_q$), 132.20 (2CH$_{Ar}$), 125.38 (C$_q$), 111.132 (2CH$_{Ar}$), 99.16 (CH), 64.78 (CH_2), 62.32 (CH_2), 52.28 (CH_2), 39.37 (CH_3), 30.70 (CH_2), 25.49 (CH_2), 19.45 (CH_2).

HRMS: m/z calculated for $C_{15}H_{22}NO_3$ $[M+H]^+$ 264.1594, found 264.1597;
calculated for $C_{15}H_{21}NNaO_3$ $[M+Na]^+$ 286.1414, found 286.1413.

[225] Watanabe, H. et al. *Dyes Pigm.* **2019**, *170*, 107615.

(*E*)-3-(4-(methyl(2-((tetrahydro-*2H*-pyran-2-yl)oxy)ethyl)amino)phenyl)acrylaldehyde[225] (D3-2)

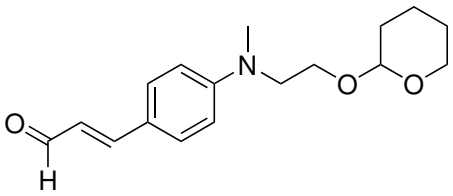

Chemical formula: $C_{17}H_{23}NO_3$

Molecular weight: 289.38 g.mol^{-1}

Procedure 1: To a stirred solution of **D3-1** (100mg, 0.380mmol) in anhydrous THF (1mL) under an argon atmosphere were added a solution of **R-2** (181mg, 0.489mmol) in anhydrous THF (1mL), then sodium hydride (60w% dispersed in mineral oil, 23.1mg, 0.578mmol) and the mixture was stirred overnight. The reaction progress was monitored by TLC (PE/AcOEt 70:30) and upon completion an aqueous saturated solution of ammonium chloride (5mL) was added and the mixture was stirred for 10mins. THF was then removed under reduced pressure and the resulting mixture was extracted 3 times with DCM, organic phases were combined, dried over magnesium sulfate, filtered over cotton and solvents were removed under reduced pressure. The crude oily residue was dissolved in a mixture of DCM and TFA (9:1, 4mL) under a dinitrogen atmosphere. The reaction progress was monitored by TLC (PE/AcOEt 70:30) and showed completion after 15mins. An aqueous saturated solution of sodium hydrogenocarbonate (20mL) was added and the mixture was stirred until no more carbon dioxide bubbles formed. The reaction mixture was then extracted 3 times with DCM, organic phases were combined, dried over magnesium sulfate, filtered over cotton and solvents were removed under reduced pressure. The crude residue was purified over silica gel (PE/AcOEt from 100:0 to 0:100) to give 40mg (36%) of the desired compound and 25mg (32%) of **D3-2'** as a deep red oil.

Procedure 2: A stirred solution of **D3-1** (14.85g, 56.4mmol) and **R-2** (23.2g, 62.8mmol) in anhydrous THF (220mL) under an argon atmosphere was cooled down to 0°C with an ice bath before slow addition of sodium hydride (60w% dispersed in mineral oil, 6.77g, 169mmol). The reaction medium was stirred another 10mins before removing the ice bath. The reaction progress was monitored by TLC (PE/AcOEt 70:30) after extracting a small amount of the mixture with AcOEt and an aqueous saturated solution of ammonium chloride and showed completion after 1.5hrs. Distilled water (100mL) was added slowly to the mixture, then organic solvents were removed under reduced pressure. After addition of DCM (200mL) to the mixture, phases were separated and the aqueous phase was further extracted two more times. The organic phases were combined (600mL), dried over magnesium sulfate, filtered on cotton and evaporated under reduced pressure. The crude was then dissolved in anhydrous DCM (140mL) and silica (40–63µm, 122mL), distilled water (5.5mL, 0.31mol) and acetic acid (0.42mL, 7.3mmol) were added. The mixture was stirred for 10 days until completion, with occasional addition of DCM to avoid drying, and the reaction progress was monitored by TLC (PE/AcOEt 70:30). The reaction medium was then concentrated under reduced pressure and the crude residue was purified over silica gel (PE/AcOEt from 100:0 to 60:40) to give 14.37g (88%) of desired compound as a deep red oil.

R_f: 0.38 (PE/AcOEt 70:30)

IR (cm^{-1}): 2941 (CH_2 *asym str*), 1664 (C=O α,β insaturated aldehyde *str*), 1591, 1523, 1437, 1383, 1329, 1263, 1186, 1117, 1072, 1033, 977, 905, 870, 810.

^{1}H NMR ($CDCl_3$, 400 MHz): δ 9.59 (d, 1H, *J* = 7.9 Hz, CHO), 7.44 (d, 2H, *J* = 8.8 Hz, $2H_{Ar}$), 7.37 (d, 1H, *J* = 15.6 Hz, Ar-CH=), 6.72 (d, 2H, *J* = 8.8 Hz, $2H_{Ar}$), 6.54 (dd, 1H, *J* = 15.6, 7.9 Hz, CHO-C*H*=CH), 4.61-4.56 (m, 1H, O-CH (THP)), 3.96-3.88 (m, 1H, N-CH_2-CH_2-O), 3.81-3.74 (m, 1H, N-CH_2-CH_2-O; O-CH2 (THP)), 3.68-3.57 (m, 3H, N-CH_2-CH_2-O), 3.50-3.43 (m, 1H, N-CH_2-CH_2-O), 3.09 (s, 3H, N-CH_3), 1.80-1.65 (m, 2H, CH_2 (THP)), 1.59-1.45 (m, 4H, $2CH_2$ (THP)).

^{13}C NMR ($CDCl_3$, 101 MHz): δ 193.97 (CHO), 154.12 (CH), 151.68 (C_q), 130.76 ($2CH_{Ar}$), 123.89 (CH), 121.91 (C_q), 111.90 ($2CH_{Ar}$), 99.18 (CH), 64.83 (CH_2), 62.34 (CH_2), 52.29 (CH_2), 39.27 (CH_3), 30.75 (CH_2), 25.52 (CH_2), 19.49 (CH_2).

HRMS: m/z calculated for $C_{17}H_{24}NO_3$ $[M+H]^+$ 290.1751, found 290.1755;
calculated for $C_{17}H_{23}NNaO_3$ $[M+Na]^+$ 312.1570, found 312.1575.

(*E*)-3-(4-((2-hydroxyethyl)(methyl)amino)phenyl)acrylaldehyde (D3-2')

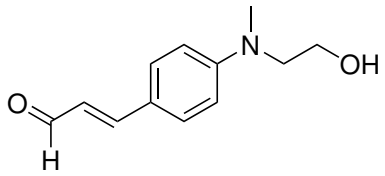

Chemical formula: $C_{12}H_{15}NO_2$

Molecular weight: 205.26 g.mol^{-1}

Compound obtained as a side product of the synthesis of **D3-2** *via* the procedure 1.

R_f: 0.07 (PE/AcOEt 70:30)

^{1}H NMR ($CDCl_3$, 400 MHz): δ 9.53 (d, 1H, *J* = 8.0 Hz, CHO), 7.42 (d, 2H, *J* = 9.0 Hz, $2H_{Ar}$), 7.34 (d, 1H, *J* = 15.6 Hz, CH-C_q), 6.75 (d, 2H, *J* = 9.0 Hz, $2H_{Ar}$), 6.48 (dd, 1H, *J* = 15.6, 8.0 Hz, CH=C), 3.86 (t, 2H, *J* = 5.6 Hz, CH_2), 3.59 (t, 2H, *J* = 5.6 Hz, CH_2), 3.09 (s, 3H, CH_3).

***N*-(4-((1*E*,3*E*)-4-(4-(methyl(2-((tetrahydro-*2H*-pyran-2-yl)oxy)ethyl)amino)phenyl)buta-1,3-dien-1-yl)phenyl)benzamide (F3-3-Bz)**

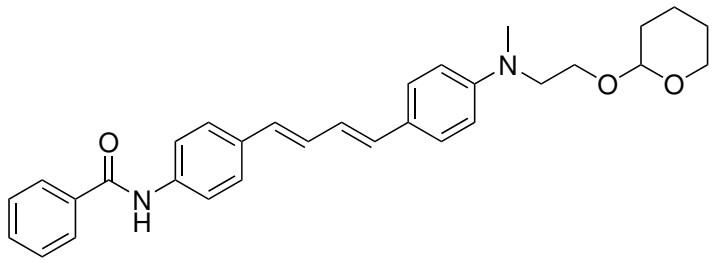

Chemical formula: $C_{31}H_{34}N_2O_3$

Molecular weight: 482.62 g.mol^{-1}

D3-2 (2.00g, 6.91mmol) and **P-Bz** (2.64g, 7.61mmol) were added to a flask under an argon atmosphere, then THF (70mL) was added. Sodium hydride (60w% dispersed in mineral oil, 1.10g, 27.5mmol) was then slowly added by portion, waiting for dihydrogen release to slow down before each addition. The reaction mixture was stirred for 4 days until completion, and the reaction progress was monitored by TLC (PE/AcOEt 70:30) after extracting a small amount of the mixture with DCM and an aqueous saturated solution of ammonium chloride. An aqueous saturated solution of ammonium chloride (25mL) was slowly added to the reaction mixture, which was then stirred until the dihydrogen release stopped. Organic solvents were then removed under reduced pressure, and distilled water (25mL) was added to redissolve some precipitated ammonium chloride. DCM was added to the mixture, the flask was sonicated then phases were separated, and this operation was repeated until no solid residue was left. Organic layers were combined (750mL), dried over magnesium sulfate, filtered on cotton and solvents were removed under reduced pressure, yielding 3.11g (93%) of the desired compound as a brown solid.

R$_f$: 0.35 (PE/AcOEt 70:30)

T$_f$: 177°C

IR (cm^{-1}): 3340, 2943 (CH_2 *asym str*), 1644, 1604, 1519, 1488, 1411, 1371, 1322, 1249, 1202, 1191, 1137, 1122, 1074, 1034, 981, 926, 902, 870, 844, 798, 715, 693, 679.

^{1}H NMR (CDCl3, 400 MHz): δ 7.86 (s, 1H, NH), 7.85-7.81 (m, 2H, $2H_{Bz}$), 7.59 (d, *J* = 8.5 Hz, 2H, $2H_{Ar}$), 7.56-7.50 (m, 1H, H_{Bz}), 7.50-7.43 (m, 2H, $2H_{Bz}$), 7.40 (d, *J* = 8.5 Hz, 2H, $2H_{Ar}$), 7.30 (d, *J* = 8.9 Hz, 2H, $2H_{Ar}$), 6.89 (dd, *J* = 15.3, 10.4 Hz, 1H, Ar-CH=CH-), 6.75 (dd, *J* = 15.3, 10.4 Hz, 1H, Ar-CH=CH-), 6.67 (d, *J* = 8.9 Hz, 2H, $2H_{Ar}$), 6.58 (d, *J* = 15.4 Hz, 1H, Ar-CH=CH-), 6.53 (d, *J* = 15.4 Hz, 1H, Ar-CH=CH-), 4.59-4.54 (m, 1H, O-CH_{THP}), 3.93-3.83 (m, 1H, N-CH_2-CH_2-O), 3.83-3.75 (m, 1H, N-CH_2-CH_2-O), 3.62-3.51 (m, 3H, N-CH_2-CH_2-O; O-$CH_{2,THP}$), 3.49-3.42 (m, 1H, N-CH_2-CH_2-O), 3.01 (s, 3H, N-CH_3), 1.78-1.73 (m, 1H, $CH_{2,THP}$), 1.72-1.63 (m, 1H, $CH_{2,THP}$), 1.56-1.44 (m, 4H, $CH_{2,THP}$).

^{13}C NMR ($CDCl_3$, 101 MHz): δ 165.49 (C_q), 148.73 (C_q), 136.60 (C_q), 134.92 (C_q), 134.33 (C_q), 133.11 (CH), 131.86 (CH), 129.55 (CH), 129.41 (CH), 128.81 ($2C_{Ar}$), 127.58 ($2C_{Ar}$), 126.99 ($2C_{Ar}$), 126.72 ($2C_{Ar}$), 125.49 (C_q), 124.95 (CH), 120.11 ($2C_{Ar}$), 112.00 ($2C_{Ar}$), 98.99 (CH), 64.78 (CH_2), 62.16 (CH_2), 52.30 (CH_2), 39.01 (CH_3), 30.61 (CH_2), 25.37 (CH_2), 19.36 (CH_2).

HRMS: m/z calculated for $C_{31}H_{35}N_2O_3$ $[M+H]^+$ 483.2642, found 483.2642;
calculated for $C_{31}H_{34}N_2NaO_3$ $[M+Na]^+$ 505.2462, found 505.2464.

***N*-(4-((1*E*,3*E*)-4-(4-((2-hydroxyethyl)(methyl)amino)phenyl)buta-1,3-dien-1-yl)phenyl)benzamide (F3-4-Bz)**

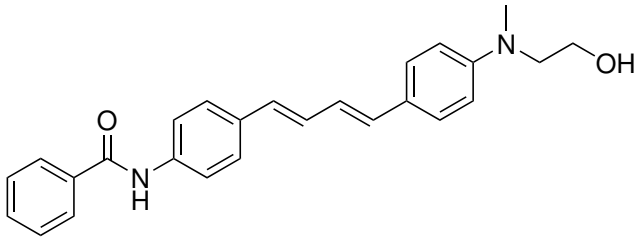

Chemical formula: $C_{26}H_{26}N_2O_2$

Molecular weight: 398.51 g.mol^{-1}

Procedure 1: To a solution of **F3-3-Bz** (2.20g, 4.55mmol) in DCM (330mL) was added an aqueous solution of hydrochloric acid (6N, 16mL), turning the solution from brown to very dark red. The mixture was then heated at 55°C for 1.5hrs, while the organic phase lightenned up to clear light yellow and a light brown precipitate formed on the flask. The reaction completion was appreciated by the organic phase color. Heating was stopped, the organic phase discarded and an aqueous solution of sodium hydroxide (4N, 36mL) was slowly added, alongside some DCM (250mL) under vigorous stirring. Distilled water (100mL) was added to increase the aqueous phase volume, phases were separated and the aqueous layer was further extracted two times. The organic layers were then combined (2.1L), dried over magnesium sulfate, filtered on cotton and solvents were removed under reduced pressure, yielding 1.70g (94%) of desired compound as a brown solid.

Procedure 2: To a solution of **F3-3-Bz** (2.01g, 4.16mmol) in iPrOH (100mL) under argon atmosphere was added PTSA monohydrate (1.55g, 8.15mmol). The reaction mixture changed color from yellow to red wine and was then heated at 55°C and stirred overnight. Reaction progress was monitored by TLC (DCM/EtOH 95:5), and upon completion solvents were removed under reduced pressure. An aqueous saturated solution of sodium hydrogenocarbonate (150mL) was slowly added to the residue which changed color from purple to pine green as carbon dioxide was released. The suspension was sonicated and filtered on a sintered glass funnel, and the precipitate was washed with distilled water (100mL) and dried under vacuum to give 1.50g (90%) of the desired compound as a pine green solid. The sample showed some solvatochromic properties, as its color heavily relies on the last solvent used, ranging from brown to green with respect to an increase in polarity.

R_f: 0.09 (PE/AcOEt 70:30)

$T_{decomposition}$: 162°C

IR (cm^{-1}): 3277, 2924 (CH_2 *asym str*), 1644, 1602, 1518, 1488, 1448, 1411, 1372, 1326, 1189, 1124, 1042, 985, 845, 800, 754, 704, 691.

^{1}H NMR (CDCl3, 400 MHz): δ 7.92-7.84 (m, 2H, $2H_{Ar}$ (Bz)), 7.82 (s, 1H, NH), 7.61 (d, 2H, *J* = 8.5 Hz, $2H_{Ar}$), 7.58-7.53 (m, 1H, H_{Ar} (Bz)), 7.53-7.46 (m, 2H, $2H_{Ar}$ (Bz)), 7.43 (d, 2H, *J* = 8.5 Hz, $2H_{Ar}$), 7.34 (d, 2H, *J* = 8.5 Hz, $2H_{Ar}$), 6.91 (dd, 1H, *J* = 15.4, 10.6 Hz, Ar-CH=C*H*-), 6.79 (dd, 1H, *J* = 15.4, 10.6 Hz, Ar-CH=C*H*-), 6.76 (d, 2H, *J* = 8.5 Hz, $2H_{Ar}$), 6.60 (d, 1H, *J* = 15.4 Hz, Ar-C*H*=CH-), 6.57 (d, 1H, *J* = 15.4 Hz, Ar-C*H*=CH-), 3.87-3.80 (m, 2H, N-CH_2-CH_2-O), 3.55-3.48 (m, 2H, N-CH_2-CH_2-O), 3.01 (s, 3H, N-CH_3), 1.72-1.68 (m, 1H, OH).

^{13}C NMR (DMSO-*d6*, 101 MHz): δ 165.43 (C_q), 148.73 (C_q), 138.17 (C_q), 134.97 (C_q), 133.04 (C_q), 132.83 (CH), 131.58 (CH), 129.36 (CH), 129.14 (CH), 128.41 ($2CH_{Ar}$), 127.68 ($2CH_{Ar}$), 127.47 ($2CH_{Ar}$), 126.24 ($2CH_{Ar}$), 124.61 (CH), 124.50 (C_q), 120.41 ($2CH_{Ar}$), 111.71 ($2CH_{Ar}$), 58.08 (CH_2), 54.09 (CH_2), 38.68 (CH_3).

HRMS: m/z calculated for $C_{26}H_{27}N_2O_2$ $[M+H]^+$ 399.2067, found 399.2070.

***N*-(4-((1*E*,3*E*)-4-(4-((2-azidoethyl)(methyl)amino)phenyl)buta-1,3-dien-1-yl)phenyl)benzamide (F3-5-Bz)**

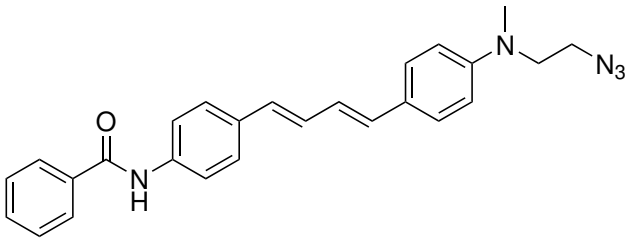

Chemical formula: $C_{26}H_{25}N_5O$

Molecular weight: 423.52 g.mol^{-1}

To a stirred solution of **F3-4-Bz** (780mg, 1.96mmol) in DCM (10mL) under argon atmosphere was added triethylamine (0.82mL, 5.9mmol), before cooling down to 0°C using an ice bath. Mesyl chloride (0.30mL, 3.9mmol) was added dropwise, and the ice bath was removed 10mins after completing the addition. The reaction progress was monitored by TLC (PE/AcOEt 50:50, identical R_f but fluorescence emission under irradiation at 365 nm was different by eye between reagent and product). Methanol (5mL) was added upon completion and the reaction mixture was stirred 10mins before addition of water (15mL) and DCM (20mL) and phase separation. Further rinsing of the organic phase was done and organic phases were reunited, dried over magnesium sulfate, filtered and solvents were thoroughsly removed under reduced pressure. The dry residue and sodium azide (637mg, 9.8mmol) were then dissolved in DMF (10mL) under argon atmosphere, before heating the reaction mixture to 90°C for 2.5hrs. The reaction progress was monitored by TLC (PE/AcOEt 50:50) after extracting a small amount of the mixture with AcOEt and distilled water. Upon completion, solvents were removed under reduced pressure and the residue was washed with distilled water before filtration on a sintered glass funnel, giving 767mg (92%) of the desired compound as a yellow solid.

R_f: 0.35 (PE/AcOEt 70:30); 0.70 (DCM/AcOEt 70:30)

$T_{decomposition}$: 105°C

IR (cm^{-1}): 3289, 2927 (CH_2 *asym str*), 2099 (N_3 *asym str*), 1646, 1602, 1518, 1487, 1447, 1411, 1323, 1262, 1188, 1125, 1073, 1027, 985, 967, 904, 846, 800, 705, 692.

^{1}H NMR ($CDCl_3$, 400 MHz): δ 7.87 (d, *J* = 8.6 Hz, 2H, $2H_{Ar}$), 7.86 (bs, 1H, NH), 7.61 (d, *J* = 8.5 Hz, 2H, $2H_{Ar}$), 7.56 (t, *J* = 6.7 Hz, 1H, H_{Ar}), 7.49 (dd, *J* = 8.4, 6.7 Hz, 2H, $2H_{Ar}$), 7.42 (d, *J* = 8.4 Hz, 2H, $2H_{Ar}$), 7.35 (d, *J* = 8.5 Hz, 2H, $2H_{Ar}$), 6.91 (dd, *J* = 15.4, 10.5 Hz, 1H, CH=C), 6.79 (dd, *J* = 15.2, 10.5 Hz, 1H, CH=C), 6.69 (d, *J* = 8.6 Hz, 2H, $2H_{Ar}$), 6.60 (d, *J* = 15.2 Hz, 1H, CH=C), 6.56 (d, *J* = 15.4 Hz, 1H, CH=C), 3.57 (t, *J* = 6.0 Hz, 2H, N-$CH_2$2-CH_2-O), 3.47 (t, *J* = 6.0 Hz, 2H, N-CH_2-CH_2-O), 3.04 (s, 3H, CH_3).

^{13}C NMR ($CDCl_3$, 101 MHz): δ 165.71 (C_q), 148.15 (C_q), 136.98 (C_q), 135.16 (C_q), 134.48 (C_q), 133.00 (CH), 132.11 (CH), 130.02 (CH), 129.62 (CH), 129.05 ($2CH_{Ar}$), 127.91 ($2CH_{Ar}$), 127.19 ($2CH_{Ar}$), 127.01 ($2CH_{Ar}$), 126.56 (C_q), 125.74 (CH), 120.37 ($2CH_{Ar}$), 112.28 (C_{Ar}), 52.05 (CH_2), 49.04 (CH_2), 39.13 (CH_3).

HRMS: m/z calculated for $C_{26}H_{26}N_5O$ $[M+H]^+$ 424.2132, found 424.2138;
calculated for $C_{26}H_{25}N_5NaO$ $[M+Na]^+$ 446.1951, found 446.1957.

***tert*-butyl (4-((1*E*,3*E*)-4-(4-((2-azidoethyl)(methyl)amino)phenyl)buta-1,3-dien-1-yl)phenyl) carbamate (F3-5-Boc)**

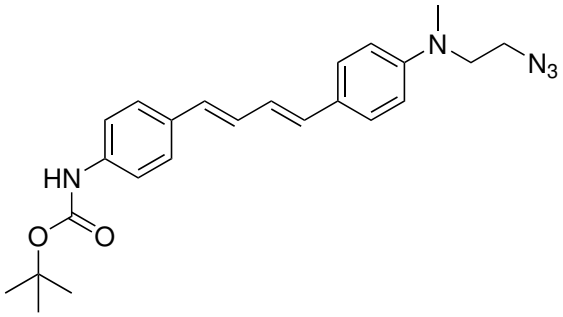

Chemical formula: $C_{24}H_{29}N_5O_2$

Molecular weight: 419.53 g.mol^{-1}

To **F3-5-Bz** (2.37g, 5.60mmol), di-*tert*-butyl dicarbonate (4.27g, 19.6mmol) and 4-dimethylaminopyridine (137mg, 1.12mmol) was added THF (50mL), and the mixture was stirred overnight. The reaction progress was monitored by TLC (PE/AcOEt 70:30) and upon completion, MeOH (5mL) was added to the reaction medium which was then stirred for 15min. Hydrazine hydrate (1.10mL, 22.4mmol) was then added and a precipitate started forming. The reaction progress was monitored by TLC in the same conditions and showed completion after an hour. A saturated aqueous solution of ammonium chloride (10mL) was added and organic solvents were removed under reduced pressure until a precipitate was left in a clear aqueous solution, solid which was then filtered off and dried under reduced pressure. The crude residue was purified over silica gel (DCM) to give 1.81g (77%) of the desired compound as a yellow solid.

R$_f$: 0.74 (PE/AcOEt 70:30)

T$_f$: 177°C

IR (cm^{-1}): 3317, 2978 (CH_3 *asym str*), 2111 (N_3 *asym str*), 1714, 1604, 1519, 1413, 1363, 1317, 1267, 1234, 1212, 1160, 1112, 1053, 1028, 1013, 985, 957, 904, 846, 799, 772, 746.

^{1}H NMR ($CDCl_3$, 400 MHz): δ 7.37-7.29 (m, 6H, 6H$_{Ar}$), 6.86 (dd, *J* = 14.9, 10.5 Hz, 1H, CH=C), 6.78 (dd, *J* = 14.8, 10.5 Hz, 1H, CH=C), 6.71-6.65 (m, 2H, 2H$_{Ar}$), 6.57 (d, *J* = 14.9 Hz, 1H, CH=C), 6.53 (d, *J* = 14.8 Hz, 1H, CH=C), 6.46 (bs, 1H, NH), 3.57 (t, *J* = 5.7 Hz, 2H, N-CH_2-CH_2-$_3$), 3.47 (t, *J* = 5.7 Hz, 2H, N-CH_2-CH_2-N_3), 3.04 (s, 3H, CH_3), 1.52 (s, 9H, ^{t}Bu).

^{13}C NMR ($CDCl_3$, 101 MHz): δ 153.60 (C_q), 152.81 (C_q), 148.52 (C_q), 137.42 (C_q), 133.03 (C_q), 132.68 (CH), 130.06 (CH), 128.96 (CH), 127.79 (2CH$_{Ar}$), 126.94 (2CH$_{Ar}$), 126.35 (C_q), 125.63 (CH), 118.75 (2CH$_{Ar}$), 112.29 (2CH$_{Ar}$), 82.52 (C_q), 63.80 (CH_2), 51.19 (CH_2), 38.92 (CH_3), 28.54 (CH_3), 27.91 (CH_3).

HRMS: m/z calculated for $C_{24}H_{30}N_5O_2$ $[M+H]^+$ 420.2394, found 420.2398;
calculated for $C_{24}H_{29}N_5NaO_2$ $[M+Na]^+$ 442.2213, found 442.2216.

***tert*-butyl (4-((1*E*,3*E*)-4-(4-((2-isothiocyanatoethyl)(methyl)amino)phenyl)buta-1,3-dien-1-yl)phenyl) carbamate (F3-6-Boc)**

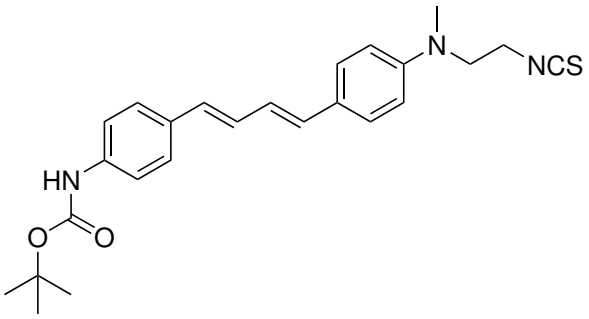

Chemical formula: $C_{25}H_{29}N_3O_2S$

Molecular weight: 435.59 g.mol^{-1}

Compound prepared by following **procedure C** on **F3-5-Boc** (620mg, 1.42mmol), yielding 592mg (92%) of the desired compound as a yellow solid.

R$_f$: 0.65 (PE/AcOEt 70:30)

T$_f$: 191°C

IR (cm^{-1}): 3353, 2983 (CH_3 *asym str*), 2188 (N=C=S *asym str*), 2109 (N=C=S *asym str*), 1707, 1688, 1604, 1582, 1513, 1450, 1433, 1410, 1362, 1319, 1287, 1238, 1190, 1155, 1057, 1030, 1013, 985, 963, 901, 877, 849, 826, 800, 774, 740, 689, 679.

^{1}H NMR (DMSO-*d6*, 400 MHz): δ 9.40 (bs, 1H, NH), 7.42 (d, 2H, *J* = 8.7 Hz, 2H$_{Ar}$), 7.35 (d, 2H, *J* = 8.9 Hz, 2H$_{Ar}$), 7.33 (d, 2H, *J* = 8.9 Hz, 2H$_{Ar}$), 6.91 (dd, 1H, *J* = 15.0, 10.7 Hz, CH=C), 6.81 (dd, 1H, *J* = 15.0, 10.7 Hz, CH=C), 6.74 (d, 2H, *J* = 8.7 Hz, 2H$_{Ar}$), 6.57 (d, 1H, *J* = 15.0 Hz, CH-C$_q$), 6.53 (d, 1H, *J* = 15.0 Hz, CH-C$_q$), 3.82 (t, 2H, *J* = 5.9 Hz, N-CH$_2$-CH$_2$-NCS), 3.69 (t, 2H, *J* = 5.9 Hz, N-CH$_2$-CH$_2$-NCS), 2.98 (s, 3H, CH_3), 1.47 (s, 9H, ^{t}Bu).

^{1}H NMR ($CDCl_3$, 400 MHz): δ 7.42-7.28 (m, 6H, 6H$_{Ar}$), 6.85 (dd, *J* = 14.9, 10.5 Hz, 1H, CH=C), 6.77 (dd, *J* = 14.9, 10.5 Hz, 1H, CH=C), 6.70-6.64 (m, 2H, 2H$_{Ar}$), 6.57 (d, *J* = 14.9 Hz, 1H, CH=C), 6.54 (d, *J* = 14.9 Hz, 1H, CH=C), 6.47 (bs, 1H, NH), 3.73-3.69 (m, 4H, N-CH$_2$-CH$_2$-NCS), 3.07 (s, 3H, CH_3), 1.52 (s, 9H, ^{t}Bu).

^{13}C NMR ($CDCl_3$, 101 MHz): δ 152.79 (C$_q$), 147.43 (C$_q$), 137.49 (C$_q$), 132.87 (C$_q$), 132.29 (CH), 130.46 (CH), 128.75 (CH), 127.89 (2CH$_{Ar}$), 126.99 (2CH$_{Ar}$), 126.16 (CH), 118.70 (2CH$_{Ar}$), 112.44 (2CH$_{Ar}$), 80.81 (C$_q$), 52.42 (CH_2), 42.72 (CH_2), 39.51 (CH_3), 28.54 (3CH_3).

HRMS: *m*/*z* calculated for $C_{25}H_{30}N_3O_2S$ $[M+H]^+$ 436.2053, found 436.2057;
calculated for $C_{25}H_{29}N_3NaO_2S$ $[M+Na]^+$ 458.1873, found 458.1881.

2.5 Synthesis of the nanotriggers

NT-4a-Boc

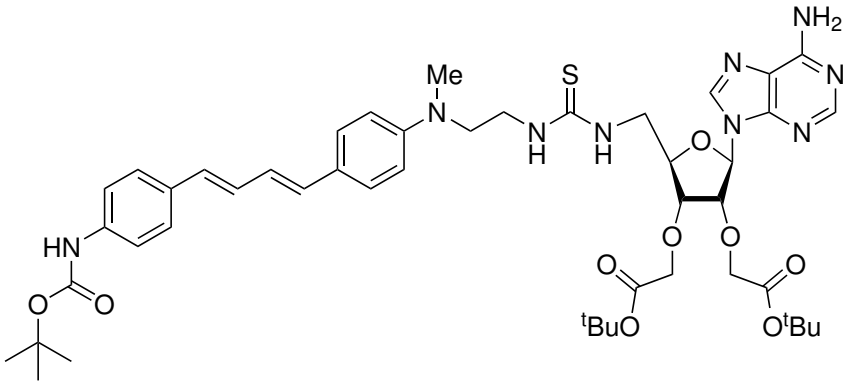

Chemical formula: $C_{47}H_{63}N_9O_9S$

Molecular weight: 930.14 g.mol^{-1}

Compound prepared using **procedure D** with **F3-6-Boc** and **A-4a**, yielding 35−94% of **NT-4a-Boc** after incomplete purification over silica gel (DCM/EtOH from 100:0 to 90:10), *before* purification over C18 silica.

R$_t$ (MeCN/H$_2$O 65:35; 1.75mL/min; 97bar): 21.12min

R$_f$: 0.47 (DCM/EtOH 95:5)

T$_{decomposition}$: 125°C

IR (cm^{-1}): 3335, 2977 (CH_3 *asym str*), 2929 (CH_2 *asym str*), 1727 (C=O ester *str*), 1635 (C−N= *str*), 1604 (N−H *def*), 1515, 1476, 1412, 1368, 1315, 1236, 1154 (C=S thiourea *str*), 1084, 1051, 985, 900, 846, 824, 798, 769, 748, 738, 718, 698, 686, 677.

^{1}H NMR (CDCl$_3$, 400 MHz): δ 8.27 (bs, 1H, NH), 8.08 (bs, 1H, H_2), 7.85 (s, 1H, H_8), 7.36-7.29 (m, 4H, 4H_{Ar}), 7.25 (d, *J* = 8.7 Hz, 2H, 2H_{Ar}), 6.84 (dd, *J* = 15.3, 10.5 Hz, 1H, CH=C), 6.73 (dd, *J* = 15.3, 10.5 Hz, 1H, CH=C), 6.69 (d, *J* = 8.7 Hz, 2H, 2H_{Ar}), 6.57 (bs, 1H, NH), 6.52 (d, *J* = 15.3 Hz, 1H, CH=C), 6.52 (d, *J* = 15.3 Hz, 1H, CH=C), 6.35-6.28 (m, 1H, NH), 5.98 (d, *J* = 5.7 Hz, 1H, $H_{1'}$), 5.85 (bs, 2H, NH_2), 4.68 (t, *J* = 5.7 Hz, 1H, $H_{2'}$), 4.49-4.44 (m, 1H, $H_{3'}$), 4.38-4.34 (m, 1H, $H_{4'}$), 4.28 (d, *J* = 16.9 Hz, 1H, CH), 4.18 (d, *J* = 16.9 Hz, 1H, CH), 4.09 (d, *J* = 16.3 Hz, 1H, CH), 3.99 (d, *J* = 16.3 Hz, 1H, CH), 3.91 (bs, 1H, NH), 3.75-3.42 (m, 6H, N-CH_2-CH_2-N, 2$H_{5'}$), 2.92 (s, 3H, CH_3), 1.52 (s, 9H, ^{t}Bu), 1.50 (s, 9H, ^{t}Bu), 1.34 (s, 9H, ^{t}Bu).

^{13}C NMR ($CDCl_3$, 101 MHz): δ 184.11 (C_q), 169.85 (C_q), 168.95 (C_q), 155.96 (C_q), 152.84 (C_q), 152.53 (C_{Ar}), 149.15 (C_q), 148.91 (C_q), 141.19 (C_{Ar}), 137.47 (C_q), 132.96 (C_q), 132.53 (C_{Ar}), 130.22 (C_{Ar}), 128.88 (C_{Ar}), 127.74 (C_{Ar}), 126.96 (C_q), 126.76 (C_{Ar}), 125.83 (C_{Ar}), 121.08 (C_q), 118.77 (C_{Ar}), 112.85 (C_{Ar}), 89.21 (CH), 82.62 (CH), 82.28 (C_q), 80.81 (C_q), 80.46 (CH), 78.75 (CH), 77.44 (CH), 68.47 (CH_2), 68.32 (CH_2), 51.92 (CH_2), 42.28 (CH_2), 38.51 (CH_3), 28.54 (^{t}Bu), 28.34 (^{t}Bu), 28.17 (^{t}Bu).

HRMS: m/z calculated for $C_{47}H_{64}N_9O_9S$ $[M+H]^+$ 930.4542, found 930.4528;
calculated for $C_{47}H_{65}N_9O_9S$ $[M+2H]^{2+}$ 465.7307, found 465.7304;
calculated for $C_{47}H_{63}N_9NaO_9S$ $[M+Na]^+$ 952.436, found 952.4346.

NT-4b-Boc

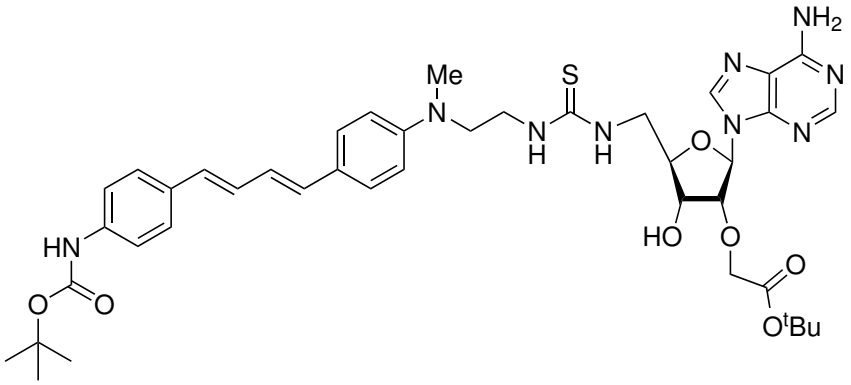

Chemical formula: $C_{41}H_{53}N_9O_7S$

Molecular weight: 815.99 g.mol^{-1}

Compound prepared using **procedure D** with **F3-6-Boc** and **A-4b**, yielding 16−70% of **NT-4b-Boc** after incomplete purification over silica gel (DCM/EtOH from 100:0 to 90:10), *before* purification over C18 silica.

R_t (MeCN/H_2O 65:35; 1.75mL/min; 97bar): 7.15min

R_f: 0.38 (DCM/EtOH 95:5)

$T_{decomposition}$: 135°C

IR (cm^{-1}): 3327, 2925 (CH_3 *asym str*), 1725 (C=O ester *str*), 1637 (C−N= *str*), 1604 (N−H *def*), 1515, 1476, 1412, 1368, 1315, 1240, 1156 (C=S thiourea *str*), 1051, 984, 901, 846, 824, 797, 765, 756, 744, 728, 715, 706, 685.

^{1}H NMR ($CDCl_3$, 400 MHz): δ 8.52 (bs, 1H, NH), 8.05 (bs, 1H, H_2), 7.79 (s, 1H, H_8), 7.34-7.29 (m, 4H, $4H_{Ar}$), 7.23 (d, J = 8.7 Hz, 2H, $2H_{Ar}$), 6.83 (dd, J = 15.2, 10.6 Hz, 1H, CH=C), 6.72 (dd, J = 15.2, 10.6 Hz, 1H, CH=C), 6.67 (d, J = 8.7 Hz, 2H, $2H_{Ar}$), 6.58 (bs, 1H, NH), 6.51 (d, J = 15.2 Hz, 1H, CH=C), 6.49 (d, J = 15.2 Hz, 1H, CH=C), 6.32 (bs, 1H, OH), 5.90 (d, J = 7.0 Hz, 1H, $H_{1'}$), 5.82 (bs, 2H, NH_2), 4.60 (s, 1H, $H_{2'}$), 4.47 (dd, J = 6.8, 4.6 Hz, 1H, $H_{3'}$), 4.42 (bs, 1H, NH), 4.39-4.34 (m, 1H, CH_2-O), 4.10-4.12 (m, 1H, CH_2-O), 3.97-3.87 (m, 1H, $H_{4'}$), 3.82-3.55 (m, 5H, N-CH_2-CH_2-N, $H_{5'a}$), 3.52-3.43 (m, 1H, $H_{5'b}$), 2.92 (s, 3H, CH_3), 1.52 (s, 9H, ^{t}Bu), 1.45 (s, 9H, ^{t}Bu).

^{13}C NMR ($CDCl_3$, 101 MHz): δ 171.10 (C_q), 156.01 (C_q), 152.85 (C_q), 152.51 (C_q), 149.17 (C_q), 148.83 (C_q), 141.71 (C_q), 137.50 (C_q), 132.92 (C_q), 132.41 (C_{Ar}), 130.34 (C_{Ar}), 128.82 (C_{Ar}), 127.71 (C_{Ar}), 126.97 (C_{Ar}), 125.95 (C_{Ar}), 121.28 (C_q), 118.80 (C_{Ar}), 112.98 (C_{Ar}), 88.52 (CH), 85.15 (CH), 84.08 (CH), 83.96 (C_q), 80.83 (C_q), 77.44 (CH), 70.56 (CH), 70.01 (CH_2), 51.97 (CH_2), 42.38 (CH_2), 38.63 (CH_3), 28.54 (^{t}Bu), 28.20 (^{t}Bu).

HRMS: m/z calculated for $C_{41}H_{54}N_9O_7S$ $[M+H]^+$ 816.3861, found 816.3864;
calculated for $C_{41}H_{55}N_9O_7S$ $[M+2H]^{2+}$ 408.6967, found 408.6971;
calculated for $C_{41}H_{53}N_9NaO_7S$ $[M+Na]^+$ 838.3681, found 816.3864.

NT-4c-Boc

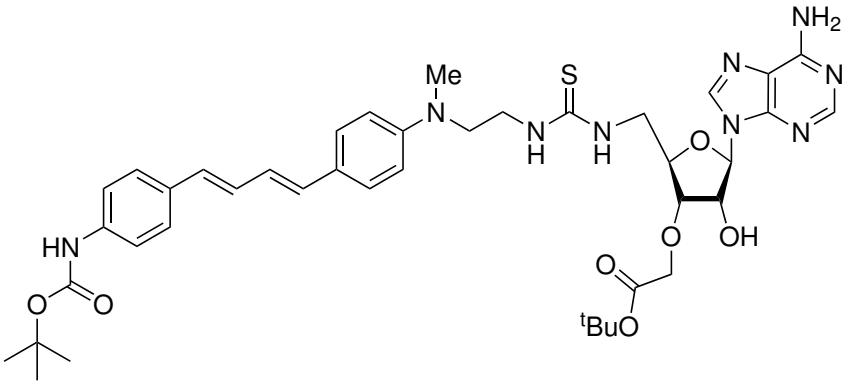

Chemical formula: $C_{41}H_{53}N_9O_7S$

Molecular weight: 815.99 g.mol^{-1}

Compound prepared using **procedure D** with **F3-6-Boc** and **A-4c**, yielding 10−71% of **NT-4c-Boc** after incomplete purification over silica gel (DCM/EtOH from 100:0 to 90:10), *before* purification over C18 silica.

R_t (MeCN/H_2O 65:35; 1.75mL/min; 97bar): 8.42min

R_f: 0.31 (DCM/EtOH 95:5)

$T_{decomposition}$: 135°C

IR (cm^{-1}): 3338, 2977 (CH_3 *asym str*), 2931 (CH_2 *asym str*), 1724 (C=O ester *str*), 1637 (C−N= *str*), 1604 (N−H *def*), 1515, 1477, 1412, 1368, 1316, 1239, 1158 (C=S thiourea *str*), 1081, 1052, 985, 847, 829, 797, 769, 746, 725, 680.

^{1}H NMR ($CDCl_3$, 400 MHz): δ 8.50 (bs, 1H, NH), 8.06 (bs, 1H, H_2), 7.79 (s, 1H, H_8), 7.36-7.28 (m, 4H, $4H_{Ar}$), 7.23 (d, J = 8.8 Hz, 2H, $2H_{Ar}$), 6.82 (dd, J = 15.3, 10.6 Hz, 1H, CH=C), 6.72 (dd, J = 15.3, 10.6 Hz, 1H, CH=C), 6.67 (d, J = 8.8 Hz, 2H, $2H_{Ar}$), 6.58 (bs, 1H, NH), 6.51 (d, J = 15.3 Hz, 1H, CH=C), 6.49 (d, J = 15.3 Hz, 1H, CH=C), 6.40 (bs, 1H, OH), 5.90 (d, J = 7.1 Hz, 1H, $H_{1'}$), 5.81 (bs, 2H, NH_2), 4.58 (s, 1H, $H_{2'}$), 4.48 (dd, J = 6.9, 4.7 Hz, 1H, $H_{3'}$), 4.42 (bs, 1H, NH), 4.39-4.34 (m, 1H, CH_2-O), 4.19-4.11 (m, 1H, CH_2-O), 3.97-3.87 (m, 1H, $H_{4'}$), 3.79-3.69 (m, 4H, N-CH_2-CH_2-N), 3.68-3.55 (m, 1H, $H_{5'a}$), 3.51-3.42 (m, 1H, $H_{5'b}$), 2.92 (s, 3H, CH_3), 1.52 (s, 9H, ^{t}Bu), 1.45 (s, 9H, ^{t}Bu).

^{13}C NMR ($CDCl_3$, 101 MHz): δ 184.16 (C_q), 171.25 (C_q), 155.98 (C_q), 152.85 (C_q), 149.17 (C_q), 148.65 (C_q), 141.33 (C_q), 137.46 (C_q), 132.99 (C_q), 132.49 (C_{Ar}), 130.21 (C_{Ar}), 128.93 (C_{Ar}), 127.65 (C_{Ar}), 126.97 (C_{Ar}), 125.90 (C_{Ar}), 121.27 (C_q), 118.78 (C_{Ar}), 112.91 (C_{Ar}), 91.51 (C_{Ar}), 83.68 (CH), 82.63 (CH), 80.81 (C_q), 77.44 (CH), 73.12 (CH), 69.93 (CH_2), 51.85 (CH_2), 46.06 (CH_2), 42.37 (CH_2), 38.26 (CH_3), 28.55 (^{t}Bu), 28.28 (^{t}Bu).

HRMS: m/z calculated for $C_{41}H_{54}N_9O_7S$ $[M+H]^+$ 816.3861, found 816.3859;
calculated for $C_{41}H_{55}N_9O_7S$ $[M+2H]^{2+}$ 408.6967, found 408.6970;
calculated for $C_{41}H_{53}N_9NaO_7S$ $[M+Na]^+$ 838.3681, found 838.3681.

NT-4i-Boc

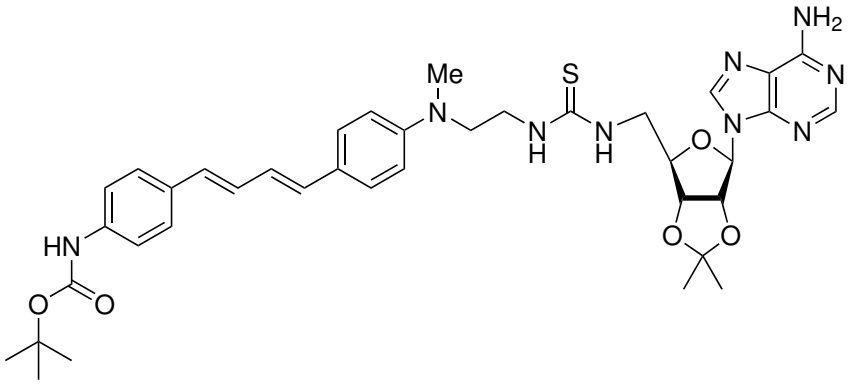

Chemical formula: $C_{38}H_{47}N_9O_5S$

Molecular weight: 741.91 g.mol^{-1}

Compound prepared using **procedure D** with **F3-6-Boc** and **A-4i**, yielding 44−88% of **NT-4i-Boc** after incomplete purification over silica gel (DCM/EtOH from 100:0 to 90:10), *before* purification over C18 silica.

R_t (MeCN/H_2O 65:35; 1.75mL/min; 97bar): 7.52min

R_f: 0.40 (DCM/EtOH 95:5)

$T_{decomposition}$: 149°C

IR (cm^{-1}): 3350, 2979 (CH_3 *asym str*), 2933 (CH_2 *asym str*), 1704, 1636 (C−N= *str*), 1604 (N−H *def*), 1514, 1475, 1412, 1370, 1316, 1235, 1187, 1157 (C=S thiourea *str*), 1090, 1053, 1027, 984, 903, 845, 817, 797, 769, 746, 724.

^{1}H NMR ($CDCl_3$, 400 MHz): δ 8.35 (bs, 1H, NH), 8.09 (bs, 1H, H_2), 7.71 (s, 1H, H_8), 7.36-7.28 (m, 4H, $4H_{Ar}$), 7.19 (d, *J* = 8.6 Hz, 2H, $2H_{Ar}$), 6.81 (dd, *J* = 15.3, 10.5 Hz, 1H, CH=C), 6.68 (dd, *J* = 15.3, 10.5 Hz, 1H, CH=C), 6.65 (d, *J* = 8.6 Hz, 2H, $2H_{Ar}$), 6.59 (bs, 1H, NH), 6.49 (d, *J* = 15.3 Hz, 1H, CH=C), 6.44 (d, *J* = 15.3 Hz, 1H, CH=C), 6.26-6.17 (m, 1H, NH), 5.84 (bs, 2H, NH_2), 5.77 (d, *J* = 4.6Hz, 1H, $H_{1'}$),5.10(dd, *J* = 6.0,4.6Hz, 1H, $H_{2'}$),4.92(dd, *J* = 6.0,2.1 Hz, 1H, $H_{3'}$), 4.55-4.46 (m, 1H, $H_{4'}$), 3.96-3.79 (m, 2H, N-CH_2), 3.65-3.50 (m, 4H, N-$CH_2$2; 2$H_{5'}$), 2.92 (s, 3H, CH_3), 1.63 (s, 3H, CH_3), 1.52 (s, 9H, ^{t}Bu), 1.37 (s, 3H, CH_3).

^{13}C NMR ($CDCl_3$, 101 MHz): δ 184.27 (C_q), 155.97 (C_q), 152.86 (C_q), 152.59 (C_q), 149.19 (C_q), 148.62 (C_q), 140.78 (C_q), 137.50 (C_q), 132.91 (C_q), 132.37 (C_{Ar}), 130.23 (C_{Ar}), 128.86 (C_{Ar}), 127.65 (C_{Ar}), 126.94 (C_{Ar}), 126.73 (C_{Ar}), 125.88 (C_{Ar}), 121.07 (C_q), 118.81 (C_{Ar}), 114.86 (C_q), 112.86 (C_{Ar}), 92.69 (C_{Ar}), 83.95 (CH), 82.50 (CH), 81.65 (CH_2), 80.82 (C_q), 77.44 (CH), 51.71 (CH_2), 46.27 (CH_2), 42.52 (CH_2), 38.30 (CH_3), 28.54 (^{t}Bu), 27.79 (CH_3), 25.56 (CH_3).

HRMS: m/z calculated for $C_{38}H_{48}N_9O_5S$ $[M+H]^+$ 742.3494, found 742.3491; calculated for $C_{38}H_{47}N_9NaO_5S$ $[M+Na]^+$ 764.3313, found 764.3300.

NT-5a

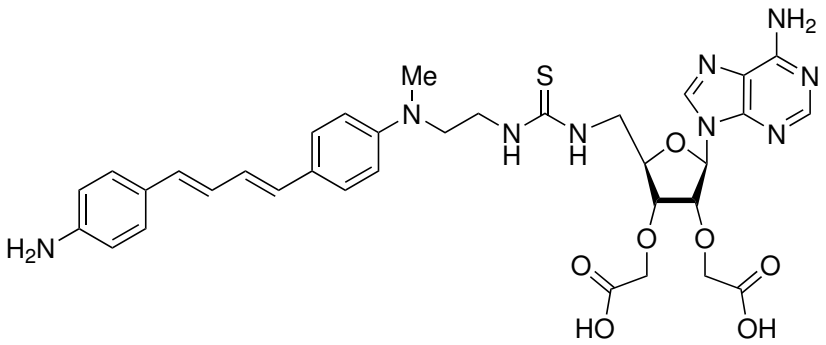

Chemical formula: $C_{34}H_{39}N_9O_7S$

Molecular weight: 717.80 g.mol^{-1}

NT-4a-Boc was dissolved in DCM/TFA 9:1 and the mixture was stirred at room temperature for 2hrs. The desired compound was recovered after removal of the solvents under reduced pressure.

R_f: 0.59 (MeCN/H_2O 60:40, C18 silica)

$T_{decomposition}$: 126°C

IR (cm^{-1}): 3321, 3099, 2926 (CH_2 *asym str*), 2610, 1671 (C−N= *str*), 1556, 1509, 1430, 1196, 1141 (C=S thiourea *str*), 989, 837, 798, 754, 722, 707.

^{1}H NMR (CD_3OD, 400 MHz): δ 8.45 (s, 1H, H_2), 8.40 (bs, 1H, H_8), 7.60 (d, J = 8.6 Hz, 2H, $2H_{Ar}$), 7.38 (d, J = 8.6 Hz, 2H, $2H_{Ar}$), 7.33 (d, J = 8.6 Hz, 2H, $2H_{Ar}$), 7.06 (dd, J = 15.4, 10.5 Hz, 1H, CH=C), 6.97 (d, J = 8.6 Hz, 2H, $2H_{Ar}$), 6.86 (dd, J = 15.4, 10.5 Hz, 1H, CH=C), 6.66 (d, J = 15.4 Hz, 1H, CH=C), 6.64 (d, J = 15.4 Hz, 1H, CH=C), 6.23 (d, J = 4.9 Hz, 1H, $H_{1'}$), 4.85-4.77 (m, 1H, $H_{2'}$), 4.49-4.43 (m, 1H, $H_{3'}$), 4.43-4.20 (m, 5H, $2CH_2$-O; $H_{4'}$), 3.90 (bs, 2H, NH_2), 3.75-3.65 (m, 2H, N-CH_2), 3.64-3.57 (m, 2H, N-CH_2), 3.29-3.22 (m, 2H, $2H_{5'}$), 3.06 (s, 3H, CH_3).

^{13}C NMR (CD_3OD, 101 MHz): δ 174.00 (C_q COOH), 173.56 (C_q COOH), 152.39 (C_q), 149.96 (CH_{Ar}), 149.00 (C_q), 146.03 (C_q), 144.58 (C_q), 140.43 (CH_{Ar}), 135.49 (=CH), 133.16 (=CH), 131.70 (C_q), 130.64 (C_q), 130.05 (=CH), 129.08 (CH_{Ar}), 128.73 (CH_{Ar}), 126.99 (=CH), 124.34 (CH_{Ar}), 121.08 (C_q), 115.15 (CH_{Ar}), 89.77 (CH), 83.40 (CH), 82.12 (CH), 79.26 (CH), 68.40 ($3CH_2$), 53.65 (CH_2), 42.54 (CH_2), 40.17 (CH_3).

HRMS: m/z calculated for $C_{34}H_{40}N_9O_7S$ $[M+H]^+$ 718.2766, found 718.2757;
calculated for $C_{34}H_{41}N_9O_7S$ $[M+2H]^{2+}$: 359.6419, found 359.6421;
calculated for $C_{34}H_{42}N_9O_7S$ $[M+3H]^{3+}$ 240.0970, found 240.0980.

NT-5b

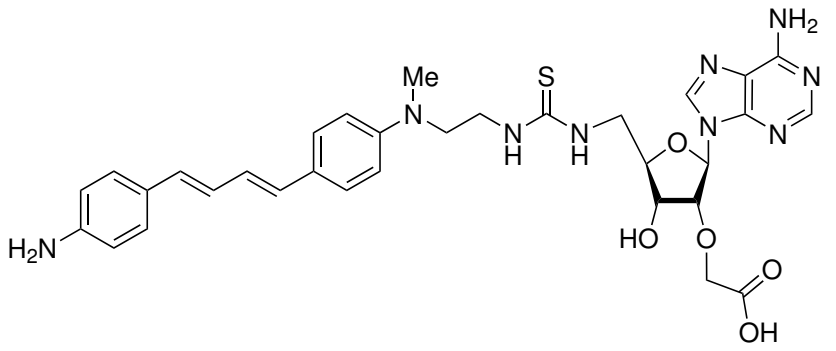

Chemical formula: $C_{32}H_{37}N_9O_5S$

Molecular weight: 659.77 g.mol^{-1}

NT-4b-Boc was dissolved in DCM/TFA 9:1 and the mixture was stirred at room temperature for 2hrs. The desired compound was recovered after removal of the solvents under reduced pressure.

R$_f$: 0.56 (MeCN/H_2O 60:40, C18 silica)

T$_{decomposition}$: 104°C

IR (cm^{-1}): 3310, 3083, 2916 (CH_2 *asym str*), 2851 (CH_2 *sym str*), 2627, 1673 (C−N= *str*), 1556, 1509, 1428, 1199, 1136 (C=S thiourea *str*), 988, 838, 798, 722, 691.

^{1}H NMR (CD_3OD, 400 MHz): δ 8.46 (s, 1H, H_2), 8.42 (bs, 1H, H_8), 7.65-7.56 (m, 2H, 2H_{Ar}r), 7.42-7.35 (m, 2H, 2H_{Ar}), 7.35-7.30 (m, 2H, 2H_{Ar}), 7.06 (dd, *J* = 15.4, 10.4 Hz, 1H, CH=C), 7.01-6.94 (m, 2H, 2H_{Ar}), 6.86 (dd, *J* = 15.4, 10.4 Hz, 1H, CH=C), 6.66 (d, *J* = 15.4 Hz, 1H, CH=C), 6.64 (d, *J* = 15.4 Hz, 1H, CH=C), 6.23-6.17 (m, 1H, $H_{1'}$), 4.73-4.59 (m, 1H, $H_{2'}$), 4.50-4.44 (m, 1H, $H_{3'}$), 4.32-4.16 (m, 3H, CH_2-O; $H_{4'}$), 3.90 (bs, 2H, NH_2), 3.75-3.68 (m, 2H, N-CH_2), 3.65-3.56 (m, 2H, N-CH_2), 3.38-3.32 (m, 2H, 2$H_{5'}$), 3.06 (s, 3H, CH_3).

^{13}C NMR (CD_3OD, 101 MHz): δ 174.14 (C_q COOH), 152.31 (C_q), 150.00 (CH_{Ar}), 145.93 (CH_{Ar}), 144.78 (C_q), 144.70 (CH_{Ar}), 140.45 (C_q), 135.33 (=CH), 133.12 (=CH), 130.60 (C_q), 130.28 (=CH), 129.12 (CH_{Ar}), 128.77 (CH_{Ar}), 127.42 (=CH), 124.39 (CH_{Ar}), 121.09 (C_q), 115.68 (CH_{Ar}), 89.63 (CH), 85.11 (CH), 83.98 (CH), 83.87 (CH), 69.56 (CH_2), 68.94 (CH_2), 54.10 (CH_2), 42.43 (CH_2), 40.58 (CH_3).

HRMS: *m*/*z* calculated for $C_{32}H_{38}N_9O_5S$ $[M+H]^+$ 660.2711, found 660.2704;
calculated for $C_{32}H_{39}N_9O_5S$ $[M+2H]^{2+}$ 330.6392, found 330.6398.

NT-5c

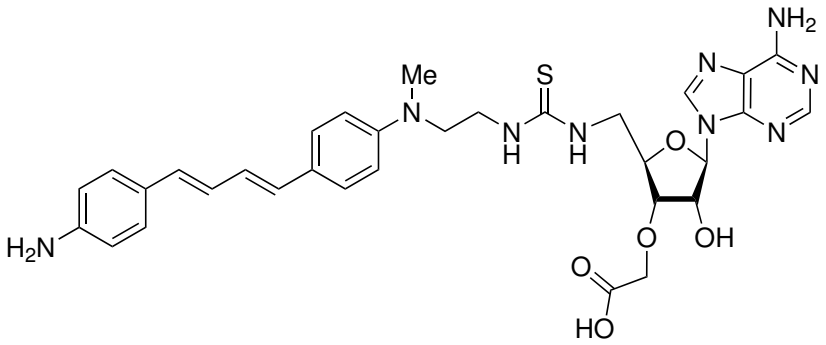

Chemical formula: $C_{32}H_{37}N_9O_5S$

Molecular weight: 659.77 g.mol^{-1}

NT-4c-Boc was dissolved in DCM/TFA 9:1 and the mixture was stirred at room temperature for 2hrs. The desired compound was recovered after removal of the solvents under reduced pressure.

R$_f$: 0.57 (MeCN/H_2O 60:40, C18 silica)

T$_{decomposition}$: 117°C

IR (cm^{-1}): 3310, 3085, 2921 (CH_2 *asym str*), 2619, 1673 (C−N= *str*), 1556, 1509, 1429, 1197, 1138 (C=S thiourea *str*), 988, 838, 798, 722, 707, 681.

^{1}H NMR (CD_3OD, 400 MHz): δ 8.43 (s, 1H, H_2), 8.39 (bs, 1H, H_8), 7.64-7.56 (m, 2H, $2H_{Ar}$), 7.44-7.36 (m, 2H, $2H_{Ar}$), 7.35-7.30 (m, 2H, $2H_{Ar}$), 7.14-6.95 (m, 3H, $2H_{Ar}$; CH=C), 6.92-6.79 (m, 1H, CH=C), 6.71-6.57 (m, 2H, 2CH=C), 6.05-5.99 (m, 1H, $H_{1'}$), 4.82-4.71 (m, 1H, $H_{2'}$), 4.40-4.24 (m, 4H, CH_2-O; $H_{3'}$; $H_{4'}$), 3.90 (bs, 2H, NH_2), 3.77-3.68 (m, 2H, N-CH_2), 3.67-3.57 (m, 2H, N-CH_2), 3.37-3.32 (m, 2H, $2H_{5'}$), 3.08 (s, 3H, CH_3).

^{13}C NMR (CD_3OD, 101 MHz): δ 174.78 (C_q COOH), 152.28 (C_q), 149.94 (CH_{Ar}), 145.91 (C_q), 144.43 (C_q), 144.35 (C_q), 140.40 (CH_{Ar}), 136.90 (C_q), 135.11 (=CH), 133.03 (=CH), 130.62 (C_q), 130.50 (=CH), 129.13 (CH_{Ar}), 128.79 (CH_{Ar}), 127.77 (=CH), 124.42 (CH_{Ar}), 121.02 (C_q), 116.09 (CH_{Ar}), 91.03 (CH), 86.79 (CH), 83.40 (CH), 81.56 (CH), 74.94 (CH_2), 69.13 (CH_2), 52.75 (CH_2), 42.42 (CH_2), 40.92 (CH_3).

HRMS: m/z calculated for $C_{32}H_{38}N_9O_5S$ $[M+H]^+$ 660.2711, found 660.2707;
calculated for $C_{32}H_{39}N_9O_5S$ $[M+2H]^{2+}$ 330.6392, found 330.6394.

NT-5

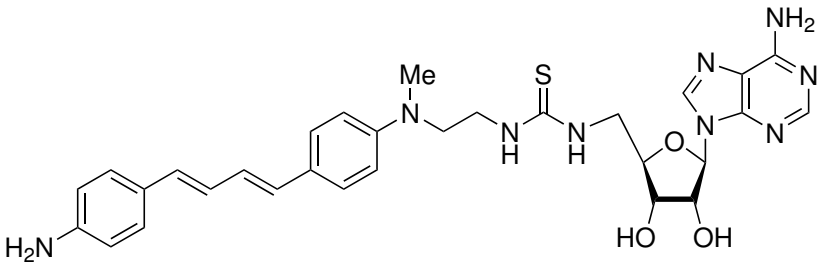

Chemical formula: $C_{30}H_{35}N_9O_3S$

Molecular weight: 601.73 g.mol^{-1}

NT-4i-Boc was dissolved in TFA/EtOH 9:1 and the mixture was stirred at room temperature for 2hrs. The desired compound was recovered after removal of the solvents under reduced pressure.

R$_f$: 0.52 (MeCN/H_2O 60:40, C18 silica)

T$_{decomposition}$: 94°C

IR (cm^{-1}): 3297, 3088, 2917 (CH_2 *asym str*), 2850 (CH_2 *sym str*), 2621, 1672 (C−N= *str*), 1558, 1509, 1428, 1197, 1135 (C=S thiourea *str*), 988, 840, 798, 722.

^{1}H NMR (CD_3OD, 400 MHz): δ 8.45 (s, 1H, H_2), 8.40 (bs, 1H, H_8), 7.64-7.58 (m, 2H, $2H_{Ar}$), 7.47-7.38 (m, 2H, $2H_{Ar}$), 7.38-7.29 (m, 2H, $2H_{Ar}$), 7.15-7.01 (m, 3H, $2H_{Ar}$; CH=C), 6.89 (dd, *J* = 15.4, 10.6 Hz, 1H, CH=C), 6.66 (d, *J* = 15.4 Hz, 1H, CH=C), 6.66 (d, *J* = 15.4 Hz, 1H, CH=C), 6.02 (d, *J* = 5.2 Hz, 1H, $H_{1'}$), 4.68 (t, *J* = 5.2 Hz, 1H, $H_{2'}$), 4.35 (dd, *J* = 5.2, 4.0 Hz, 1H, $H_{3'}$), 4.26-4.19 (m, 1H, $H_{4'}$), 3.90 (bs, 2H, NH_2), 3.76-3.70 (m, 2H, N-CH_2), 3.69-3.61 (m, 2H, N-CH_2), 3.38-3.31 (m, 2H, $2H_{5'}$), 3.10 (s, 3H, CH_3).

^{13}C NMR (CD_3OD, 101 MHz): δ 152.39 (C_q), 149.94 (C_q), 148.75 (C_q), 146.04 (CH_{Ar}), 144.41 (CH_{Ar}), 140.35 (C_q), 135.33 (=CH), 133.09 (=CH), 130.67 (C_q), 130.18 (=CH), 129.07 (CH_{Ar}), 128.73 (CH_{Ar}), 127.20 (=CH), 124.37 (CH_{Ar}), 121.03 (C_q), 115.41 (CH_{Ar}), 91.19 (CH), 85.33 (CH), 75.58 (CH), 72.61 (CH), 70.70 (CH_2), 53.92 (CH_2), 42.51 (CH_2), 40.33 (CH_3).

HRMS: *m*/*z* calculated for $C_{30}H_{36}N_9O_3S$ $[M+H]^+$ 602.2656, found 602.2647;
calculated for $C_{30}H_{37}N_9O_3S$ $[M+2H]^{2+}$ 301.6365, found 301.6372;
calculated for $C_{30}H_{35}N_9NaO_3S$ $[M+Na]^+$ 624.2476, found 624.2469.

2.6 Synthesis of the non-commercially available reagents

dibenzyl phosphorochloridate (R-1)[168]

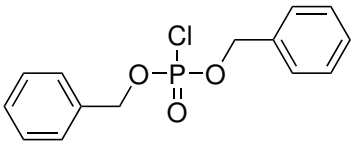

Chemical formula: $C_{14}H_{14}O_3PCl$

Molecular weight: 296.69 g.mol^{-1}

To a solution of *N*-chlorosuccinimide (4.32g, 32.4mmol) in anhydrous toluene (80mL) under an argon atmosphere was added dibenzylphosphite (2.42g, 9.23mmol) and the solution was stirred overnight. The excess *N*-chlorosuccinimide was precipitated by addition of PE and filtered off. Solvents were then removed under reduced pressure to give the desired compound used without further purification.

((1,3-dioxolan-2-yl)methyl)tributylphosphonium bromide (R-2)[144]

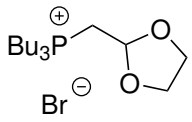

Chemical formula: $C_{16}H_{34}O_2PBr$

Molecular weight: 369.32 g.mol^{-1}

2-Bromomethyl-1,3-dioxolane (6.50mL, 62.8mmol) and tributylphosphine (15.50mL, 62.8mmol) were mixed in a flask under argon, and stirred at 95°C overnight. Stirring was set to 180 rotation per minute (RPM) to keep an even stirring even when the mixture thickens over the progress of the reaction. The reaction progress was monitored by ^{1}H NMR and was considered complete when reagents signals accounted for less than 5% of the desired compound signals. The desired compound was recovered as a pale yellow very viscous oil and used without further purification.

IR (cm^{-1}): 2958 (CH_3 *asym str*), 2932 (CH_2 *asym str*), 2872 (CH_2 *asym str*), 1464, 1383, 1231, 1130, 1097, 1017, 971, 942, 918, 817, 718.

^{1}H NMR (CDCl3, 400 MHz): δ 5.26 (dt, 1H, $J_{3,P-H}$ = 11.2 Hz, $J_{3,H-H}$ = 4.3 Hz, O-CH), 4.08 (t, 2H, J = 7.1 Hz, CH_2-O), 3.94 (t, 2H, J = 7.1 Hz, CH_2-O), 3.10 (dd, 2H, $J_{2,P-H}$ = 13.0 Hz, $J_{3,H-H}$ = 4.3 Hz, CH_2-P), 2.55-2.43 (m, 6H, $3CH_2$), 1.61-1.50 (m, 12H, $3CH_2$-CH_2), 0.98 (t, 9H, J = 6.9 Hz, $3CH_3$).

HRMS: m/z calculated for $C_{16}H_{34}O_2PBr$ $[M-Br]^+$ 289.2291, found 289.2290.

diethyl (4-benzamidobenzyl)phosphonate (P-Bz)[195,144]

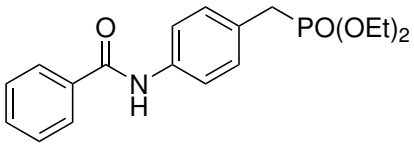

Chemical formula: $C_{18}H_{22}NO_4P$

Molecular weight: 347.35 g.mol^{-1}

To diethyl-4-aminobenzylphosphonate (14.60g, 60.02mmol) under an argon atmosphere was added toluene (450mL) and triethylamine (12.1mL, 86.8mmol). Slow addition of benzoyl chloride (7.7mL, 66.3mmol) was then performed and the mixture was stirred overnight. The reaction progress was monitored by TLC (PE/AcOEt 20:80) and upon completion distilled water (400mL) and DCM (450mL) were added. Phases were separated, the aqueous layer was further extracted 3 times with DCM, then the organic layers were combined, dried over magnesium sulfate, filtered on cotton and evaporated under reduced pressure. The crude residue was purified over silica gel (PE/AcOEt from 100:0 to 0:100) to give 19.60g (94%) of the desired compound as a white solid.

R_f: 0.17 (PE/AcOEt 20:80)

T_f: 159°C

IR (cm^{-1}): 3242, 2985 (CH_3 *asym str*), 1651 (C=O secondary amide *str*), 1601, 1579, 1532, 1514, 1492, 1447, 1414, 1323, 1246, 1182, 1144, 1101, 1057, 1030 (P−OC_2H_5), 972, 958, 897, 841, 797, 736, 702, 688.

^{1}H NMR ($CDCl_3$, 400 MHz): δ 8.57 (bs, 1H, NH), 7.92 (d, 2H, J = 8.0 Hz, $2H_{Ar}$), 7.64 (d, 2H, J = 8.3 Hz, $2H_{Ar}$), 7.56-7.50 (m, 1H, H_{Ar}), 7.50-7.40 (m, 2H, $2H_{Ar}$), 7.26 (dd, 2H, J = 8.3, 2.4 Hz, $2H_{Ar}$), 3.97 (dq, 2H, J = 8.0, 7.0 Hz, O-CH_2), 3.97 (dq, 2H, J = 8.0, 7.0 Hz, O-CH_2), 3.12 (d, 2H, $J_{2,P-H}$ = 21.5 Hz, P-CH_2), 1.23 (t, 6H, J = 7.1 Hz, $2CH_3$).

^{13}C NMR ($CDCl_3$, 101 MHz): δ 166.16 (C_q), 137.47 (d, J = 4 Hz, C_q), 135.28 (C_q), 131.87 (C_{Ar}), 130.49 (C_{Ar}), 130.43 (C_{Ar}), 128.78 ($2C_{Ar}$), 127.49 ($2C_{Ar}$), 127.29 (d, J = 9.1 Hz, C_q), 120.66 (C_{Ar}), 120.64 (C_{Ar}), 62.40 (CH_2), 62.34 (CH_2), 33.29 (d, J = 138.6 Hz, P-CH_2), 16.60 (CH_3), 16.54 (CH_3).

***tert*-butyl (4-((diethoxyphosphoryl)methyl)phenyl)carbamate (P-Boc)[144]**

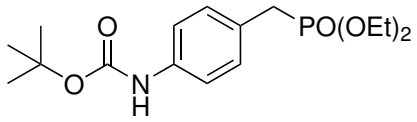

Chemical formula: $C_{16}H_{26}NO_5P$

Molecular weight: 343.36 g.mol^{-1}

To a stirred solution of diethyl-4-aminobenzylphosphonate (4.94g, 20.4mmol) in anhydrous THF (20mL) under a dinitrogen atmosphere was added a solution of di-*tert*-butyl dicarbonate (10.40g, 47.7mmol) in anhydrous THF (20mL). The reaction mixture was heated to 75°C and stirred overnight. The reaction progress was monitored by TLC (PE/AcOEt 50:50) and upon completion solvents were removed under reduced pressure. To the crude oily residue was added a saturated solution of ammonium chloride (30mL), distilled water (10mL) and DCM (30mL). Phases were separated, and the aqueous layer was further extracted 2 times with DCM, organic layers were combined, dried over magnesium sulfate, filtered on cotton and evaporated under reduced pressure. The crude residue was purified over silica gel (PE/AcOEt from 100:0 to 0:100) to give 6.41g (92%) of the desired compound as a white solid.

R$_f$: 0.12 (PE/AcOEt 50:50)

T$_f$: 121°C

IR (cm^{-1}): 3270, 2979 (CH_3 *asym str*), 1708, 1598, 1532, 1451, 1412, 1391, 1364, 1320, 1241, 1161, 1102, 1051, 1031 (P−OC_2H_5), 964, 907, 850, 819, 774, 727.

^{1}H NMR ($CDCl_3$, 400 MHz): δ 7.31 (d, 2H, J = 8.6 Hz, 2H$_{Ar}$), 7.21 (dd, 2H, J = 8.6, 2.3 Hz, 2H$_{Ar}$), 6.50 (bs, 1H, NH), 4.08-3.93 (m, 4H, 2xO-CH_2), 3.10 (d, 2H, $J_{2,P-H}$ = 21.4 Hz, P-CH_2), 1.51 (s, 9H, ^{t}Bu), 1.24 (t, 6H, J = 7.1 Hz, 2CH_3).

***tert*-butyl (*tert*-butoxycarbonyl)(4-((diethoxyphosphoryl)methyl)phenyl)carbamate (P-2Boc)**

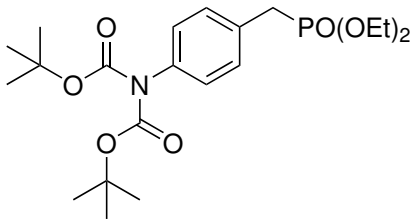

Chemical formula: $C_{21}H_{34}NO_7P$

Molecular weight: 443.48 g.mol^{-1}

P-Boc (505mg, 1.47mmol), di-*tert*-butyl dicarbonate (489mg, 2.24mmol), 4-dimethylaminopyridine (20mg, 0.16mmol) and triethylamine (0.20mL, 1.48mmol) were dissolved in anhydrous DCM (3mL, 0.5M) under a dinitrogen atmosphere and stirred for 4 days. The reaction progress was monitored by TLC (PE/AcOEt 50:50) and upon completion a saturated solution of sodium hydrogenocarbonate was added until no more carbon dioxide bubbles formed. The mixture was then extracted 3 times with DCM, organic phases were reunited, dried over magnesium sulfate, filtered over cotton and solvents were removed under reduced pressure. The crude residue was then purified over neutralized silica gel (PE with 5% triethylamine/AcOEt from 100:0 to 40:60) yielding 687mg (quant.) of the desired compound mixed with grease.

R_f: 0.18 (PE/AcOEt 50:50); 0.68 (AcOEt/EtOH 85:15)

^{1}H NMR ($CDCl_3$, 400 MHz): δ 7.30 (dd, 2H, J = 8.3, 2.1 Hz, $2H_{Ar}$), 7.08 (dd, 2H, J = 8.3 Hz, $2H_{Ar}$), 4.08-3.90 (m, 4H, 2xO-CH_2), 3.16 (d, 2H, $J_{2,P-H}$ = 21.7 Hz, P-CH_2), 1.40 (s, 18H, ^{t}Bu), 1.24 (t, 6H, J = 6.9 Hz, $2CH_3$).

diethyl (4-((diphenylmethylene)amino)benzyl)phosphonate (P-Bp)

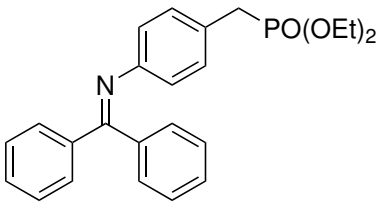

Chemical formula: $C_{24}H_{26}NO_3P$

Molecular weight: 407.45 g.mol^{-1}

Diethyl-4-aminobenzylphosphonate (1.00g, 4.13mmol), PTSA monohydrate (71mg, 0.41mmol) and benzophenone (759mg, 4.17mmol) were dissolved in toluene (4mL, 1M) before heating to reflux under stirring for 3 days. The reaction progress was monitored by TLC (DCM/MeOH 95:5) and upon reaching the maximum progress a saturated solution of sodium hydrogenocarbonate (5mL) was added and the mixture was stirred until no more carbon dioxide bubbles formed. Then toluene was evaporated under reduced pressure and the resulting mixture was extracted 3 times with DCM, organic phases were reunited, dried over magnesium sulfate, filtered over cotton and solvents were removed under reduced pressure. The crude residue was purified over silica gel (DCM/MeOH from 100:0 to 90:10) to give 612mg (36%) of the desired compound as a yellow solid.

R_f: 0.15 (PE/AcOEt 50:50); 0.51 (DCM/MeOH 95:5)

^{1}H NMR ($CDCl_3$, 400 MHz): δ 7.73 (d, 2H, J = 8.2 Hz, $2H_{Ar}$), 7.47 (t, 1H, J = 6.9 Hz, H_{Ar}), 7.40 (t, 2H, J = 7.6 Hz, $2H_{Ar}$), 7.28-7.20 (m, 3H, $3H_{Ar}$), 7.14-7.05 (m, 4H, $4H_{Ar}$), 6.68 (d, 2H, J = 8.2 Hz, $2H_{Ar}$), 3.99-3.79 (m, 4H, 2xO-CH_2), 3.04 (d, 2H, $J_{2,P-H}$ = 21.3 Hz, P-CH_2), 1.18 (t, 6H, J = 7.1 Hz, $2CH_3$).

Bibliography

(1) Balard, A.-J. *Ann. Chim. Phys.* **1844**, *12*, 294–330.

(2) Guthrie, F. *Q. J. Chem. Soc.* **1859**, *11*, 245–252.

(3) Brunton, T. L. *Lancet* **1867**, *90*, 97–98.

(4) Sobrero, A. *C. r. hebd. séances Acad. sci.* **1847**, 247–248.

(5) Murrell, W. *Lancet* **1879**, *113*, 80–81.

(6) Hill, N. S.; Antman, E. M.; Green, L. H.; Alpert, J. S. *CHEST* **1981**, *79*, 69–76.

(7) Miller, M. R.; Megson, I. L. *Br. J. Pharmac.* **2007**, *151*, 305–321.

(8) Hay, M. *Earth Environ. Sci. Trans. R. Soc. Edinb.* **1883**, *32*, 67–86.

(9) Krantz, J. C.; Carr, C. J.; Forman, S. E.; Cone, N. *J. Pharmacol. Exp. Ther.* **1940**, *70*, 323–327.

(10) Rath, M. M.; Krantz, J. C. *J. Pharmacol. Exp. Ther.* **1942**, *76*, 33–38.

(11) Schultz, K.-D.; Schultz, K.; Schultz, G. *Nature* **1977**, *265*, 750–751.

(12) Katsuki, S.; Arnold, W.; Mittal, C.; Murad, F. *J. Cyclic Nucleotide Res.* **1977**, *3*, 23–35.

(13) Murad, F.; Mittal, C. K.; Arnold, W. P.; Katsuki, S.; Kimura, H. *Adv. Cyclic Nucleotide Res.* **1978**, *9*, 145–158.

(14) Kukovetz, W. R.; Holzmann, S.; Wurm, A.; Pöch, G. *Naunyn-Schmiedeberg's Arch. Pharmacol.* **1979**, *310*, 129–138.

(15) Ignarro, L. J.; Lippton, H.; Edwards, J. C.; Baricos, W. H.; Hyman, A. L.; Kadowitz, P. J.; Gruetter, C. A. *J. Pharmacol. Exp. Ther.* **1981**, *218*, 739–749.

(16) Parks, N. J.; Krohn, K. A.; Mathis, C. A.; Chasko, J. H.; Geiger, K. R.; Gregor, M. E.; Peek, N. F. *Science* **1981**, *212*, 58–60.

(17) Bennett, B. M.; Marks, G. S. *Trends Pharmacol. Sci.* **1984**, *5*, 329–332.

(18) Romanin, C.; Kukovetz, W. R. *J. Mol. Cell. Cardiol.* **1988**, *20*, 389–396.

(19) Deguchi, T.; Yoshioka, M. *J. Biol. Chem.* **1982**, *257*, 10147–10151.

(20) Moncada, S.; Gryglewski, R.; Bunting, S.; Vane, J. R. *Nature* **1976**, *263*, 663–665.

(21) Furchgott, R. F.; Zawadzki, J. V. *Nature* **1980**, *288*, 373–376.

(22) Ferreira, S. H.; Moncada, S.; Vane, J. R. *Nat. New Biol.* **1971**, *231*, 237–239.

(23) Moncada, S.; Palmer, R. M. J.; Higgs, E. A. In *Biology and Pathology of Platelet-Vessel Wall Interactions*, Academic Press, London; Orlando, 1986, pp 289–304.

(24) Busse, R.; Trogisch, G.; Bassenge, E. *Basic Res. Cardiol.* **1985**, *80*, 475–490.

(25) Cocks, T. M.; Angus, J. A.; Campbell, J. H.; Campbell, G. R. *J. Cell. Physiol.* **1985**, *123*, 310–320.

(26) Gryglewski, R. J.; Moncada, S.; Palmer, R. M. J. *Br. J. Pharmac.* **1986**, *87*, 685–694.

(27) Vane, J. R. *Br. J. Pharmacol. Chemother.* **1964**, *23*, 360–373.

(28) Azuma, H.; Ishikawa, M.; Sekizaki, S. *Br. J. Pharmac.* **1986**, *88*, 411–415.

(29) Radomski, M. W.; Palmer, R. M.; Moncada, S. *Br. J. Pharmacol.* **1987**, *92*, 181–187.

(30) Radomski, M. W.; Palmer, R. M. J.; Moncada, S. *Lancet* **1987**, *330*, 1057–1058.

(31) Radomski, M. W.; Palmer, R. M. J.; Moncada, S. *Biochem. Biophys. Res. Commun.* **1987**, *148*, 1482–1489.

(32) Gruetter, C. A.; Gruetter, D. Y.; Lyon, J. E.; Kadowitz, P. J.; Ignarro, L. J. *J. Pharmacol. Exp. Ther.* **1981**, *219*, 181–186.

(33) Gryglewski, R. J.; Palmer, R. M. J.; Moncada, S. *Nature* **1986**, *320*, 454–456.

(34) Rubanyi, G. M.; Vanhoutte, P. M. *Am. J. Physiol. Heart Circ.* **1986**, *250*, H822–H827.

(35) Moncada, S.; Palmer, R. M.; Gryglewski, R. J. *Proc. Natl. Acad. Sci. U. S. A.* **1986**, *83*, 9164–9168.

(36) Arnold, W. P.; Mittal, C. K.; Katsuki, S.; Murad, F. *Proc. Natl. Acad. Sci. U. S. A.* **1977**, *74*, 3203–3207.

(37) Craven, P. A.; DeRubertis, F. R. *J. Biol. Chem.* **1978**, *253*, 8433–8443.

(38) Martin, W.; Smith, J. A.; White, D. G. *Br. J. Pharmac.* **1986**, *89*, 563–571.

(39) Ignarro, L. J.; Byrns, R. E.; Wood, K. S. In *Vasodilation: Vascular Smooth Muscle Peptides, Autonomic Nerves and Endothelium*, Vanhoutte, P. M., Ed.; Raven Press, pp 401–414.

(40) Furchgott, R. F. In *Vasodilation: Vascular Smooth Muscle Peptides, Autonomic Nerves and Endothelium*, Vanhoutte, P. M., Ed.; Raven Press, pp 401–414.

(41) Ignarro, L. J.; Buga, G. M.; Wood, K. S.; Byrns, R. E.; Chaudhuri, G. *Proc. Natl. Acad. Sci. U. S. A.* **1987**, *84*, 9265–9269.

(42) Dale, H. H. *Bull. Johns Hopkins Hosp.* **1933**, *53*, 297–347.

(43) Moncada, S.; Radomski, M. W.; Palmer, R. M. J. *Biochem. Pharmacol.* **1988**, *37*, 2495–2501.

(44) Moncada, S.; Palmer, R. M.; Higgs, E. A. *Hypertension* **1988**, *12*, 365–372.

(45) The Nobel Prize in Physiology or Medicine 1998, https://www.nobelprize.org/prizes/medicine/1998/summary/.

(46) Chen, Z.; Zhang, J.; Stamler, J. S. *Proc. Natl. Acad. Sci. U. S. A.* **2002**, *99*, 8306–8311.

(47) Kleschyov, A. L.; Oelze, M.; Daiber, A.; Huang, Y.; Mollnau, H.; Schulz, E.; Sydow, K.; Fichtlscherer, B.; Mülsch, A.; Münzel, T. *Circ. Res.* **2003**, *93*, e104–e112.

(48) Opelt, M.; Eroglu, E.; Waldeck-Weiermair, M.; Russwurm, M.; Koesling, D.; Malli, R.; Graier, W. F.; Fassett, J. T.; Schrammel, A.; Mayer, B. *J. Biol. Chem.* **2016**, *291*, 24076–24084.

(49) Opelt, M.; Wölkart, G.; Eroglu, E.; Waldeck-Weiermair, M.; Malli, R.; Graier, W. F.; Kollau, A.; Fassett, J. T.; Schrammel, A.; Mayer, B.; Gorren, A. C. F. *Mol. Pharmacol.* **2018**, *93*, 335–343.

(50) Liu, X.; Miller, M. J. S.; Joshi, M. S.; Sadowska-Krowicka, H.; Clark, D. A.; Lancaster, J. R. *J. Biol. Chem.* **1998**, *273*, 18709–18713.

(51) Goridis, C.; Morgan, I. *FEBS Lett.* **1973**, *34*, 71–73.

(52) Kimura, H.; Murad, F. *Life Sci.* **1975**, *17*, 837–843.

(53) Denninger, J. W.; Marletta, M. A. *Biochim. Biophys. Acta - Bioenerg.* **1999**, *1411*, 334–350.

(54) Bellamy, T. C.; Wood, J.; Garthwaite, J. *Proc. Natl. Acad. Sci. U. S. A.* **2002**, *99*, 507–510.

(55) Horst, B. G.; Yokom, A. L.; Rosenberg, D. J.; Morris, K. L.; Hammel, M.; Hurley, J. H.; Marletta, M. A. *eLife* **2019**, *8*, ed. by van der Donk, W. A.; Cole, P. A.; Mattevi, A.; Beuve, A., e50634.

(56) Kots, A. Y.; Martin, E.; Sharina, I. G.; Murad, F. In *cGMP: Generators, Effectors and Therapeutic Implications*, Schmidt, H. H. H. W., Hofmann, F., Stasch, J.-P., Eds.; Handbook of Experimental Pharmacology; Springer: Berlin, Heidelberg, 2009, pp 1–14.

(57) Stryer, L. *Annu. Rev. Neurosci.* **1986**, *9*, 87–119.

(58) Francis, S. H.; Corbin, J. D. *Urol. Clin. North Am.* **2005**, *32*, 419–429.

(59) Francis, S. H.; Busch, J. L.; Corbin, J. D. *Pharmacol. Rev.* **2010**, *62*, 525–563.

(60) Surks, H. K.; Mochizuki, N.; Kasai, Y.; Georgescu, S. P.; Tang, K. M.; Ito, M.; Lincoln, T. M.; Mendelsohn, M. E. *Science* **1999**, *286*, 1583–1587.

(61) Münzel, T.; Daiber, A.; Gori, T. *Circulation* **2011**, *123*, 2132–2144.

(62) Sharma, J. N.; Al-Omran, A.; Parvathy, S. S. *Inflammopharmacology* **2007**, *15*, 252–259.

(63) Pfeilschifter, J.; Eberhardt, W.; Hummel, R.; Kunz, D.; Mühl, H.; Nitsch, D.; Plüss, C.; Walker, G. *Cell Biol. Int.* **1996**, *20*, 51–58.

(64) Kim, Y.-M.; Bombeck, C. A.; Billiar, T. R. *Circ. Res.* **1999**, *84*, 253–256.

(65) Brüne, B.; Götz, C.; Meßmer, U. K.; Sandau, K.; Hirvonen, M.-R.; Lapetina, E. G. *J. Biol. Chem.* **1997**, *272*, 7253–7258.

(66) Picón-Pagès, P.; Garcia-Buendia, J.; Muñoz, F. J. *Biochim. Biophys. Acta Mol. Basis Dis.* **2019**, *1865*, 1949–1967.

(67) Knowles, R. G.; Moncada, S. *Biochem. J.* **1994**, *298*, 249–258.

(68) Michel, T.; Feron, O. *J. Clin. Invest.* **1997**, *100*, 2146–2152.

(69) Kobzik, L.; Reid, M. B.; Bredt, D. S.; Stamler, J. S. *Nature* **1994**, *372*, 546–548.

(70) Vizzard, M. A.; Erdman, S. L.; de Groat, W. *J. Neurosci.* **1995**, *15*, 4033–4045.

(71) Guo, F. H.; Raeve, H. R. D.; Rice, T. W.; Stuehr, D. J.; Thunnissen, F. B.; Erzurum, S. C. *Proc. Natl. Acad. Sci. U. S. A.* **1995**, *92*, 7809–7813.

(72) Belhassen, L.; Kelly, R. A.; Smith, T. W.; Balligand, J. L. *J. Clin. Invest.* **1996**, *97*, 1908–1915.

(73) Daff, S. *Nitric Oxide* **2010**, *23*, 1–11.

(74) Brenman, J. E.; Chao, D. S.; Gee, S. H.; McGee, A. W.; Craven, S. E.; Santillano, D. R.; Wu, Z.; Huang, F.; Xia, H.; Peters, M. F.; Froehner, S. C.; Bredt, D. S. *Cell* **1996**, *84*, 757–767.

(75) Sessa, W. C.; Garca-Cardea, G.; Liu, J.; Keh, A.; Pollock, J. S.; Bradley, J.; Thiru, S.; Braverman, I. M.; Desai, K. M. *J. Biol. Chem.* **1995**, *270*, 17641–17644.

(76) Liu, J.; García-Cardeña, G.; Sessa, W. C. *Biochemistry* **1996**, *35*, 13277–13281.

(77) Roman, L. J.; Martásek, P.; Masters, B. S. S. *Chem. Rev.* **2002**, *102*, 1179–1190.

(78) Stuehr, D. J. *Biochim. Biophys. Acta - Bioenerg.* **1999**, *1411*, 217–230.

(79) Chen, P.-F.; Wu, K. K. *J. Biol. Chem.* **2000**, *275*, 13155–13163.

(80) Roman, L. J.; Martásek, P.; Miller, R. T.; Harris, D. E.; de la Garza, M. A.; Shea, T. M.; Kim, J.-J. P.; Masters, B. S. S. *J. Biol. Chem.* **2000**, *275*, 29225–29232.

(81) Garcin, E. D.; Bruns, C. M.; Lloyd, S. J.; Hosfield, D. J.; Tiso, M.; Gachhui, R.; Stuehr, D. J.; Tainer, J. A.; Getzoff, E. D. *J. Biol. Chem.* **2004**, *279*, 37918–37927.

(82) Bredt, D. S.; Snyder, S. H. *Proc. Natl. Acad. Sci. U. S. A.* **1990**, *87*, 682–685.

(83) Feng, C.; Tollin, G.; Holliday, M. A.; Thomas, C.; Salerno, J. C.; Enemark, J. H.; Ghosh, D. K. *Biochemistry* **2006**, *45*, 6354–6362.

(84) Welland, A.; Garnaud, P. E.; Kitamura, M.; Miles, C. S.; Daff, S. *Biochemistry* **2008**, *47*, 9771–9780.

(85) Feng, C.; Tollin, G.; Hazzard, J. T.; Nahm, N. J.; Guillemette, J. G.; Salerno, J. C.; Ghosh, D. K. *J. Am. Chem. Soc.* **2007**, *129*, 5621–5629.

(86) Palmer, R. M. J.; Ashton, D. S.; Moncada, S. *Nature* **1988**, *333*, 664–666.

(87) Feng, C. *Coord. Chem. Rev.* **2012**, *256*, 393–411.

(88) Liu, Q.; Gross, S. S. In *Methods in Enzymology*; Nitric Oxide Part A: Sources and Detection of NO; NO Synthase, Vol. 268; Academic Press: 1996, pp 311–324.

(89) Divakaran, S.; Loscalzo, J. *J. Am. Coll. Cardiol.* **2017**, *70*, 2393–2410.

(90) Vidal, M. J.; Romero, J. C.; Vanhoutte, P. M. *Eur. J. Pharmacol.* **1988**, *149*, 401–402.

(91) Cooke, J. P.; Losordo, D. W. *Circulation* **2002**, *105*, 2133–2135.

(92) Sinzinger, H.; Fitscha, P.; Sinzinger, H.; Fitscha, P.; O'Grady, J.; Rauscha, F.; Rogatti, W.; Vane, J. *Lancet* **1990**, *335*, 627–628.

(93) Pacher, P.; Beckman, J. S.; Liaudet, L. *Physiol. Rev.* **2007**, *87*, 315–424.

(94) Liu, Y.; Feng, Q. *Differentiation* **2012**, *84*, 54–61.

(95) de Mel, A.; Murad, F.; Seifalian, A. M. *Chem. Rev.* **2011**, *111*, 5742–5767.

(96) Brüne, B.; von Knethen, A.; Sandau, K. B. *Eur. J. Pharmacol.* **1998**, *351*, 261–272.

(97) Koshland, D. E. *Science* **1993**, *262*, 1953–1953.

(98) Park, D.; Saravanakumar, G.; Kim, W. J. In *Therapeutic Application of Nitric Oxide in Cancer and Inflammatory Disorders*, Morbidelli, L., Bonavida, B., Eds.; Academic Press: 2019, pp 191–218.

(99) Andrade, S. P.; Bakhle, Y. S.; Hart, I.; Piper, P. J. *Br. J. Cancer* **1992**, *66*, 821–826.

(100) Oliveira-Paula, G. H.; Lacchini, R.; Tanus-Santos, J. E. *Gene* **2016**, *575*, 584–599.

(101) Korneev, S. A.; Park, J.-H.; O'Shea, M. *J. Neurosci.* **1999**, *19*, 7711–7720.

(102) Lowenstein, C. J.; Alley, E. W.; Raval, P.; Snowman, A. M.; Snyder, S. H.; Russell, S. W.; Murphy, W. J. *Proc. Natl. Acad. Sci. U. S. A.* **1993**, *90*, 9730–9734.

(103) Balligand, J.-L.; Feron, O.; Dessy, C. *Physiol. Rev.* **2009**, *89*, 481–534.

(104) Förstermann, U.; Sessa, W. C. *Eur. Heart J.* **2012**, *33*, 829–837, 837a–837d.

(105) Nakane, M.; Mitchell, J.; Förstermann, U.; Murad, F. *Biochem. Biophys. Res. Commun.* **1991**, *180*, 1396–1402.

(106) Bernátová, I. *Interdiscip. Toxicol.* **2011**, *4*, 63–68.

(107) Dedio, J.; König, P.; Wohlfart, P.; Schroeder, C.; Kummer, W.; Müller-Esterl, W. *FASEB J.* **2001**, *15*, 79–89.

(108) Bauer, P. M.; Fulton, D.; Boo, Y. C.; Sorescu, G. P.; Kemp, B. E.; Jo, H.; Sessa, W. C. *J. Biol. Chem.* **2003**, *278*, 14841–14849.

(109) Dimmeler, S.; Fleming, I.; Fisslthaler, B.; Hermann, C.; Busse, R.; Zeiher, A. M. *Nature* **1999**, *399*, 601–605.

(110) Fulton, D.; Gratton, J.-P.; McCabe, T. J.; Fontana, J.; Fujio, Y.; Walsh, K.; Franke, T. F.; Papapetropoulos, A.; Sessa, W. C. *Nature* **1999**, *400*, 792–792.

(111) Matsubara, M.; Hayashi, N.; Jing, T.; Titani, K. *J. Biochem* **2003**, *133*, 773–781.

(112) Ravi, K.; Brennan, L. A.; Levic, S.; Ross, P. A.; Black, S. M. *Proc. Natl. Acad. Sci. U. S. A.* **2004**, *101*, 2619–2624.

(113) Stuehr, D. J.; Fasehun, O. A.; Kwon, N. S.; Gross, S. S.; Gonzalez, J. A.; Levi, R.; Nathan, C. F. *FASEB J.* **1991**, *5*, 98–103.

(114) Li, Y.; Wang, H.; Tarus, B.; Perez, M. R.; Morellato, L.; Henry, E.; Berka, V.; Tsai, A.-L.; Ramassamy, B.; Dhimane, H.; Dessy, C.; Tauc, P.; Boucher, J.-L.; Deprez, E.; Slama-Schwok, A. *Proc. Natl. Acad. Sci. U. S. A.* **2012**, *109*, 12526–12531.

(115) Rouaud, F.; Romero-Perez, M.; Wang, H.; Lobysheva, I.; Ramassamy, B.; Henry, E.; Tauc, P.; Giacchero, D.; Boucher, J.-L.; Deprez, E.; Rocchi, S.; Slama-Schwok, A. *Oncotarget* **2014**, *5*, 10650–10664.

(116) Schini, V. B.; Vanhoutte, P. M. *J. Pharmacol. Exp. Ther.* **1992**, *261*, 553–559.

(117) Werner, E. R.; Pitters, E.; Schmidt, K.; Wachter, H.; Werner-Felmayer, G.; Mayer, B. *Biochem. J.* **1996**, *320*, 193–196.

(118) Víteček, J.; Lojek, A.; Valacchi, G.; Kubala, L. *Mediators Inflamm.* **2012**, *2012*, e318087.

(119) Macallister, R.; Whitley, G.; Vallance, P. *Kidney Int.* **1994**, *45*, 737–742.

(120) Vallance, P.; Leone, A.; Moncada, S.; Calver, A.; Collier, J. *Lancet* **1992**, *339*, 572–575.

(121) Young, R. J. et al. *Bioorganic Med. Chem. Lett.* **2000**, *10*, 597–600.

(122) Wolff, D. J.; Datto, G. A.; Samatovicz, R. A.; Tempsick, R. A. *J. Biol. Chem.* **1993**, *268*, 9425–9429.

(123) Drago, R. S.; Paulik, F. E. *J. Am. Chem. Soc.* **1960**, *82*, 96–98.

(124) Scicinski, J.; Oronsky, B.; Ning, S.; Knox, S.; Peehl, D.; Kim, M. M.; Langecker, P.; Fanger, G. *Redox Biol.* **2015**, *6*, 1–8.

(125) Scicinski, J.; Oronsky, B.; Taylor, M.; Luo, G.; Musick, T.; Marini, J.; Adams, C. M.; Fitch, W. L. *Drug Metab. Dispos.* **2012**, *40*, 1810–1816.

(126) Ellis-Davies, G. C. R. *Nat. Methods* **2007**, *4*, 619–628.

(127) Vuilleumier, J.; Gaulier, G.; De Matos, R.; Ortiz, D.; Menin, L.; Campargue, G.; Mas, C.; Constant, S.; Le Dantec, R.; Mugnier, Y.; Bonacina, L.; Gerber-Lemaire, S. *ACS Appl. Mater. Interfaces* **2019**, *11*, 27443–27452.

(128) Fraix, A.; Parisi, C.; Seggio, M.; Sortino, S. *Chem. Eur. J.* **2021**, *27*, 12714–12725.

(129) Stoddard, B. L.; Cohen, B. E.; Brubaker, M.; Mesecar, A. D.; Koshland, D. E. *Nat. Struct. Biol.* **1998**, *5*, 891–897.

(130) Ursby, T.; Weik, M.; Fioravanti, E.; Delarue, M.; Goeldner, M.; Bourgeois, D. *Acta Crystallogr. D. Biol. Crystallogr.* **2002**, *58*, 607–614.

(131) Allin, C.; Ahmadian, M. R.; Wittinghofer, A.; Gerwert, K. *Proc. Natl. Acad. Sci. U. S. A.* **2001**, *98*, 7754–7759.

(132) Dunn, A. R.; Dmochowski, I. J.; Winkler, J. R.; Gray, H. B. *J. Am. Chem. Soc.* **2003**, *125*, 12450–12456.

(133) Belliston-Bittner, W.; Dunn, A. R.; Nguyen, Y. H. L.; Stuehr, D. J.; Winkler, J. R.; Gray, H. B. *J. Am. Chem. Soc.* **2005**, *127*, 15907–15915.

(134) Seymour, C. P.; Tohda, R.; Tsubaki, M.; Hayashi, M.; Matsubara, R. *J. Org. Chem.* **2017**, *82*, 9647–9654.

(135) Parisi, C.; Seggio, M.; Fraix, A.; Sortino, S. *ChemPhotoChem* **2020**, *4*, 742–748.

(136) Ieda, N.; Hotta, Y.; Yamauchi, A.; Nishikawa, A.; Sasamori, T.; Saitoh, D.; Kawaguchi, M.; Kimura, K.; Nakagawa, H. *ACS Chem. Biol.* **2020**, *15*, 2958–2965.

(137) Perdicakis, B.; Montgomery, H. J.; Abbott, G. L.; Fishlock, D.; Lajoie, G. A.; Guillemette, J. G.; Jervis, E. *Bioorg. Med. Chem.* **2005**, *13*, 47–57.

(138) Beaumont, E.; Robin, A.-C.; Berka, V.; Tsai, A.-L.; Blanchard-Desce, M.; Lambry, J.-C.; Slama-Schwok, A. *Nitric Oxide* **2006**, *14*, 14–15.

(139) Robin, A.-C.; Gmouh, S.; Mongin, O.; Jouikov, V.; Werts, M. H. V.; Gautier, C.; Slama-Schwok, A.; Blanchard-Desce, M. *Chem. Commun.* **2007**, 1334–1336.

(140) Beaumont, E.; Lambry, J.-C.; Gautier, C.; Robin, A.-C.; Gmouh, S.; Berka, V.; Tsai, A.-L.; Blanchard-Desce, M.; Slama-Schwok, A. *J. Am. Chem. Soc.* **2007**, *129*, 2178–2186.

(141) Beaumont, E.; Lambry, J.-C.; Robin, A.-C.; Martasek, P.; Blanchard-Desce, M.; Slama-Schwok, A. *ChemPhysChem* **2008**, *9*, 2325–2331.

(142) Beaumont, E.; Lambry, J.-C.; Blanchard-Desce, M.; Martasek, P.; Panda, S. P.; van Faassen, E. E. H.; Brochon, J.-C.; Deprez, E.; Slama-Schwok, A. *ChemBioChem* **2009**, *10*, 690–701.

(143) Lambry, J.-C.; Beaumont, E.; Tarus, B.; Blanchard-Desce, M.; Slama-Schwok, A. *J. Mol. Recognit.* **2010**, *23*, 379–388.

(144) Nguyen, N.-H. Synthèse de Nano-Déclencheurs Photo-Activables Pour Le Contrôle Spatio-Temporel de La Formation de NO, These de Doctorat, Ecole normale supérieure de Cachan, 2015.

(145) Nguyen, N.-H.; Bogliotti, N.; Chennoufi, R.; Henry, E.; Tauc, P.; Salas, E.; Roman, L. J.; Slama-Schwok, A.; Deprez, E.; Xie, J. *Org. Biomol. Chem.* **2016**, *14*, 9519–9532.

(146) Chennoufi, R.; Cabrié, A.; Nguyen, N. H.; Bogliotti, N.; Simon, F.; Cinquin, B.; Tauc, P.; Boucher, J.-L.; Slama-Schwok, A.; Xie, J.; Deprez, E. *Biochim. Biophys. Acta Gen. Subj.* **2019**, *1863*, 1127–1137.

(147) Overman, L. E.; Paone, D. V. *J. Am. Chem. Soc.* **2001**, *123*, 9465–9467.

(148) Lal, B.; Pramanik, B. N.; Manhas, M. S.; Bose, A. K. *Tetrahedron Lett.* **1977**, *18*, 1977–1980.

(149) Mitsunobu, O.; Obata, T.; Mukaiyama, T. *J. Org. Chem.* **1965**, *30*, 1071–1073.

(150) Mitsunobu, O.; Yamada, M. *BCSJ* **1967**, *40*, 2380–2382.

(151) Mitsunobu, O.; Yamada, M.; Mukaiyama, T. *BCSJ* **1967**, *40*, 935–939.

(152) Comstock, L. R.; Rajski, S. R. *Tetrahedron* **2002**, *58*, 6019–6026.

(153) Beddoe, R. H.; Sneddon, H. F.; Denton, R. M. *Org. Biomol. Chem.* **2018**, *16*, 7774–7781.

(154) Batesky, D. C.; Goldfogel, M. J.; Weix, D. J. *J. Org. Chem.* **2017**, *82*, 9931–9936.

(155) Hu, F.-H.; Wang, L.-S.; Cai, S.-F. *J. Chem. Eng. Data* **2009**, *54*, 1382–1384.

(156) Sun, H.; Yeo, W. L.; Lim, Y. H.; Chew, X.; Smith, D. J.; Xue, B.; Chan, K. P.; Robinson, R. C.; Robins, E. G.; Zhao, H.; Ang, E. L. *Angew. Chem. Int. Ed.* **2016**, *55*, 14277–14280.

(157) Darzens, A. G. *C. r. hebd. séances Acad. sci.* **1911**, *152*, 1601–1603.

(158) Peterson, M. A.; Oliveira, M.; Christiansen, M. A.; Cutler, C. E. *Bioorganic Med. Chem. Lett.* **2009**, *19*, 6775–6779.

(159) Bertho, A.; Maier, J. *Liebigs Ann.* **1932**, *498*, 50–61.

(160) Wang, T.; Lee, H. J.; Tosh, D. K.; Kim, H. O.; Pal, S.; Choi, S.; Lee, Y.; Moon, H. R.; Zhao, L. X.; Lee, K. M.; Jeong, L. S. *Bioorganic Med. Chem. Lett.* **2007**, *17*, 4456–4459.

(161) Zhang, G.; Richardson, S. L.; Mao, Y.; Huang, R. *Org. Biomol. Chem.* **2015**, *13*, 4149–4154.

(162) Staudinger, H.; Meyer, J. *Helv. Chim. Acta* **1919**, *2*, 635–646.

(163) Xie, J. *Eur. J. Org. Chem.* **2002**, *2002*, 3411–3418.

(164) Uchida, T.; Egami, F. *J. Biochem* **1967**, *61*, 44–53.

(165) Uzawa, S. *J. Biochem* **1932**, *15*, 1–10.

(166) Fox, J. W. *Toxicon* **2013**, *62*, 75–82.

(167) Borio, A.; Hofinger, A.; Kosma, P.; Zamyatina, A. *Tetrahedron Lett.* **2017**, *58*, 2826–2829.

(168) Lehar, S. M. et al. *Nature* **2015**, *527*, 323–328.

(169) Wagner, D.; Verheyden, J. P. H.; Moffatt, J. G. *J. Org. Chem.* **1974**, *39*, 24–30.

(170) Wei, W.-C.; Chang, C.-C. *Eur. J. Org. Chem.* **2017**, *2017*, 3033–3040.

(171) Dilly, S.; Roman, L. J.; Bogliotti, N.; Xie, J.; Deprez, E.; Slama-Schwok, A. *Antioxidants* **2020**, *9*, 89.

(172) Komnenos, T. *Liebigs Ann.* **1883**, *218*, 145–167.

(173) Michael, A. *J. prakt. Chem.* **1887**, *35*, 349–356.

(174) Tokoroyama, T. *Eur. J. Org. Chem.* **2010**, *2010*, 2009–2016.

(175) Fischer, O.; Müller, A.; Vilsmeier, A. *J. prakt. Chem.* **1925**, *109*, 69–87.

(176) Vilsmeier, A.; Haack, A. *Ber. Dtsch. Chem. Ges.* **1927**, *60*, 119–122.

(177) Wittig, G.; Geissler, G. *Liebigs Ann.* **1953**, *580*, 44–57.

(178) Wittig, G.; Schöllkopf, U. *Chem. Ber.* **1954**, *87*, 1318–1330.

(179) Spangler, C. W.; McCoy, R. K. *Synth. Commun.* **1988**, *18*, 51–59.

(180) Gu, Y.; Tian, S.-K. In *Stereoselective Alkene Synthesis*, Wang, J., Ed.; Topics in Current Chemistry; Springer: Berlin, Heidelberg, 2012, pp 197–238.

(181) Tamura, R.; Kato, M.; Saegusa, K.; Kakihana, M.; Oda, D. *J. Org. Chem.* **1987**, *52*, 4121–4124.

(182) Tamura, R.; Saegusa, K.; Kakihana, M.; Oda, D. *J. Org. Chem.* **1988**, *53*, 2723–2728.

(183) Horner, L.; Hoffmann, H.; Wippel, H. G. *Chem. Ber.* **1958**, *91*, 61–63.

(184) Horner, L.; Hoffmann, H.; Wippel, H. G.; Klahre, G. *Chem. Ber.* **1959**, *92*, 2499–2505.

(185) Wadsworth, W. S.; Emmons, W. D. *J. Am. Chem. Soc.* **1961**, *83*, 1733–1738.

(186) Wadsworth, D. H.; Schupp, O. E.; Seus, E. J.; Ford, J. A. *J. Org. Chem.* **1965**, *30*, 680–685.

(187) Schotten, C. *Ber. Dtsch. Chem. Ges.* **1884**, *17*, 2544–2547.

(188) Baumann, E. *Ber. Dtsch. Chem. Ges.* **1886**, *19*, 3218–3222.

(189) Milas, N. A.; Sussman, S. *J. Am. Chem. Soc.* **1936**, *58*, 1302–1304.

(190) Eames, J.; Mitchell, H. J.; Nelson, A.; O'Brien, P.; Warren, S.; Wyatt, P. *J. Chem. Soc., Perkin trans. 1* **1999**, 1095–1104.

(191) Jacobsen, E. N.; Marko, I.; Mungall, W. S.; Schroeder, G.; Sharpless, K. B. *J. Am. Chem. Soc.* **1988**, *110*, 1968–1970.

(192) Sharpless, K. B.; Amberg, W.; Bennani, Y. L.; Crispino, G. A.; Hartung, J.; Jeong, K. S.; Kwong, H. L.; Morikawa, K.; Wang, Z. M. *J. Org. Chem.* **1992**, *57*, 2768–2771.

(193) VanRheenen, V.; Kelly, R. C.; Cha, D. Y. *Tetrahedron Lett.* **1976**, *17*, 1973–1976.

(194) Pappo, R.; Allen D., J.; Lemieux, R.; Johnson, W. *J. Org. Chem.* **1956**, *21*, 478–479.

(195) Bellucci, C.; Gualtieri, F.; Chiarini, A. *Eur. J. Med. Chem.* **1987**, *22*, 473–477.

(196) Mladenova, M.; Ventelon, L.; Blanchard-Desce, M. *Tetrahedron Lett.* **1999**, *40*, 6923–6926.

(197) Leonelli, F.; Trombetta, A.; Bella, A. L.; Lucarelli, G.; Demitri, N.; Lamba, D.; Migneco, L. M.; Bettolo, R. M. *Eur. J. Org. Chem.* **2019**, *2019*, 1594–1599.

(198) Burk, M. J.; Allen, J. G. *J. Org. Chem.* **1997**, *62*, 7054–7057.

(199) Janczewski, Ł.; Gajda, A.; Gajda, T. *Eur. J. Org. Chem.* **2019**, *2019*, 2528–2532.

(200) Li, H.; Zhang, X.; Shi, X.; Ji, N.; He, W.; Zhang, S.; Zhang, B. *Adv. Synth. Catal.* **2012**, *354*, 2264–2274.

(201) Rodríguez-Lucena, D.; Benito, J. M.; Álvarez, E.; Jaime, C.; Perez-Miron, J.; Ortiz Mellet, C.; García Fernández, J. M. *J. Org. Chem.* **2008**, *73*, 2967–2979.

(202) Xiong, J.; Wei, X.; Ding, M.-W. *Synlett* **2017**, *28*, 1075–1078.

(203) Despras, G.; Hain, J.; Jaeschke, S. O. *Chem. Eur. J.* **2017**, *23*, 10838–10847.

(204) García-Moreno, M. I.; Díaz-Pérez, P.; Benito, J. M.; Ortiz Mellet, C.; Defaye, J.; García Fernández, J. M. *Carbohydr. Res.* **2002**, *337*, 2329–2334.

(205) Li, R.; Martin, M. P.; Liu, Y.; Wang, B.; Patel, R. A.; Zhu, J.-Y.; Sun, N.; Pireddu, R.; Lawrence, N. J.; Li, J.; Haura, E. B.; Sung, S.-S.; Guida, W. C.; Schonbrunn, E.; Sebti, S. M. *J. Med. Chem.* **2012**, *55*, 2474–2478.

(206) Doknic, D.; Abramo, M.; Sutkeviciute, I.; Reinhardt, A.; Guzzi, C.; Schlegel, M. K.; Potenza, D.; Nieto, P. M.; Fieschi, F.; Seeberger, P. H.; Bernardi, A. *Eur. J. Org. Chem.* **2013**, *2013*, 5303–5314.

(207) Banik, B. K.; Manhas, M. S.; Bose, A. K. *J. Org. Chem.* **1993**, *58*, 307–309.

(208) Ramage, R.; MacLeod, A. M.; Rose, G. W. *Tetrahedron* **1991**, *47*, 5625–5636.

(209) Valeur, B. In *Molecular Fluorescence*; John Wiley & Sons, Ltd: 2001; Chapter 3, pp 34–71.

(210) Rurack, K.; Spieles, M. *Anal. Chem.* **2011**, *83*, 1232–1242.

(211) Brouwer, A. M. *Pure Appl. Chem.* **2011**, *83*, 2213–2228.

(212) Göppert-Mayer, M. *Ann. Phys.* **1931**, *401*, 273–294.

(213) Rumi, M.; Perry, J. W. *Adv. Opt. Photon.* **2010**, *2*, 451–518.

(214) Friedrich, D. M. *J. Chem. Educ.* **1982**, *59*, 472.

(215) Melnikov, A. S.; Serdobintsev, P. Y.; Vedyaykin, A. D.; Khodorkovskii, M. A. *J. Phys.: Conf. Ser.* **2017**, *917*, 062029.

(216) Gottlieb, H. E.; Kotlyar, V.; Nudelman, A. *J. Org. Chem.* **1997**, *62*, 7512–7515.

(217) Doddrell, D. M.; Pegg, D. T.; Bendall, M. R. *J. Magn. Reson.* **1982**, *48*, 323–327.

(218) Piotto, M.; Bourdonneau, M.; Elbayed, K.; Wieruszeski, J.-M.; Lippens, G. *Magn. Reson. Chem.* **2006**, *44*, 943–947.

(219) Socrates, G., *Infrared and Raman Characteristic Group Frequencies: Tables and Charts*, 3rd ed; Wiley: Chichester ; New York, 2001.

(220) Devkota, K.; Lohse, B.; Liu, Q.; Wang, M.-W.; Stærk, D.; Berthelsen, J.; Clausen, R. P. *ACS Med. Chem. Lett.* **2014**, *5*, 293–297.

(221) Swarbrick, J. M.; Graeff, R.; Garnham, C.; Thomas, M. P.; Galione, A.; Potter, B. V. L. *Chem. Commun.* **2014**, *50*, 2458–2461.

(222) Tang, K.-C.; Mariuzza, R.; Coward, J. K. *J. Med. Chem.* **1981**, *24*, 1277–1284.

(223) Anglin, J. L.; Deng, L.; Yao, Y.; Cai, G.; Liu, Z.; Jiang, H.; Cheng, G.; Chen, P.; Dong, S.; Song, Y. *J. Med. Chem.* **2012**, *55*, 8066–8074.

(224) Shah, P. N.; Min, J.; Kim, H.-J.; Park, S.-Y.; Lee, J.-S. *Macromolecules* **2011**, *44*, 7917–7925.

(225) Watanabe, H.; Miki, Y.; Shimizu, Y.; Saji, H.; Ono, M. *Dyes Pigm.* **2019**, *170*, 107615.

(226) Daly, C. J. In *Biomedical Visualisation : Volume 1*, Rea, P. M., Ed.; Advances in Experimental Medicine and Biology; Springer International Publishing: Cham, 2019, pp 97–106.

(227) Eukaryote, https://en.wikipedia.org/w/index.php?title=Eukaryote&oldid=1048742473, 2021.

(228) Transcription (Biology), https://en.wikipedia.org/w/index.php?title=Transcription_(biology) &oldid=1047615721, 2021.

(229) DNA and RNA Codon Tables, https://en.wikipedia.org/w/index.php?title=DNA_and_RNA_codon_tables&oldid=1044190903, 2021.

(230) Spoel, S. H. *J. Exp. Bot.* **2018**, *69*, 4499–4503.

(231) Vedejs, E.; Peterson, M. J. In *Topics in Stereochemistry*; John Wiley & Sons, Ltd: 1994, pp 1–157.

(232) Reichardt, C. *Chem. Rev.* **1994**, *94*, 2319–2358.

List of Figures

List of Tables

Appendix A

Biology precisions

A.1 Structure of vascular vessels

Vascular vessel are composed of three principal parts, as shown in **Figure** A.1[226]. The external layer, or tunica externa, composed of adipous tissue and the perivascular innervation. The internal layer, or tunica intima, composed of an elastic matrix coated with endothelial cells in contact with the bloodstream. The intermediate layer, or tunica media is located between the two former, surrounded by another elastic layer and composed of smooth muscle cells.

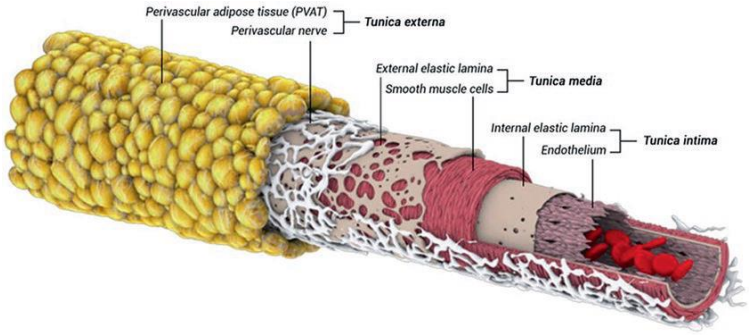

Figure A.1: Tridimensionnal reconstruction of a vascular vessel[226].

[226] Daly, C. J. In *Biomedical Visualisation : Volume 1*, Rea, P. M., Ed.; Advances in Experimental Medicine and Biology; Springer International Publishing: Cham, 2019, pp 97–106.

A.2 Main structures in eukaryotic cells

The most important structures of eukaryotic cells are presented in **Figure** A.2[227].

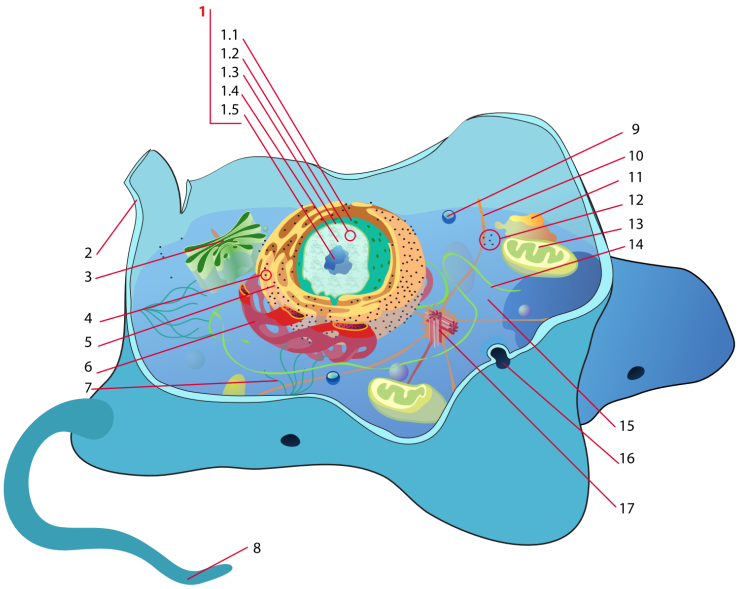

Figure A.2: Representation of an eukaryotic cell[227].

1. Nucleus: 1.1. Nuclear pore; 1.2. Chromatin; 1.3. Nuclear enveloppe; 1.4. Nucleus; 1.5. Nucleolus. **2.** Plasmic membrane. **.3** Golgi apparatus. **4.** Ribosomes. **5.** Rough endoplasmic reticulum. **6.** Smooth endoplasmic reticulum. **7.** Actin filaments. **8.** Flagellum (not in all eukaryotic cells). **9.** Peroxysome. **10.** Microtubule. **11.** Lysosome. **12.** Free ribosomes. **13.** Mitochondrion. **14.** Intermediate filaments. **15.** Cytoplasm or cytosol. **16.** Secretory vesicle. **17.** Centrosome.

[227] Eukaryote, https://en.wikipedia.org/w/index.php?title=Eukaryote&oldid=1048742473, 2021.

A.3 From gene to protein and regulation

The main steps of cellular protein synthesis are detailed below in a simplified manner.

A.3.1 Transcription

The transcription is a biological process in which an enzyme called the RNA-polymerase binds the DNA helix, creates a zone where the two strands are separated before creating a matching RNA copy of the read DNA sequence, as shown on **Figure** A.3[228]. The DNA genomic information is thus transcripted into the polymerised RNA strands.

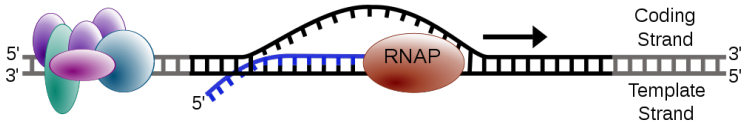

Figure A.3: Schematic representation of the biosynthesis of mRNA (blue) from DNA (black) by RNA-polymerase (brown)[228]. The colored ellipses represent the different transcription cofactors enabling the transcription in the first place.

More precisely, eukaryotes have four kinds of RNA polymerases, three of which exists in animals, and the mRNA involved in peptidic synthesis is produced by RNA polymerase II. It requires a very complex succession of controlled events to properly produce a functionnal mRNA. This enzyme requires a promoter sequence which allows its binding to the double helix, such as a TATA box composed mainly of adenine (A) and thymine (T) nucleic bases. Its recruitment is facilitated by proteic transcription factor such as TATA binding protein (TBP), which itself is regulated by TBP associated factors (TAFs). Some other transcription factors specific of RNA polymerase II lead to the formation of the pre-initiation complex (PIC). Then the double helix is finally opened, the DNA strand transfered towards the active site , and the mRNA starts being polymerised. The initiation step ends when the enzymatic complex leaves the promoter sequence.

Other processes can also influence the transcription of DNA into mRNA. In the nucleus, DNA is mostly under the form of chromatin, which is a condensed state where its strands are wrapped around histones. The transcription levels are dependant on the condensation level of the DNA strands. Nonetheless, histones can be modified by co-activation factor, that are proteic factors able to recruit RNA Pol II, recognize activation factors and promote chromatin remodelling.

The synthesized mRNA still undergoes some modifications before being converted into a protein.

A.3.2 Post-transcriptional modification

The previously formed RNA strand can then undergo maturation, in an operation called post-transcriptional modification. The mRNA can have some portions enzymatically removed and some added in order to become a mature mRNA, ready to be converted into a protein.

More precisely, specific sequences are recognized and spliced out of the mRNA by spliceosomes. Other enzymatic complexes located in the same cellular region add a polyadenyl tail, which is also a part of the maturation process. The same starting mRNA can be spliced in different ways, *in fine* producing different proteins from the same genomic information. The excised sequences are called introns and the one that will be translated into a peptidic sequence are named exons.

[228] Transcription (Biology), https://en.wikipedia.org/w/index.php?title=Transcription_(biology) &oldid=1047615721, 2021.

A.3.3 Translation

The previously formed mature mRNA will then be used by ribosomes to convert the genomic sequence into a peptidic sequence, in a process called translation. The ribosome matches the desired amino acid with respect to a sequence of 3 bases on the mRNA using transfer RNAs (tRNAs), with a redundant code shown in **Figure** A.4[229]. The mRNA strand is read by the ribosome from the 5' end towards the 3' end.

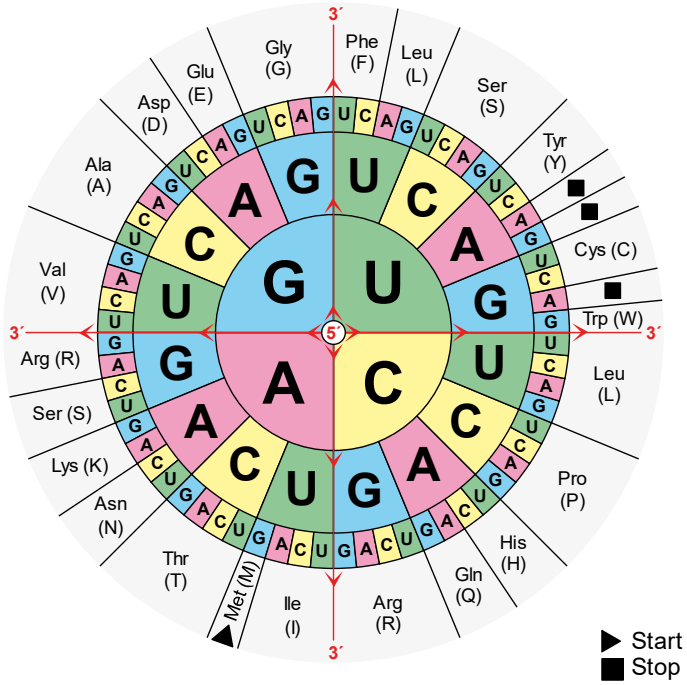

Figure A.4: RNA redundant codon table used to translate the genome into a peptidic sequence[229].

The protein polymerised this way is not readily functional. A key step to produce a functionnal protein is its proper folding, sometimes requiring external help such as chaperonines, but this process will not be further detailed.

A.3.4 Post-translational modifications

A wide array of post-translational modifications can occur on proteins after their synthesis, as shown on **Figure** A.5[230]. They can modify various properties of the protein, from activation to inhibition of its activity, change its cellular localization or start its degradation process. Palmitoylation or is also a kind of post-translational modification involved in addressing the proteins to membranes.

[229] DNA and RNA Codon Tables, https://en.wikipedia.org/w/index.php?title=DNA_and_RNA_codon_tables&oldid=1044190903, 2021.
[230] Spoel, S. H. *J. Exp. Bot.* **2018**, *69*, 4499–4503.

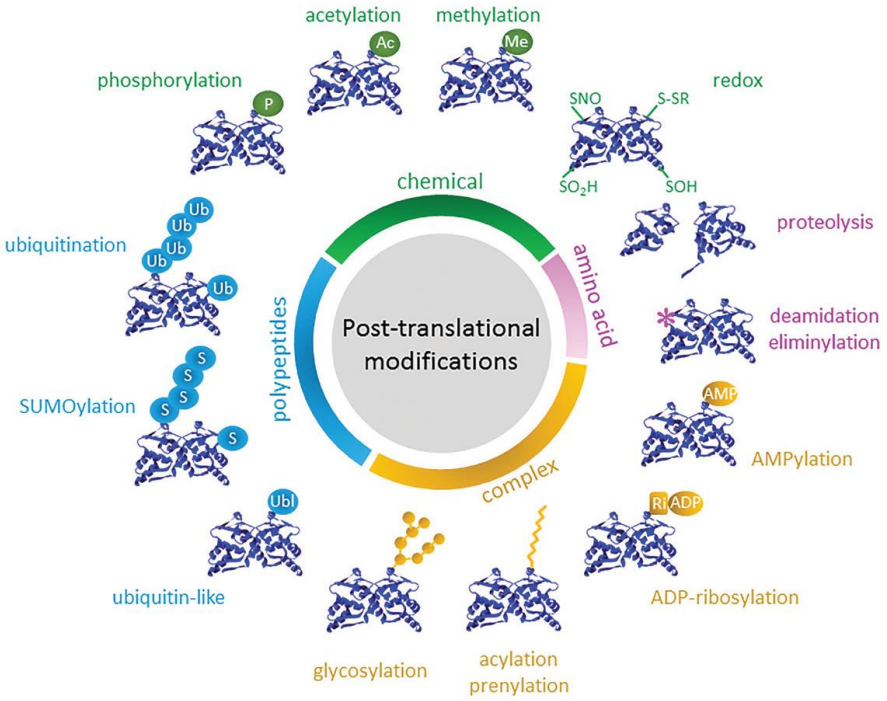

Figure A.5: Various possibilities for a protein post-translational modification[230].

A.4 Detailed catalytic cycle forming NO in NOSs by L-arg oxidation into L-cit

The detailed catalytic cycle of NO formation at the heme of NOSs is presented in **Figure** A.6[73].

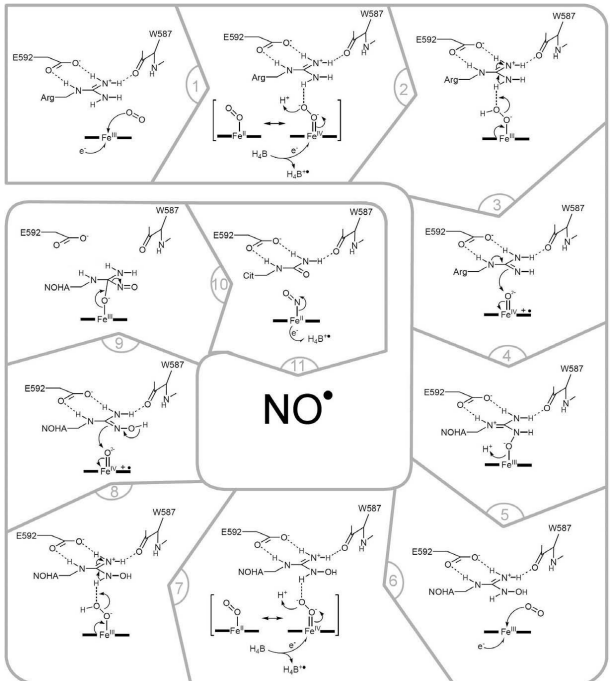

Figure A.6: Catalytic NO formation through an oxyferryl complex[73].

Appendix B

Synthesis precisions

B.1 Reaction progress by ^{31}P NMR

In order to determine the success of the transformation of dibenzylphosphite into dibenzyl phosphoryl chloride **R-2**, TLC was not an option due to the compounds instability. A fairly elegant solution was found with the use of ^{31}P NMR, by recording spectra for the starting material and the crude product, as well as a mixture of the two. The coupling constant between ^{13}C and ^{31}P is relatively small (around 10-20Hz) compared to the coupling between ^{31}P and ^{1}H (around 200Hz in PH_3). As shown on **Figure** B.1, dibenzylphosphite shows a great coupling constant of around 700Hz that disappear in the crude residue, represented by a singlet if the small carbon couplings are ignored. These informations are consistent with the formation of the desired compound.

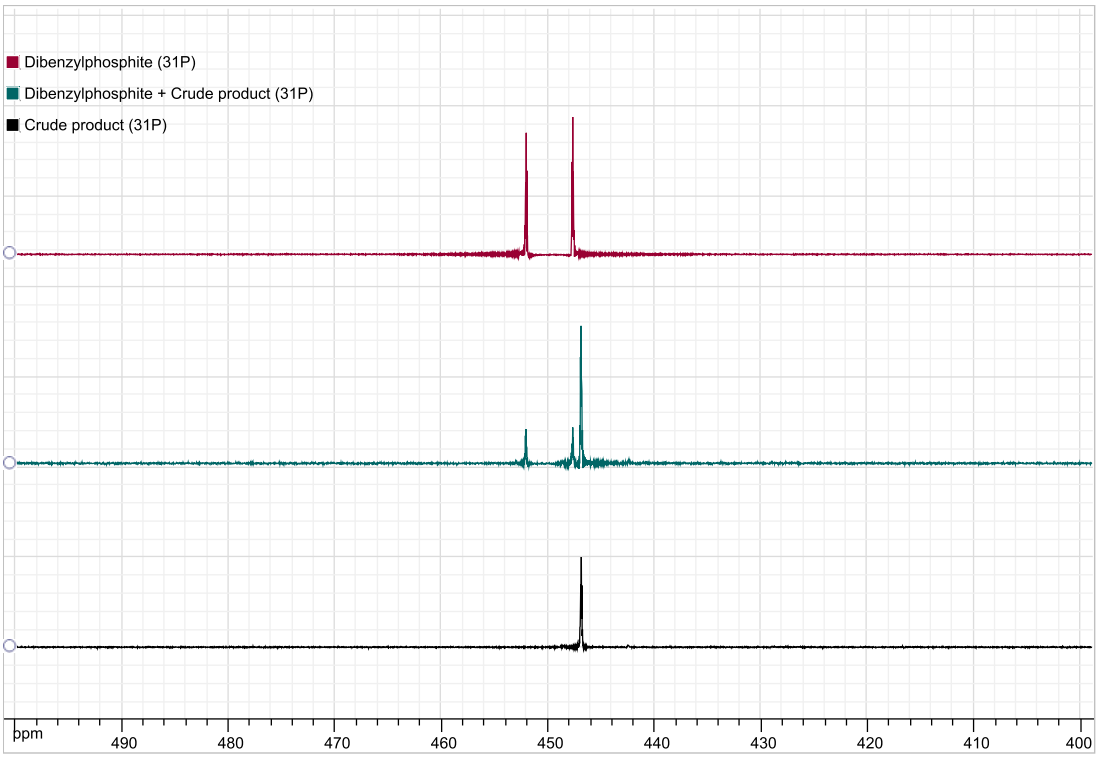

Figure B.1: Superimposed ^{31}P NMR spectra of dibenzylphosphite (red), the crude product of the reaction (black) and a mixture of both (green).

Additionally, the ^{1}H NMR of the compound showed degradation after a couple of days, with the appearance of a clear broad singlet, probably signifying the hydrolysis of the dibenzylphosphoryl chloride into the respective phosphoric acid because of moisture, as shown on **Figure** B.2.

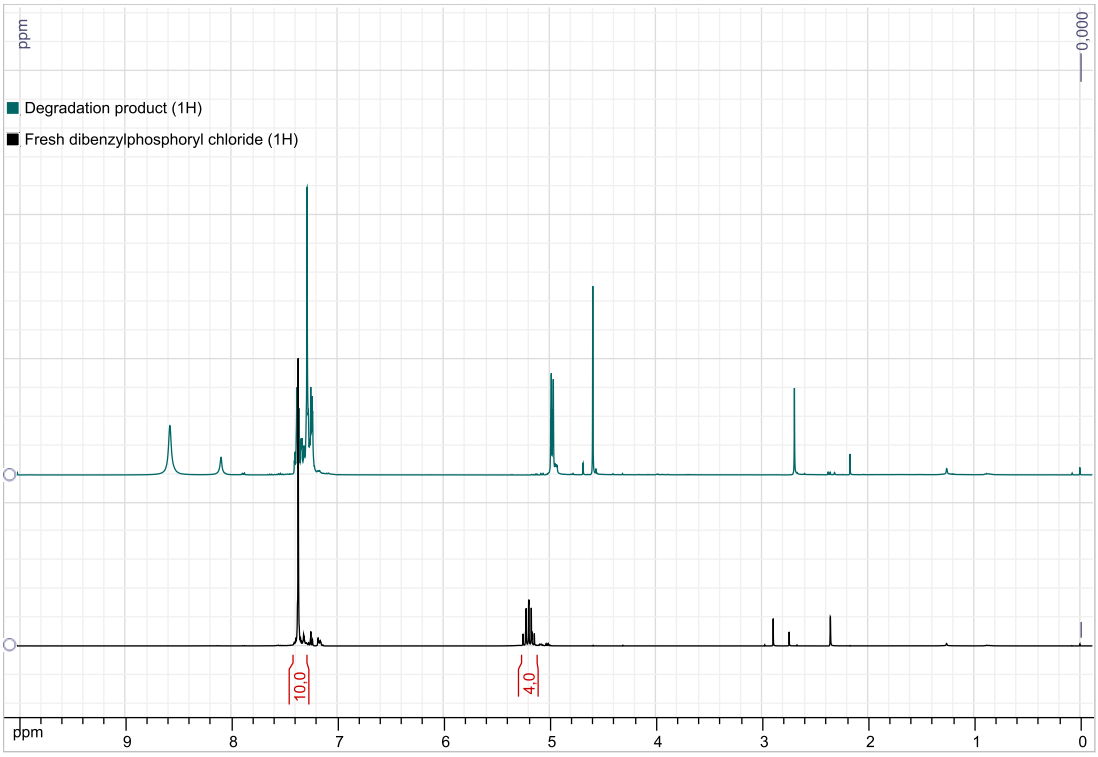

Figure B.2: Superimposed ^{1}H NMR spectra of dibenzylphosphoryl chloride (black) and its degradation product after two days (green).

B.2 Stereoselectivity of the Wittig olefination

The stereochemistry of the Wittig olefination is thought to derive from steric interactions as the two reactive moieties approach each other, with several transition states possible and several ways of proceeding towards the products through an oxaphosphetane, as shown on **Figure** B.3[180].

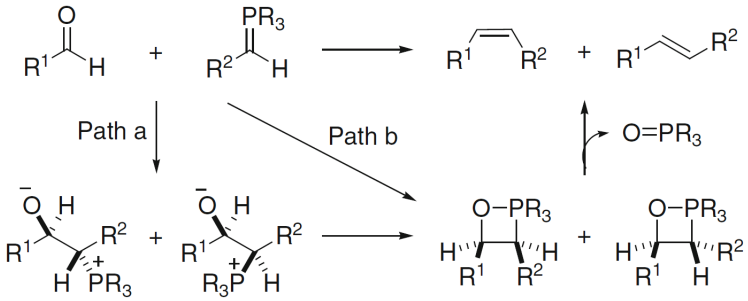

Scheme B.3: Mechanistic pathways of the Wittig's olefination[180].

A transition state model was thought of by Vedejs[231], shown on **Figure** B.4, explaining the stereochemical outcome of this reaction. The four-center transition states (TSs) (C-C-P-O) can adopt

[231] Vedejs, E.; Peterson, M. J. In *Topics in Stereochemistry*; John Wiley & Sons, Ltd: 1994, pp 1–157, (p.135).

either a *cis* TS or *trans* TS. The *cis* puckered TS geometry leading to *Z* olefins relieves the TS from 1,2 steric interactions between the ylide and the aldehyde substituent compared to the *cis* planar TS. The *trans* planar TS forming *E* olefins decreases the 1,3 steric interactions compared to the *trans* puckered TS.

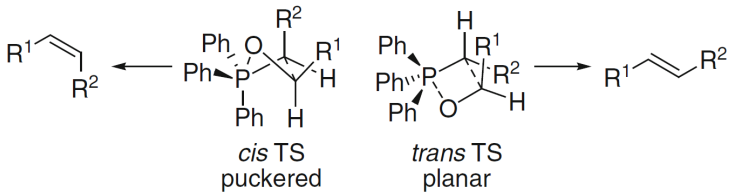

Scheme B.4: Vedejs transition states model explaining the stereochemistry of Wittig's olefination[180].

Additionally, replacing the common phenyl substituents by butyl groups on the ylides usually leads to an increase towards *E* olefin formation[180]. In the Wittig's olefinations described in **Chapter 2**, the aryl substitution of the aldehyde and the 1,3-dioxolanyl substitution on the ylide seem to have very high levels of 1,2 steric interactions, as exclusive *E* formation was observed by measurement of the *J* couplings of the vinylic protons in 1D ^{1}H NMR spectra.

B.3 Stereoselectivity of the HWE olefination

The HWE olefination is under both thermodynamic and kinetic control[180]. The formation and equilibrium between the *erythro* and *threo* intermediates is under thermodynamic control, as shown on **Figure** B.5, but their irreversible transformation into alkenes is determined by kinetic factors. Thus the stereochemical outcome of this transformation can be tuned towards the desired stereoselectivity. Usually the thermodynamically favored *E* olefin is the major compound, and in the olefination described in **Chapter 2** no *Z* form was formed, as observed by looking at the *J* couplings of the vinylic protons in 1D ^{1}H NMR spectra.

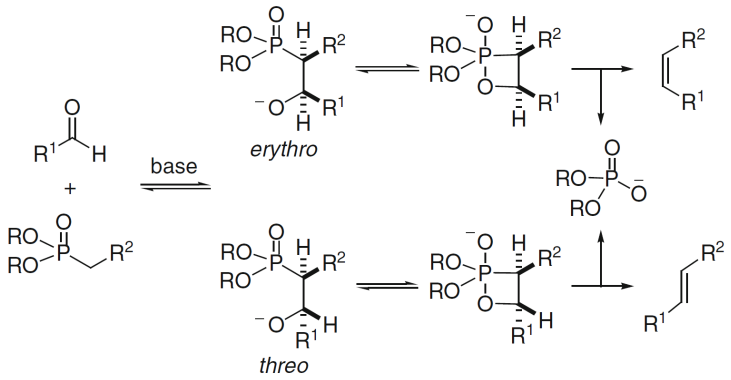

Scheme B.5: Equilibria at stakes during the HWE olefination[180].

B.4 HPLC

During HPLC analysis, a quantification method was needed in order to assess the purity of the compounds. To that extent, four channels (190nm, 254nm, 390nm and 450nm) were recorded on a batch of **NT-4c-Boc** which was the less pure substance available. Absorbance at 450nm was discarded as its maximum was 500 fold below the other ones, close to the background noise. The three wavelegth left showed non-superimposable chromatograms, even after normalization, as shown in **Figure** B.6. Spectroscopic properties of similar compound was already known to have maxima of absorbance at around 370nm in a Tris buffer and 390nm in DMSO[145]. Thus the choice was made to use the postulated highest absorption wavelength, 390nm, to analyse the chromatograms.

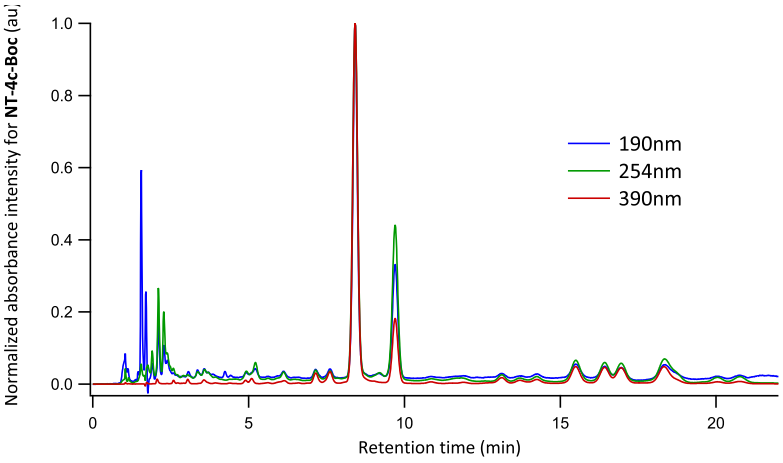

Figure B.6: Chromatograms of the normalized absorptions of **NT-4c-Boc** at 190nm, 254nm and 390nm.

The optical purity was then assessed by integration of the area under the visible peaks and division by the total area under the peaks, as described in **Appendix C.2**.

Appendix C

Spectroscopy precisions

C.1 TICT state investigation

The Franck-Condon excited state reached upon irradiation can induce large changes among the electronic density around a molecule[209]. The latter can then evolve from the locally excited (LE) planar state towards a TICT state, with a geometrical change of the molecule, breaking conjugation and further increasing the charge separation, as shown on **Figure** C.1. From the structure of the synthesized nanotriggers, bearing a fairly large conjugated system along with several possible rotations enriched by amines, the existence of a TICT state could be possible.

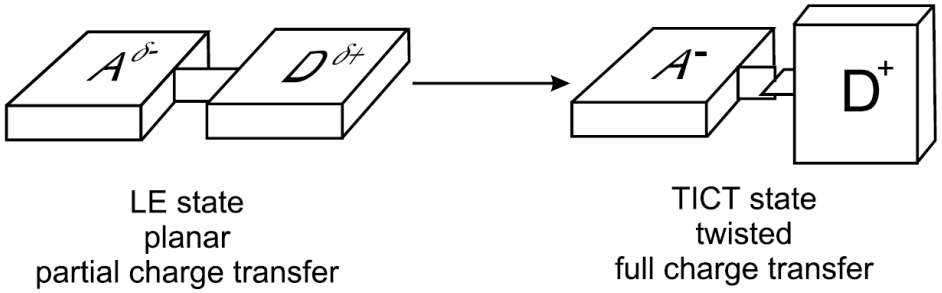

Figure C.1: Representation and formation of a TICT state from a Franck-Condon state[209], involving charge transfer in molecules bearing an electron-donating moiety (D) and electron-accepting moiety (A).

In order to probe the existence of a TICT state, the study of the fluorescence properties of the compounds can be studied in solvents of increasing polarity. The higher a solvent polarity, the more this excited state can undergo a solvent relaxation, leading to a relaxed intramolecular charge transfer (ICT) state, and the more red-shifted and broad is its emission.

For these reasons, the absorption and fluorescence emission properties of the nanotriggers were studied in THF, DMSO and EtOH[232], as presented in **Figure** C.2, with the results summarized in **Tables** C.1 & C.2.

[232] Reichardt, C. *Chem. Rev.* **1994**, *94*, 2319–2358.

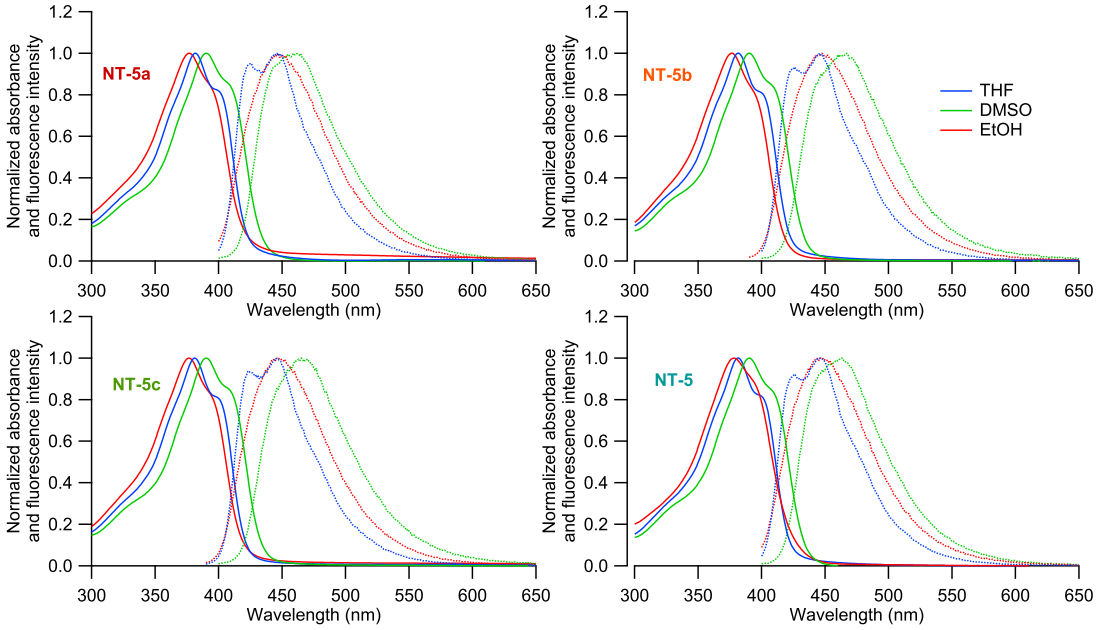

Figure C.2: Absorption and emission properties of the synthesized nanotriggers in solvents of different polarity.

Solvent	**Polarity**†	$\lambda_{max,abs}$ **5a** (nm)	$\lambda_{max,abs}$ **5b** (nm)	$\lambda_{max,abs}$ **5c** (nm)	$\lambda_{max,abs}$ **5** (nm)
THF	0.207	382	382	381	381
DMSO	0.444	390	388	392	390
EtOH	0.654	377	376	377	378

Table C.1: Absorbance properties of the compounds in THF, DMSO and EtOH.

† Normalized empirical parameters of solvent polarity[232].

Solvent	**Polarity**†	$\lambda_{max,em}$ **5a** (nm)	$\lambda_{max,em}$ **5b** (nm)	$\lambda_{max,em}$ **5c** (nm)	$\lambda_{max,em}$ **5** (nm)
THF	0.207	446 (426)‡	446 (426)‡	445 (423)‡	446 (426)
DMSO	0.444	459	467	465	463
EtOH	0.654	447	448	448	447

Table C.2: Fluorescence emission properties of the compounds in THF, DMSO and EtOH. Excitation at the previously described absorbance maximum in each solvent.

† Normalized empirical parameters of solvent polarity[232].
‡ Maximum of the second lower emission band beetween parentheses.

The spectra shown in **Figure** C.2 show a similar shift for all the compounds in the three solvents, either with respect to their absorbance or fluorescence emission. The bands resolution seems to increase when the polarity of the solvent deacreases, as seen with the smooth bell shape of the spectra in EtOH, the appearance of a small shouldering at longer wavelength in DMSO, and the two clear visible bands in THF. This observation is valid for either absorption or emission spectra, but does not support the TICT state as no clear red-shifted band can be observed in EtOH. The resolved bands observed are energetically shifted by around 1050cm^{-1} in THF, typically in the energy range of molecular vibrations. Thus, the observed bands are most likely coming from different vibrational levels of the excited state.

C.2 Multiphoton processes

C.2.1 Generalities

Multiphoton processes are a very large family of processes, as shown on **Figure** C.3 with several biphoton examples[214]. Multiphoton processes can be used to probe the symmetry of the excited states of molecules, *via* selection rules controlled by symmetry, but this feature will not be further detailed.

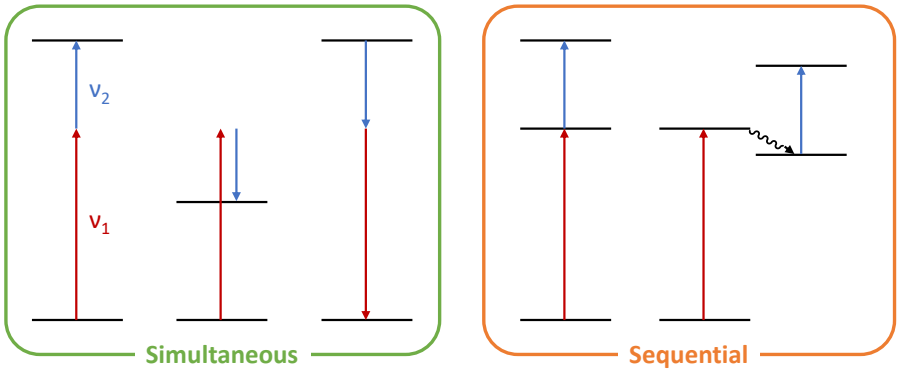

Figure C.3: Examples of multiphoton processes, with either a simultaneous or sequential two-photon absorption. Simultaneous events *do not* go through an intermediate excited state as often referred to, it is a single quantum jump. Sequential events *do* proceed through an existing excited state.

In the following will only be discussed simultaneous processes. The general schemes presented are roughly a few examples, as any number of photons could theoretically be absorbed at once, if some symmetry considerations are respected. Nonetheless, more photons absorbed simultaneously is a less probable event, because the presence of the molecule and all involved photons at the same position is required for it to occur. Another approach to these kind of phenomena is through the energetic point of view, as electromagnetic interactions between the entities involved. Photons are harmonic *vibration modes* of the electromagnetic field and do not interact with each other. The *vibrational modes* of molecules are coupled and do not interact with each other. In the close proximity of a molecule, those electromagnetic entities are able to interact and simultaneously redistribute the sum of all their energy.

An illustration of the potency of multiphoton processes is shown on **Figure** C.4, with the comparison between Raman scattering and coherent anti-Stokes Raman scattering (CARS).

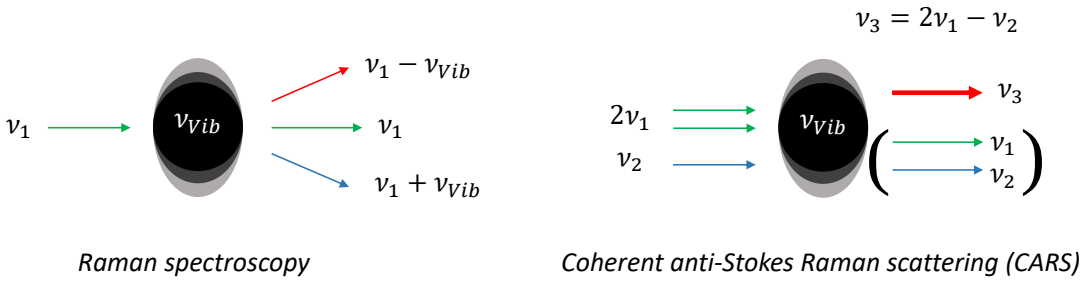

Figure C.4: Example of the more sensitive Coherent anti-Stokes Raman scattering (CARS) multiphoton process, with respect to Raman spectroscopy.

The first one is caused by the inelastic scattering of light, either adding or substracting a molecular vibrational frequency to the scattered light, thus giving information on the vibrational structure. The scattering happening in all directions, the Raman signal can be quite weak. This issue was solved by CARS, a multiphoton improvement of Raman spectroscopy.

A simple way of increasing the output signal is to make it coherent, thus directionnal and consequently more intense. The production of photons of frequency ν_3 is resonant when $\nu_1 - \nu_2 = \nu_{vib}$ (Raman resonance), as shown on **Figure** C.5. Despite being a third order process, thus much less likely to occur compared to the first order Raman scattering, the coherence of photons ν_3 produced by CARS makes the output beam bright enough to give a good output signal.

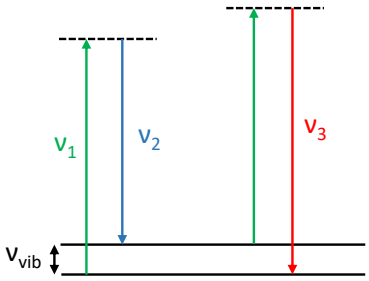

Figure C.5: Energy diagram representing the CARS multiphoton process. Dashed lines are displayed for the sake of clarity and do not represent an existing state.

Processes involving two photons with $\nu_1 = \nu_2 = \nu$ are particularly used, mainly because it only requires one powerful source of monochromatic photons. As high power lasers are not cheap, these conditions are much easier to set up. Additionally, the energy range of a two-photon excitation with an infrared source is equivalent to a one-photon excitation in the UV range, without their known consequences on living organisms. Nonetheless, a noteworthy feature is that a high energy beam of infrared photons can also lead to molecular degradation by excitation of the vibrational levels. Two-photon measurements were used for the characterization of the nanotriggers described in the main matter, and as such these will be the main focus of the following discussion.

C.2.2 Two-photon absorption: a non-linear phenomenon

In order to unveil the non-linear aspect of two-photon absorption, some mathematical definitions should be set:

$$\mathrm{I} = [h\nu] \times c \tag{C.1}$$

I = Light intensity ($photons.\mathrm{cm}^{-2}.\mathrm{s}^{-1}$)
[hν] = Photon concentration ($photons.\mathrm{cm}^{-3}$)
c = Speed of light ($\mathrm{cm.s}^{-1}$)

The italic *portion of units is presented for the sake of clarity but not part of the International System of Units (SI).*

In the upcoming discussion, the concentration of non-excited molecules will be assumed to be constant. First because of the very low lifetime of most molecular excited states, and second because it enables the use of the method of flooding of Ostwald. Thus, for an ordinary unidimensional one-photon process, *ie* at low light intensity, the absorption transition can be described with the following first order rate equation:

$$-\frac{d[h\nu]}{dt} = -\frac{d\mathrm{N}^*}{dt} = k\mathrm{N} \times [h\nu] = \frac{k\mathrm{N}}{c} \times \mathrm{I} = -\frac{d\mathrm{I}}{dx} \tag{C.2}$$

N = Concentration of molecules M ($molecules.\mathrm{cm}^{-3}$), hypothesized constant
N^* = Concentration of excited molecules M^*
k = Rate constant of the one-photon absorption process ($photon/molecule^{-1}.\mathrm{cm}^3.\mathrm{s}^{-1}$)

A solution with respect to the light intensity is given by:

$$\mathrm{I}(x) = \mathrm{I}_0 \times e^{-\frac{k\mathrm{N}}{c}x} = \mathrm{I}_0 \times e^{-\sigma \mathrm{N} x} \tag{C.3}$$

$\sigma = \frac{k}{c}$ = One-photon absorption cross-section ($\mathrm{cm}^2.molecule^{-1}$)

One can recognize here an expression of Beer-Lambert law across a path of length ℓ:

$$\mathrm{A} = \log\left(\frac{\mathrm{I}_0}{\mathrm{I}}\right) = \varepsilon \ell [\mathrm{M}] \quad \text{with} \quad \varepsilon = \frac{\sigma \times \mathrm{N_A}}{\ln 10 \times 10^3} = \frac{k \times \mathrm{N_A}}{c \times \ln 10 \times 10^3} \tag{C.4}$$

ℓ = Cuvette length (cm)
[M] = Concentration of molecules M ($\mathrm{mol.L}^{-1}$)
ε = Molar absorption coefficient ($\mathrm{L.mol}^{-1}.\mathrm{cm}^{-1}$)
$\mathrm{N_A}$ = Avogadro constant (6.022×10^{23} $molecules.\mathrm{mol}^{-1}$)

The same approach can describe multiphoton processes using a higher order rate equation, becoming the following second order rate equation for two-photon absorption:

$$-\frac{d[h\nu_1]}{dt} = -\frac{d[h\nu_2]}{dt} = -\frac{d\mathrm{N}^*}{dt} = k_{2h\nu}\mathrm{N} \times [h\nu_1][h\nu_1] \tag{C.5}$$

$k_{2h\nu}$ = Rate constant of the two-photon absorption process ($molecule/photon^{-1}.photon^{-1}\mathrm{cm}^6.\mathrm{s}^{-1}$)

The latter changes to the following if $\nu_1 = \nu_2 = \nu$:

$$-\frac{1}{2}\frac{d[h\nu]}{dt} = -\frac{dN^*}{dt} = k_{2h\nu} N \times [h\nu]^2 \tag{C.6}$$

Including the light intensity in the latter gives:

$$-\frac{dI}{dx} = -2\frac{k_{2h\nu} N}{c^2} \times I^2 = -2\sigma_{TPA} N \times I^2 \tag{C.7}$$

$\sigma_{TPA} = \frac{k_{2h\nu}}{c^2}$ = Two-photon absorption cross-section ($cm^4.s.molecule^{-1}$)

The two-photon absorption cross-section σ_{TPA} is usually very small, as demonstrated by its most adapted unit, the Goeppert-Mayer ($1GM = 10^{-50} cm^4.s.molecule^{-1}$). Thus, a solution of this particular equation can be simplified using Taylor series:

$$I(x) = \frac{I_0}{1 + 2I_0\sigma_{TPA} N x} \quad \text{which becomes} \quad I(x) \approx I_0 - I_0^2 \sigma_{TPA} N x + ... \quad \text{when} \quad 2I_0\sigma_{TPA} N x \ll 1 \tag{C.8}$$

By combination of equation **C.2**, **C.3** and **C.7** arise the following:

$$-\frac{dI}{dx} = \sigma N I + 2\sigma_{TPA} N I^2 \tag{C.9}$$

As stated as a preliminary remark, the intensity and respective absorption cross-sections are functions of ν. Following equation **C.9**, in order to study the very low two-photon absorption cross-section σ_{TPA} an important premice is to have no one-photon absorption of the excitation beam, as it would be a lot of orders of magnitude higher. The nanotriggers **NT-a**, **NT-b** and **NT-c** did not display one-photon absorbance in the range where their σ_{TPA} were studied, enabling these two-photon characterizations.

C.2.3 Two-photon absorption cross-section measurements

As discussed in the main matter, the two-photon absorption cross-section σ_{TPA} of the previous generation of nanotriggers was determined by comparison with a known reference, Coumarin 102[215]. As previously stated, the evolution of the excited state reached is independant of its one- or two-photon excitation, the key parameter is its energy. Thus TPIF can be correlated to σ_{TPA}. The two-photon fluorescence quantum yield $\phi_{F,2h\nu}$ can be described accurately by ϕ_F, if looked through the same lens as before. Fluorescence quantum yield is the ratio of emitted photons over absorbed photons, or the ratio of emitted photons over the number of adequate excited states reached. Thus, the pathway towards excitation of the molecule should not have a huge impact on the $\phi_{F,2h\nu}$ value *versus* ϕ_F.

The unknown values of σ^i_{TPA} of the nanotriggers can be obtained through TPIF measurements *via* the described values of a reference (superscript *R*) using the following equation[213]:

$$\sigma^i_{TPA} = \sigma TPA^R \frac{\phi^R_F \cdot N^R \cdot G^R}{\phi^i_F \cdot N^i \cdot G^i} \frac{I^i_{TPIF}}{I^R_{TPIF}} \tag{C.10}$$

G = Correction factor dependant on experimental parameters
I_{TPIF} = Integral of the TPIF signal

The correction factor G depends on many parameters, such as the difference in refractive index between the source beam wavelength and the fluorescence wavelength, the reabsorption of fluorescence, or optical parameters within the setup. Its influence can be minimised by comparing the samples to the reference as well as adjusting the laser power to a fixed value at every wavelength investigated. Additionally, the concentration for the samples and the nanotriggers were the same. Approximating $G \approx 1$, the former equation becomes:

$$\sigma^{i}_{\mathrm{TPA}} = \sigma^{\mathrm{R}}_{\mathrm{TPA}} \times \frac{\Phi^{\mathrm{R}}_{\mathrm{F}}}{\Phi^{i}_{\mathrm{F}}} \frac{\mathrm{I}^{i}_{\mathrm{TPIF}}}{\mathrm{I}^{\mathrm{R}}_{\mathrm{TPIF}}} \tag{C.11}$$

Equation **C.11** was used in order to calculate the values of σ_{TPA} for **NT-a**, **NT-b** and **NT-c** for two-photon excitation wavelengths ranging from 740nm to 900nm with 10nm steps between each point, as presented in **Chapter 3**.

Appendix D

Automation of fastidious tasks

D.1 HPLC analysis (Wavemetrics Igor Pro)

A user-friendly graphical user interface (GUI) was programmed in order to perform quantification measurements on chromatograms obtained by HPLC. The latter enabled integration of the peaks area and returned the spectral purity, defined as the contribution of a single peak over all the peaks.

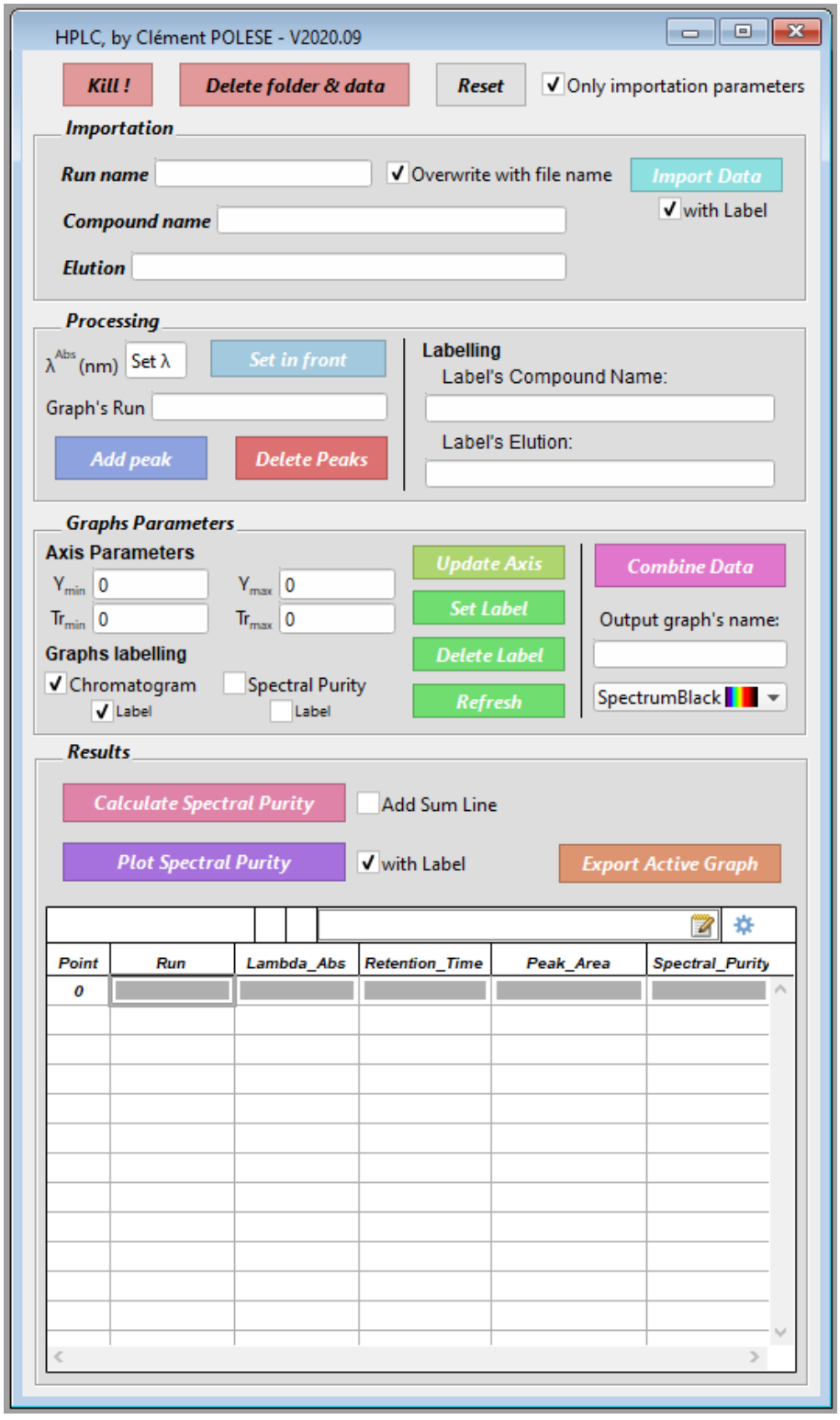

Figure D.1: GUI programmed to enable user foreign to Igor Pro programming to perform HPLC quantification.

D.2 NMR redaction (Microsoft Excel)

In order to avoid the repetitive and tedious process of converting NMR spectra into publication-ready paragraphs, a Visual Basic for Applications (VBA) macro was coded for Microsoft Excel. Settings allow the choice of the nucleus, solvent, journal to format the output. Then, after filling the chemical shifts, signal type, coupling constants, integration and attribution, the press of a button converts the table into a fully formatted paragraph adapted to the chosen journal standards. Another button enables to convert it into LaTeX format.

Nucleus	Type	Frequency	Solvent	Journal	Preview
^{1}H	1D	400 MHz	MeOD-*d4*	ACS	^{1}H NMR (MeOD-*d4* , 400 MHz): δ

COMPILATION | LaTeX | CLEAR

δ (ppm)	Type	Coupling (Hz)	Integration	Attribution	Preview
8.33	s		1	H_2	8.33 (s, 1H, H_2),
8.20	s		1	H_8	8.20 (s, 1H, H_8),
6.16	d	3.6	1	H_1'	6.16 (d, 1H, *J* = 3.6 Hz, H_1'),
5.28	dd	6.1, 3.6	1	H_2'	5.28 (dd, 1H, *J* = 6.1, 3.6 Hz, H_2'),
5.04	dd	6.1, 2.3	1	H_3'	5.04 (dd, 1H, *J* = 6.1, 2.3 Hz, H_3'),
4.38	ddd	3.9, 3.2, 2.3	1	H_4'	4.38 (ddd, 1H, *J* = 3.9, 3.2, 2.3 Hz, H_4'),
3.79	dd	12.1, 3.2	1	H_{5a}'	3.79 (dd, 1H, *J* = 12.1, 3.2 Hz, H_{5a}'),
3.71	dd	12.1, 3.9	1	H_{5b}'	3.71 (dd, 1H, *J* = 12.1, 3.9 Hz, H_{5b}'),
1.62	s		3	CH_3	1.62 (s, 3H, CH_3),
1.38	s		3	CH_3	1.38 (s, 3H, CH_3).
					^{1}H NMR (MeOD-*d4* , 400 MHz): δ 8.33 (s, 1H, H_2), 8.20 (s, 1H, H_8), 6.16 (d, 1H, *J* = 3.6 Hz, H_1'), 5.28 (dd, 1H, *J* = 6.1, 3.6 Hz, H_2'), 5.04 (dd, 1H, *J* = 6.1, 2.3 Hz, H_3'), 4.38 (ddd, 1H, *J* = 3.9, 3.2, 2.3 Hz, H_4'), 3.79 (dd, 1H, *J* = 12.1, 3.2 Hz, H_{5a}'), 3.71 (dd, 1H, *J* = 12.1, 3.9 Hz, H_{5b}'), 1.62 (s, 3H, CH_3), 1.38 (s, 3H, CH_3).
					^{1}H NMR (MeOD-\textit{d}\textit{4}, 400 MHz): δ 8.33 (s, 1H, H$_{2}$), 8.20 (s, 1H, H$_{8}$), 6.16 (d, 1H, \textit{J} = 3.6 Hz, H$_{1}$'), 5.28 (dd, 1H, \textit{J} = 6.1, 3.6 Hz, H$_{2}$'), 5.04 (dd, 1H, \textit{J} = 6.1, 2.3 Hz, H$_{3}$'), 4.38 (ddd, 1H, \textit{J} = 3.9, 3.2, 2.3 Hz, H$_{4}$'), 3.79 (dd, 1H, \textit{J} = 12.1, 3.2 Hz, H$_{5a}$'), 3.71 (dd, 1H, \textit{J} = 12.1, 3.9 Hz, H$_{5b}$'), 1.62 (s, 3H, CH$_{3}$), 1.38 (s, 3H, CH$_{3}$).

Figure D.2: Microsoft Excel macro programmed in VBA to format NMR experiments towards a written medium.

D.3 Epsilon characterizations (Wavemetrics Igor Pro)

An user-friendly GUI was programmed with the precious help of Stéphane Maisonneuve, as shown in **Figure** D.3, in order to ease and shorten the time required to process the data aquired from the spectrophotometers and obtain the desired results. The latter also enables the simple display and study of absorbance evolution *versus* the concentration, as in **Chapter 3**.

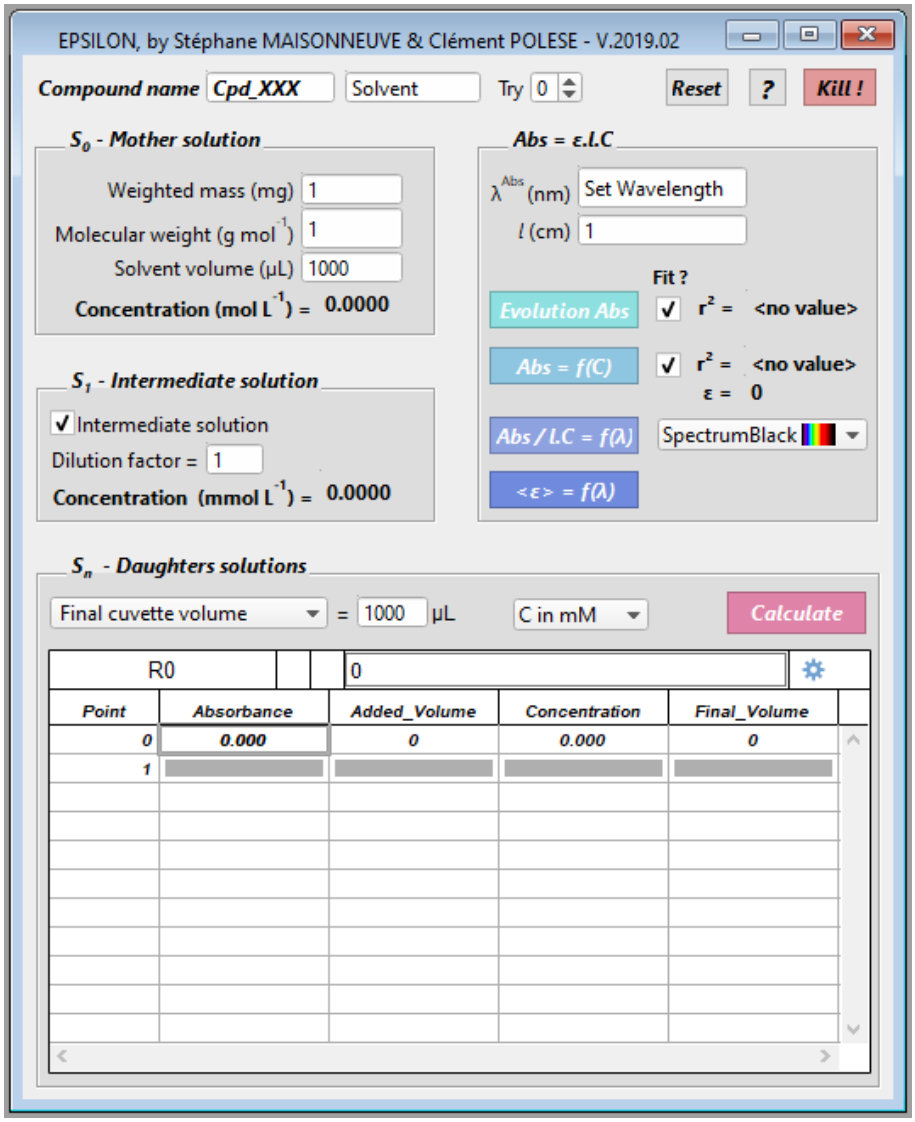

Figure D.3: GUI programmed to enable user foreign to Igor Pro programming to perform simple absorptivity measurements.

université PARIS-SACLAY

ÉCOLE DOCTORALE
Sciences Chimiques: Molécules, Matériaux, Instrumentation et Biosystèmes (2MIB)

Titre: Synthèse et caractérisation d'analogues photoactivables de NADPH

Mots clés: Monoxyde d'azote, Nanodéclencheur, Nitric Oxide Synthase, NOS

Résumé: Le monoxyde d'azote (NO) est une molécule avec un rôle majeur de signalisation impliquée dans des processus biologiques variés. Impliqué dans la relaxation des muscles lisses induite par des dérivés nitrés, parmi lesquels certains sont utilisés depuis presque 150 ans dans le traitement de problèmes cardiaques. Plus récemment, il a été montré sa place centrale dans un mécanisme complexe de transduction du signal découvert à la fin des années 1980, en lien avec une régulation en amont de p53 et donc une capacité pro-apoptotique. De nombreuses physiopathologies ont été corrélées à une libération endogène ou exogène de NO, telles que certaines maladies cardiaques, rénales, l'obésité, l'impuissance ou le cancer. Dans l'optique d'élucider les processus biologiques régulés par NO et leurs mécanismes sous-jacents, l'utilisation de la lumière comme déclencheur des phénomènes est une méthodologie prometteuse, permettant la plus grande précision spatiotemporelle disponible. Plusieurs stratégies ont été développées dans le but de photo-libérer du NO, parmi lesquelles une particulièrement intéressante repose sur l'utilisation de mimes photoactivables de NADPH, appelés nanodéclencheurs. Ces composés peuvent intéragir avec l'enzyme productrice de NO, permettant le déclenchement de son cycle catalytique par transfert électronique photoinduit. Une nouvelle génération de ces analogues ont été synthétisés et caractérisés, comportant un dérivé d'adénosine pour reconnaître le domaine réductase de l'enzyme, ainsi qu'une structure basée sur un motif diarylbutadiène capable de donner des électrons dans un état excité. Les structures de ces derniers ont été conçues à l'aide de données de modélisation moléculaire de manière à cibler les Nitric Oxide Synthases (NOSs). Ces nouveaux composés pourraient permettre d'étudier des processus biologiques impliquant des doses précises de NO, comme pour l'existence d'une concentration seuil pour influer sur l'angiogénèse.

Title: Synthesis and characterization of photoactivatable NADPH mimics

Keywords: Nitric oxide, Nanotrigger, Nitric Oxide Synthase, NOS

Abstract: Nitric oxide (NO) is a major signalling molecule in various biological processes. It is involved in the smooth muscle relaxation induced by nitrovasodilators, some of which are clinically used for more than 150 years in the treatment of cardiac pathologies. More recently, it was shown to play a key role in a complex signal transduction pathway discovered in the late 1980s, related to p53 upregulation and able to trigger apoptosis. Numerous physiopathologies were correlated with endogenous or exogenous release of NO, such as cardiovascular diseases, renal dysfunction, obesity, erectile dysfunction or cancer. In order to further elucidate the bioprocesses regulated by NO and their underlying mechanism, light-triggered phenomena are the most promising methodology, achieving the most precise space-time control available. Several strategies towards NO photorelease were developped but one of particular interest relies on photoactivatable mimics of NADPH, called nanotriggers. These compounds can interact with the NO-producing enzyme and trigger its catalytic transformation upon photoinduced electron transfer. A new generation of these analogs was synthesized and characterized, bearing an adenosine derivative towards recognition of the enzyme reductase domain alongside a diarylbutadiene moiety capable of giving away electrons while in an excited state. The latter were designed with insights from molecular modelling to be targeted at the Nitric Oxide Synthases (NOSs). These new compounds could enable further investigations on biological processes involving precise NO-release, such as the existence of a concentration threshold for NO to affect angiogenesis.

Université Paris-Saclay
Espace Technologique / Immeuble Discovery
Route de l'Orme aux Merisiers RD 128 / 91190 Saint-Aubin, France